TAILORING ARCHITECTURE IN WHEAT BY MANIPULATING GENES IN BRASSINOSTEROID PATHWAY

Manpartik Singh Gill

Thesis submitted to The University of Nottingham for the degree of Doctor of Philosophy

November 2023

Abstract

Due to increasing human population growth it is predicted that wheat yields will need to increase by 60% by 2050. Overwhelming evidence suggests that during grain filling wheat yield potential is sink-limited, as carbon accumulation is limited by the storage capacity of the grains. Therefore, strategies to improve grain number is one of the most important avenues in the genetic improvement of yield potential. A strategy for increasing grain number is to increase the spike density within the crop. This can potentially be achieved by altering canopy architecture to improve radiation use efficiency and allow a higher planting density. Brassinosteroids (BRs) are phytohormones that have an important role in controlling architecture and assimilate partitioning. It is well established that lesions in the BR biosynthesis and signalling pathway can produce more upright canopy architecture in cereals. For example, partial suppression of the *OsBRI1* gene in transgenic rice confers a beneficial erect-leaf phenotype that increases grain yield under higher planting density. Based on studies in other cereals, we targeted *TaBRI1*, which encodes the BR receptor, and the BR-biosynthesis genes *TaDWF1* and *TaDWF4* as candidates for gene characterisation and mutation in wheat. TILLING and EMS mutagenesis-based screens enabled identification of homoeologous loss-of-function mutations in these genes. These were then stacked in the common background Cadenza followed by backcrossing to stabilize the mutants for characterization. *tabri1* mutants displayed reduced sensitivity, whereas *tadwf1* and *tadwf4* mutants showed hypersensitivity to external BR application. BR analysis found elevated levels of the biologically active BRs brassinolide, castasterone and 24-epicastasterone as well as the biosynthesis precursors campesterol (CR), 6-oxocampestanol (6-oxoCN), typhasterol and 6-deoxotyphasterol in the triple receptor mutant *tabri1-a.1bd* compared to non-mutant controls, potentially due to restricted feedback regulation because of compromised signal transduction. There was a 126-fold reduction in the level of CR in the triple *tadwf1-abd* mutant in which the conversion of 24-methylenecholesterol to CR is blocked. Additionally, the levels of the intermediates campestanol, 6-oxoCN and 6-deoxocathasterone were reduced in this mutant compared to non-mutant controls. No differences in BR levels could be detected in the triple *tadwf4-abd* mutant compared to controls. To determine the phenotype associated with these mutations in the

TaBRI1, *TaDWF1* and *TaDWF4* genes, the mutants were grown under glasshouse and field conditions. Interestingly, *tabri1-a.1b*, *tabri1-bd*, *tabri1-a.1d*, with mutations in two *TaBRI1* homoeologues, and the triple *tadwf4-abd* mutant exhibited increased leaf erectness without negative pleotropic effects on other agronomically important traits such as stem elongation and grain size both under glasshouse and field conditions. In contrast, *tabri1-a.3bd* and *tadwf1-abd* mutants showed alterations in canopy architecture coupled with negative effects on stem elongation and grain characteristics. As a strategy to understand the physiological mechanisms through which BRs control leaf angle, anatomical studies using low-vacuum scanning electron microscopy and laser ablation tomography were conducted on *tadwf1-abd* and *tadwf4-abd* mutants at the seedling stage. Reduced cell elongation in the auricle region and increased number of adaxial and abaxial sclerenchyma cell layers in the lamina joint were observed in these mutants compared to Cadenza. Taken together, we established the role of BR pathway genes i.e., *BRI1*, *DWF1* and *DWF4* in altering above ground architecture in wheat. Leading to identification of some upright leaf angle mutants having no negative pleotropic effects on agronomically important traits which could potentially improve grain yields of wheat under dense planting density.

Acknowledgements

First and foremost, I am immensely grateful to my Rothamsted Research (RRES) supervisors, Steve, and Peter, for their unwavering support, invaluable guidance, constructive feedback, and for sharing their expertise throughout this research journey. I owe special thanks to my University of Nottingham supervisor, John for his continuous encouragement and cooperation throughout the degree. I am grateful to Andy for his great suggestions and advice.

I would like to extend my sincere thanks to Darren, Jon, and Steph at the University of Nottingham for letting me use their fantastic Laser Ablation Tomography (LAT) and their constructive discussions throughout my stay at the University. I am also grateful to Hannah and Kirstie in Bioimaging Facility at RRES for helping me use Scanning Electron Microscope (SEM) enabling me to acquire some pretty images around the lamina joint.

I am grateful to Nicolas and the high throughput phenotyping team here at RRES for sowing and generating useful physiological data throughout the life cycle of BR mutants growing under the Field Scanalyzer. I am thankful to John for keeping patience and for teaching me some basics for my stats analysis. Special thanks to Fiona, Jill, Andrea, Jack, and Tom for their great help and cooperation throughout my glasshouse trials at RRES. I express my gratitude to Helen, Chris, and the farm team for organizing every operation during my field trails at RRES (especially feeding the plots with some extra water during the dry summer months).

A big thank you to my wheat architecture lab members i.e., Pat, Stephen, Alison, and Matt for their continuous support and help during the degree. Thank you, Graham, in VCU unit for clicking great photographs of my mutants, bringing some life to my PPTs and thesis chapters.

Additionally, I would like to acknowledge my friends Mohsin, Anil, Satnam, Gurpreet, Navneet, Anam, Komal, Rimal, Sanjula, and Rahul for motivating, and providing occasional distractions, making this academic journey memorable, joyful and full of new experiences.

I am grateful to my entire family (Gill, Basra, Grewal, Matharoo, Patara, and Aujla) for always being there for me during the ups and downs of this journey. I am grateful to my wife Bhavjot, mom Parminder and dad Manav and grandparents for being there for me every day, providing great support, advice, and encouragement, believing in me when I didn’t, and having patience, enabling me to reach the end of a 4.5-year long marathon. Without you all I wouldn’t have reached this far.

Finally, I am extremely grateful to the University of Nottingham, Future Food Beacon, Rothamsted Research, and Designing Future Wheat for providing funding and scholarship throughout this project.

Table of Contents

List of Figures

List of Tables

Abbreviations

µg	Microgram
µl	Microlitre
µM	Micromolar
µm	Micrometre
3D	Three dimensional
ABA	Abscisic Acid
ANOVA	Analysis of variance
AS	ABNORMAL SHOOT
ATP	Adensine Triphosphate
$BC_{(1,2,3)}$	Back Cross
bHLH	Basic helix-loop-helix
BIN2	BR-INSENSITIVE 2
BKI	BRI Kinase Inhibitor
BL	Brassinolide
BR	Brassinosteroid
BRI1	Brassinosteroid Inhibitor 1
BSB	Blade-sheath boundary
BSK	BRASSINOSTEROID-SIGNALLING KINASE
BSU	BRI1-SUPPRESSOR1
BZR	BRASSINAZOLE RESISTANT
CAD	Cadenza
Cas	CRISPR-associated
CC	Canopy cover
CDG	CONSTITUTIVE DIFFERENTIAL GROWTH
CIMMYT	International Maize and Wheat Improvement Center
CK	Cytokinase
CN	Campestanol
CoA	Carboxylase
CPD	Carboxypeptidase D
CR	Campesterol
CRISPR	Clustered regularly interspaced short palindromic repeats
CS	Castasterone
CT	Cathasterone
CT	C-terminal tail
CYC	CYCLOIDEA
DIM	*DIMINUTO*
DNA	Deoxyribonucleic acid
DOXP	1-deoxy-D-xylulose 5-phosphate
DPA	Days post anthesis
DS	Dolichoesterone

DT	Dehydroteasterone
DWF	Dwarf
ED	extracellular domain
EMS	Ethyl methanesulfonate
$F_{(1,2,3)}$	Filial
FAD	flavin adenine dinucleotide
FLA	Flag leaf angle
G x E	Genotype X Environment
GA	Gibberellin
GH	Greenhouse
GS	Growth stage
His	Histidine
HMG-CoA	3-hydroxy-3-methyloglutaryl-CoA
HTTP	High throughput phenotyping platform
I2	Internode 2
I3	Internode 3
I4	Internode 4
I5	Internode 5
IFR	Isofucosterol
INDEL	Insertions/deletions
IPP	Isopentenyl pyrophosphate
IWGSC	International wheat genome sequencing consortium
JA	Jasmonic Acid
JM	Juxtamembrane segment
KASP	Kompetitive Allele Specific PCR
KD	Kinase domain
LA	Leaf angle
LAI	Leaf area index
LAT	Laser ablation tomography
LIC	Tiller angle increased controller
LJ	Lamina Joint
LRR-RLK	leucine-rich repeat receptor-like kinase
LSD	Least Significant Difference
MEcPP	Plastidial metabolite, methylerythritol cyclodiphosphate
MEP	Methylenelophenol
Mm	Millimetre
mM	Millimolar
MVA	Mevalonate
NDVI	Normalized difference vegetation index
NGS	Next generation sequencing
NS	Null segregant
PCR	Polymerase Chain Reaction
PIF	Phytochrome interacting factors
PLB	Preligule band

PP2A	PROTEIN PHOSPHATASE 2A
QTL	Quantitative Loci/Locus
RGB	Red, green and blue
RHT	Reduced height
RNA	Ribonucleic acid
RNA-seq	RNA sequencing
ROS	Reactive oxygen species
ROT	ROTUNDIFOLIA
RPM	Revolutions per minute
RUE	Radiation use efficiency
SD	Standard Deviation
SED	Standard error of a difference between two means
SEM	Scanning Electron Microscope
Ser/Thr	Serine/ Threonine
SL	Strigolactones
SMO	Sterol methyl oxidase
SMT	Sterol methyltransferase
SNP	Single Nucleotide Polymorphism
STR	Sitosterol
TE	Teasterone
TF	Transcription factor
TGW	Thousand grain weight
TILLING	Targeting induced local lesions in genomes
TY	Typhasterol
UHPLC	Ultra-High-Performance liquid chromatography

Chapter 1: Introduction

1.1 Wheat crop

Wheat (*Triticum aestivum* L) is one of the three most important cereal crops grown in the world accompanying maize and rice. In 2021, approximately 770 million tonnes of wheat were produced globally (http://faostat.fao.org/). Wheat is grown on approximately 220 million hectares of land (FAOSTAT, 2021) from 67º N in Scandinavia and Russia to 45º S in Argentina, including elevated regions in the tropics and sub-tropics (Feldman et al 1995). Currently, 95% of the wheat grown worldwide is hexaploid bread wheat and the remaining 5% is tetraploid durum wheat. Harvested wheat grain provides approximately 20% of carbohydrate and 20% of total protein, dietary fibre, and mineral requirements for the global human population.

Modern wheat varieties are very different from those that were grown 10,000 years ago when it was first cultivated by humans. The earliest forms of wheat originating in south-eastern part of Turkey, were diploid (AA) and tetraploid (AABB) wheats (Dubcovsky and Dvorak, 2007). These spread to Near East where the first forms of hexaploid wheat originated about 9000 years ago (Feldman, 2001). A genome of wheat came from wild and cultivated einkorn, while the B genome was probably derived from S genome of *Aegilops speltoides*. The S genome was closely related to G genome in *T. timopheevi* (having A and G genomes). The D genome was derived from T. tauschii (Feldman, 2001). Wheat was then spread to Europe (via Anatolia to Greece) during 8000BP, then to Italy, France, and Spain during 7000BP. Reaching UK and Scandinavia by 5000BP then to Iran, Central Asia and China, Africa, and Egypt during 3000BP. Finally reached Mexico and Australia during 1529 and 1788 respectively. (Shewry, 2009). In subsequent years, domesticated wheat was improved by farmers following non-formal plant breeding principles to develop superior yielding cultivars compared to their grassy wild relatives. A few specific traits were modified in the progenitors making them fit for large scale cultivation. The loss of shattering of the spike at maturity was achieved by manipulating the *Brittle rachis* locus (Nalam et al., 2006). Shattering was an important trait for wild relatives enabling successful seed dispersal, but it was detrimental for modern varieties as it led to significant yield losses. Hulled grains (adhering tightly to grains) were bred for

allowing easy threshing of grains from the spike. This was achieved by modifying the *Q* locus to supress the effects of the *Tenacious Glume* locus (Dubcovsky and Dvorak, 2007; Simons et al., 2006).

But at this stage, wheats were tall (lodging susceptible) and low yielding due to less responsiveness to external fertiliser application. Therefore, interventions were needed at this stage to produce more wheat to alleviate food insecurity and poverty (Nelson et al., 2019).

1.2 Manipulation of wheat architecture fuelled the Green Revolution

Wheat varieties grown before the Green Revolution era tended to be tall and were prone to lodging caused by wind and rain. The use of higher fertiliser applications was avoided by the farmers to prevent these wheat varieties from lodging. Short stemmed wheats were identified in Japan by Dr SC Salmon (an American scientist) where he was assigned as agricultural advisor after World War II by the US army. In 1945 he brought 16 dwarf lines from Japan to USA, including Norin 10. Dr Orville Vogel a USDA scientist at Washington State University was the first to note the high yielding potential of Norin 10. By 1949 he had crossed it with various local varieties. During this period Dr Norman Borlaug was working at CIMMYT in Mexico and he had achieved significant success in developing rust resistant varieties in wheat. By 1953, Borlaug obtained segregating lines from a cross of Norin 10 x Brevor from Dr Vogel (Law et al 1978). By late 1950s Borlaug and colleagues identified high yielding semi dwarf wheat varieties which were seen for the first time in 1961 growing in fields at Sonora valley. By 1962, two high- yielding semi dwarf wheat varieties, Pitic 62 and Penjamo 62 were made commercially available across the world (Borlaug, 1983) and became the basis of international breeding programs. This led to a huge increase in the wheat yields under higher fertiliser doses and arguably saved the world from hunger. Today, approximately 70% of the modern wheat varieties contain at least one of the two Green Revolution semi-dwarfing alleles, designated *Rht-B1b* and *Rht-D1b* which were both derived from Norin 10 (Hedden, 2003). These dwarfing genes caused accumulation of less resources in the straw and more partitioning to the developing grains, ultimately causing an increase in harvest index by 60% (Khush GS, 2001). Importantly, these short stemmed varieties were lodging resistant, allowing higher fertiliser doses to be applied thus increasing grain yields further. The introduction of these alleles was a major factor in increasing grain

yields during the Green Revolution. Between 1960 and 2000, wheat grain yields for all the major developing countries rose by 208% (FAO, 2004). If there was no widespread adoption of Green Revolution technologies, it has been estimated that the world food and feed prices would have been higher by as much as 36- 65% and average caloric availability would have declined by 11-13% (Evenson R, Rosegrant M; 2003).

1.3 Wheat yields need to double to feed the global population by 2050

Despite the successes of the Green Revolution, in recent years there has been stagnation in improving global wheat grain yields. Currently the global average rate of increase in wheat yield is 0.9%, but a non-compounding ~2.4% rate of increase in grain yield is needed to feed the hungry planet by 2050 (Ray et al., 2013). It is reported that world has already lost one third of the arable land in last 40 years due to soil erosion and pollution. Furthermore, the impact of climate change including an increase in global temperatures, drought and increased severity of extreme weather events threatens global food security (Asseng et al., 2015; Trnka et al., 2015; Zampieri et al., 2017). Recent global instability are also having an impact, with the war in Ukraine highlighting the issues of fragility in global wheat exports. Taken together, it is apparent that increasing wheat grain yields and providing resilience to environmental pressures is a high priority for wheat breeders.

'Breeding of crop ideotypes' is a concept first proposed by Donald in 1968. It is postulated that using their knowledge of physiology scientists could alter plant architecture for improving plant traits based on the target environment. This approach was greatly successful for breeding high yielding wheat and rice cultivars. It was proposed that cultivars having reduced final plant height, erect leaves, lower tiller number, increased number of grains/ panicle or spike, and increased stem stiffness could contribute towards increasing grain yields in rice and wheat (Khush, 1993; Rajaram and van Ginkel, 1996). In relation to altering cereal leaf angle to be more upright, it has been demonstrated to allows a greater number of plants be accommodated in an area and increase radiation use efficiency (RUE) thus improving grain yields. This strategy has been widely adopted in maize hybrids with planting density increasing from 30,000 plants/ ha in 1930s to 75,000 plants/ ha in 2000s in the US (Duvick, 2005). Plant hormones have been demonstrated to have an important role in controlling leaf canopy architecture, with brassinosteroids (BRs) have been

identified as key regulators of leaf angle in cereal crops (as discussed in section 1.9.5.2).

1.4 How tailoring BRs can contribute towards crop improvement

Brassinosteroids are phytohormones that control a multitude of developmental processes including organ expansion, senescence, reproductive development, and tolerance to biotic and abiotic stresses at whole plant level (Clouse, 2011; Divi and Krishna, 2009; Vriet et al 2012; Nolan et al., 2020).

Our understanding of the role of BRs has largely been elucidated through the identification and characterisation of BR-deficient and BR-insensitive mutants. In rice, the BR-deficient mutant, *brd1* displayed abnormal cell organisation and reduced stem elongation (Hong et al., 2002). in barley, the *uzu.1a* allele has been demonstrated to cause BR-insensitive growth defects including reduced stem elongation and an erect leaf phenotype (Chono et al., 2003). These characteristics have allowed the *uzu.1a* allele to be widely utilised in barley breeding programs, ultimately provide lodging resistance and allowing dense planting under field conditions in these varieties. During the 1930s barley *uzu* varieties were cultivated in almost 70% of acreage in Japan and more than 30% acreage in the Korean peninsula. During the 2000s almost all hull-less barley cultivars in southern Japan had *uzu* allele and they have been further utilised in East Asia, Korea, and China (Saisho et al., 2004).

Leaf angle is another important trait that is controlled by BRs. This trait is conferred by regulation of lamina joint inclination at the cellular level (discussed in further detail in section 1.9.5.1). As indicated above, this trait has been exploited in barley using the BR-insensitive *uzu.1a* alleles (Chono et al., 2003). BR-deficient mutants also display an upright leaf architecture. Notably, the rice *osdwf4-1* mutant displaying upright leaf angles but lacked other negative pleiotropic effects often associated with severe BR-deficient mutants (Sakamoto et al., 2006). Field trials conducted using the *osdwf4-1* mutant demonstrated an increase in grain yields of 32% under a higher planting density regime (Sakamoto et al., 2006).

BRs also play an important role in reproductive development. For instance, severe mutants in Arabidopsis and rice have reduced male fertility thus affecting seed yield

(Kim et al., 2005; Hong et al., 2005). The effects of reduced BR signalling on male fertility include defects in tapetum and microspore development (Yu et al., 2010).

BRs have also been reported to regulate the response of plants to abiotic stresses such as drought, heat and cold (Nolan et al., 2017). For instance, BR deficient or insensitive mutants displayed increased drought tolerance, mediated through an interaction with the ABA phytohormone pathway (Feng et al., 2015; Northey et al., 2016; Nolan et al., 2017; Zhang et al., 2009).

Based on our understanding of the role of BRs in controlling key cereal traits outlined above, manipulation of this pathway provides promise for grain yield improvement in wheat under changing climatic conditions.

1.5 Brassinosteroids (BRs)

1.5.1 History

BRs are a class of steroidal phytohormones which play an essential role in plant growth and development. Originally named Brassins, they were first identified in pollen extract of *Brassica napus* and shown to promote internode elongation in bean (Mitchell et al., 1970). After a decade of research, 4mg of Brassin was purified from 227 kg of bee collected *B. napus* pollen. The chemical structure was determined by X- ray crystallography and shown to be (22*R*,23*R*,24*S*)-2α,3α,22,23-tetrahydroxy-24-methyl-B-homo-7-oxa-5α-c-holestan-6-one, which was ultimately named brassinolide (Grove et al., 1979; Figure 1). The stereo isomer, 24-epiBL was chemically synthesised two years later, enabling extensive research to understand the physiological roles of BRs in plant development (Cutler, 1991). Currently, nearly 70 BRs have been identified in plants. Based on bioassays, brassinolide (BL) and/or castasterone (CS) are the most abundant BRs found in plants having biological activity (Yokota et al., 1982). The other identified BRs are intermediates of BR biosynthesis pathway or inactivated products of BR catabolism.

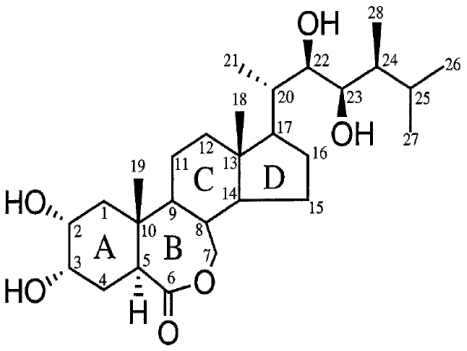

Figure 1. 1 Chemical structure of brassinolide (BL) {(22*R*,23*R*,24*S*)-2α,3α,22,23-tetrahydroxy-24-methyl-B-homo-7-oxa-5α-cholestan-6-one}. Adapted from Fujioka and Yokota, 2003.

1.5.2 Chemical structure of brassinosteroids

Based on the number of carbon molecules, BRs are sub-divided into three groups that are C27, C28 and C29 molecules having 5a-cholestane skeleton 5a-ergostane, and 5a-stigmastane respectively (Bajguz et al., 2020). Brassinolide (BL) one of the major bioactive BR is polyhydroxylated derivative of 5α -cholestan, namely (22R,23R,24S)-2α,3α,22,23-tetrahydroxy-24-methyl-B-homo-7-oxa-5α-cholestan-6-one (Figure 1.1). Other BRs differ from BL through. variation at C-2 and C-3 position in the A-ring; presence of ketone, lactone or de-oxo function at C-6 position in the B-ring; stereochemistry of hydroxyl group on side chain; presence or absence of methylene or ethylene group at the C-24 position. In general, these modifications arise through oxidation and reduction reactions. BRs have also been demonstrated to be conjugated with glucose and fatty acid moieties (Wendeborn et al., 2017).

1.6 BR biosynthesis pathway

Production of C27, C28 and C29 BRs is a result of three pathways that are interconnected. The earliest steps in the biosynthesis of BR precursors are the MVA or non-MVA pathways which produce cycloartenol and cycloartanol. Cycloartanol is utilised for production of Cholesterol via the sterol biosynthesis pathway, leading to production C27 BR via BR-specific biosynthesis pathway. On another hand, Cycloartenol is utilised in sterol pathway for production of Campesterol (CR) which is the precursor to bioactive BRs (C28) such as CS and BL. Another pathway involves the production of Sitosterol via the sterol pathway, which is the precursor to

C29 BRs. Currently, most of our knowledge is around the components that participate in the C28 biosynthesis pathway, and this has been elucidated from the study of model plants, mainly those involving Arabidopsis (Fujioka et al., 2002; Chung and Choe, 2013; Kim et al., 2018; Rozhon et al., 2019; Bajguz et al., 2020). The pathways are discussed in greater details in the following sections.

1.6.1 The mevalonate pathway provides substrates for sterol biosynthesis

BRs are synthesised in plants from precursors generated by the early mevalonate (MVA) or non-MVA pathway which sequentially leads to the cycloartenol-dependent sterol pathway. The non-MVA pathway most commonly operates in lower plants whereas the MVA pathway predominates in higher plants. The non-MVA pathway starts from D-glyceraldehyde 3-phosphate and pyruvate and results in the production of isopentenyl pyrophosphate (IPP) via series of steps that produce the intermediates DOXP, MEP, CDP-ME, CDP-MEP, MEcPP and HMB-PP (Lichtenthaler, 2000). The reactions are catalysed by a range of synthase, kinase and reductase enzymes. The MVA pathway starts with acetyl-CoA which is converted to 3-hydroxy-3-methyloglutaryl-CoA by HMG-CoA synthase. HMG-CoA reductase then converts this compound to MVA. IPP is then synthesized from MVA through the two phosphorylated intermediates MVA-phosphate and MVA-pyrophosphate (Miziorko, 2011). These reactions are catalysed by MVA kinase, phospho-MVA kinase and MVA-PP decarboxylase, respectively (Wang et al., 2017).

IPP is the key building block that is converted to squalene by squalene synthase. Cycloartenol and cycloartanol are then produced via synthase and reductase enzymes, respectively and are key precursors required to drive the sterol biosynthetic pathway (Wang et al., 2017). The pathway is described indicated in Figure 1.2.

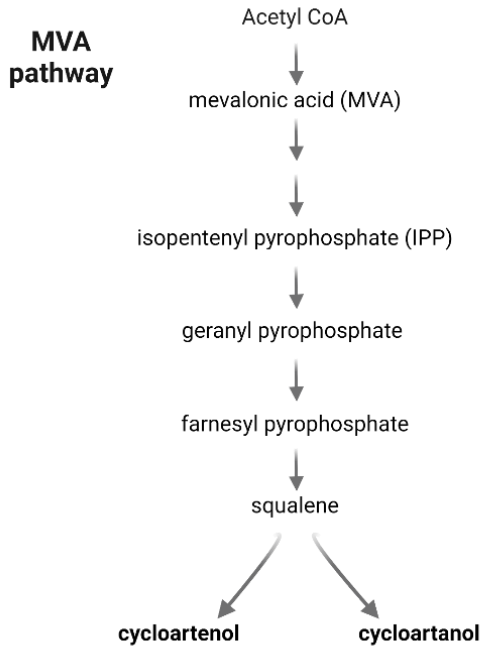

Figure 1. 2 The MVA pathway. Acetyl CoA is converted to IPP via MVA. IPP is the precursor for squalene biosynthesis and is converted via geranyl pyrophosphate and farnesyl pyrophosphate. At this step the pathway bifurcates into two steps leading to production of cycloartenol and cycloartanol which are key precursors for sterol biosynthesis.

1.6.2 Sterol pathway leads to BR-biosynthesis pathway

The precursors of C27-type BRs are generated through series of reactions in which cycloartanol is converted to cholesterol, (Figure 1.3; Wang et al., 2017). In contrast, cycloartanol is the precursor of C29- and C28-type BRs. Cycloartanol is initially converted to 24-methylenecycloartanol and then through a series of reactions resulting in the sterol intermediates 4a-methylergostatrienol, 4a-methylergostadienol and 24-methylenelophenol (Wang et al., 2017). 24-methylenelophenol is utilised by two independent sterol pathway routes leading to production of β-sitosterol and campesterol which are precursors of C29- and C28-type BRs respectively (Sonawane et al., 2016). The key genes and enzymes involved in the sterol pathway are indicated in figure 1.3 and described below.

***Sterol methyltransferase1* (*SMT1*)** gene encodes an early enzyme in the sterol pathway which converts cycloartenol to 24-methylenecycloartenol by addition of a single methyl group at the C-24 position. Arabidopsis contains three genes, *SMT1*, *SMT2* and *SMT3* which are homologous to ERG6 gene in yeast (Carland et al., 2010).

Mutations in the *SMT1* gene caused poor development, loss of fertility and improper embryo morphogenesis in Arabidopsis, demonstrating the importance of BRs in growth and development in Arabidopsis. Additionally, these mutants had higher cholesterol accumulation and reduced content of C-24 alkylated sterols (Diener et al., 2000).

***Sterol 4α-methyl oxidase1* and *2* (*SMO1* and *SMO2*)** genes encode for key enzymes involved in removal of first and second methyl groups at C-4 position, respectively. There are three *SMO1* genes and two *SMO2* genes in Arabidopsis. The three single *smo1* and *smo1-1smo1-3* double mutants didn't display any phenotypic abnormalities, however, the *smo1-1smo1-2* double mutant displayed embryo lethality. This phenotype was associated with dysregulated auxin and cytokinin biosynthesis, transport, and utilisation. The *smo1-1smo1-2* mutant was also shown to accumulate elevated levels of 4,4-dimethylsterols. (Song et al., 2019).

FACKEL encodes a C-14 reductase which is responsible for reduction of 4α-methylergostatrienol to 4α-methylergostadienol. Mutations in this gene in Arabidopsis results in pleotropic effects such as defects in embryo development, multiple shoot meristems and stunted roots. (Schrick et al., 2000; Jang et al., 2000).

HYDRA encodes a sterol 8,7 isomerase which converts 4α-methylergostadienol to 24-methylenelophenol. The Arabidopsis *hydra* mutant displays defective vascular patterning in the shoot which is associated with ectopic cell divisions. The expression of *AtHB8* homeobox gene is disrupted and mislocalization of PIN proteins occurs in the mutant embryos and seedlings. Interestingly, the mutant phenotype can be partially rescued by inhibiting auxin and ethylene signalling but not by exogenous sterol or BR application (Pullen et al., 2017; Souter et al., 2002).

DWF7/STE1 encodes a C-5(6) desaturase enzyme which converts Episterol to 5-Dehydroepisterol and Avenasterol to 5-Dehydroavenasterol in the sterol pathway. The phenotype of *dwf7* is characteristic of other BR mutants, displaying dark-green leaves, reduced height, pedicels, siliques size, fertility, and a slower rate of development. Additionally, the levels of 24-MC, CR and CN were significantly reduced in the mutant compared to wild-type, demonstrating the blockage in the mutant is prior to 24-MC production (Choe et al., 1999).

DWF5 encodes a 7-dehydrocholesterol reductase enzyme which catalyses the conversion of 5-Dehydroepisterol and 5-Dehydroavenasterol to 24-Methylenecholesterol (24-MC) and Isofucosterol (IFR), respectively. The phenotype of *dwf5* mutants includes short internodes, reduced stature, rounded leaves, and increased number of inflorescences in Arabidopsis. Interestingly fertility was not compromised in these mutants, but the germination rate is reduced which could be enhanced by external BL or nutrient supplementation. Thus, demonstrating essential role of BRs in controlling various developmental processes in Arabidopsis (Choe et al., 2000).

DWF1/DIM/CBB1 gene encodes a sterol side chain reductase1 which is involved in the conversion of 24-MC and IFR to Campesterol (CR) and Sitosterol (STR), respectively. Phenotypically, the mutants in Arabidopsis displayed short stature, rounded leaves, a tightly packed rosette and fertility was compromised (Choe et al., 1999). In rice, the mutants had reduced stature with dark-green, erect leaves coupled with reduced fertility and root elongation. Interestingly, the severity of the mutants varied considerably in rice and Arabidopsis. The Arabidopsis *dwf1* mutant had severe phenotypic abnormalities (Takahashi et al., 1995), but in rice the *DWF1 (brd2)* mutant showed a moderate phenotype (Hong et al., 2005). Estimation of BR levels confirmed presence of CS (Castasterone) in the *brd2* mutant, suggesting the presence of an alternative BR biosynthesis pathway in rice. After detailed hormone estimations, it was established activation of 24-methylene-type pathway might be causing accumulation of Dolichosterone (DS) in the *brd2* mutant compared to wild-type. Feeding experiments confirmed that DS had biological activity and might explain why the *brd2* mutant does not exhibit a severe BR-deficient phenotype (Hong et al., 2005).

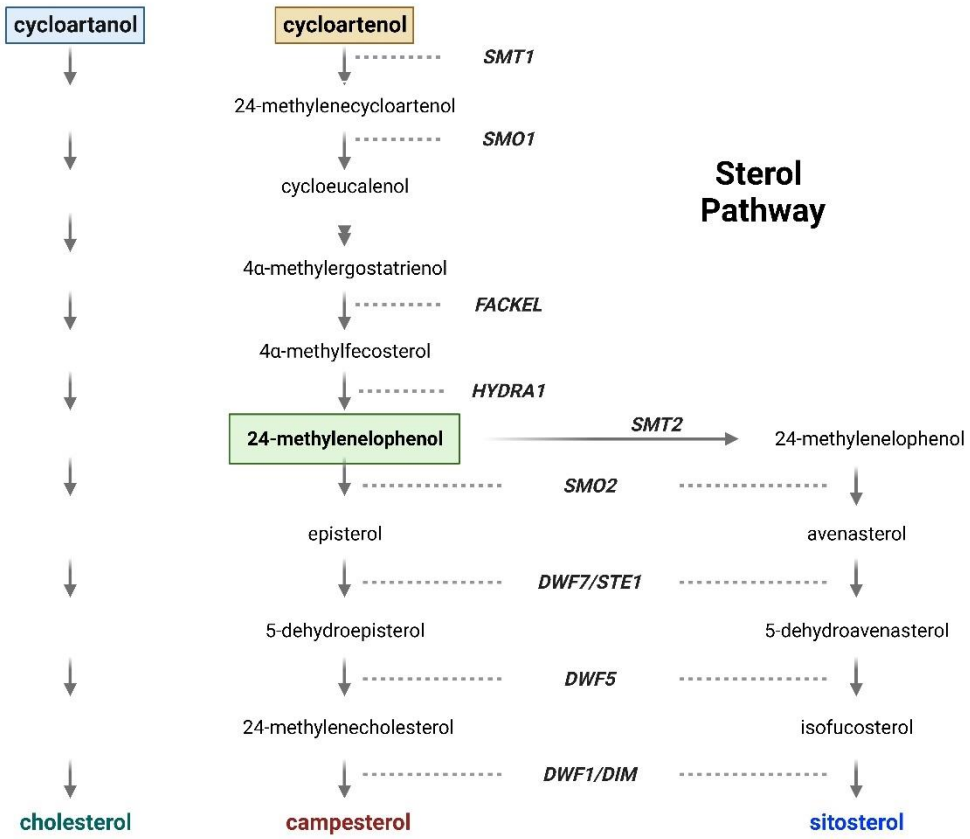

Figure 1. 3 The sterol biosynthesis pathway. Cycloartanol produced by MVA pathway leads to production to cholesterol which is the precursor of C27 BRs. In parallel, cycloartenol leads to production of 24-methylenelophenol. At this step the pathway bifurcates into two routes leading to production of campesterol (CR) and b-sitosterol which are the precursors of C28 BRs and C29 BRs respectively. The key genes/ enzymes catalysing various steps are described in bold and italics on the arrow heads. The pathway was produced using BioRender.com**.**

1.6.3 BR-specific biosynthetic pathway

Campesterol (CR) produced via the sterol pathway is converted to campestanol (CN) and then finally to CS and BL following two parallel routes known as the late and early C-6 oxidation pathways. Studies in in a range of different plant species led to our current understanding about the steps involved in the production of bioactive BRs (Bajguz et al., 2020). Conversion of 6-oxoCN to CT was demonstrated in C. roseus cells (Fujioka et al., 2000). The conversion of CN to 6-deoxoCT to 6-deoxoTE (steps in late C-6 oxidation pathway) were uncovered in Arabidopsis thaliana (Choi et al, 1997; Noguchi et al., 2000). Whereas conversion of TE to CS and 6-deoxoCS to CS was discovered using seedlings of rice and tobacco (Choi et al., 1996; Suzuki et al.,

1995). Additionally, conversion of TE to TY via 3-dehydroTE was uncovered in cultured and cell-free systems in Marchantia polymorpha and lily cells (Nomura et al., 1999).

The early C-6 oxidation pathway leads to the conversion of CN to 6-oxoCN, which is modified through a series of reactions to produce BL. In contrast, the late C-6 oxidation pathway results in the conversion of CN to 6-deoxoCT and then to other parallel C-6 deoxy forms. This route is also known as CN-dependent pathway, in which late C-22 oxidation reactions are catalysed. Another route in the pathway runs via early C-22 oxidation steps to produce CS and BL via the CN-independent branch (Fujioka et al., 2002; Ohnishi et al., 2012). Furthermore, a C-23 hydroxylation pathway also exists and leads to conversion of 22-OH-3-one and 3-epi-6-deoxoCT to 6-deoxo3DT and 6-deoxoTY, respectively (Ohnishi et al., 2006).

The pathways leading to the production of bioactive BRs varies amongst higher plant species. For instance, in Arabidopsis, rice, pea and zinnia the steps in early and late C-6 oxidation pathway are interlinked via the reactions catalysed by BR6ox (Hong et al., 2002; Yamamuro et al., 2000; Nomura et al., 1999; Nomura et al., 1997; Yamamoto et al., 2001). In contrast, steps in late C-6 oxidation pathway are followed for production of bioactive BRs in tomato and tobacco (Bishop et al., 1999; Koka et al., 2000; Yokota et al., 2001).

Most of the enzymes involved in the BR-biosynthesis pathway belong to the cytochrome P450 (CYP450) monooxygenase superfamily, except for DET2 (Li et al., 1996; Ohnishi et al., 2012). The CYP450 enzymes are integral membrane proteins that are in the endoplasmic reticulum (ER), which therefore appears to be the site of BR production. The BR-specific biosynthesis pathway, including the genes and encoded enzymes involved are described below and shown in Figure 1.4.

Deetiolated2 (DET2) encodes for a steroid 5α-reductase which catalyses the conversion of (24R)-ergost-4-en-3-one to (24R)-5α-ergostan-3-one and (22S,24R)-22-hydroxyergost-4-en-3-one to (22S,24R)- 22-hydroxy-5α-ergostan-3-in the early, and late C-22 oxidation, respectively. Additionally, DET2 is also involved in conversion of (22S)-22-hydroxycholest-4-en-3-one to (22S)-22-hydroxy-5α-cholestan-3-one in C27-type BR biosynthesis (Fujioka et al., 1997). BR analysis revealed three-fold accumulation of (24R)-24-methylcholest-4-en-3-one whereas

downstream BR levels were substantially reduced in the mutant compared to wild-type (Fujioka et al., 1997). Phenotypically, Arabidopsis *det2* dark grown mutants had many characteristics of light-grown plants such as hypocotyl growth inhibition, expansion of cotyledons, primary leaf initiation, accumulation of anthocyanin (Chory et al., 1991). The BR-deficient phenotype of *det2* mutants was recovered by external BR application. (Fujioka et al., 1997; Noguchi et al., 1999).

DWF4 **(CYP90B1) and** ***DWF11*** **(CYP72B1)** genes encode 22a-hydroxylase enzymes which catalyse multiple parallel steps including the conversion of CR to 22-OHCR, 4-en-3-one to 22-OH-4-en-3-one, 3-one to 22-OH-3-one, campestanol (CN) to 6-deoxoCT and 6-oxoCN to cathasterone (CT) (Fujita et al., 2006; Zhao and Li, 2012; Sakamoto et al., 2006). The *osdwf4* mutant seedlings were rescued by application of CT and 6-deoxoCT but did not respond to 6-oxoCN, demonstrating that 22α-hydroxylation is blocked and causative of the BR-deficient phenotype that is observed in the mutant (Choe et al., 1998). Additionally, DWF4 has been shown to catalyse a rate-limiting steps in the BR pathway (Sakamoto et al., 2006). *DWF4* and *DWF11* appear to have some overlapping roles in controlling BR-responsive growth in rice. The *osdwf4-1* mutant exhibits an erect leaf architecture, but with only a slight reduction in plant height. In contrast, the *osdwf11* exhibited a more substantial reduction in stem elongation, erect statured, reduced seed size and a compacted panicle phenotype in rice (Sakamoto et al., 2006; Guo et al 2014). These finding suggest that *DWF11* has a more important role than *DWF4* in controlling some aspects of BR-responsive growth, including stem elongation. Interestingly, overexpression of *DWF4* has been shown to increase biomass and seed yields in a range of plant species (Choe et al., 2001; Li et al., 2018; Sahni et al., 2016; Milner et al., 2022; Liu et al., 2020).

Constitutive photomorphogenesis and dwarfism (CPD) encodes an enzyme that catalyses the C-3 oxidation step in the BR-biosynthesis pathway. The *cpd* mutants have been demonstrated to accumulate 22-OHCR and not CR (Ohnishi et al., 2012). The Arabidopsis *cpd* mutant of displayed a de-etiolated phenotype and derepression of light induced genes in dark and dwarfism, reduced male fertility in the light (Kauschmann et al., 1996; Szekeres et al., 1996). The phenotype of the mutant was restored to wild type after application of C23-hydroxylated brassinolide precursors (Szekeres et al., 1996). There are two homologues of this gene in rice i.e., *OsCPD1/*

CYP90A3 and *OsCPD2/ CYP90A4.* The single knockout mutants of these genes show no visible phenotypic abnormalities, whereas double knock-out mutant displayed multiple BR-related growth defects including dwarfism, shorter tortuous erect leaves and smaller grains (Zhan et al., 2022).

***ROT3* (CYP90C1) and CYP90D1** encode enzymes involved in multiple parallel C-23 hydroxylation reactions, including the conversion of cathasterone (CT), 6-deoxoCT, 22-OHCR and 22-OH-4-en-3-one to teasterone (TE), 6-deoxoTE, 22,23-diOHCR and 22,23-diOH-4-en-3-one in the BR-pathway (Ohnishi et al., 2006). CYP90C1 and CYP90D1 are closely related genes which are essential for regulating leaf length in Arabidopsis. It was observed that the double knockout mutant of *ROT3* and CYP90D1 were severely dwarfed with small leaves in Arabidopsis (Kim et al., 2005).

***DWF2* (CYP90D2)** encodes an enzyme that catalyses the C-23 hydroxylation step in the pathway, including the conversion of teasterone (TE) and 6-deoxoTE to 3-dehydroteasterone (3DT) and 6-deoxo3DT (Sakamoto et al., 2012). The rice *dwf2* mutant displayed slightly rolled and dark green leaves, reduced stem elongation and sterility (Jiang et al., 2013) The phenotype of this mutant could be recovered by application of exogenous BL (Hong et al., 2003).

***BR-6-ox1, 2* (CYP85A1, A2)** encode C-6 oxidases, involved in the conversion of 6-deoxoTE to TE, 6-deoxo3DT to 3DT, 6-deoxoTY to TY and 6-deoxoCS to CS (Zhao and Li, 2012). Interestingly, CYP85A2 is only involved in the Baeyer-Villiger oxidation step that leads to the conversion of castasterone (CS) to brassinolide (BL) in Arabidopsis (Kim et al., 2005). The double knockout mutant displayed dwarfism similar to other BR-biosynthetic mutants of Arabidopsis (Kwon et al., 2005). Interestingly, the CYP85A1/ CYP85A2 mutants displayed elevated drought tolerance in maize and Arabidopsis that was mediated through an interaction with the ABA pathway (Castorina et al., 2018; Northey et al., 2016).

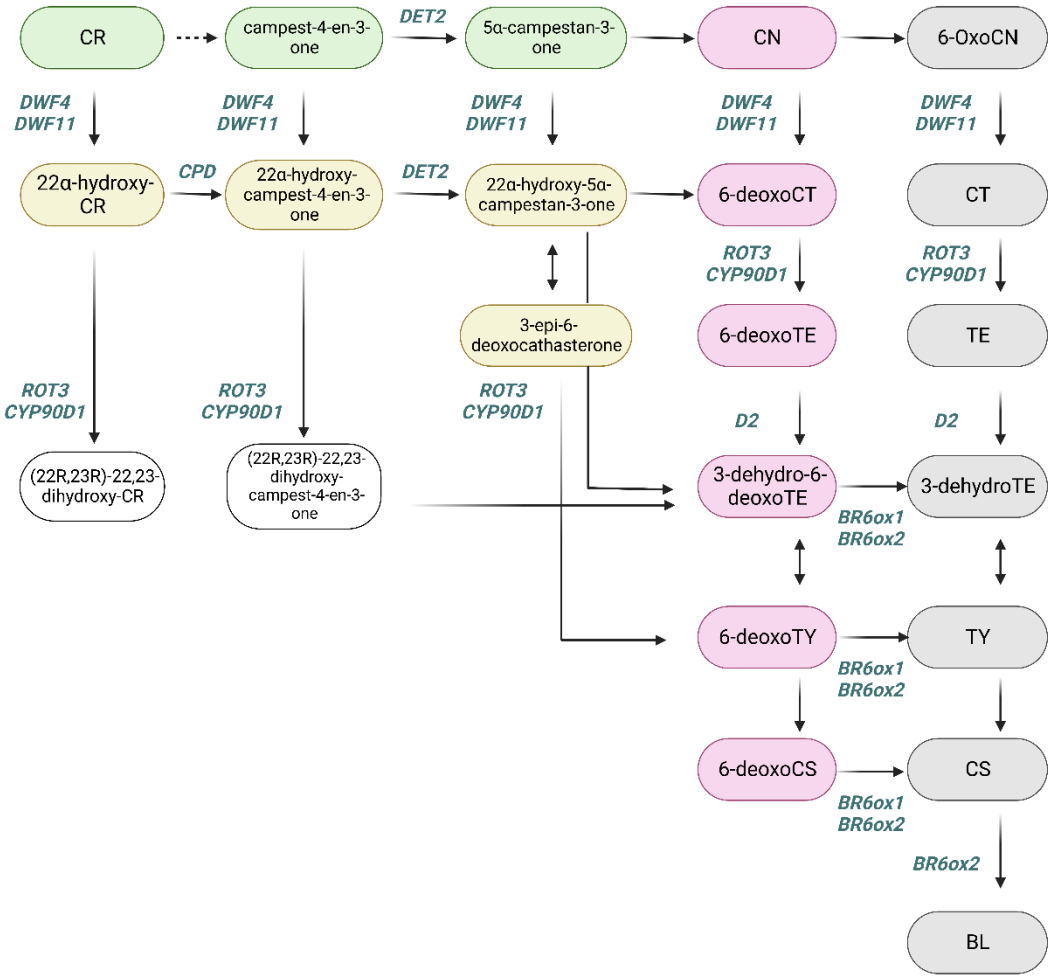

Figure 1. 4 Steps involved in C28 BR-specific biosynthesis pathway. Campesterol (CR) produced by sterol pathway is the first substrate needed for the BR-specific biosynthesis pathway. The pathway has four main routes i.e., late C-22 oxidation, early C-22 oxidation, late C-6 oxidation, and early C-6 oxidation steps are highlighted in green, yellow, pink, and grey respectively. Castasterone (CR) and Brassinolide (BL) are the bioactive BRs produced because of the pathway which are utilised by the BR-receptor to initiate BR signalling pathway. The key genes/ enzymes catalysing various steps are described in bold and italics on the arrow heads. The pathway was produced using BioRender.com**.**

1.6.4 Transport of BRs

In view of the plasma membrane localisation of the BR receptor, it is likely that transport of bioactive BRs from the ER to the extracellular matrix/ cell surface is required to initiate BR-signalling. It is known that BRs do not undergo long-distance transport, following a paracrine mode of signalling (Symons et al., 2008). It is currently not known how BRs reach the extracellular matrix from the site of

production. It is conceivable that this could occur by binding to transporters to be then released in the apoplast. Alternatively, vesicular transport via the Golgi apparatus could occur or potentially via simple diffusion across the plasma membrane (Vukašinovic and Russinova, 2018).

1.7 BR signalling pathway

1.7.1 Perception of BRs by BRASSINOSTEROID INSENSITIVE 1 (BRI1)

The Arabidopsis *bri1* mutants were identified based on their insensitivity to exogenously applied BRs in hypocotyl elongation and primary root inhibition assays (Clouse et al., 1996). In contrast, they retained sensitivity to other phytohormones such as auxin, cytokinin, GA, ethylene and ABA. Phenotypically, the mutant displayed severe dwarf stature, thickened and dark green leaves, male sterility and they were deetiolated when grown in the dark.

The *BRI1* gene was demonstrated to encode a leucine-rich repeat receptor-like kinase (LRR-RLK) containing an extracellular domain or ED containing N-terminal signal peptide, leucine-zipper motif, leucine rich repeats, island domain. A transmembrane domain and a cytoplasmic serine/threonine kinase domain containing juxtamembrane, kinase domain and C-terminal tail (Li and Chory, 1997; Oh et al., 2000). The ED forms a helical solenoid structure with LRRs and ID, and BL binds to the hydrophobic surface groove of the protein (Hothorn et al., 2011; She et al., 2011). Specific mutations in the ED domain of block the interaction between BL and *BRI1* leading to reduced BR signalling and BR-insensitive growth defects (Hothorn et al., 2011).

Mutants have been identified in the *BRI1* genes in Arabidopsis, rice and barley displaying a range of phenotypes (Sun et al., 2017; Dockter et al., 2014; Yamamuro et al., 2000; Chono et al., 2003; Morinaka et al., 2006). For instance, in rice, *d61-3* and *d61-4* displayed severe phenotypic abnormalities whereas *d61-1*, *d61-2* and *d61-7* produced less severe, potentially agronomically beneficial, phenotypes including erect leaves and semi-dwarf stature (Morinaka et al., 2006). Furthermore, the barley *uzu1.a* allele contains a lesion in *HvBRI1* gene and has been used extensively to produce semidwarf and upright statured barley in East Asia, Japan, Korean peninsula and China over many decades (Siasho et al., 2004).

1.7.2 BR signalling mediated by BRI1

In the absence of BRs, BRI1 is inhibited by the association of BRI1 KINASE INHIBITOR1 (BKI1) to the C-terminal kinase domain of BRI1. BRI1 activation by BRs results in its binding to the kinase-domain of BRI1-ASSOCIATED RECEPTOR KINASE1 (BAK1) and dissociation with BKI1 (Guo et al., 2012; Nam and Li, 2002; Jaillais et al., 2011; Wang and Chory, 2006). BAK1 is a small transmembrane LRR-RLK protein containing five LRRs and a cytoplasmic kinase domain (Nam and Li, 2002). Phosphorylation assays demonstrated that BRI1 and BAK1 can both autophosphorylate and transphosphorylate each other resulting in activation or deactivation of BRI1, respectively (Wang et al., 2005). There are approximately 12 *in vitro* autophosphorylation sites that exist within the juxtamembrane, kinase and C-terminal domain of the BRI1 protein (Oh et al., 2000).

Following activation, BRI1 phosphorylates two additional plasma membrane localised cytoplasmic kinases BRASSINOSTEROID-SIGNALLING KINASE1 (BSK1) and CONSTITUTIVE DIFFERENTIAL GROWTH1 (CDG1) (Kim et., 2011 and Tang et al., 2008). These cytoplasmic kinases then phosphorylate BRI1-SUPPRESSOR1 (BSU1) which inactivates a negative regulator of BR signalling, GSK3-like kinase BRASSINOSTEROID INSENSITIVE2 (BIN2) by dephosphorylating a conserved tyrosine residue which is (Kim and Wang, 2010). Consequently, in the absence of BRs, BRI1 and BKI1 are strongly associated, thus preventing BIN2 inactivation and allowing the phosphorylation of two transcription factors BRASSINAZOLE RESISTANT1 (BZR1) and BRI1-EMS-SUPPRESOR1 (BES1; also referred to as BZR2). This has the function of reducing the DNA-binding activity of BZR1 and BZR2 inhibiting their direct regulation of primary target genes that regulate BR-responsive growth (He et al., 2002; Wang et al., 2002). In the presence of BRs, BRI1 dissociates from BKI1 and interacts with BAK1, which phosphorylates the protein kinases, leading to inactivation of BIN2 and subsequent dephosphorylation of BZR1 and BZR2 via PROTEIN PHOSPHATASE 2A (PP2A) (Tang et al., 2011). This allows nuclear localisation of BZR1/BZR2 which are then available to activate/repress downstream BR-regulated genes that ultimately promote growth responses (Yin et al., 2005; Yu et al., 2011). The pathway is described in figure 1.5.

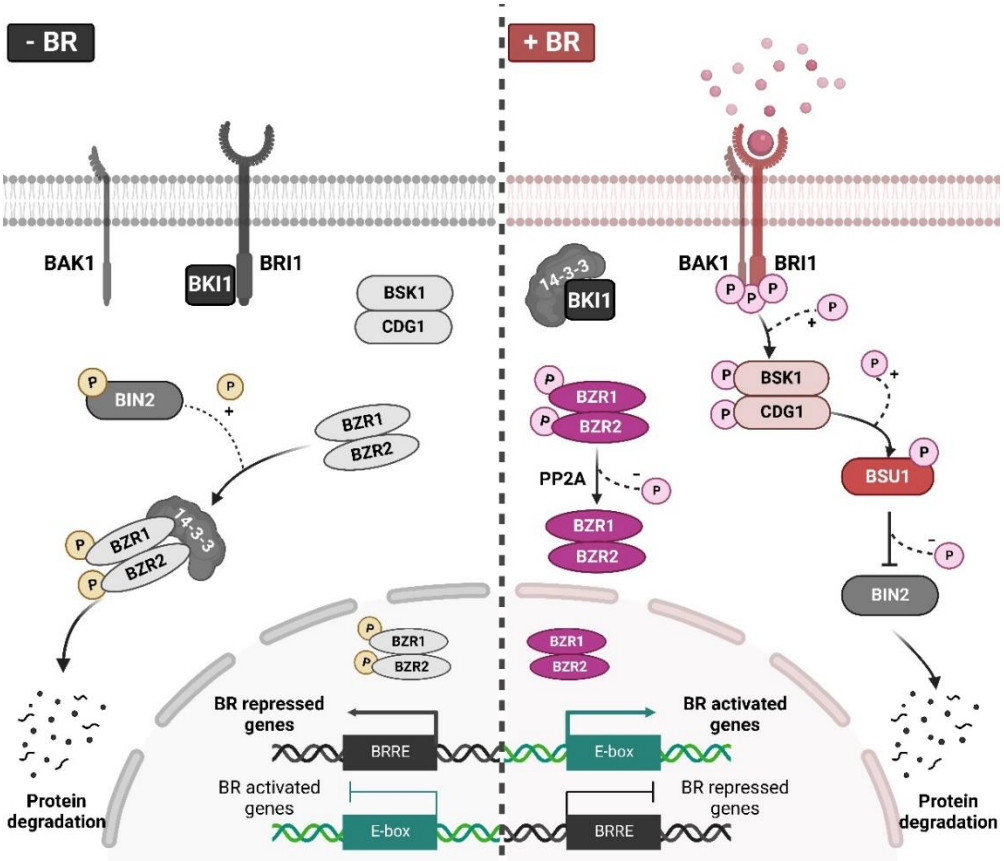

Figure 1. 5 The BR signal transduction pathway. In the absence of BRs, the negative regulator BKI1 attaches with BRI1 inhibiting binding with its co-receptor BAK1. And the transcription factors BZR1 and BZR2 are also phosphorylated by BIN2 which enables their degradation and induces expression of BR-repressed genes in the nucleus and vice-versa happens in the presence of bioactive BR molecules such as BL/ CS which are produced by BR-biosynthesis pathway. The pathway was produced using BioRender.com

1.7.3 Regulation of BR-responsive genes controlling growth and development

Physiological studies indicate BRs promote cell elongation and enhance tolerance to various biotic and abiotic factors thus potentially providing opportunities for improving or sustaining crop yields in a changing environment. However, the exact mechanism of how BRs regulate a variety of developmental processes is still unknown. Genetic studies have demonstrated that BZR1 and BZR2 are the central players in the signalling pathway which regulate gene expression and BR-specific development (Wang et al., 2002; Yin et al., 2002). BZR1 and BZR2 share around 90% protein sequence identity (He et al., 2005).

To further understand the tissue and developmental specific regulation of the downstream genes regulated by BZR1 and BZR2, two independent studies employed chromatin immunoprecipitation-based approaches (ChiP-chip) with an aim to understand direct targets of these TFs in Arabidopsis. In the first study, nearly 953 genes were directly regulated by BZR1 and in the second, nearly 250 genes regulated by BZR2 (Sun et al., 2010; Yu et al., 2011). Thus, demonstrating BZR1 and BZR2 function by activating and suppressing target genes by interacting with BRRE and E-Box motifs in the promotors. It was established that BZR1 also binds to the promotors of various hormone biosynthesis, transport and signal transduction genes regulating auxin, GA, ABA, ethylene, cytokinin and jasmonate biosynthesis and signalling, but the mechanisms by which these interactions regulate growth and development is still unknown (Sun et al., 2010; Yu et al., 2011).

1.8 BR homeostasis

1.8.1 Metabolism

The BR biosynthetic pathway is regulated by bioactive BRs through a homeostatic feedback mechanism. This is illustrated by the observations that external BR application leads to the downregulation in expression of sterol and BR biosynthetic genes, including *HYD2*, *DWF7*, *DWF5*, *DWF4*, *CPD*, *D2* and *BR6ox1*,*2*. Conversely, the expression of these genes is upregulated following the application of a BR biosynthetic inhibitor (Mathur et al., 1998; Tanaka et al., 2005; Sun et al., 2010; Yu et al., 2011). The BR signalling pathway is responsible for controlling this homeostatic mechanism via the BZR1 and BZR2 TFs, which directly regulate expression of BR biosynthetic genes (Wang et al., 2002; Yin et al., 2002). For example, when the BR levels are low these TFs are phosphorylated and inactive, but in the presence of high levels of BRs they are active and repress expression of BR biosynthetic genes. Demonstrating BZR1 and BZR2 not only regulated expression of many downstream genes controlling BR-regulated growth and development but they are also responsible for feedback inhibition of BR biosynthesis pathway genes by directly binding to their promoter regions (He et al., 2005; Sun et al., 2010; Yu et al., 2011).

1.8.2 Developmental and environmental regulation of BR biosynthesis

Some recent reports also suggest that BR regulation is also dependent on quality of light and day length. For instance, blue light promotes expression of *BRD1/CYP85A1* and *CYP90A3/4* in arial tissue, whereas far-red light promotes BR-biosynthesis in roots in rice (Asahina et al., 2014). Another report suggests BR metabolism is diurnally regulated with BES1/BZR2 repressing BR biosynthesis during the day. At dawn, elevated PIF4 binds to the *DWF4* and *BR6ox2* promotors, competing with BES1, resulting in elevated expression that drives BR biosynthesis (Martinez et al., 2018; Park et al., 2003; Wei et al., 2017).

1.8.3 BR Catabolism

BR catabolism results in reduced endogenous levels of bioactive BRs leading to attenuated BR signalling. Multiple mechanisms leading to the inactivation of BRs have been uncovered and the classes of enzymes catalysing these reactions include hydroxylases, glycosyltransferases, reductase, acyltransferases, and sulfotransferases (Wei and Li, 2020).

Hydroxylases perform C26 hydroxylation on CS or BL to produce C26 hydroxylated derivates which inhibits binding of the BRs to the pocket of BRI1 (Neff et al., 1999; Turk et al., 2003; Horthorn et al., 2011; She et al., 2011; Ohnishi et al., 2006). For instance, BAS1/CYP734A1 in Arabidopsis and CYP734A7 in tomato perform this C26 hydroxylation on the BL or CS ultimately to reduce BR signalling. In rice, this enzyme additionally performs additional oxidation steps that produce aldehyde and carboxylate groups at C26 position (Sakamoto et al., 2011).

Glycosylation is another form of BR inactivation. UDP-glycosyltransferases including UGT73C5 and UGT73C6 can glycosylate BL or CS at the C2-, C3-, C22-, and C23- positions resulting in inactivation (Soeno et al., 2006). Suppression of these genes has been demonstrated to induce BR signalling in Arabidopsis, suggesting that they play a physiological role in regulating levels of bioactive BRs.

BEN1 or BRI1-5 ENHANCED1 encodes a dihydroflavonol 4-reductase-like protein which inhibits the reduction of 6-oxo BR to 6-deoxo counterparts (Yuan et al., 2007). In Arabidopsis, acyltransferases such as BRASSINOSTEROID INACTIVATOR1 (BIA1)/ ABNORMAL SHOOT1 (ABS1), BIA2, PIZZA (PIZ)/ BR-RELATED ACYLTRANSFERASE1 (BAT1/ DWARF AND ROUND LEAF1 (DRL1) have

been shown to acetylate BL or CS, thus reducing activity of these molecules (Gan et al., 2020; Zhang and Xu, 2018; Schneider et al., 2012; Choi et al., 2013; Zhu et al., 2013).

BNST3 and BNST4, encode steroid sulfotransferases in Brassica napus, which catalyse the O-sulfonation of 24-epiBRs such as 24-epicathasterone thus reducing biosynthesis of 24-epiBL followed by CS and BL (Rouleau et al., 1999; Marsolais et al., 2004). Similarly, in Arabidopsis the homologue of BNST3 and BNST4, AtST1 perform a similar functions in inactivating 24-epiBRs (Marsolais et al., 2007).

1.9 Role of BRs in determining agronomically important traits

In cereals, BRs are known to regulate many important agronomic traits such as stem elongation, leaf angle, grain size, flowering time and senescence (Divi and Krishna 2009; Khripach et al 2000). In the following sections, the role of BRs in regulating various architectural traits of agronomic importance is discussed.

1.9.1 Stem elongation

Severe dwarfism is reported in BR-deficient mutants of Arabidopsis, maize and rice, demonstrating an important role for BRs in regulating stem elongation (Clouse et al., 1996; Kir et al., 2015; Yamamuro et al., 2000; Sun et al., 2017). Some reports suggest that crosstalk between the BR and GA pathways is responsible for regulating stem elongation. For instance, a physical interaction between BZR1 and DELLA proteins (a negative regulator of GA signalling) has been demonstrated in Arabidopsis. GA production leads to degradation of DELLA thereby releasing BZR1 from the BZR1-DELLA complex to promote cell elongation (Bai et al., 2012; Gallego-Bartolome et al., 2012). Crosstalk between the GA and BR pathway, also involves regulation of phytohormone levels. GA levels were shown to be reduced in BR deficient mutants, whereas seedling height was increased in BR-overexpressing mutants due to elevated levels of GA (Tong et al., 2014). BZR1 has also been shown to promote cell elongation by directly regulating TFs such as DLT, LIC, RLA/SMOS1, OFP8 which are positive regulators of this process (Castorina and Consonni, 2020).

There are many reports demonstrating the role of BR pathway genes in regulating final plant height in cereals such as rice, maize, and barley. For instance, a semidwarf phenotype was observed in the barley *uzu* mutant (figure 1.6), containing a nucleotide substitution in the *BRI1* gene (Chono et al., 2003). The *uzu* gene has been introduced

into hull-less barley cultivars in Japan to confer a semi-dwarf and lodging resistant phenotype suitable for higher yields. In rice, *OsBRI1* mutants displayed a range of phenotypes (Morinaka et al., 2006). A weak allele, *d61-7* displayed semi-dwarfness, erect leaves and had 35% higher biomass at maturity under dense planting conditions compared to wild-type. But due to smaller grains in this mutant compared to wild type there was no yield advantage when growing them under higher density field conditions (Morinaka et al., 2006). In maize, the *na2-1* mutant containing a mutation in *ZmDWF1*) was severely dwarfed, with a final plant height that was reduced 90% compared to the wild-type. It was also reported that all internodes were evenly reduced in length due to defects in cell elongation (Best et al., 2016).

Figure 1. 6 Phenotype of the barley *uzu* mutant. The wild type is shown on the left and the *uzu* mutant on the right. Bar length, 1meter. Adapted from Chono et al., 2003).

In contrast to BR-deficient mutant, a transgenic maize line overexpressing *ZmDWF4* displayed a significant increase in the final plant height and leaf area (Liu et al., 2020). A similar increase in biomass and height was also reported in BR overexpressing lines of *Brassica napus* and *Arabidopsis* (Sahni et al., 2016; Choe et al., 2001).

1.9.2 Seed development

Seed size and weight are major yield determining traits which have been extensively selected during domestication. This trait also holds importance for the end consumers. For instance, people in Southern China, most parts of Asia and USA prefer long and slender grain varieties whereas, people in Northern China, Japan and South Korea prefer shorter and round grain varieties of rice (Weng et al., 2008; Bai et al., 2010; Shao et al., 2010). Seed size is determined by phytohormones, ubiquitination-mediated proteasomal degradation pathway and G-protein signalling pathway (Zuo and Li, 2014; Zhang et al., 2014 and Hu et al., 2013).

Many reports demonstrate a role of BRs in controlling seed development in different plat species such as Arabidopsis, pea, tomato, wheat and rice (Liu et al., 2018; Fang et al., 2016; Feng et al., 2016; Jiang et al., 2013; Morinaka et al., 2006; Hong et al., 2005; Tanabe et al., 2005). For instance, BR-deficient mutants in rice had reduced seed length (Hong et al., 2005; Morinaka et al., 2006) whereas BR-overexpressing mutants demonstrated sn increase in seed size in rice (Wu et al., 2008; Figure 1.7). In Arabidopsis, the *det2* mutant has smaller seeds with reduced seed cavity, endosperm volume and integument cell length compared to wild type (Jiang et al., 2013). Mechanistically, it was shown that BRs, acting through BZR1, regulate seed size in Arabidopsis by represseing negative regulators *APETALA2* and *ARF2* and promoting the positive regulators *HAIKU2*, *MINISEED3* and *SHOOT HYPOCOTYL UNDER BLUE1*) (Jiang et al., 2013).

Figure 1. 7 Seed phenotype of mutants overexpressing *OsDWF4* gene (A) 10 seeds aligned length wise, (B) 10 seeds aligned width wise. Adapted from Li et al., 2018.

Interestingly, the *osdwf4-1* mutant did not display alterations in grain size (Sakamoto et al., 2006). displayed no undesirable grain morphology. It is noteworthy that *OsD11* (CYP724B1) catalyses the same C-22 hydroxylation step in BR biosynthesis as OsDWF4 (CYP90B1) and appears to have a more important role controlling grain

development. This is illustrated by the *d11-4* mutant having smaller grains. This demonstrates that expression of *OsD11* is key in maintaining bioactive levels of BR for seed development.

1.9.3 Spike development

Spike length, number of spikelets and floret fertility are agronomically important traits which determine final grain yield. Spike length and compactness have strong correlations with plant height and lodging resistance (Wu et al., 2014; Yao et al., 2019; Li et al., 2020). It has also been demonstrated that manipulating the number of spikelets on an ear can contribute to final grain yields in wheat (Guo et al., 2017).

BRs have been demonstrated to have an important function in controlling spike and panicle development in cereals (Hong et al., 2005; Dockter et al., 2014). Often, BRdeficient or insensitive mutants possess compressed panicles or spikes in cereals such as rice, maize, barley, and wheat (Hong et al., 2005; Best et al., 2016; Dockter et al., 2014; Gasperini et al., 2012). For example, *Rht8c* an alternative to GA-insensitive alleles, having reduced sensitivity to BRs and adapted to hotter and drier climates, possessed decreased spike length without demonstrating a reduction in the spikelet number (Kowalski et al., 2016). In barley, the reduced spike length in the *uzu1.a* mutant (of barley, possessed shorter spikes and awns due to reduced rachis-internode length (Figure 1.8) at the base and tip of the spike (Dockter et al., 2014). Similarly, the rice *brd2* mutant displayed malformed panicles, a reduced number of spikelets and decreased fertility (Hong et al., 2005).

Figure 1. 8 Spike phenotype of the barley *uzu1.a* mutant. The spike is shorter due to reduced rachis-internode elongation in the mutant compared to wild-type (Bowman). Bar length, 10cm. Adapted from Dockter et al., 2014.

During spike development, the grain number is influenced by floret fertility. Anther and pollen development are important factors that affect this agronomically important trait in cereals. Phytohormones such as auxin, GA, ethylene, CK, JA and BR are well known to have an essential role in determining male fertility (Huang et al., 2003; Cecchetti et al., 2008; Kieber et al., 1993; Park et al., 2002; Singh et al., 2002; Yu et al., 2010). Consequently, mutants that exhibit hormone deficiency or insensitivity display anther developmental defects that impact fertility. BRs have a positive role in determining male fertility by promoting anther development and filament elongation (Ye et al., 2010). In Arabidopsis, BR-deficient mutants, including *cpd*, *bin2*, *dwf4* and *bri1-201* have reduced male fertility due to abnormalities in pollen development. These defects include reduced pollen number, microspore mother cells, failure in pollen tube elongation (causing failure of pollen to reach stigma) and vacuolated tapetal cells causing lower pollen load thus, difficulty of release of pollens from the anthers compared to wild type (Szekeres et al., 1996; Li et al., 2001; Kim et al., 2005; Clouse, 2008; Yu et al., 2010; Bouquin et al., 2001; Dong et al., 2005).

1.9.4 Tillering

Tillering or tiller number is an important agronomic trait in cereals that has a crucial role in determining yield potential, grain quality and overall plant architecture.

Strigolactones (SLs) are phytohormones that have an important role controlling tillering cereals (Al-Babili and Bouwmeester, 2015). A recent study by Fang and colleagues 2020 demonstrated that tiller number determination in rice in controlled by the crosstalk between by SL and BR signalling. In contrast to Arabidopsis, it was reported that BR signalling promotes bud outgrowth and tillering in rice (Stirnberg et al., 2002; Wang et al., 2013; Fang et al., 2020). It was established that SL and BR coordinate rice tillering by stabilizing the interaction of D53 (a negative regulator of SL signalling) with OsBZR1 and reducing the expression level of an inhibitor of shoot branching, *FC1*. Tiller number was significantly reduced in BR-deficient mutants, but transgenic mutants having elevated BR-signalling had a greater number of tillers (Fang et al., 2020; Figure 1.9). Thus, demonstrating role of BRs along with SL in determining bud outgrowth and tiller number in rice.

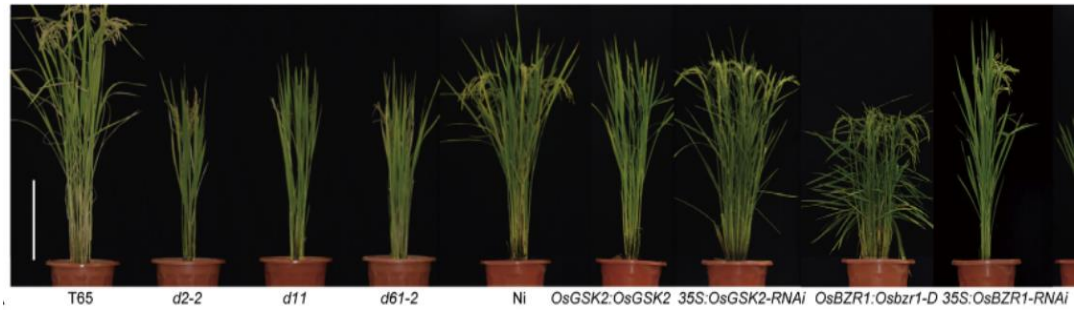

Figure 1. 9 Tillering phenotype of rice BR mutants and transgenic lines with altered BR signalling. Rice mutants and transegic *d2-2*, *d11*, *d61-2*, *OsGSK2:OsGSK2*, *35S:OsGSK2-RNAi*, *OsBZR1:Osbzr1-D*, *35S:OsBZR1-RNAi* compared to wild types (T65 and Ni) at headng stage.. Bar length, 40cm. Adapted from Fang et al., 2020.

1.9.5 Leaf angle/ canopy architecture

The net light energy absorbed by the plant is based on the organization of leaves forming a 3- dimensional spatial structure with a specific total surface area. Both the amount of radiation captured and the way it is distributed in time and space determines the canopy photosynthesis and growth rate (Murchie et al 2019). Leaf angle in cereals determines radiation use efficiency (RUE) and planting density which in turn determine final grain yield.

In maize, the effects of tailoring leaf angle to improve light interception and photosynthetic rate was demonstrated by producing two near isogenic lines having contrasting leaf angle caused by differences at the *LIGULELESS2* locus. The erect

statured lines produced 40% more grain as compared to their counterparts having horizontal leaves, due to improved RUE on per plant basis (Pendleton et al., 1968). Similarly, hybrid 'Pioneer 3306' having horizontal leaves had 14% increase in grain yield by manual manipulation of upper leaves to angle of 10° (Pendleton et al., 1968). Demonstrating that combination of erect leaf architecture along with greater leaf area index (LAI) increased light interception capacity by 14% in modern maize hybrids compared to varieties released in 1930 to late 1960s (Lee and Tollenaar, 2007). This was a factor in the >20% improvement in grain yields observed during this period in the maize crop (Duvick, 2005; Lee and Tollenaar, 2007; Lauer et al., 2012). Another advantage of erect leaf architecture is the ability of accommodating a greater number of plants per unit area thus improving grain yields (Lambert and Johnson, 1978; Ma et al., 2014). It has been reported that maize yields have 50% increase in in US solely due to erect canopy architecture and increased plant densities (Duvick, 2005). A similar increase was also reported in Canada and China due to modifications in planting density, greater LAI, stay-green phenotype in modern hybrids compared to those released in 1950s (Tollenaar and Wu, 1999; Tollenaar and Lee, 2006; Ma et al., 2014). Thus, in summary, plants with upright canopy architecture facilitated better light penetration throughout the canopy which improved photosynthetic efficiency allowing farmers to grow maize under higher planting density leading to significant increase in maize yields over the last nine decades (Pendleton et al., 1968, Duvick, 2005, Tian et al., 2011).

In barley, semidwarf and erect-statured cultivars containing the *uzu.1a* were lodging resistant and supported dense planting were widely grown in approximately 70% of the land in Japan and in parts of China and Korean peninsula during 1930s. Although 1000-grain weight was reduced in these cultivars, improved photosynthesis, lodging resistance and adoption of higher planting densities they performed well and have been preferred by farmers in these regions (Chono et al., 2003; Saisho et al., 2004).

In rice, erect statured cultivars had higher light interception, photosynthesis rate and yielded higher than the cultivars having horizontal leaves (Murchie et al., 1999; Sakamoto et al., 2006; Kumagai et al., 2014). It was reported that erect statured rice genotypes had near maximum photochemical quenching (qP) at midday coupled with less light stress, higher photo-inhibition under light saturation, maximum photosynthetically active radiation (PAR) and better carbon assimilation at plant

level (Murchie et al., 1999). Mutations in *Osdwarf4* gene resulted in erect canopy architecture in rice mutants (Figure 1.10) leading to improved gain yield under dense planting density without any increase in fertilizer application (Sakamoto et al., 2006). Due to which this was an important ideotype characteristic of 'super' high yielding hybrid rice which were developed by crossing elite indica lines with tropical improved japonica cultivars having flag, second and third leaf angle of 5, 10 and 20 degrees respectively (Yuan, 2001; Yao et al., 2000; Bingsong et al., 2002; Peng et al., 2008). Additionally, these erect statured rice varieties 'Liangyoupeijiu' had 13% higher photosynthesis rate than its counterpart 'Shanyou63' and yielded 8-15% higher in farmer's fields (Zong et al., 2000).

Figure 1. 10 Shows erect leaf angle in *osdwf4-1* knockout mutant compared to wild-type. lb stands for leaf blade and ls stands for leaf sheath. Bar length, 3cm. Adapted from Sakamoto et al., 2006.

In wheat, studies have reported that genotypes with narrow and erect statured phenotype had enhanced LAI, higher dry matter production and grain yields (Choudhury, 2000; Parry et al., 2011; Richards et al 2019). For example, mapping populations segregating for erectophile and planophile architecture were developed and tested under field conditions by Richards and colleagues (2019). Associations between canopy architecture and yield related traits were assessed and it was reported that grain yield was 13% more in erectophile lines which was mainly associated with higher above-ground biomass (11%) as compared to planophile lines. Additionally, although the grain weight in these lines was reduced by 9% there were 24% more grains per unit area. Mapping for understanding genetic control of canopy

architecture was then conducted which resulted in detection of various QTLs across most chromosomes but low G x E values demonstrated that the trait is highly heritable and stable across their experiments and environments.

These studies demonstrate the importance of leaf architecture for wheat grain yield improvement, and it was one of the important traits being prioritised in wheat and durum wheat breeding programs at CIMMYT (Shearman et al., 2005).

1.9.5.1 Anatomical basis of leaf angle determination in cereals

Leaf angle is determined by the cell size in the lamina joint region, which connects the leaf blade to leaf sheath. The lamina joint consists of two structures, the ligule and a pair of auricles. Developmentally, leaf angle formation is divided into three stages i.e., formation of blade-sheath boundary (BSB), preligule band (PLB) and development of ligule and auricle (Sylvester et al., 1990). At the BSB stage there is no differentiation between the cells forming leaf blade and sheath. At PLB stage the ligule region is detectable due to rapid cell differentiation. Later, the formation of ligule occurs due to periclinal cell division of the cells at the base of preligule and cell division and elongation behind the ligule leads to formation of auricle tissue (Sylvester et al., 1990; Becraft et al., 1990).

The size of auricle is responsible for providing mechanical strength to the leaf blade which determines the final leaf angle in cereals. Several reports suggest a role of BRs in determining the leaf angle formation by altering either the number of sclerenchyma cell layers in the abaxial or adaxial end of LJ or by determining the cell division or proliferation patterns in the auricle region of LJ (Sun et al., 2015; Tian et al., 2019; Feng et al., 2016; Guo et al., 2021; Zhao et al., 2010). For instance, it is reported BRs inhibit cell proliferation of sclerenchyma cells on the abaxial end of LJ in rice. Molecular analysis revealed expression of *CYC U4;1* in the LJ promoted proliferation of sclerenchyma cell layers. Additionally, it was established that BES1 inhibits expression of *CYC U4;1*, whereas the negative regulator of BR signalling, BIN2 interacts with *CYC U4;1* to promote DNA binding and replication and enhance cell division. Therefore, indicating that *CYC U4;1* functions antagonistically to BR signalling to control leaf angle in rice (Sun et al., 2015). In contrast, a QTL, *Upright Plant Architecture2* (*UPA2*) on chromosome 2 in maize which controls erect leaf

angle in mutant by promoting sclerenchyma cell layer proliferation on adaxial end of lamina joint (Tian et al., 2019).

The length of adaxial end of lamina joint at the auricle region is greater in the BR overexpressing mutants and shorter in BR-deficient mutants in rice and maize. Anatomical studies indicated these differences were associated with differential cell length elongation in this auricle region of LJ in these mutants (Feng et al., 2016; Guo et al., 2021; Zhao et al., 2010, 2013). For instance, *slg-D* mutant overexpressing BRs resulted in enlarged leaf angles as compared to wild-type due to increased cell length in adaxial end of lamina joint in rice (Feng et al., 2016).

1.9.5.2 How BR's and interplay with other phytohormones govern canopy architecture in cereals

Brassinosteroids are extensively reported as one of the key regulators of lamina joint development in cereals such as rice, maize, barley, and sorghum (Morinaka et al., 2006; Sakamoto et al., 2006; Dockter et al 2014; Sun et al., 2015; Feng et al., 2016; Tian et al., 2019). For example, in maize *ZmDWF1* loss-of-function mutant had upright canopy architecture and dwarfism due to reduced cell elongation (Best et al., 2016). In rice, patrial suppression of *OsBRI1* caused upright leaf angle in the mutants which yielded 30% more compared to the wild type under dense planting density (Morinaka et al 2006).

Gibberellins control leaf angle by playing positive and negative role in conjunction with BRs. For instance, transcription of *OsGSR1*, a GA-stimulated transcript, is induced in the presence of external GA and reduced by presence of BR. And *OsGSR1-RNAi* lines had phenotype like BR deficient mutants, which could be rescued by external BR application (with BL). Further investigation reported that *OsGSR1* interacts with *DWF1/DIM1* gene in the BR biosynthesis pathway thereby regulating BR-signal transduction (Wang et al., 2009). This demonstrates a positive role of GA pathway in leaf angle regulation mediated through BRs (Shimada et al., 2006; Jang et al., 2021). In contrast, Tong and colleagues (2014) demonstrated excessive application of BR, leads to GA inactivation via upregulation of a GA-inactivation gene, *GA2OX3*. Furthermore, elevated GA levels downregulated BR biosynthesis and response thus playing a negative role in leaf angle development

which is different in rice compared to model species Arabidopsis thaliana (Tong et al., 2014).

Auxins plays a negative role in regulating leaf angle in rice, as numerous mutants defective in either auxin biosynthesis or signalling display enlarged leaf angle (Bian et al., 2012; Du et al., 2012; Song et al., 2009; Yoshikawa et al., 2014). For instance, in maize *BRACHYTIC2* or *BR2* gene and sorghum *DWARF3* or *Dw3* containing mutants had elevated levels of free indole acetic content causing increased auxin polar transport and reducing leaf angle (Pilu et al., 2007; Truong et al., 2015). Whereas three auxin suppressors *OsARF1*, *OsARF11* and *OsARF19* likely promote *OsBRI1* and *OsGH3s* expression, resulting in enlarged leaf angles in rice (Attia et al., 2009; Liu et al., 2018; Zhang et al., 2015).

Strigolactones (SLs) play a negative role in leaf angle regulation as defective SL biosynthesis and signalling mutants (*d10*, *d17*, *d27*, *d3* and *d14*) display enlarged leaf angle in rice (Li et al., 2014). For instance, it is reported that tillering and leaf angle in rice is controlled by SL and BR pathway, as D53 (OsDWARF53, negative regulator of SL) induced BR signalling component OsBZR1, thus increasing leaf angles in rice, whereas OsDWARF3 a positive regulator of SL pathway, leads to degradation of OsBZR1 leading to reduced leaf angles in rice (Fang et al., 2020).

Although we have considerable knowledge about the genes and pathways regulating leaf angle there are limited alleles suitable for cereal breeding, mainly due to negative pleiotropic effects often associated with changing leaf angle (Hong et al., 2002, 2003, 2005; Tanabe et al., 2005; Tong et al., 2012). The precise manipulation of the expression of these genes or selection of new favourable alleles is required to develop potential crop improvement strategy. For instance, *RNAi-OsBRI1* transgenic plants with a slight reduction in expression produced 30% more grains under higher planting density (Morinaka et al., 2006). Additionally, by manipulating expression of specific genes such as *DWF4*, *BU1* and *LIC* specifically reduced leaf angle without any other pleiotropic effects on plant development could be further exploited to potential gains (Sakamoto et al., 2006; Wang et al., 2008; Zhang et al., 2012; Tanaka et al., 2009). Identification and utilisation of natural alleles in the natural population could also be explored for improving the leaf angle in modern crops. For instance, a recent study demonstrated that two naturally occurring QTLs *Upright Plant Architecture1*

(*UPA1*) and *Upright Plant Architecture2* were utilised to breed for upright leaf architecture and enhanced grain yield in maize (Tian et al., 2019). Thus, demonstrating that with better biotechnology tools currently available new alleles to alter canopy architecture can be identified and deployed rapidly, which should ultimately improve food security in a changing environment.

1.10 Objectives of this study

Overwhelming evidence suggests that during grain filling wheat yield potential is sink-limited, as carbon accumulation is limited by the storage capacity of the grains. Therefore, strategies to improve grain number are one of the most important avenues in the genetic improvement of yield potential. During the last 50 years, the *Rht-1* dwarfing alleles have been essential for increasing grain yields and providing lodging resistance in most wheat varieties. However, under certain growing conditions *Rht-1* alleles are suboptimal and can confer a yield penalty. Brassinosteroids (BRs) are phytohormones that also have an important role controlling architecture and assimilate partitioning. It is well established that lesions in the BR signalling pathway can produce beneficial traits in cereals. For example, the barley *uzu1* dwarfing alleles, containing lesions in the BR receptor (*BRI1*), have been widely used in breeding programs in East Asia. In addition, partial suppression of the *OsBRI1* gene in transgenic rice confers a beneficial erect-leaf phenotype that could provide an estimated 30% increase in grain yields under dense planting density. In barley, other BR signalling components, including the biosynthetic gene *HvDWF1/HvDIM*, have also been demonstrated as targets for developing dwarfing and erect statured genotypes. Additionally, the rice *brd2* (*OsDWF1* gene) mutant displayed erect stature and semi-dwarf height which was less severe than other BR deficient mutants in cereals due to production of DS from an alternative BR-biosynthesis pathway. Similarly, *osdwf4-1* mutant (having deleterious mutation in *OsDWF4* gene) displayed erect leaf architecture without any negative impacts on other agronomically important traits such as plant height and reproductive development. Leading to nearly 32% yield increase in field compared to wild type under dense planting density. Demonstrating huge potential of yield improvement by tailoring expression/ activity of BR pathway genes in wheat.

The aim of this PhD project is to alter architecture (specifically canopy architecture) of wheat by targeting BR biosynthesis and signalling components using a

combination of reverse and forward genetics-based approaches. It is expected that this will allow the development of novel BR alleles that can be used for potentially improve grain yields in wheat under field conditions.

Objective 1: Characterise the *TaBRI1*, *TaDWF1* and *TaDWF4* genes in wheat.

Based on studies of BR biosynthesis and signalling genes in other cereals, the *TaBRI1*, *TaDWF1* and *TaDWF4* genes have been identified as potential targets for improving wheat architecture. The first objective of this project is to identify and characterise these genes in wheat using a reverse genetics-based approach. This will be achieved by screening the Cadenza TILLING population (Krasileva et al 2017) to identify deleterious mutations in these genes of interest and produce combinatorial mutants for each target gene. The backcrossed mutants generated will be subjected to a detailed phenotypic characterisation under glasshouse and field conditions. This will include an assessment of key agronomic traits including plant architecture and reproductive development. Additionally, we will establish the anatomical basis of erect leaf architecture in some of the BR mutants.

Objective 2: Identify and characterise novel *TaBRI1-A* mutations.

The hexaploid nature of bread wheat often precludes the identification of recessive mutations that could be beneficial for breeding. To overcome this hurdle, we will aim to conduct a novel screen to identify weak *tabri1-A* alleles that have the potential to be used for optimising wheat architecture in breeding programs. Preliminary studies have demonstrated that the *TaBRI1* homoeologues appear to have functionally redundant roles controlling BR-responsive growth. To overcome the genetic redundancy, we will conduct an EMS-mutagenesis based screen using *tabri1-bd* double mutant. A field-based screen of M2 plants enabled identification of two novel alleles in the *TaBRI1-A* gene, displaying a dwarf and/or erect flag leaf phenotype that is characteristic of altered BR signalling. To establish role of mutations in *TaBRI1* genes on flux of BR pathway hormonal, transcriptomic and physiological studies will be conducted under glasshouse conditions.

Chapter 2: Materials and Methods

2.1 General Molecular Biology Methods

2.1.1 Genomic DNA extraction

Approximately 40-50 mg (fresh weight) of leaf tissue at seedling stage (2-leaf stage) was collected into 96 deep well blocks which were subsequently covered with a sealing matt. Harvested leaf material was frozen at -80 ℃ and then lyophilised using the Edwards Mondulyu RV8 Freeze dryer (Crawley, Sussex, UK) for 2-3 days. The lyophilised tissue was then homogenised at 1750rpm for 4 minutes using 1×3mm stainless steel ball bearings in a 2010 GenoGrinder® (SPEX SamplePrep, New Jersey, USA). Genomic DNA was extracted from leaf material by the addition of 600µl of extraction buffer (described below) using a multidropper and the samples were incubated at 65 ℃ for 1 hour. Next, 200µl of 5M KAc was then added to the samples followed by shaking for 2 minutes at 1750 RPM in the GenoGrinder®. Cell debris was pelleted by centrifugation at 3000 RPM for 15 minutes. Using a multichannel pipettor, 300µl of the supernatant was transferred to a new plate containing 165µl chilled isopropanol. The plate was then inverted 5-6 times to mix the solutions followed by a 10-minute incubation at 4 ℃. The DNA was precipitated by centrifuging the blocks at 3000 RPM for 20 minutes. The supernatant was discarded, and the DNA pellet washed with 500µl of 70% ethanol added using multidropper and plates inverted 3-4 times. Plates were centrifuged at 3000 RPM for 7 minutes followed by removal of the supernatant. The DNA pellets were dried at 50 ℃ for 20 minutes and re-suspended in 200µl of TE0.1R buffer (components described below) in the samples using multidropper followed by a 1-hour incubation at 50 ℃ to enable resuspension of the genomic DNA. The samples were stored at 4 ℃ overnight to aid resuspension and then transferred to -20 ℃ for long term storage of the DNA samples.

2.1.2 DNA quantification

DNA concentrations were measured using a NanoDrop^{TM} ND-1000 spectrophotometer (LabTech International LTD., U.K.).

2.1.3 Polymerase Chain Reaction (PCR)

A PCR reaction for genotyping and sequencing was performed using pair of primers mentioned in supplementary table 1. Hot Shot Diamond Mastermix (Clent Life Science, Stourbridge, UK) was used to amplify the DNA fragments of DNA. Amplification was performed (using a C1000 Thermal Cycler Bio-Rad Laboratories, Hercules, California, U.S.A) in a 20 µl reaction volume containing 10 µl of Hot Shot Dimond Master mix, 7 µl of double distilled RNAase free water, 0.5 µl of 10 µM forward primer, 0.5 µl of 10 µM reverse primer and 2 µl DNA template. The thermal cycler was programmed at 98 ^{o}C for 5 minutes for initial denaturation, followed by 43 cycles at 97 ^{o}C for 30s for denaturation, 55-65 ^{o}C (based on primer pair Tm) for 30s for annealing, 72 ^{o}C for 60s per kb for extension and lastly 7 min at 72 ^{o}C for final extension yielding PCR products needed for genotyping or sequencing.

2.1.4 Purification and sequencing of PCR products

PCR products were purified using QIAquick PCR Purification kit (Qiagen, Hilden, Germany). When required, DNA fragments were extracted from an agarose gel using a Qiagen Gel Extraction kit (Qiagen, Hilden, Germany). The PCR products were purified using the manufacturer's protocol. The purified products were outsourced for sequencing to Eurofins Genomics (Wolverhampton, U.K.) using Sanger sequencing.

2.1.5 Agarose gel electrophoresis

The amplified PCR products were separated and visualized by agarose gel electrophoresis. Agarose gel was prepared (1-2.5% (w/v) depending on the fragment length) by dissolving agarose powder (Fisher Scientific, Loughborough, U.K.) in the 0.5X TBE buffer (45 nM Tris- borate, 1nM EDTA, pH 8.3) with the aid of heat. Ethidium bromide was added to a concentration of 0.5 µg/µl.

The DNA samples were mixed with 1X Loading Dye containing bromophenol blue and xylene cyanol FF, (Thermo Scientific, Hemel Hempsted, U.K.) and approximately 15-20 µl of the product was loaded in wells along. The size of DNA fragments was ascertained by comparing against a 1kb or 100bp DNA ladder (Thermo Scientific, Hemel Hempstead, U.K.). Electrophoresis was conducted for 30-120 minutes at 100mV, depending on the expected product size. The gel was then

visualised under UV excitation using SynGene GelDoc image documentation equipment (Synoptics Ltd, Cambridge, U.K.).

2.1.6 Kompetitive Allele Specific PCR (KASP) genotyping

KASP low-ROX Mastermix (LGC, Teddington, UK) was used and added to 2 forward primers allowing SNP specificity (FAM, HEX or VIC tails) and a common reverse primer. Genomic DNA was used as a template and was diluted to ~50 ng/µl. The KASP primer mix used contained the following constituents 12 µl KASP SNP primer 1 (WT) (100 µM), 12 µl KASP SNP primer 2 (mut) (100 µM), 30 µl KASP common primer (100 µM) and 46 µl water. To perform the assays, 2µl of DNA was aliquoted into the white qPCR 96- well plate (4titude Ltd., Surrey, U.K.), including a minimum of two positive and two negative controls. To this template, 8µl of the assay mix containing 0.14 µl KASP primer mix, 2.86 µl water and 5.00 µl KASP low-ROX mix (LRK) was added. After preparing the reaction, the plate was covered with a clear seal (4titude Ltd., Surrey, UK). The plate was then spun down using Labnet MPS 1000 Mini plate spinner (Sigma- Aldrich Company Ltd., Dorser, U.K.). The KASP reaction was then carried out using a BIO-RAD C1000^{TM} Thermal cycler (California, USA) or ABI 7500 Real Time PCR system (Applied Biosystems, California, USA). The reaction conditions were initial denaturation at 95°C for 15 min followed by 10 cycles at 95°C for 20 seconds and annealing at 61°C for 60 seconds (reducing 0.6°C per cycle) and remaining 27 cycles at 95°C for 20 seconds and annealing at 55°C for 60 seconds. The plates were read with the 7500 Fast Software v2.3 (Applied Biosystems, Foster City, California, USA) and analysed using the KlusterCaller™ software (LGC, Teddington, UK).

2.1.7 RNA Extraction

Seedlings were harvested into liquid nitrogen and crushed to form a fine powder using a sterile pestle and mortar. Approximately 50-75mg of frozen plant material was transferred into a sterilized 2ml tube and stored at -70^{o}C until the extractions were performed. RNA was extracted from frozen tissue using a Monarch® Total RNA Miniprep Kit (New England Biolabs, Ipswich, Massachusetts, USA) according to the manufacturer's instructions and including the DNase treatment. To assess RNA concentration and quality, Agilent 2100 Bioanalyzer (Agilent, Santa Clara, California, USA) and Agilent 6000 Nano RNA Kit (Agilent, Santa Clara, California,

USA) was used according to the manufacturer's instructions. Extracted RNA samples were stored at -80°C.

2.2 Bioinformatics

2.2.1 Identification of *BRI1, DWF1* and *DWF4* genes in wheat

BlastP was performed on Ensembl-Plants within *Triticum aestivum* varirty Chinese spring database (TGACv1 genome assembly, Clavijo et al., 2017) against the translated amino acid sequences of *BRI1, DWF1* and *DWF4* genes from *Oryza sativa, Hordeum vulgare* and *Arabidopsis thaliana*. The top blast hits having lowest E value, highest sequence similarity and maximum coverage was selected in wheat. Followed by identification of the homoeologous genes in wheat.

2.2.2 Phylogenetic analysis

The amino acid alignment was performed in Geneious 10.2.3 software using ClustalW program followed by construction of phylogenetic trees using neighbour ending joining in Geneious 10.2.3 software.

2.2.3 Identification of protein domains

To identify various domains, present in *TaBRI1*, *TaDWF1* and *TaDWF4* publications were screened where the protein was characterised in related/model species. This enabled the identification of conserved domains and motifs that were present in the predicted proteins.

2.2.4 Identification of TILLING mutations

Deleterious EMS mutations used to generate loss-of-function mutants were identified using the wheat TILLING website (http://www.wheat-tilling.com/) (Krasileva et al., 2017).

2.2.5 Primer Design

PCR primers (for gene amplification and KASP-based genotyping) were designed using Geneious version 10.2.3 (BioMatters Ltd, Auckland, New Zealand). Gene-specific primers were designed with a GC content of around 40-60%, 18-24 base-pairs in size and Tm of 58-62°C. Homologue-specific SNP's were included on the 3' end of the primer.

2.2.6 RNA sequencing

RNA was sent to Novogene Bioinformatics Technology Co. Ltd. (Cambridge, UK) for mRNA-sequencing. The resultant raw fasta files were processed by pairing of reads and trimming of the Illumina-specific adapters, using Trimmomatic 0.39 software (Bolger et al., 2014) was used (SLIDINGWINDOW:4:20; MINLEN:50). The raw fasta.q files were then mapped to wheat IWGSC RefSeq v2.1 genome assembly using STAR 2.7.8a (Dobin et al., 2013) (outFilterMismatchNmax 6; --alignIntronMax 10000). The number of mapped reads was counted using HTSeq 0.11.3 (Putri et al., 2022) and then converted to TPMs (transcripts per million). Differentially expressed genes (based on two-fold or higher changes with adjusted P-value of ≤0.05) were then identified by running Bioconductor tool DESeq2 (Love et al., 2014) in RStudio version 4.1.1717 (RStudioTeam, 2015). Differential expression was visualised by generating heatmaps for the BR-pathway genes using Heatmapper (http://www.heatmapper.ca/).

2.3 Plant material and growth conditions

2.3.1 Growth Conditions under glasshouse conditions

Wheat cv. Cadenza was used for all molecular, physiological and TILLING experiments. Wheat seeds were imbibed on damp filter paper in petri plates. The petri plates were then transferred to the cold room at 4℃ for 4-5 days to break the innate dormancy. The plates were then transferred to 20℃ to stimulate germination. Once the coleoptile had emerged, they were transferred to germination trays containing Rothamsted potting mix (75% peat, 12% sterilised loam, 3% vermiculite and 10% grit) and placed in the glasshouse nursery. Once the seedlings attained the 2-3 leaf stage, they were transferred to 15-cm pots containing the same potting mix. Subsequently, the pots were transferred to the standard glasshouse cabinet which maintained approximately 18-20 ℃ day and 14-15℃ night temperature and a 16-hour photoperiod using natural and artificial light supplementation from LED lights (400-1000 μmolm-2s-1 PAR). To protect the plants from insect pests and fungal diseases, yellow sticky traps, Amblyline sachets (Bioline AgroSciences, Holland Road, UK) and sulphur dioxide open- air fumigation were used respectively, as pest and pathogen control measures.

2.3.2 Crossing wheat plants

The spikes to be pollen acceptors and pollen donors were selected based on the stage of development. Selected female parents were emasculated by excision of pale green/yellow immature anthers 1-3 days prior to anthesis. The bottom three and top two spikelets, and two innermost florets of all remaining spikelets were removed. Emasculated spikes were enclosed in transparent plastic crossing bags and labelled with the genotype and the date. When selected male parents entered anthesis, single pollen shedding spikes were excised, lemma and palea cut to ease the emergence of the anthers and placed upside-down inside the crossing bag with the emasculated spike. After agitation to spread pollen around all available florets, pollen donor spikes were held in place upside-down against the female parent using paperclips. Pollen donor spikes were replaced as required. Grains were left to develop for 20-25 days before collection. The scheme for stacking TILLING mutations and generating combinatorial mutants in shown in Figure 2.1.

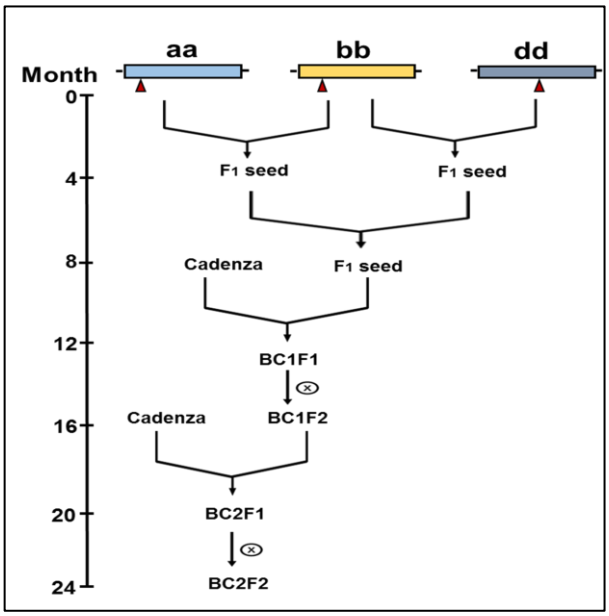

Figure 2. 1 Crossing scheme followed for stacking TILLING mutations. After identification of the mutations in the three homeologues the TILLING lines were inter-crossed to stack the mutations in common background. Followed by at least two rounds of backcrossing to reduce the number of EMS-derived background mutations and the identification of combinatorial mutants to allow subsequent phenotypic characterisation.

2.3.3 Wheat EMS mutagenesis-based screening

The M1 seed obtained was planted in the field in March 2018 with a sowing density of 100 grains/m^2 in twelve separate plots (1.8 x 12m plots). At maturity the M2 seed was combine harvested from each plot to generate twelve individual M2 pools for conducting screening. The bulked M2 seed from individual pools was sown in the field in March 2019. Eight plots of 1.8 x 12 m per pool were sown at a planting density of 100 grains /m^2 giving a total of 96 plots. Visual screening of the plots was conducted from GS65 to GS87 to identify mutants displaying altered height and/or leaf erectness in individual M2 plants. M3 seed was collected from selected individual plants at maturity.

2.4 Phenotypic characterisation of *tabri1*, *tadwf1*, *tadwf4* mutants under glasshouse

2.4.1 Leaf angle

The leaf angle was defined as the angle between the vertical stem and the midrib of the leaf as illustrated in Figure 2.2. Leaf angle was measured at seedling stage (2nd leaf) and reproductive stage on flag-leaf. For measuring flag-leaf angle the date of ear emergence and anthesis was recorded on a representative primary tiller. The leaf angle was measured using a protractor and was recorded using the Zadoks scale at ear emergence (GS-55), anthesis (GS-61), completion of anthesis (GS-69), soft dough (GS-77), late milk (GS-85) and ripening stage (GS-93) on the primary tiller.

Figure 2. 2 Leaf angle formed between the stem and the midrib. This angle was measured on the flag-leaf of Cadenza growing in the glasshouse during anthesis stage (GS-61) using a protractor.

2.4.2 Flag leaf area

Flag leaf width and length were measured on the primary tiller at the widest and longest point of the leaf. Measurements were conducted at GS85. The leaf area (mm^2) was calculated using the equation: length x width x 0.835 (Miralles et al. 1998).

2.4.3 Final plant height

Final plant height in mm was recorded as the length of the tallest tiller from the base of the stem touching the soil to the tip of the spike at the time of maturity.

2.4.4 Internode lengths

Internode measurements were taken from 2-3 tallest tillers per plant. The measurements (mm or cm) taken were for the individual internodes: peduncle, internode 2 (I2), internode 3 (I3), internode 4 (I4) and total stem length (excluding the spike).

2.4.5 Spike parameters

Spike length was measured from the base of the first spikelet to end of the terminal spikelet just beneath the base of the awns. The number of spikelets producing grain per spike was also measured.

2.4.6 Grain characteristics

The Marvin grain analyser (INDOSAW, India) was used to determine grain, width, length, and area. Approximately 3-5 gm of clean threshed seed was spread evenly (without any overlap) on the tray within the Marvin grain analyser. The length, width, and area (in mm^2) of each individual seed were measured and the means were calculated for each genotype.

2.5 Field assessment of wheat mutants

2.5.1 Phenotypic evaluation of Spring-sown field trial

To access the agronomic performance of the wheat BR mutants under field conditions a field trial was planted in Spring 2022 at Rothamsted Research. The size of the plots was $1m^2$. The layout of the trial is shown in figure 2.3.

Traits such as flag-leaf angle (anthesis stage and 2-weeks post anthesis stage), final plant height, internode elongation, spike characteristics (spike length and number of spikelets/spike) and grain characteristics (grain area and weight) were recorded in

these genotypes as mentioned in section 2.4 above. Approximately 10-15 recordings (per trait) were collected in a genotype/block. There were some exceptions on how I recorded these measurements. First, as the heterogeneity within the plot was higher than what I usually observed within a pot under the glasshouse, I tagged 10-15 uniform tillers (at same GS). Flag-leaf angles were then recorded on these selected tillers using a protractor. For measuring the final plant height and internode lengths were recorded on tallest tillers/plot. Static thrasher was used to thrash the spikes (as opposed to manual thrashing in GH) procured from the plots to get clean seeds which could be used for recording grain measurements.

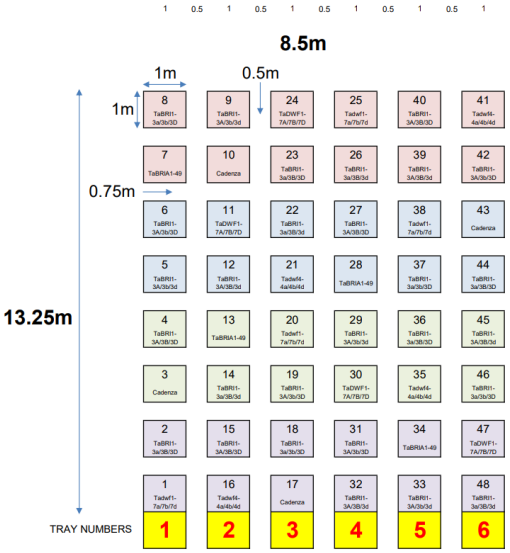

Figure 2. 3 WS2232 field trial layout. Four biological reps of each genotype were randomly planted in complete block design under the field during Spring 2022 at Rothamsted Research farms, Harpenden. Size of each block was 1m^2. 48 genotypes were accommodated in six rows (with 8 genotypes/ row).

2.5.2 High throughput phenotyping under Field Scanalyzer

To assess physiological characteristics including green canopy cover, plant height and spike density, the *tadwf1-abd* mutant and Cadenza were Autumn sown under the Field Scanalyzer in 2020.

Three biological reps of these genotype were grown in randomised in 0.6m^2 plots. The RGB images were captured using high-resolution visible cameras and 3D laser scanners in camera bay of the Scanalyzer in real-time during the life cycle of the crop (i.e., from seedling establishment to harvesting stage) as mentioned in Virlet et al.,

2016. Followed by processing of these images through published pipelines to get quantitative data on plant height (Lyra et al., 2020), green canopy cover (Sadeghi-Tehran et al., 2017) and ear/ spike density (Sadeghi- Tehran et al., 2019) during the various growth stages in the crop cycle.

2.6 Brassinosteroid hormone profiling

BR hormone profiling was outsourced to The Laboratory of Growth Regulators, Palacky University, Olomouc, Czech Republic using the published protocol based on UPLC-ESI-MS/MS (Tarkowska et al 2016).

As the triple mutant is severely dwarfed compared to Cadenza, a greater number of leaves (i.e., 7) were pooled to make sufficient sample/ biological replicate as compared to other mutants and Cadenza (for which 4 leaves were pooled). The leaf tissue from seedlings was collected in 1.5 ml falcon tubes, followed by snap freezing in liquid nitrogen. The fresh weight of the tissue was noted (before snap-freezing) followed by freeze drying. Samples were sent to Olomouc for BR estimation.

2.7 Lamina joint inclination assay

To determine the sensitivity of wheat mutants to BRs, lamina joint inclination assays were conducted on seedlings. The wheat lines were sown in germination trays and grown under 16 hours light period for 10-14 days until they the second leaf emerged. Uniformly developed seedlings from each genotype to be tested were sampled, and 2 cm sections containing the 2nd leaf lamina joint, leaf sheath, and leaf blade were excised. These samples were then allowed to float in petri plates containing autoclaved water for 10 minutes. The seedling samples were then transferred to 10^{-5}M epiBL solution or autoclaved water contained in 90 mm × 15 mm petri dishes. The petri dishes were sealed using parafilm and transferred to an incubator set at 29°C in the dark for 2 days. The leaf angles were then recorded using a protractor (Li et al., 2017).

2.8 Histological analysis of lamina joint

2.8.1 Scanning electron microscopy (SEM)

Wheat seedlings were grown for 10-14 days under 16-hour photoperiod in the glasshouse. Leaf segments (approx. 1cm) including the lamina joints of the 2nd leaf were harvested. The leaf samples were then attached to aluminium stubs having

50:50 mixture of graphite and TissueTek and immediately immersed in liquid nitrogen. The samples were then transferred to a GATAN ALTO 2100 cryo-prep system and sputtered with argon gas and coated with a thin layer of gold. Micrographs were collected using JEOL JSM-6360LV scanning electron microscope (SEM) imaging software. Cell lengths were calculated using ImageJ 1.48v software. The elaborated procedure is available at: https://www.rothamsted.ac.uk/sites/default/files/Cryo-LowVac-SEM-Protocol.pdf.

2.8.2 Laser ablation tomography (LAT)

Wheat seedlings were grown for 11-12 days under 16-hour photoperiod in the growth chamber. Leaf segments (approx. 1cm) including the lamina joints of the 2nd leaf were harvested and dipped in fresh water for 5-10 minutes. These leaf segments were transferred to 100% methanol (fixation) for 2 days at 4 degree Celsius. Followed by transferring these segments to 100% ethanol (dehydration) for 2 days at 4 degree Celsius. These samples were then transferred to critical point dryer (Leica EM CPD300) to remove all the liquid from the samples without affecting the cellular structures within the tissue. Then these samples were allowed to sit (till the time for LAT imaging) in sealed containers having activated silica gel desiccant. The dried samples were attached to a magnetic clamp and transferred to LAT machine (LatScan 2.0, L4IS). The images were captured at an interval of 10 μm at 5X magnification. Number of sclerenchyma cell layers were counted manually and the widths in LJ cross section were calculated using ImageJ 1.48v software. The elaborated procedure for LAT and image capture are described in detail in recent publication (Schneider et al., 2023; Strock et al., 2019).

2.9 Statistical analysis

2.9.1 Randomisation

The genotypes to be tested were divided into blocks to reduce statistical variation in the experiment. Each block had an equal number of genotypes being tested in the experiment. These genotypes within the block were randomised using Genstat software (21.1st Edition).

2.9.2 Analysis of variance (ANOVA)

Analysis of variance was conducted for estimating statistical differences amongst various genotypes/ treatments being compared in an experiment. ANOVA was

performed using Genstat software (21.1st Edition). Which yielded *p*-values, SED, and LSD at 5% level of significance. Statistical significant difference between mutants and controls were further tested from Fisher's LSD unprotected test providing *P*-values for the comparison. Mean and residual plots for each dataset were generated to access the normality. The graphs using individual values, means, SEM and *p*-values (obtained using Fisher's unprotected LSD test) were made in Graphpad Prism software (version 9.4.0).

Chapter 3: Induced variation in the *BRI1* gene modifies plant architecture in wheat

3.1 Introduction

3.1.1 Brief introduction to the *BRI1* gene

Brassinosteroids are perceived by the transmembrane receptor known as *BRI1* (*BRASSINOSTEROID INSENSITIVE1*) which is a member of serine-threonine protein kinases (Li et al., 2001). The protein has three major domains which are essential for its function i.e., extracellular domain, transmembrane domain, and serine-threonine kinase domain (Li and Chory, 1997). The extracellular domain further comprises of the N-terminal region containing a signal peptide followed by multiple leucine-rich repeats (25 or 22 which is specific to dicots or monocots species, respectively, Navarro et al., 2015) and a 70-amino acid island domain (Noguchi et al., 1999) which is essential for BR recognition and binding (Li, 2003; Li and Jin, 2006). The extracellular domain and the cytoplasmic kinase domain are separated via a transmembrane domain. The kinase domain of the protein is highly conserved and is responsible for initiation of signal transduction by phosphorylating downstream signalling components in the pathway (Li and Chory, 1997; Noguchi et al., 1999; Friedrichsen and Chory, 2001).

3.1.2 Altered activity of the *BRI1* gene changes plant architecture in cereals

Identification of mutations in *BRI1* has led to a better understanding of the physiological roles of the gene in various species such as Arabidopsis, barley and rice (Clouse et al., 1996; Gruszka et al., 2011; Dockter et al., 2014; Morinaka et al., 2006; Sun et al., 2017). Numerous point mutations identified in the *OsBRI1* gene produced a range of phenotypes from severe to subtle (Yamamuro et al., 2000; Nakamura et al., 2006; Morinaka et al., 2006). For instance, severe alleles such as *d61-3* and *d61-4* result in extreme dwarfism and malformed leaves with the plants having no agronomic value. In contrast, a weaker allele, *d61-7* has upright leaves and

a semi-dwarf stature, yielding 35% higher biomass compared to wild-type when grown at high planting density. However, due to the smaller grains in the *d61-7* mutant, no increase in grain yield was observed compared to wild-type under the high-density planting regime. This demonstrates the negative pleiotropic effects of constitutively reduced BR signalling as it controls multiple developmental processes. Therefore, tissue specific alteration might be required to achieve upright canopy architecture, but not impacting other developmental processes, especially grain development. But partial suppression of *OsBRI1* expression using co-suppression strategy with the constitutive rice actin promoter produced more upright canopy without altering grain size thereby increasing grain yield by 30% under higher planting density (Morinaka et al., 2006).

The *uzu* barley landraces (having mutation in *HvBRI1*) have been in cultivation for over a century in central and southern Japan and southern coastal parts of Korea (Miyake and Imai 1922; Saisho et al., 2004). *uzu1.a* results in reduced plant height (80% of the wild type) due to restricted internode elongation, more upright canopy architecture (thus supporting dense planting and heavy manuring) leading to higher biomass and lodging resistance under field conditions. Due to these favourable traits, by the 1930s *uzu* varieties were grown in >70% of entire arable land in Japan and >30% in Korean peninsula (Takahashi and Yamamoto 1951). By the early 2000s all the cultivated hull-less barley varieties grown in Japan were the *uzu* type. Similarly, out of 350 semi-dwarf barley varieties developed in China during the 1950s, 68.4% were derived from *uzu* lines (Jing and Wanxia, 2003), demonstrating the widespread cultivation and adaptability of these lines in Eastern Asia. It was later discovered that these *uzu* lines had reduced sensitivity to external BR application and accumulated higher BR-related compounds compared to their non-mutant counterparts (Honda et al., 2003; Chono et al., 2003). This altered phenotype was due to a SNP mutation at A2612G location causing an amino acid substitution of His-857 with Arg-857 in the kinase domain of the protein (Chono et al., 2003). However, due to low adaptability to deep seeding and a preference for a relatively warm and humid climate, these landraces were not adopted worldwide (apart from Eastern Asia, Saisho et al., 2004).

Thus, altering activity in this gene has huge potential for tailoring plant architecture and ultimately crop improvement under changing climatic conditions.

3.1.3 *BRI1* gene family in wheat

There are some recent reports describing the identification and initial characterisation of the *BRI1* gene family in hexaploid wheat (Navarro et al., 2015; Sharma and Khurana, 2022). A high level of conservation in the gene sequence is observed across monocot and dicot species implying an essential role of the BR receptor for regulating developmental processes in these species (Navarro et al 2015; Sharma and Khurana 2022). *TaBRI1* has 94%, 89%, 84%, 82%, 74% and 69% nucleotide sequence similarity compared to *HvBRI1*, *BdBRI1*, *OsBRI1*, *ZmBRI1*, *AtBRI1* and *GmBRI1*, respectively. The *TaBRI1* genes (orthologous to *AtBRI1*) were physically mapped onto the long arms of the chromosomes 3A, 3B and 3D (Navarro et al., 2015). The predicted protein structure of TaBRI1 is very similar to AtBRI1, both containing an extracellular region with multiple LRRs forming a super-helix which has an essential role in BR binding and activation of BR-induced signalling (Navarro et al., 2015; She et al., 2011).

The *BRI1* gene family consists of four paralogues in Arabidopsis and rice namely *AtBRI1*, *AtBRL1*, *AtBRL2*, *AtBRL3* and *OsBRI1*, *OsBRL1 (BRI1-LIKE)*, *OsBRL2* and *OsBRL3* respectively (Caño-Delgado et al. 2004; Zhou et al. 2004; Nakamura et al. 2006). However, a recent study identified 106 members in the *BRI1* gene family in hexaploid wheat. These were further divided into nine paralogue groups and a representative member from each group i.e., *BRI1.1*, *BRI1.2*, *BRI1.3*, *BRI1.4*, *BRI1.5*, *BRI1.6*, *BRL1.1*, *BRL1.2* and *BRL1.3* was studied for structure prediction, phylogenetic, promoter and expression analysis (Sharma and Khurana et al., 2022).
To evaluate the phenotypic and physiological effect of reducing expression of the *BRI1* gene in wheat (orthologous to *OsBRI1*), two single knockout mutants in *TaBRI-A1* and *TaBRI-D1* were isolated in the Xiaoyan81 variety via ion beam-induced mutagenesis. It was reported that these single knockout mutants exhibited erect leaf architecture during seedling development and across the reproductive stages (0 to 30 days post anthesis). These mutants had a significant reduction in final plant height, 1000-grain weight, harvest index without any differences in the number of spikelets per spike or number of grains per spike. Additionally, these mutants had reduced photosynthetic efficiency and increased susceptibility to high light and temperature stresses (Fang et al., 2020). It is worth noting that as these mutants were backcrossed

just once (especially after isolating from a forward genetic screen) there is uncertainty about the specificity of these mutations. Thus, there is a need of a full range of sufficiently backcrossed, stable combinatorial mutants (singles, doubles, and triples) which can be used to phenotypically characterise the gene and explore its potential for wheat genetic improvement.

3.1.4 Utilizing a TILLING-based approach for understanding gene function in wheat

A technique known as TILLING (Targeting Induced Local Lesions IN Genomes) was developed almost twenty years ago as an alternative to insertional mutagenesis in *Arabidopsis thaliana* (Till et al., 2003). This technique exploited classical mutagenesis, genome sequence accessibility and high-throughput screening for nucleotide polymorphisms (SNPs) or insertions/ deletions (INDELS) in any targeted sequence (Kurowska et al., 2011). It provides an allelic series of silent, missense, nonsense, and splice-site mutations to inspect the effect of specific mutations on gene function. TILLING is recognized as an effective and efficient approach for functional genomic experiments in several plant species (Barkley and Wang 2008).

Ethyl methane sulphonate (EMS) is used as a mutagen in various TILLING experiments due to the fact it causes high mutation saturation without much DNA damage (Gilchrist and Haughn, 2005). EMS alkylates guanine which then pairs with thymine resulting in G/C to A/T transitions in the mutagenized population. As the cost of sequencing per sample has substantially reduced due to the introduction of next-generation sequencing platforms, now mutation discovery in the TILLING population is based on whole genome re-sequencing or exome capture (King et al., 2015; Krasileva et al., 2017; Mo et al., 2018).

An extensive fully mapped and annotated TILLING populations containing more than 10 million mutations in protein coding regions in 2735 mutant lines in tetraploid (Kronos var.) and hexaploid (Cadenza var.) wheat were generated by Krasileva et al. in 2017. An average of 35-40 mutations per 1000 bases per population were detected with the aid of an 84-Mb exome capture array developed by NimbleGen. It also reported the presence of approximately 23-24 missense and at least one deleterious mutation (premature stop codon or splice-site mutation) in more than 90% of the wheat genes, making it a powerful resource for gene characterization in wheat (Krasileva et al., 2017).

3.1.5 Objectives of the current study

The main aim of this work was to alter architecture (specifically canopy architecture) in wheat by manipulating BR signalling as it was beneficial in improving grain yields in other cereals. Although the *BRI1* gene was recently identified in wheat, there is still a lack of *tabri1* mutants which could be characterised in detail both phenotypically and physiologically. Therefore, we generated various combinatorial mutants using reverse genetics (after identifying deleterious mutations from the Cadenza TILLING population). In addition, we used a forward genetics approach to identify two novel alleles in *TaBRI1A* by mutation in the *tabri1-bd* background. These were sufficiently backcrossed to generate stable mutants which could be characterised in detail. To confirm the effect of *tabri1* mutations on BR biosynthesis and signalling, we analysed the BR content and performed mRNA-sequencing on the representative *tabri1* mutants at the seedling stage. In addition, a lamina joint inclination assay was used to determine sensitivity of these mutants to external BR application. A detailed evaluation of the phenotype associated with these mutations was carried out on plants grown under glasshouse conditions. Traits comprising flag-leaf angle at reproductive stage (as it determines radiation use efficiency and planting density), plant height, internode elongation (as semi-dwarf wheat varieties were lodging resistant even under higher fertiliser application which was basis of green revolution), spike and grain characteristics (as it determines the final grain yield) were recorded. This study will lead to better understanding of role of the *BRI1* gene in determining growth and development, generating mutants which could potentially improve grain yields in wheat in the farmer's field.

3.2 Results

3.2.1 Identification of *BRI1* genes in wheat

To identify orthologues of the *BRI1* genes in wheat, the rice *OsBRI1* gene sequence was used to blast against the *Triticum aestivum* var. Chinese spring, TGACv1 genome assembly (Clavijo et al., 2017). This search enabled identification of three homoeologous genes as identified in other wheat studies (Feng et al., 2020; Navarro et al., 2016) present on chromosomes 3A, 3B and 3D, namely TraesCS3A02G245000, TraesCS3B02G275000 and TraesCS3D02G246500. Orthologues of *BRI1* (using protein sequence of *OsBRI1*) in related cereal species and Arabidopsis was determined by blast analysis (Table 3.1). A phylogenetic tree was constructed to understand the relatedness of *TaBRI1* genes with those in other model species (Fig. 3.1).

Table 3. 1 Percent similarity of *BRI1* genes amongst model species. BlastP was performed in Ensembl to identify orthologues of the gene using the amino acid sequence of *OsBRI1*. The table provides the gene identifiers and their % identity with respect to *OsBRI1*.

S.No.	Species	Gene ID	Target %id
1	*Arabidopsis thaliana*	AT4G39400	78
2	*Triticum aestivum*	TraesCS3A02G245000	82.72
3	*Triticum aestivum*	TraesCS3B02G275000	77.49
4	*Triticum aestivum*	TraesCS3D02G246500	82.83
5	*Sorghum bicolor*	SORBI_3003G277900	79.2
6	*Hordeum vulgare*	HORVU.MOREX. r3.3HG0285210	82.92

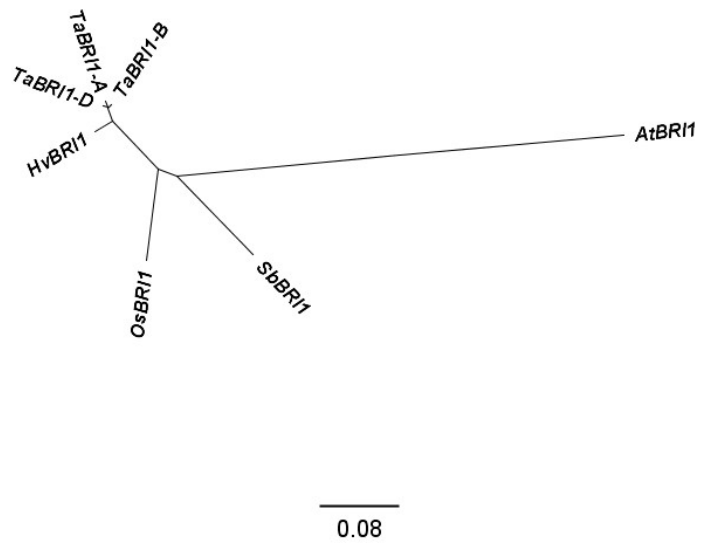

Figure 3. 1 Phylogenetic tree for *BRI1*. This tree was constructed using *BRI1* protein sequences isolated from some related species and Arabidopsis on Geneious10.2.3 software using Neighbor-joining method. The scale bar shows length of the branch.

3.2.2 Identification of conserved motifs in the *TaBRI1* protein

Cloning of the *BRI1* gene in Arabidopsis led to the understanding that the protein encodes for an LRR-RLK (Leucine Rich Repeat-Receptor Like Kinases) falling in LRR subgroup X (Li and Chory, 1997). AtBRI1 protein has N-terminal signal peptide, a leucine-zipper motif, 25 LRR (leucine rich repeats) in the extracellular domain (ED), a transmembrane region and a cytoplasmic region containing a juxtamembrane segment (JM), kinase domain (KD) and a C-terminal tail (CT**)** (Li and Chory 1997; Oh et al. 2000; Wang et al. 2005).

The ED forms a helical solenoid structure with an island domain on the concave surface (Hothorn et al. 2011; She et al. 2011). Brassinolide (BL) and castasterone (CS) which are bioactive BRs bind on the extracellular domain forming a groove (containing island domain spanning 70 amino acids and LRRs from 21 to 25) which induces BRI1 autophosphorylation (Wang et al. 2001, 2005, Kinoshita et al. 2005). There are structural rearrangements between the two loops, linking ED and the flanking LRRs upon binding with BL. Thus, after BL binding the disordered loop becomes ordered allowing a protein-protein interaction followed by initiation of BR signalling (Hothorn et al., 2011; She et al.,2011).

The cytoplasmic domain of BRI1 has three distinctive components: a juxtamembrane region, a kinase domain, and a C-terminal tail (Li and Chory, 1997). As the name suggests, the Ser/Thr kinase domain is composed of serines which are autophosphorylated (Friedrichsen et al. 2000; Oh et al. 2000). There are at least 12 autophosphorylation sites identified *in vitro* by mass spectrometry, five in the juxtamembrane region, five in the kinase domain and two in the carboxyl terminus (Oh et al., 2000). Four sites i.e. Ser-838, Thr-842, Thr-846, and Ser-858 are present in juxtamembrane region; Six sites i.e. Thr-872, Thr-880, Thr-982, Thr-1039, Ser-1042, and Thr-1049 in the kinase domain; Ser-1168 in the C-terminal region and Ser-891 in the glycine-rich loop (G-loop) of the kinase domain (functioning as a negative feedback response for reducing ATP binding (Oh et al. 2012).

Following developments in Arabidopsis, the *BRI1* gene was cloned from rice and barley in early 2000s and its role in development of these plants was investigated (Yamamuro et al 2000; Chono et al 2003). There was a high level of similarity between the orthologues except there are 22 tandem copies of LRRs in the extracellular domain in both monocot species as opposed to 25 in Arabidopsis (as shown in figure 3.3). Additionally, the 70 amino acid island domain is present between the 21st and 22nd LRR in Arabidopsis whereas it is located between the 18th and 19th LRR in rice and barley. Furthermore, the kinase domain (in the cytoplasmic region of the protein) in OsBRI1 contained all the eleven sub-domains and a high level of similarity compared to AtBRI1, as reported by Yamamuro et al in 2000.

Based on the amino acid alignment of BRI1 proteins as seen in figure 3.2 (generated using ClustalW programme in Geneious 10.2.3 software), the wheat BRI1 protein (across the homoeologues). There are 22 LRRs in wheat as reported in rice and barley (Yamamuro et al 2000; Chono et al 2003). Additionally, it is observed that much higher level of similarity exists between the protein kinase domains as compared to the extracellular domains (including the LRRs and other motifs) across various species.

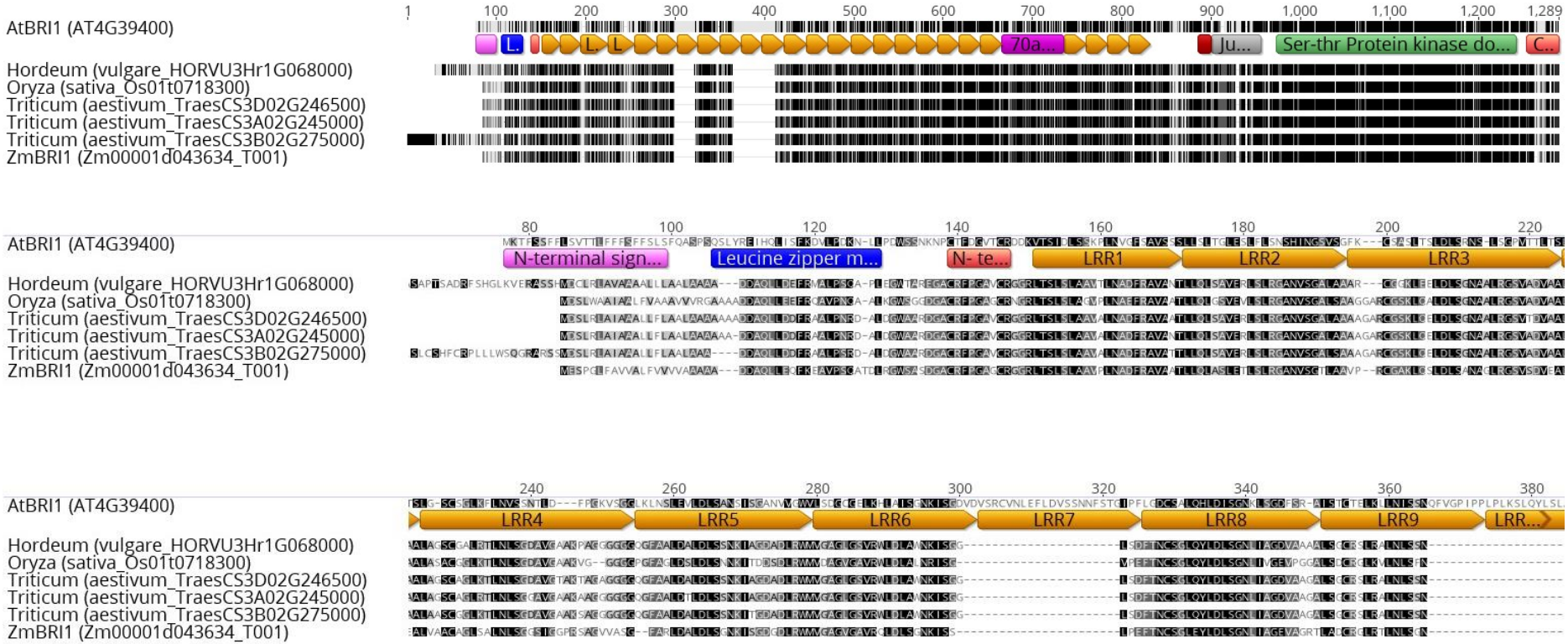
AtBRI1 (AT4G39400)
Hordeum (vulgare_HORVU3Hr1G068000)
Oryza (sativa_Os01t0718300)
Triticum (aestivum_TraesCS3D02G246500)
Triticum (aestivum_TraesCS3A02G245000)
Triticum (aestivum_TraesCS3B02G275000)
ZmBRI1 (Zm00001d043634_T001)
1
100
200
300
400
500
600
700
800
900
1,000
1,100
1,200
1,289
70a...
Ju...
Ser-thr Protein kinase do...
N-terminal sign...
Leucine zipper m...
N- te...
LRR1
LRR2
LRR3
LRR4
LRR5
LRR6
LRR7
LRR8
LRR9
LRR...

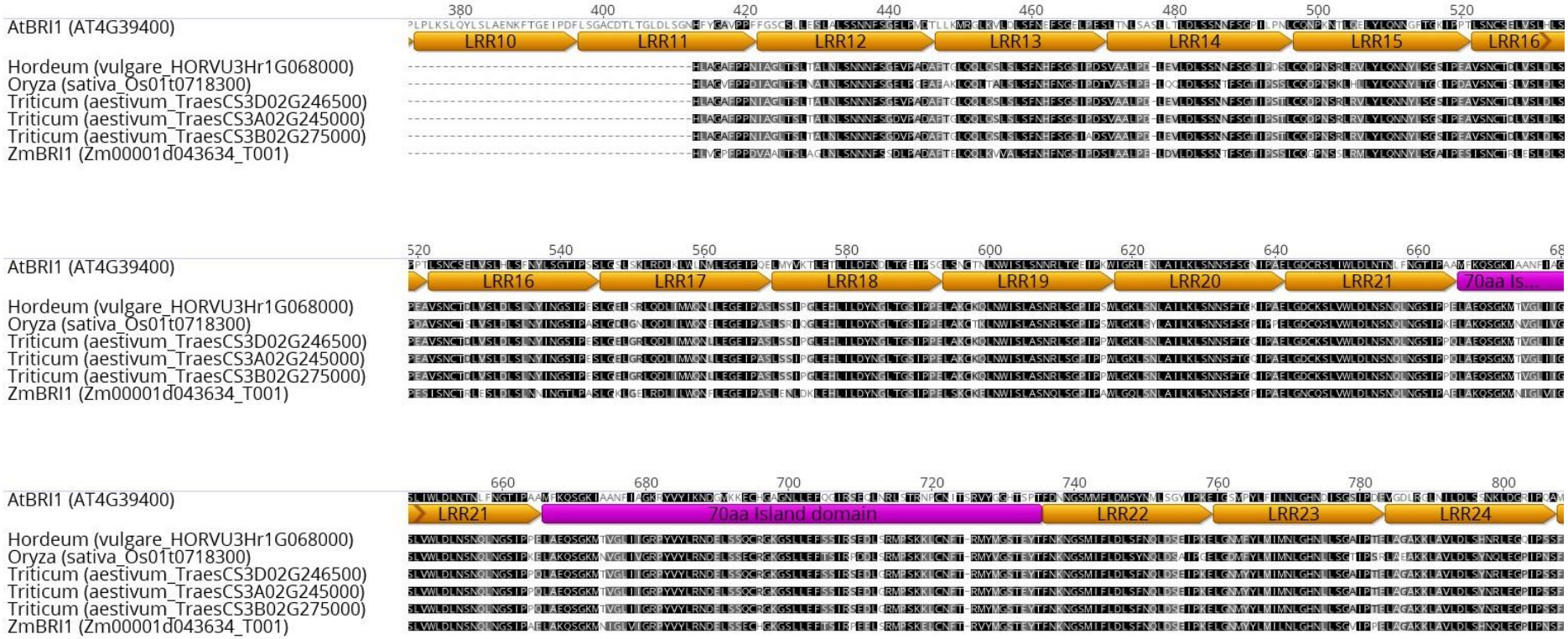
AtBRI1 (AT4G39400)
LRR10
LRR11
LRR12
LRR13
LRR14
LRR15
LRR16
LRR17
LRR18
LRR19
LRR20
LRR21
70aa Island domain
LRR22
LRR23
LRR24
Hordeum (vulgare_HORVU3Hr1G068000)
Oryza (sativa_Os01t0718300)
Triticum (aestivum_TraesCS3D02G246500)
Triticum (aestivum_TraesCS3A02G245000)
Triticum (aestivum_TraesCS3B02G275000)
ZmBRI1 (Zm00001d043634_T001)

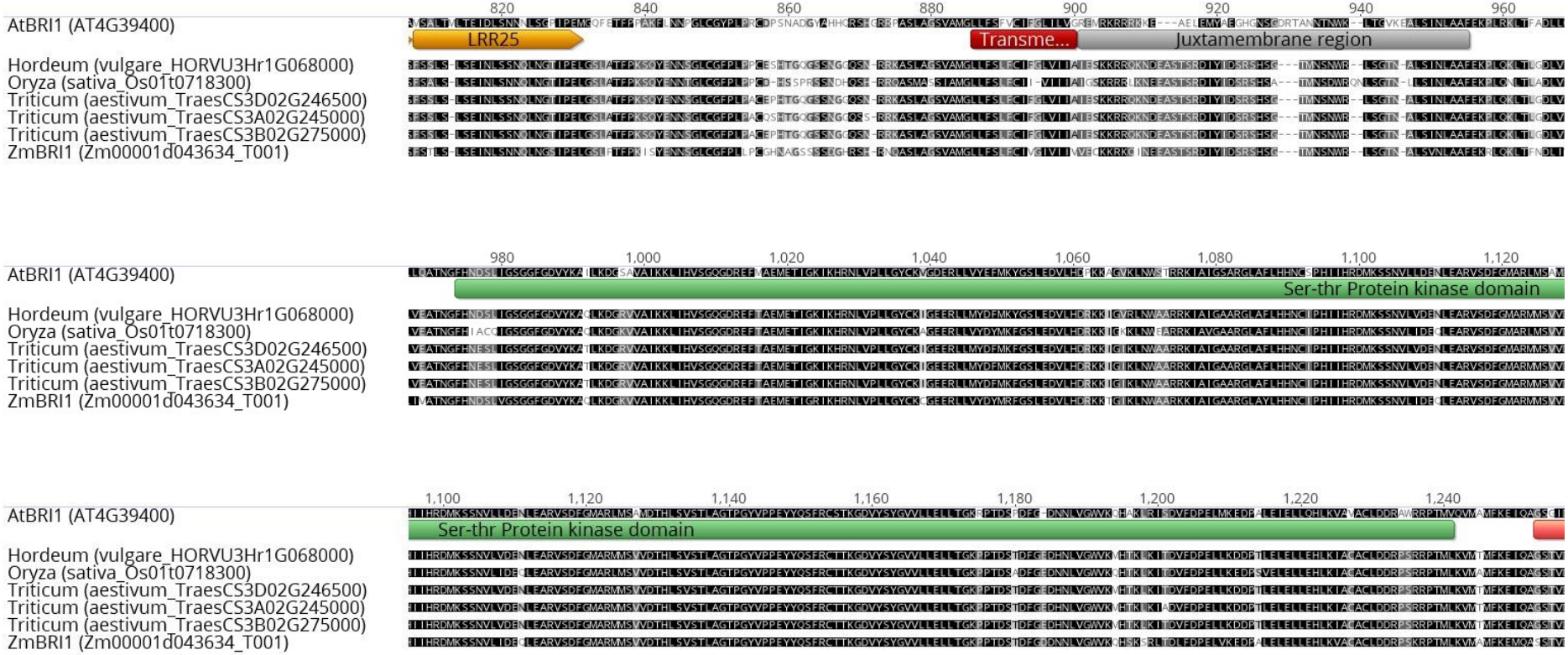
820
840
860
880
900
920
940
960
AtBRI1 (AT4G39400)
LRR25
Transme...
Juxtamembrane region
Hordeum (vulgare_HORVU3Hr1G068000)
Oryza (sativa_Os01t0718300)
Triticum (aestivum_TraesCS3D02G246500)
Triticum (aestivum_TraesCS3A02G245000)
Triticum (aestivum_TraesCS3B02G275000)
ZmBRI1 (Zm00001d043634_T001)
980
1,000
1,020
1,040
1,060
1,080
1,100
1,120
AtBRI1 (AT4G39400)
Ser-thr Protein kinase domain
Hordeum (vulgare_HORVU3Hr1G068000)
Oryza (sativa_Os01t0718300)
Triticum (aestivum_TraesCS3D02G246500)
Triticum (aestivum_TraesCS3A02G245000)
Triticum (aestivum_TraesCS3B02G275000)
ZmBRI1 (Zm00001d043634_T001)
1,100
1,120
1,140
1,160
1,180
1,200
1,220
1,240
AtBRI1 (AT4G39400)
Ser-thr Protein kinase domain
Hordeum (vulgare_HORVU3Hr1G068000)
Oryza (sativa_Os01t0718300)
Triticum (aestivum_TraesCS3D02G246500)
Triticum (aestivum_TraesCS3A02G245000)
Triticum (aestivum_TraesCS3B02G275000)
ZmBRI1 (Zm00001d043634_T001)

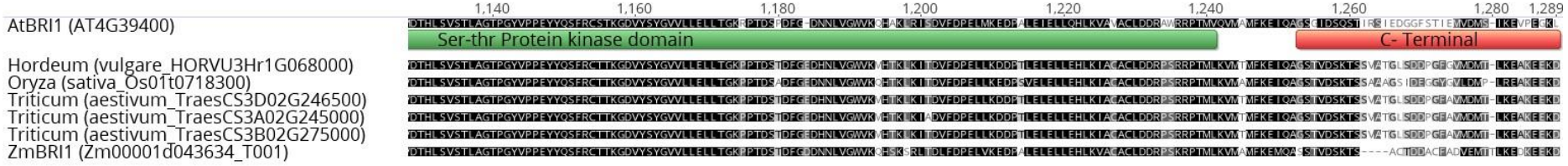

Figure 3. 2 Domains and motifs present in BRI1 proteins. The amino acid alignment compares the BRI1 proteins from Arabidopsis, maize (*Zea mays*), rice (*O. sativa*), barley (*H. vulgare*), and wheat (TraesCS3A02G245000, TraesCS3B02G275000, TraesCS3D02G246500). The positions of various domains, repeats and motifs are annotated on the AtBRI1 sequence (Li and Chory, 1997). They include the N-terminal signal peptide (pink), leucine zipper motif (blue), N-terminal (red) LRR repeats (golden), 70 aa island (magenta), transmembrane region (maroon), juxtamembrane region (grey), serine- threonine kinase domain (green) and C-terminal (red). The alignment was generated using ClustalW programme in Geneious 10.2.3 software.

3.2.3 Identification of mutations in *TaBRI1* genes and generation of combinatorial mutants

Mutations are changes in the genetic sequence which enables diversity amongst the organisms. These could be nonsynonymous (i.e., changing the amino acid sequence), synonymous (not changing the aa sequence also known as silent mutations) insertions or deletions which occur either naturally or are induced by mutagens. In genetics, mutations play a key role in understanding the molecular and physiological function of the gene (either by knocking-out or over-expressing). As hexaploid wheat (*Triticum aestivum*) usually contains three homoeologous copies of each gene that have functionally redundant roles, it is often necessary to knockout all three simultaneously to observe a mutant phenotype.

To identify loss-of-function mutations in the three homoeologous *TaBRI1* genes, we utilised the Cadenza TILLING population (cv. Cadenza) developed by Krasileva et al., 2016. The TILLING lines CAD-802, 313 and 119 were identified as containing nonsense mutations (causing premature termination of the protein) at codons 509, 273 and 447 in the coding sequence of the *TaBRI1A, TaBRI1B* and *TaBRI1D* genes, respectively (Steve Thomas personal communications). This information is also provided in Table 3.2. To confirm the presence of these mutations we amplified and sequenced the regions of *TaBRI1* gene using gene-specific markers (supplementary table1). Figure 3.3 is a schematic diagram showing the position of the premature stop-codon in tabri1 -A, -B and -D protein due to these deleterious mutations in the *TaBRI1* homoeologues. Due to the absence of 70-aa island region, transmembrane region and protein kinase domain which are essential for the protein activity (as discussed in section 3.2.2), the truncated proteins are expected to be non-functional.

Table 3. 2 *BRI1* homoeologues in wheat and the position of TILLING mutations. The position of nonsense mutations (leading to premature stop grained) identified from Cadenza TILLING population, in the *TaBRI1* genes are indicated below.

S. No.	Gene	Chromosome	Gene Id	Variant	Amino Acid substitution	Cadenza TILLING Line
1	*TaBRI1A*	3A	TraesCS3A02G245000	stop_gained	Q509*	0802
2	*TaBRI1B*	3B	TraesCS3B02G275000	stop_gained	W273*	0313
3	*TaBRI1D*	3D	TraesCS3D02G246500	stop_gained	W447*	0119

The TILLING lines containing the*TaBRI1* mutations were then stacked by inter-crossing and then backcrossed three times with wild type Cadenza to obtain the stable BC3F2 generation (as outlined in section 2.3.2). KASP-based SNP markers were designed (supplementary table 2) and were used for high-throughput genotyping of the BC3F2 generation to isolate all combinatorial mutants i.e., singles (*tabri1-a.1*, *tabri1-b* and *tabri1-d*), doubles (*tabri1-a.1b*, *tabri1-a.1d* and *tabri1-bd*) and triples (*tabri1-a.1bd* and *TaBRI1-NS*) required for phenotypic characterisation. Interestingly, the *tabri1-a.1bd* triple knockout mutant displayed a severe dwarf phenotype, with malformed leaves and the plants were completely infertile (Fig. 3.4 B) which is characteristic of *bri1* mutants identified in Arabidopsis (Clouse at al 1996). This observation provides strong evidence that the three homoeologous *TaBRI1* genes that were targeted have a major role in perceiving BRs in wheat. Additionally, Figure 3.4 (B) shows phenotype of the other combinatorial mutants at grain filling stage grown under glasshouse conditions. We observed subtle phenotypic differences (primarily in flag-leaf angle and thousand grain weight) amongst the single and double mutants compared to the *TaBRI1-NS*, which is described in greater detail in section 3.2.6 below.

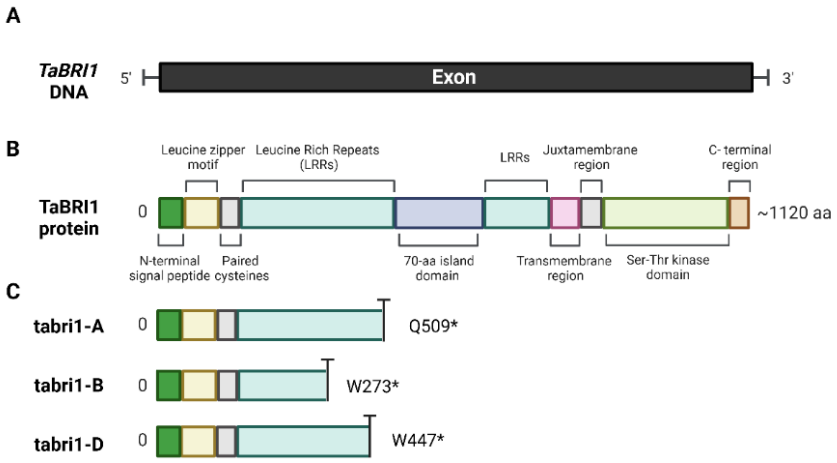

Figure 3. 3 Schematic diagram of *TaBRI1* gene and site of stop codons in the protein. (A) *TaBRI1* genes in wheat have a single exon and no intronic region, (B) Structure of TaBRI1 protein with various residues and domains. The length of the protein is approximately 1120 amino acids long, (C) The positions of the premature stop-gained in the tabri1-A, -B and -D protein leading to production of truncated non-functional protein due to absence of key domains essential for the protein function. Produced using Biorender.com.

A

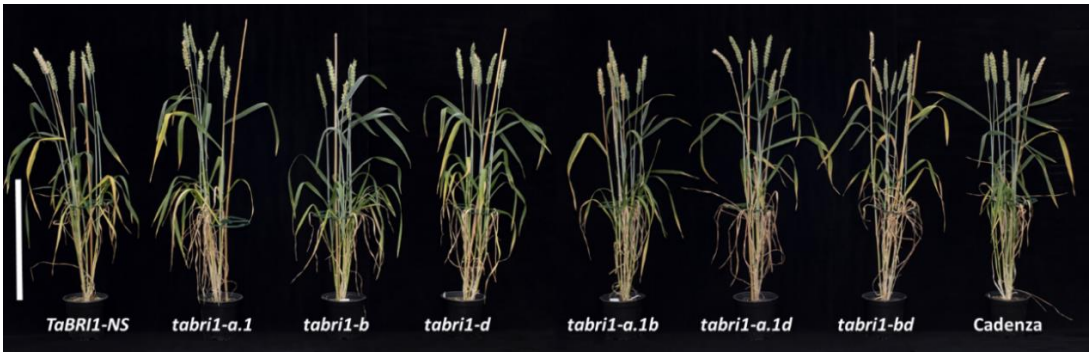

B

Figure 3. 4 Gross morphology of *tabri1* combinatorial mutants. (A) Singles, doubles, *TaBRI1-NS* and Cadenza were photographed under glasshouse conditions at GS-83. Bar length (in left) is equivalent to 40 cm. (B) Phenotype of the triple *tabri1-a.1bd* knockout mutant at 2 months after germination growing under glasshouse conditions (bar length 2.5 cm).

3.2.4 Identification of mutations in *TaBRIA1* gene using forward genetic approaches

Forward genetics is a phenotype-based approach which involves selection of the mutants (often generated using chemical or ion-beam mutagenesis) based on the trait of interest followed by identification of causative mutations responsible for the altered phenotype. For instance, various *osbri1* mutants were isolated using chemical and irradiation screens having a range of phenotype from severe (*d61-3* to *d61-6*) to weak (*d61-7* to *d61-9*) in Morinaka et al., 2006. This technique is widely used to identify novel alleles in the gene of interest. The best practical utilisation of this approach is the naturally occurring *uzu* allele (having mutation in the *HvBRI1* gene) which was widely utilised in parts of Japan, Korea, and China over the decades for making modern barley cultivars erect statured and semi-dwarf (Chono et al., 2003).

As we observed high level of functional redundancy amongst *TaBRI1* genes (as shown in Figure 3.4), we wanted to identify leaky mutations in the gene which could

potentially improve grain yields in wheat. To achieve this, we used EMS mutagenized *tabri1-bd* double knockout mutant, to identify novel leaky mutations in *TaBRI1-A* (in combination with *tabri1-b* and *-d*). The aim was to produce an allelic series of *tabri1a* mutants ranging in height from tall to severe dwarf with altered canopy architecture (upright).

Based on alteration in plant height and leaf angle (or canopy architecture) approximately 450 M2 plants were selected from 6 pools, showing either dwarfness or/and erect stature. At the time of harvesting the selected individuals were classified into <20, 20-40, 40-60, >60 cm classes (based on final plant height) with the aim to categorise the individuals based on the severity of mutations (plant height of Cadenza is ~80-90 cm in the field) as shown in Figure 3.5. A total of 9,64, 272 and 106 lines, respectively, were selected from these height classes.

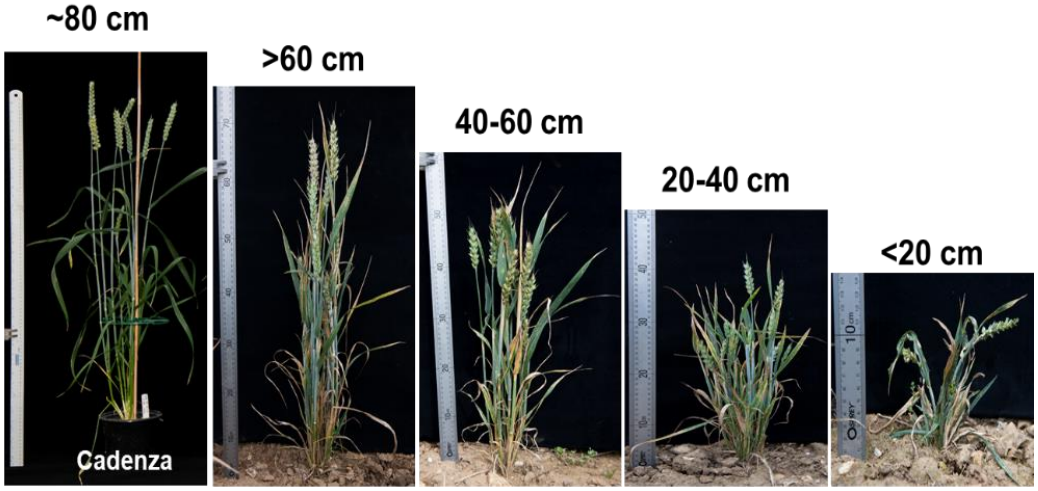

Figure 3. 5 Classification of M2 individuals based on height. Shortlisted M2 individuals were grouped into 4 height classes (i.e., <20, 20-40, 40-60 and >60 cm) during the field-based forward genetics screen in 2019.

We then initiated screening of the M3 generation derived from the M2 lines by sowing them in the glasshouse. We selected as high priority, 150 M2-derived M3 lines (having reduced height and erect canopy architecture during harvesting stage in field) and sowed them in duplicates. These M3 lines were evenly spread across the four height classes stated above. From this screen, we identified two mutants namely *M3-31* and *M3-49* as shown in Figure 3.6. *M3-31* was a more severe mutant compared to *M3-49* but as it transitioned into reproductive stage and set some seeds it was less severe than the *tabri1-a.1bd* triple knockout mutant. Phenotypically, both

these mutants had reduced plant height compared to *tabri1-bd* or *TaBRI1-NS*. Interestingly, *M3-49* displayed more erect flag leaf angles (at reproductive stage) compared to *tabri1-bd* double knockout mutant, but *M3-31* produced malformed leaves. But as these mutants were not backcrossed so it was not possible to draw many conclusions from the phenotype at this stage. However, as these mutants resembled some *BRI1* mutants in rice and barley they were interesting targets for further studies (Yamamuro et al., 2000; Morinaka et al., 2006; Dockter et al., 2014).

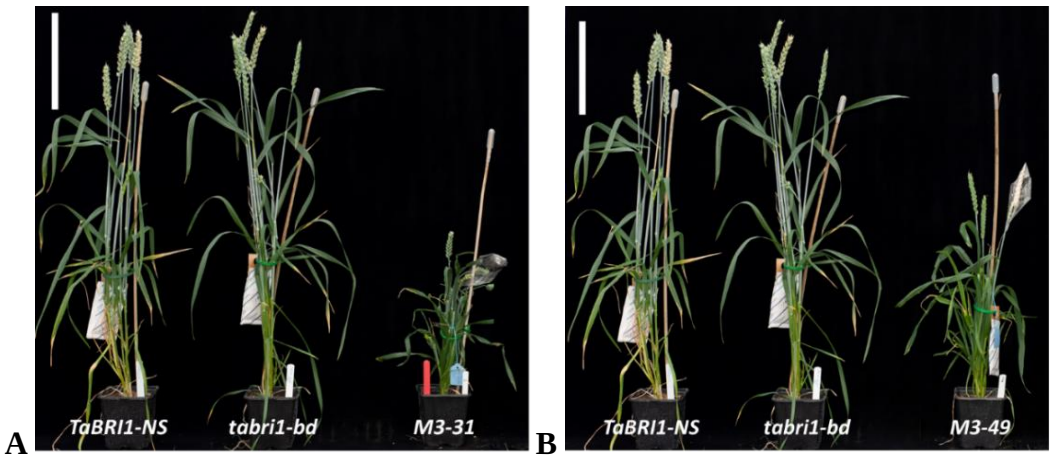

Figure 3. 6 Gross morphology of novel *tabri1* triple mutants. Phenotype of *M3-31* (A) and *M3-49* (B), *tabri1-bd* and *TaBRI1-NS*. These photographs were taken when the genotypes at GS-73 stage under glasshouse conditions. Bar length (on left) is 20 cm.

Our next objective was to uncover the genetic basis for the altered phenotype in these mutants isolated from the field screen. To start with, as the EMS treatment was done on *tabri1-bd* mutant, we hypothesized the phenotype we observe might be due to leaky mutations in the third functional copy of the gene i.e., *TaBRI1-A*. To uncover this, we sequenced the *TaBRI1-A* gene (in *M3-31* and *M3-49*) using four overlapping gene-specific primer pairs (as the approximate length of the gene was near 4kb, each primer pair could amplify approximately 1kb region in the gene) and sequenced the PCR products (using set protocols mentioned in section 2.1). The strategy followed for doing this is shown in Figure 3.7. The amplified PCR products were then aligned against the *TaBRI1-A* gene sequence (obtained from Cadenza and *TaBRI1-NS*) to identify the presence of mutations (if any) in *M3-31* and *M3-49*.

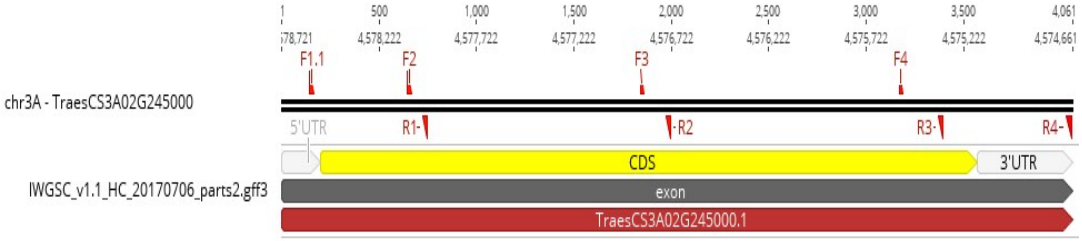

Figure 3. 7 Overlapping primer-pairs used to amplify *TaBRI1-A*. Positions of the overlapping pair of primers used to sequence the *TaBRI1-A* gene to identify SNP-based polymorphism (if any) compared to the reference sequence. Geneious software (v.10.2.3) was used for designing these primers and sequence alignment against TraesCS3A02G245000.

Following this approach, we identified two novel missense mutations in the *TaBRI1-A* gene at C2011T (cDNA position changing Cca to Tca) or P671S (protein position) in *M3-31* mutant and G3023A (cDNA position changing gGg to gAg) or G1008E (protein position) in *M3-49* mutant. The G to A and C to T substitution is the common feature of EMS-based mutagenesis resulting in SNP variation (Krasileva et al., 2017). These mutants were then named *tabri1-a.2bd* (*M3-31*) and *tabri1-a.3bd* (*M3-49*). The mutation in 671st aa corresponds to 22nd LRR and 1008th aa corresponds to serine-threonine kinase domain of the gene as demonstrated schematically in figure 3.8 below.

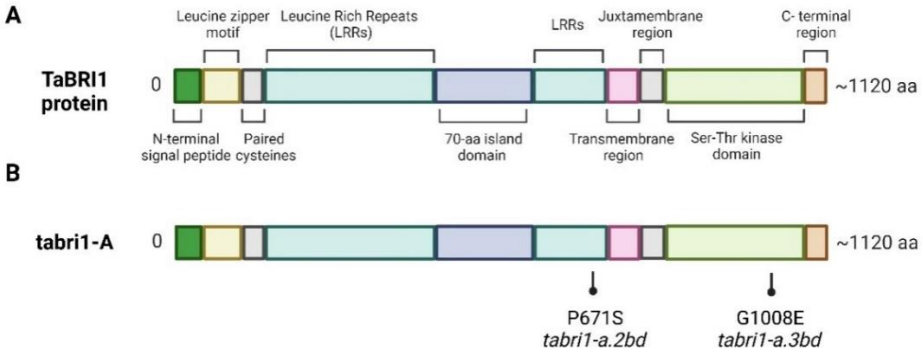

Figure 3. 8 Positions of novel missense mutations in tabri1-A protein. (A) Shows the schematic diagram of TaBRI1 protein with various domains and residues designated with different colour boxes. The length of the protein is approximately 1120 amino acids. (B) Relative position of missense mutations in *TaBRI1-A* gene in *tabri1-a.2bd* (P671S on protein or G2212A on cDNA sequence) and *tabri1-a.3bd* (G1008E on protein or C3224T on cDNA sequence) mutant identified in *tabri1-bd* background using EMS-based forward genetic screen. Produced using Biorender.com.

Luckily, both these mutations (on same residues of *TaBRIA1* gene) were also present in the Cadenza TILLING population. Cad1138 line had P671S aa change as observed in *tabri1-a.2bd* mutant. Cad0527 line had G1008E aa change as identified in *tabri1-a.3bd* mutant. Therefore, to validate the phenotype of our novel *tabri1* triple mutants (as the phenotype observed could be due to any other unidentified mutation as they were isolated from a TILLING population which is a random mutagenesis approach) we crossed the above stated Cadenza TILLING lines with the *tabri1-bd* mutant (followed by selfing to generate the F2 population). The aim from generating this cross was to try replicating the phenotype of the triple mutants we identified, but using mutations from separate TILLING populations (i.e., Cad TILLING lines will have different set of background mutations compared to our mutant population). Interestingly, the phenotype of *tabri1-a.2bd* mutant (mutation in *TaBRI1A* gene identified from our TILLLING population) was very similar to *tabri1-a.2'bd* mutant (same mutation in *TaBRI1A* gene identified from Cadenza TILLING population) at flowering stage (GS65) as shown in figure 3.9 below. This demonstrates that the phenotype we observe in the *tabri1-a.2bd* mutant is primarily due to mutations in *tabri1A*. Similarly, we crossed the Cad0527 mutant with the *tabri1-bd* mutant to replicate the phenotype of the *tabri1-a.3bd* mutant. However, we did not observe a similar phenotype (not shown) in this mutant due to unidentified reasons.

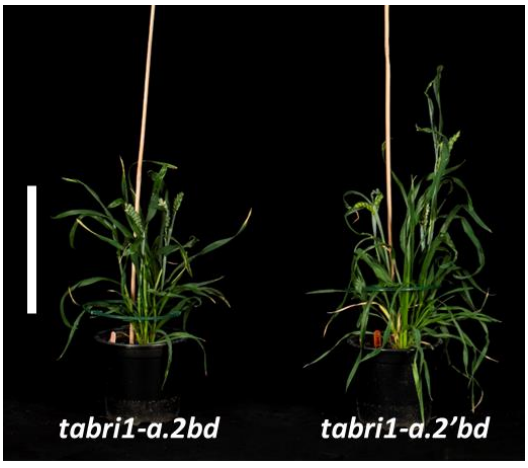

Figure 3. 9 Gross morphology of *tabri1-a.2bd* and *tabri1-a.2'bd* mutant. Phenotype of *tabri1-a.2bd* mutant (mutation in *TaBRI1A* gene identified from our EMS-based TILLING population) and *tabri1-a.2'bd* mutant (same mutation in *TaBRI1A* gene but identified from Cadenza TILLING population) was very similar at flowering stage (GS65). Bar length (on left) is 20 cm.

3.2.5 *tabri1* mutants display reduced sensitivity to external BR application

BR insensitive mutants (especially having mutation in the *BRI1* gene) displayed reduced sensitivity to external BR application in rice and barley (Yamamuro et al., 2000; Chono et al., 2003), demonstrating inability of these *bri1* mutants to utilise endogenous bioactive BRs for initiating growth and development.

The lamina joint inclination assay is a robust method for testing sensitivity of the mutants (biosynthetic and signalling) to external BR application (Li et al., 2017). The assay was performed on the triple mutants (*tabri1-a.2bd* and *tabri1-a.3bd* excluding the most severe, *tabri1-a.1bd* mutant due to seed shortage), a representative double knockout mutant i.e., *tabri1-bd* and controls *TaBRI1-NS* and Cadenza. The single and other double mutants were excluded from the experiment as we observed only subtle phenotypic changes due to these mutations due to functional redundancy of the *TaBRI1* homeologues.

Leaf angles were measured after treating the lines with 10^{-5}M epiBL and water. A paired *t*-test was performed to estimate statistically significant differences (if any) in the genotypes before and after treatment. Interestingly, no significant increase in the LA was observed after treatment of the triple mutants (*tabri1-a.2bd* and *tabri1-a.3bd*), with 10^{-5}M epiBL whereas a significant increase in the LA was observed in *tabri1-bd, TaBRI1-NS* and Cadenza after treatment with 10^{-5}M epiBL compared to the water control (Figure 3.10). This result confirms our hypothesis that these novel mutations in *TaBRI1A* (in the *tabri1-bd* background) reduce BR-sensitivity by suppressing downstream signalling.

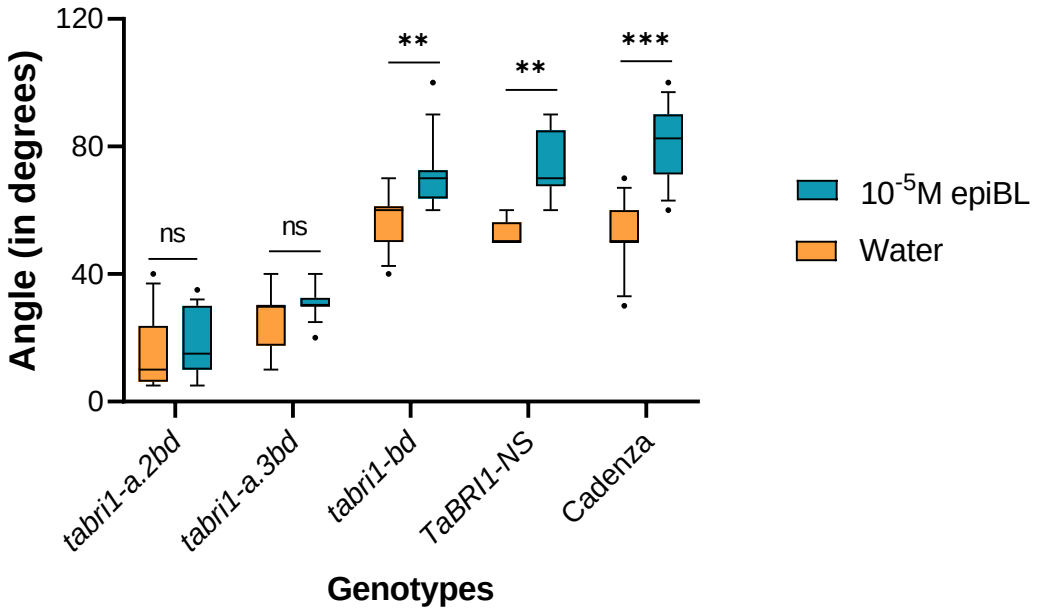

Figure 3. 10 Response of *tabri1* mutants to external BR application. The lamina joint inclination assay was performed on *tabri1-a.2bd*, *tabri1-a.3bd* and *tabri1-bd* mutant along with *TaBRI1-NS* and Cadenza as controls. Leaf angles were noted (n=15) in these genotypes with (10^{-5}M epiBL) and without (water) BR treatment. The data are plotted as a box and whisker plot. The line in the middle (of the box) is median, edges of the box representing 25 and 75 percentiles, whiskers are 10 and 90 percentiles and dots above/ below these are outliers. Statistical significances were denoted by adjusted *P* values * < 0.05, ** < 0.01, *** < 0.001 (obtained by Pairwise *t*-test).

3.2.6 *tabri1* mutants accumulate intermediates and bio-active products of the BR biosynthesis pathway

BR-insensitive mutants in Arabidopsis, rice and barley accumulate higher levels of bioactive BRs such as BL or CS when compared to the wild-type controls (Nomura et al., 1997; Noguchi et al., 1999; Choe et al., 2002; Yamamuro et al 2000). The elevated BR levels in BR-insensitive mutants are due to suppression of the feedback mechanism that down-regulates expression of BR biosynthesis genes in response to BR signal transduction (Yu et al, 2011). It is known that the sterol pathway provides the precursors for BR biosynthesis, in which campesterol (CR) is converted to campestanol (CN) leading to the production of the bio-active BRs brassinolide (BL) and castasterone (CS) via two parallel routes namely the early and late C-6 oxidation pathways as shown in Figure 3.11 **(**a detailed description of the pathway is provided in section 1.6.3).

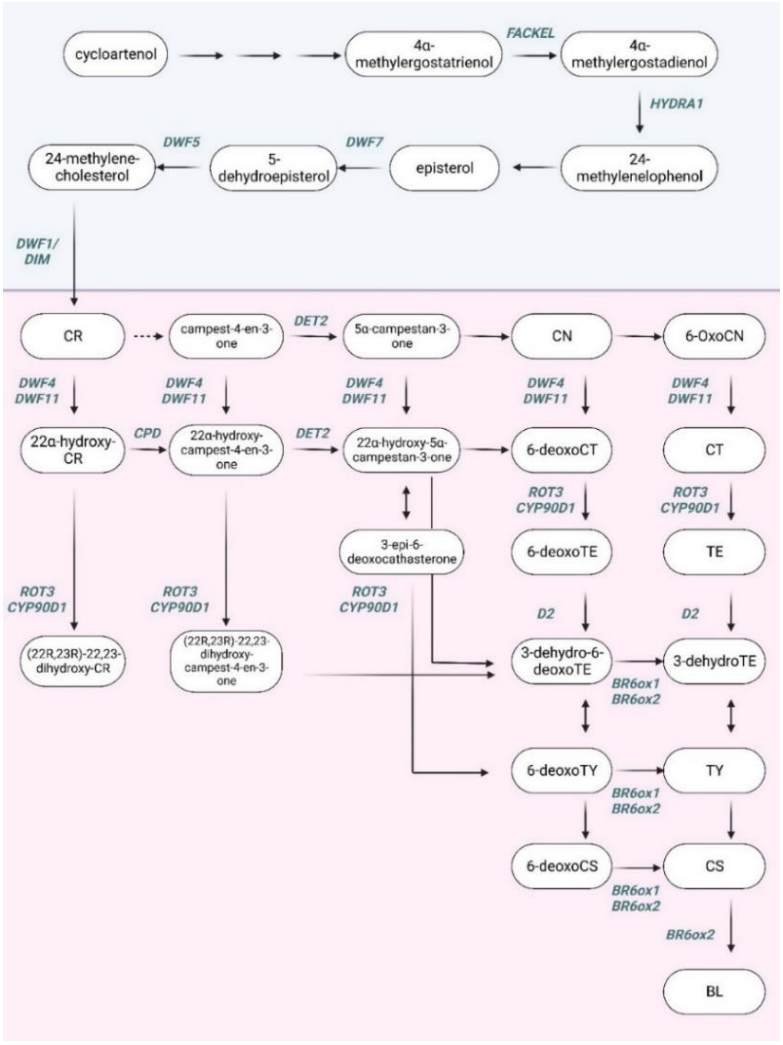

Figure 3. 11 Steps in sterol and BR-biosynthesis pathway. Products of the sterol pathway (in blue background) are precursors for the BR-specific biosynthesis pathway (in pink background). C28-BR-specific biosynthesis pathway leads to production of bioactive BRs such as castasterone (CS) and brassinolide (BL). The names of the genes and enzymes catalysing each step is shown above the arrows. Pathway was produced using Biorender.com.

There is limited information available about the BRs present in wheat. Five BRs i.e., 3-dehydroTE, TY, TE, 6-deoxoCS and CS were detected in wheat grain by Yokota et al., 1994 and three BRs i.e., 24-epiBL, BL and CS were detected from wheat seedlings in a study by Janeczko and Swaczynova, 2010. No information is currently available about the impact of mutations in *TaBRI1* on the flux through the BR-biosynthesis pathway. Therefore, we designed an experiment to estimate the BR content in seedlings of the *tabri1* mutants i.e., triple mutants (*tabri1*-a1.bd, *tabri1-a.2bd* and *tabri1-a.3bd*), double mutant *tabri1-bd* (as novel tabri1 mutations were identified in this background) and controls *TaBRI1-NS* and Cadenza grown in

continuous light. Samples were analysed by UHPLC-MS/MS at The Laboratory of Growth Regulators, Palacky University, Olomouc, Czech Republic using a published protocol for measuring 22 BRs and related sterols (Tarkowska et al., 2016).

The data generated was analysed using One-way ANOVA which yielded *p*-values, SED, and LSD at 5% level of significance which are presented below in Table 3.3 and illustrated in Figure 3.12. For the pairwise comparison amongst the mutants Fisher's unprotected LSD test was performed and the data are displayed diagrammatically in figure below.

Nine BRs were detected in *tabri1* wheat mutants and Cadenza namely CR, CN, 6-oxoCN, 6-deoxoCT, 6-deoxoTY, TY, CS, BL, and epiCS (which are more than reported for wheat in previous studies). ANOVA confirmed statistically significant differences for BR content, amongst *tabri1* mutants as the *p*-values obtained were <0.001. The levels of the bioactive BRs like CS were increased by 390-, 12- and 2.7-fold in the triple mutants *tabri1-a.1bd, tabri1-a.2bd* and *tabri1-a.3bd* respectively, compared to *TaBRI1-NS* but its increase was not significant in the double mutant, *Tabri1-bd*. We observed approx. 9- fold accumulation in the BL content in the most severe triple knockout mutant i.e., *tabri1-a.1bd* compared to the *TaBRI1-NS* with no significant differences for the other BR mutants. Thus, demonstrating elevated levels of CS and BL in the triple mutants is in agreement with the previous studies in Arabidopsis, rice, and barley (Nomura et al., 1997; Noguchi et al., 1999; Choe et al., 2002; Yamamuro et al 2000). Interestingly, Brassinolide (BL) was also detected, as reported by Janeczko and Swaczynova, 2010, while it was not detected in other cereals such as rice and barley (Chono et al., 2003, Yamamuro et al., 2000; Kim et al., 2008).

Additionally, we observed significant accumulation of TY and 6-oxoCN, which are intermediates in the early C-6 oxidation pathway, in the *tabri1-a1.bd* mutant compared to *TaBRI1-NS*. There was also a significant accumulation of 6-deoxoCT, an intermediate in the late C-6 oxidation pathway, in *tabri1-a.1bd* compared to *TaBRI1-NS*. We also observed a 1.2- fold increase in the level of the late intermediate CR in the *tabri1-a.1bd* mutant compared to the null-segregant.

These results demonstrate that in the severe triple mutant (*tabri1-a.1bd*) the feed-back loop is inactive even at elevated levels of CS/BL. This agrees with the previous

known information, that BL/CS upon binding with the *BRI1*-receptor not only activates various downstream genes via *BZR2* and *BZR1* transcription factors but is also responsible for activating feedback inhibition of various BR biosynthesis pathway genes to suppress their expression and down-regulate BR biosynthesis (He et al., 2005; Yu et al., 2011).

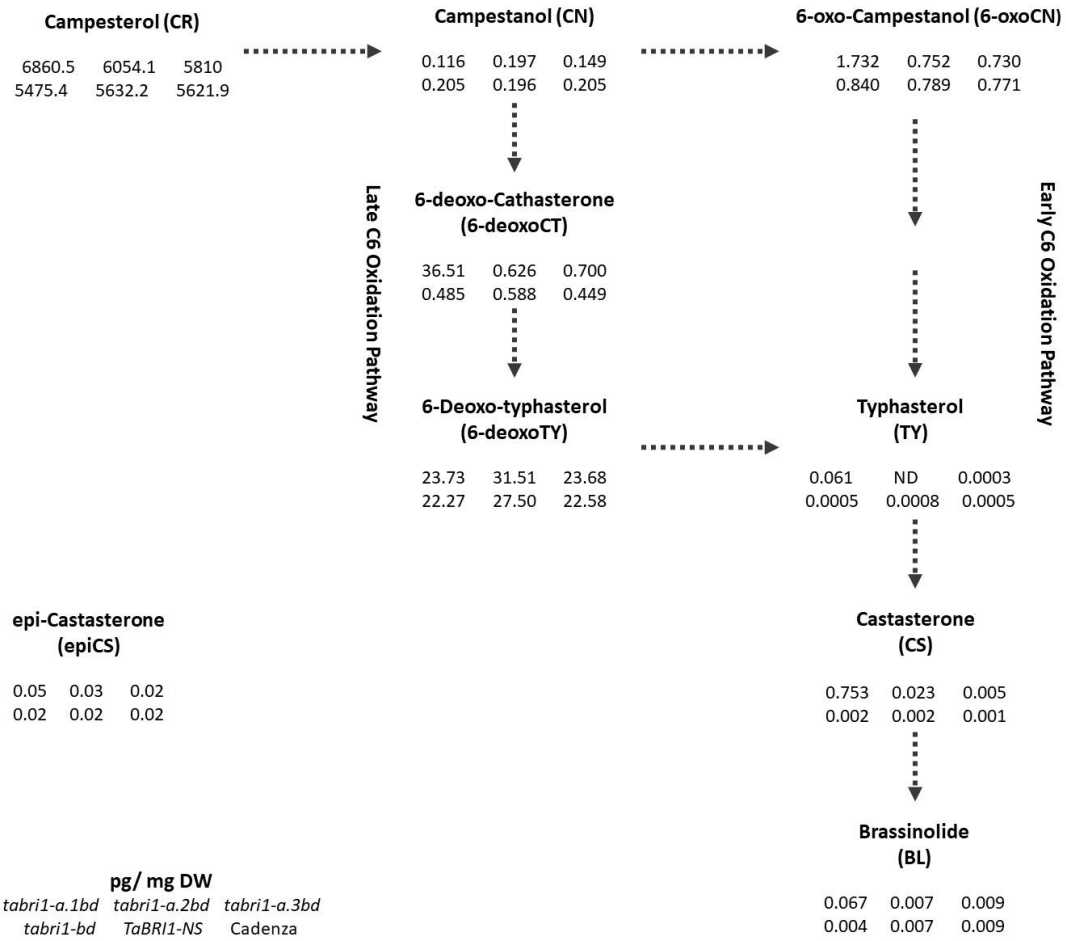

Figure 3. 12 BR hormone levels in *tabri1* mutants and controls. The mean values of BR contents (in pg/mg DW) were estimated in *tabri1* mutants (*tabri1-a.1bd*, *tabri1-a.2bd*, *tabri1-a.3bd*, *tabri1-bd*) and controls (*TaBRI1-NS* and Cadenza). CR is the first substrate of the BR-biosynthesis pathway in which it is converted to CN. 6-deoxoCT and 6-deoxoTY are substrates in the Late C6 oxidation pathway whereas, 6-oxoCN, TY, CS and BL are BRs specific to the Early C6 oxidation pathway.

		tabri1-a.1bd	*tabri1-a.2bd*	*tabri1-a.3bd*	*tabri1-bd*	*TaBRI1-NS*	Cadenza	*p*-value	SED	LSD at 5%
BR content (pg /mg DW)	**CR**	6860.5 ± 690.9***	6054.1 ± 238.6	5810 ± 247.5	5475.4 ± 544.7	5632.2 ± 427.3	5621.9 ± 241.6	<0.001	237.3	498.6
	CN	0.116 ± 0.01**	0.197 ± 0.02	0.149 ± 0.01*	0.205 ± 0.05	0.196 ± 0.02	0.205 ± 0.02	0.001	0.019	0.04
	6-oxoCN	1.732 ± 0.11***	0.752 ± 0.06	0.730 ± 0.09	0.840 ± 0.08	0.789 ± 0.15	0.771 ± 0.04	<0.001	0.057	0.119
	6-deoxoCT	36.51 ± 4.11***	0.626 ± 0.06	0.700 ± 0.07	0.485 ± 0.06	0.588 ± 0.06	0.449 ± 0.07	<0.001	0.788	1.655
	6-deoxoTY	23.73 ± 3.51	31.51 ± 1.89*	23.68 ± 2.82	22.27 ± 4.62*	27.50 ± 1.29	22.58 ± 2.81*	<0.001	1.877	3.943
	TY	0.061 ± 0.01***	ND	0.0003 ± 0.00	0.0005 ± 0.00	0.0008 ± 0.00	0.0005 ± 0.00	<0.001	0.002	0.004
	CS	0.753 ± 0.02***	0.023 ± 0.00***	0.005 ± 0.00	0.002 ± 0.00	0.002 ± 0.00	0.001 ± 0.00	<0.001	0.004	0.009
	BL	0.067 ± 0.02***	0.007 ± 0.00	0.009 ± 0.00	0.004 ± 0.00	0.007 ± 0.00	0.009 ± 0.01	<0.001	0.006	0.012
	epi-CS	0.04 ± 0.01****	0.03 ± 0.01	0.02 ± 0.01	0.02 ± 0.00	0.02 ± 0.01	0.02 ± 0.01	<.001	0.004	0.009

Table 3. 3 BR levels (pg/mg DW) in *tabri1* mutants and controls. Mean values (pg/mg DW) ± SD are shown for four *tabri1* mutants along with controls i.e., *TaBRI1-NS* and Cadenza at the seedling stage. The data were analysed using one-way ANOVA which yielded *p*-values, SED, and LSD at 5% level of significance. Fisher's unprotected LSD test was performed for multiple pair-wise comparisons. Statistically significant difference between mutants and *TaBRI1-NS* were denoted *$P < 0.05$, **$P < 0.01$, ***$P < 0.001$, ****$P < 0.0000$ (obtained from Fisher's LSD unprotected test).

3.2.7 BR pathway genes are differentially expressed in the *tabri1* mutants

Mutations in the *BRI1* gene leads to upregulation of BR-biosynthesis genes and an accumulation of bioactive BRs and some intermediates due to blockage in BR signalling (Noguchi et al., 1999; Noguchi et al., 2000). Thus, an intact BR signalling pathway is critical for regulating BR homeostasis. On the other hand, the presence of bioactive BRs and intact BR perception complex, are required for activation of the cascade of events occurring in the cell with the aid of various transcription factors (such as *BZR1* and *BZR2*) which activate the BR signalling machinery that promotes expression of BR-induced genes for regulating growth and development (Yin et al., 2005 and Yu et al., 2011). The BR-induced signalling pathway is described briefly in Figure 3.14 and is described in greater detail under section 1.7 of the general introduction.

To understand the effect of the mutations in *TaBRI1* on the expression of genes involved in the sterol, BR-specific biosynthesis and signalling pathway mRNA-sequencing was performed with *tabri1-a.1bd*, *tabri1-a.2bd*, *tabri1-a.3bd*, *tabri1-bd*, *TaBRI1-NS* and Cadenza (on the same tissue i.e., entire above ground seedling at 2nd leaf stage, as used for BR estimation). Table 3.4 shows the total number of reads, total mapped reads, and mapping efficiency (%) for these genotypes from mRNA-sequencing.

Table 3. 4 Number of read counts per genotype from mRNA sequencing. The number of total reads, total mapped reads, and mapping efficiency (%) calculated based on the number of counts/gene/genotypes.

	Number of counts					
	tabri1-a.1bd	***tabri1-a.2bd***	***tabri1-a.3bd***	***tabri1-bd***	***TaBRI1-NS***	**Cadenza**
Total mapped reads	32937529.33	30788795.5	29003801	26376738.25	32108424.5	32309016
Total reads	40934022.67	38222113.25	35860754.5	32398203.5	39398513.25	40096748.25
Mapping efficiency (%)	80.44	80.55	80.87	81.41	81.48	80.59

We observed significant accumulation of BR levels in our most severe triple mutants i.e., *tabri1-a.1bd* and *tabri1-a.2bd*, which we hypothesized is due to increased transcript abundance of biosynthetic genes. Additionally, there might be a change in the expression levels of BR-signalling and down-stream transcription factor genes in these mutants. Therefore, differential gene expression (DEG) of BR pathway genes was determined from TPMs (templates per million) for the set of genes reported in Ptošková et al., 2022.The results are represented by heatmaps displayed in Figure 3.13 and 3.14. Differential expression was determined by pairwise comparison between the mutants and *TaBRI1-NS* (using DEseq2 package on R) from which log_2fold changes and adjusted *p*-values were calculated. The maximum differentially expressed genes (related to BR-pathway) were observed in the most severe triple mutants i.e., in *tabri1-a.1bd* followed by in *tabri1-a.2bd* and the least differences in *tabri1-a.3bd* (supplementary Table 3**).** No significant differences in DEG were observed in the less severe *tabri1-bd* double mutant compared to *TaBRI1-NS* (data not shown).

Expression of the BR biosynthesis pathway genes *DWF4*, *CPD*, *ROT3*, *BR6oxs* (*DWF*) was significantly up-regulated in the *tabri1-a.1bd* and *tabri1-a.2bd* mutants compared to *TaBRI1-NS* with adjusted *p*-values <0.05 (supplementary Table 3). This is consistent with the elevated levels of the bioactive BRs CS and BL in these mutant as discussed in section 3.2.6 and supports earlier studies (Noguchi et al., 1999; Noguchi et al., 2000).

Expression of the BR signalling genes *TaBZR1*, *TaBAS1*, *TaBEN1* and *TaCDG1* was significantly reduced in the *tabri1-a.1bd* mutant compared to *TaBRI1-NS* with adjusted *p*-values <0.05 (supplementary Table 3). However, this was not observed for the less severe *tabri1* mutants *tabri1-a.2bd*, *tabri1-a.3bd* and *tabri1-bd* compared to *TaBRI1-NS*.

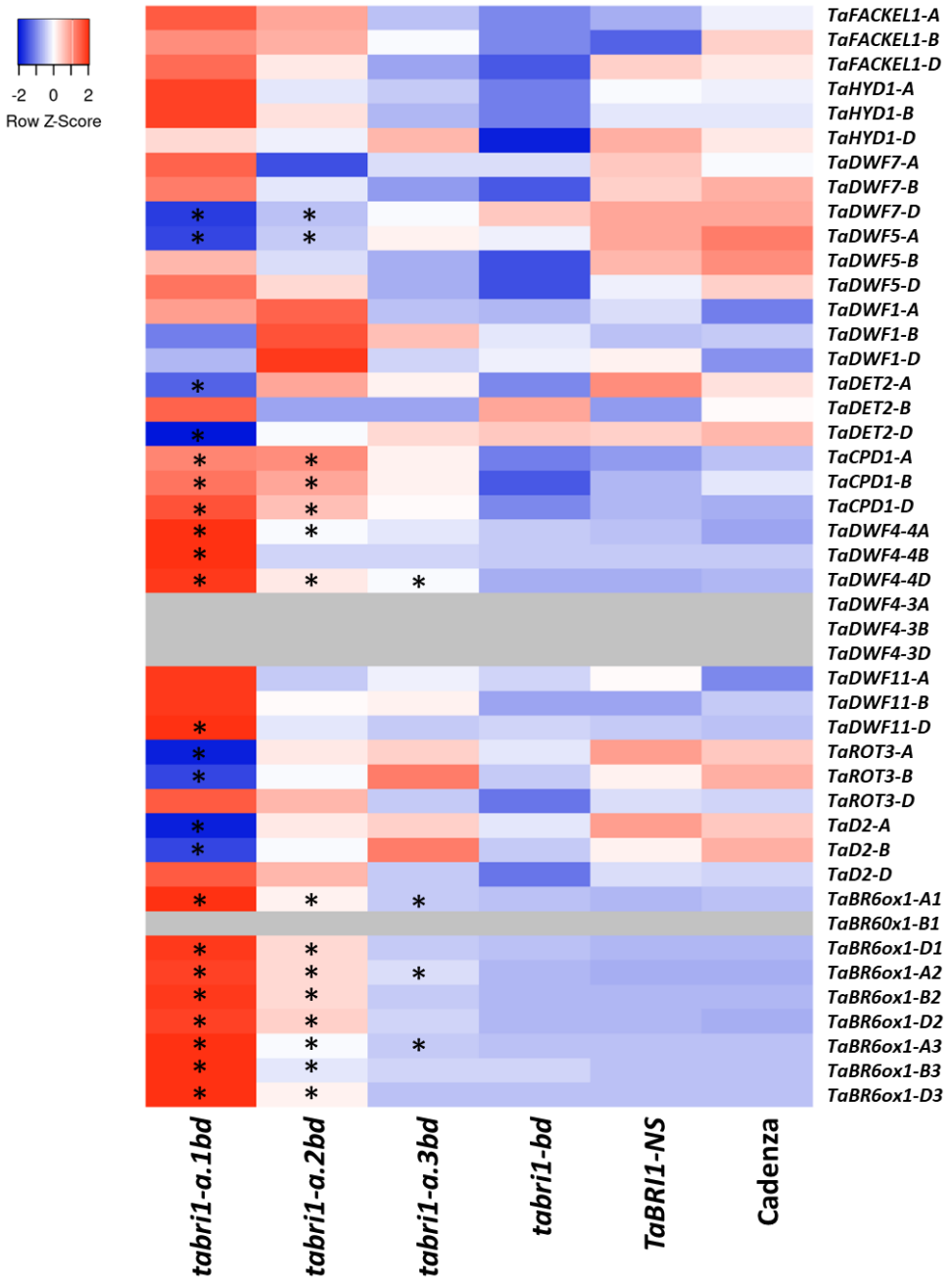

Figure 3. 13 Expression of BR biosynthesis pathway genes in *tabri1* mutants. The heatmaps compare expression levels of genes in sterol and BR-biosynthesis pathway in the *tabri1-a.1bd*, *tabri1-a.2bd* and *tabri1-a.3bd*, *tabri1-bd* mutants and controls *TaBRI1-NS* and Cadenza using normalised number of counts/genes generated using Heatmapper (http://www.heatmapper.ca/). Statistical significant differences in gene expression in mutants compared to *TaBRI1-NS* are highlighted using asterisks (*).

A

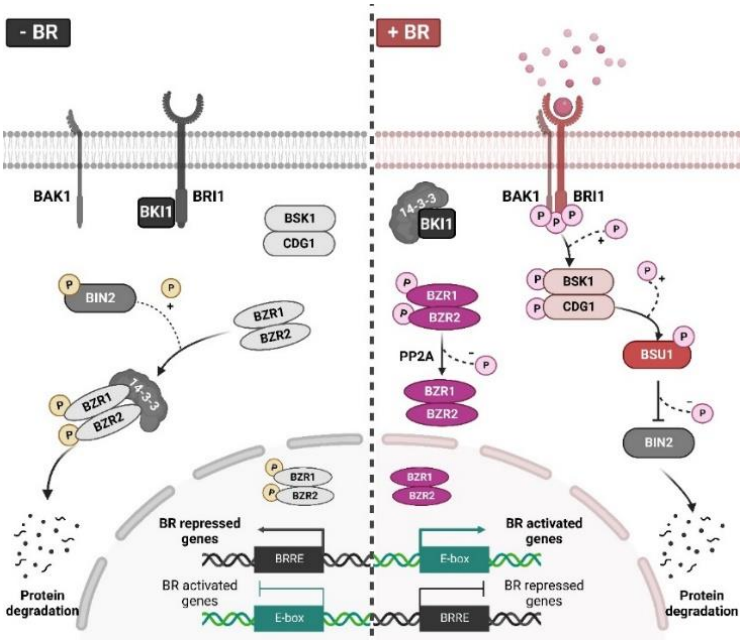

B

BRI1

↓

BKI1

↓

BAK1

↓

BSK1/ CDG1

↓

BZR1/ BZR2

↓

BIN2

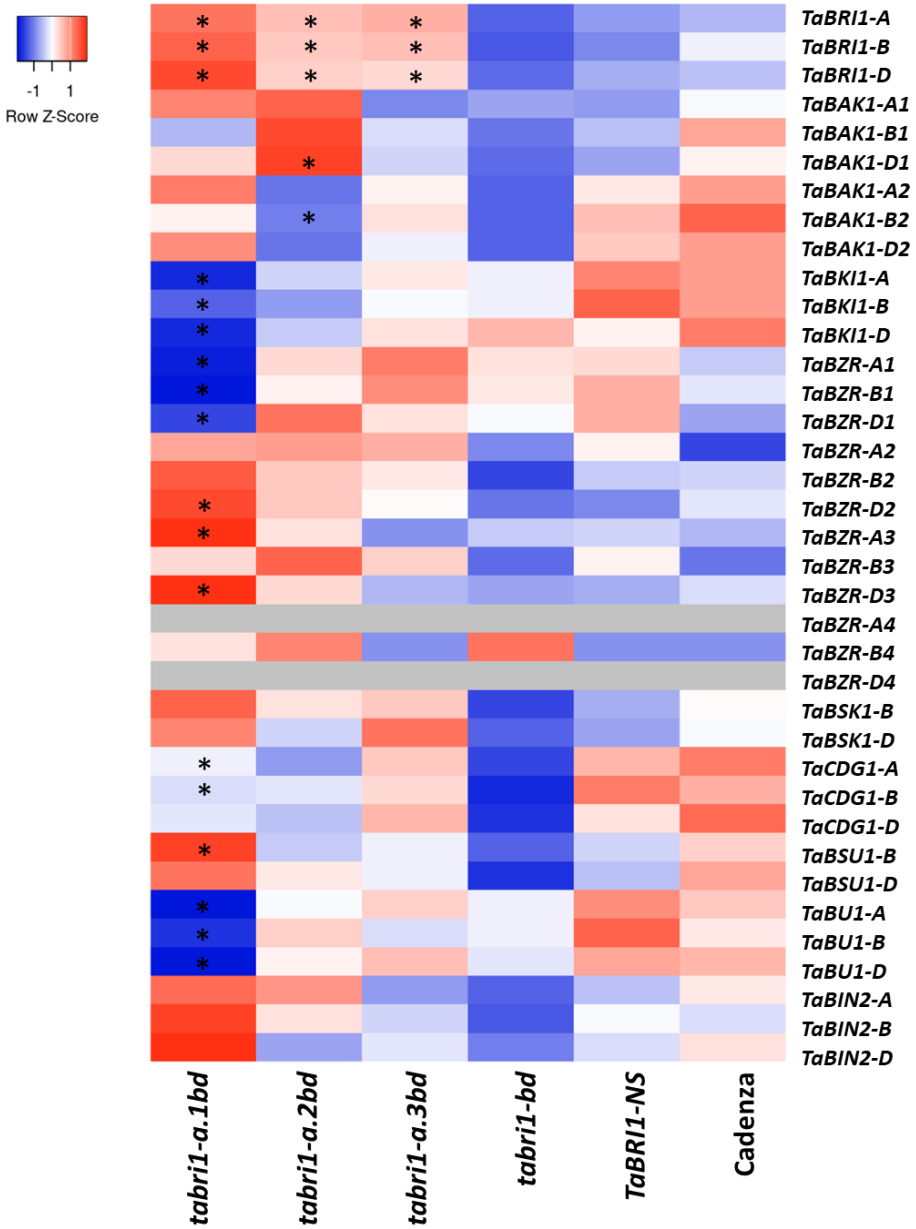

C

Figure 3. 14 Expression of BR signalling genes in *tabri1* mutants. (A) Represents various steps involved in the BR signalling pathway both in the absence and presence of bioactive BR molecules (such as CS/BL). (B) shows simplified version of the steps in the BR-signalling pathway (C) Heatmaps showing relative expression of genes in BR-signalling pathway in *tabri1-a.1bd*, *tabri1-a.2bd* and *tabri1-a.3bd*, *tabri1-bd* mutants and controls *TaBRI1-NS* and Cadenza using normalised number of counts/genes generated using Heatmapper (http://www.heatmapper.ca/). Statistical significant differences in gene expression in mutants compared to *TaBRI1-NS* are highlighted using asterisks (*).

3.2.8 Phenotypic characterization of *tabri1* mutants under glasshouse conditions

The effects on final plant height, leaf angle, leaf area, days to flowering, grain size and weight have been reported in *bri1* mutants of major cereal crops such as rice, maize, and barley (Kir et al 2015; Dockter et al 2014; Gruzka et al 2011; Morinaka et al 2006). Some mutants are severe causing extreme dwarfism and erect canopy architecture, but these are not agronomically important due to a reduction in grain size and grain number. However, some weaker mutants are also reported, and these are semi-dwarfs with erect stature without negative effects on seed size, thus improving biomass under dense planting, and are therefore agronomically important (Morinaka et al 2006).

To establish the phenotype associated with loss-of-function mutations in the wheat *BRI1* genes, we performed phenotypic characterisation of the wheat *tabri1* mutants grown under glasshouse (GH) conditions in years 2021 (experiment GH2021) and 2022 (GH2022). Six to eight biological replicates of each mutant i.e., singles (*tabri1-a.1*, *tabri1-b*, and *tabri1-d*), doubles (*tabri1-a.1b*, *tabri1*-a.*1d*, and *tabri1-bd*) and triples (*tabri1-a.2bd* and *tabri1-a.3bd*) along with Cadenza and *TaBRI1-NS* were planted in a randomised complete block design. The *tabri1-a.1bd* mutant was excluded from this experiment as it fails to elongate, transition into reproductive phase and set any seed and thus could not be compared with the other *tabri1* mutants generated in this study. The data on flag-leaf angle, final plant height, internode length, grain size and weight and spike characteristics (spike length and number of spikelets/spike) were recorded as these traits are reported to be affected in *bri1* mutants of rice, barley, and maize.

3.2.8.1 Flag-leaf angles

As the primary goal of this project was to produce more erect canopy architecture (supporting higher planting density and RUE), the flag-leaf angles (LA) on primary tillers were recorded at anthesis. The *tabri1-a.2bd* triple mutant was not included due to the severity of phenotype which included twisted and disoriented leaves). The data were analysed using ANOVA and are presented in Figure 3.16 and Table 3.5.

ANOVA confirmed statistically significant differences in flag-leaf angle amongst these mutants in GH2022 and GH2021 experiments [$F(8,49) = 8.35$, $p < .001$], [F

(8,71) = 14.29, p<.001], respectively. There was no significant difference in flag-leaf angles between *TaBRI1-NS* and Cadenza during both experiments (as the *p*-values were 0.1999 and 0.0998 for GH2022 and GH2021, respectively). Therefore, either of these genotypes could be used as a control. For this study, we compared the flag-leaf angle of the various mutants against *TaBRI1-NS*. Interestingly, we observed big differences in the flag-leaf angle for a specific genotype between these independent experiments, which could be mainly due to environmental factors such as light intensity etc, but the trends of leaf angle across the genotypes were similar. We observed significant reductions in the flag-leaf angle in the double (*tabri1-a.1b*, *tabri1-a.1d* and *tabri1bd*) and triple *tabri1-a.3bd* knockout mutants compared to *TaBRI1-NS* (as the *p*-values obtained were significantly lower than 0.05 in these mutants). The *tabri1-d* mutant had a significant reduction in the LA compared to *TaBRI1-NS* during GH2021, but not during GH2022. We observed approximately 30% and 60% reduction in the LA in the double and triple mutants, respectively, compared to *TaBRI1-NS* (figure 3.15), demonstrating the role of these BR signalling in regulating canopy architecture in wheat. Flag leaf angles were also recorded at other GS (ear emergence, watery endosperm, soft dough, and ripening stage), but due to strong correlation between the GS's (p <0.001) as shown in supplementary figure 1. Its analysis was not included in this chapter.

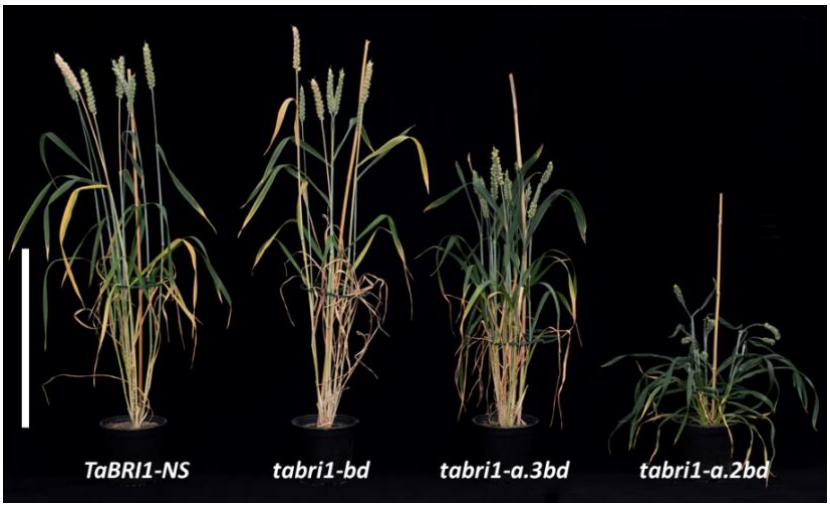

Figure 3. 15 Gross morphology of *tabri1* mutants during grain filling phase. The triple mutants (*tabri1-a.2bd* and *tabri1-a.3bd*), a representative double mutant (*tabri1-bd*) and control *TaBRI1-NS* were photographed during GH2021 at GS83. Bar length (in the left) is 40cm.

A

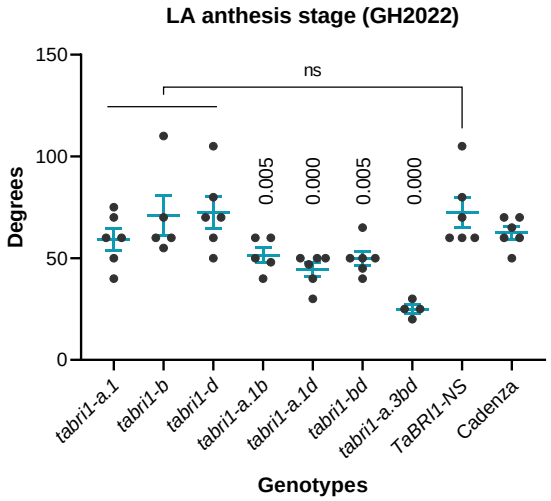

B

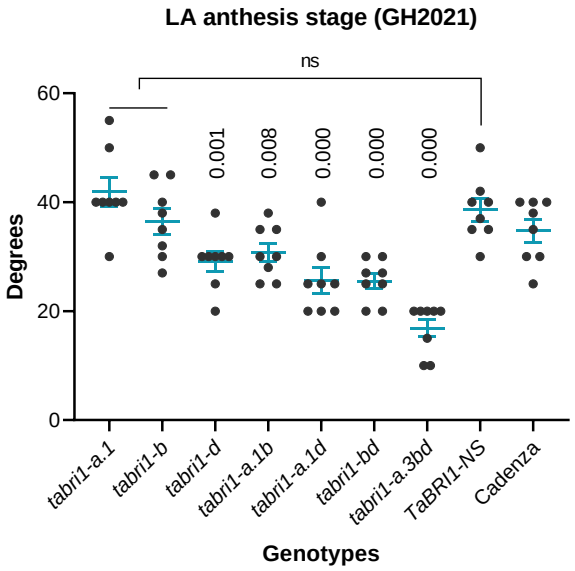

Figure 3. 16 Graphs of flag-leaf angles in *tabri1* mutants at anthesis stage. LAs were recorded in the *tabri1* mutants along with Cadenza during GH2022 (A, n=6) and GH2021 (B, n=8). *P*-values for differences between mutants and *TaBRI1-NS* were obtained using Fisher's unprotected LSD test are also shown.

Table 3. 5 Flag leaf angles of *tabri1* mutants. Flag-leaf angles (mean ± SD) of the various *tabri1* mutants and control lines recorded at anthesis during GH2022 and GH2021. The % change in the leaf angles compared with *TaBRI1-NS* control is also shown. General ANOVA output i.e., *p*-values, SED, and LSD at 5% level of significance are also described below. Statistically significant differences between mutant and *TaBRI1-NS* were denoted *$p < 0.05$, **$p < 0.01$, ***$p < 0.001$ (obtained from Fisher's LSD unprotected test).

Genotype	Leaf angle (in degrees) at anthesis stage				*p*-value		SED		LSD	
	GH2022	% Change compared to *TaBRI1-NS*	GH2021	% Change compared to *TaBRI1-NS*	2022	2021	2022	2021	2022	2021
tabri1-a.1	59.2 ± 12.8	-18.34	41.8 ± 7.5	8.3	<.001	<.001	7.66	2.907	15.53	5.823
tabri1-b	71.7 ± 22.5	-1.1	36.5 ± 6.7	-5.4						
tabri1-d	72.5 ± 18.9	0	29.1 ± 5.1**	-24.6						
tabri1-a.1b	50 ± 8.5**	-31.03	30.8 ± 4.8**	-20.2						
tabri1-a.1d	44.5 ± 8.1***	-38.62	25.6 ± 6.8***	-33.7						
tabri1-bd	50 ± 8.4**	-31.03	25.5 ± 3.9***	-33.7						
tabri1-a.3bd	25.8 ± 4.1***	-64.41	16.9 ± 4.6***	-56.2						
TaBRI1-NS	72.5 ± 17.8	_	38.6 ± 6	_						
Cadenza	62.5 ± 7.6	-13.79	34.8 ± 5.8	-9.8						

3.2.8.2 Final plant height and internode elongation

Final plant height, including the spike, was recorded on the tallest tiller per plant on 6-8 biological replicates per mutant in experiments GH2022 and GH2021. The data were analysed using ANOVA and are presented in Table 3.6 and Figure 3.18. ANOVA confirmed significant differences between mutants for final plant height in both experiments [F (9,55) = 74.45, p <.001], [F (9, 79) = 193.63, p <.001], respectively. Specifically, approx. 52% and 22% reductions in the final plant height in the triple mutants *tabri1-a.2bd* and *tabri1-a.3bd*, respectively, compared to *TaBRI1-NS* were observed in GH2021 (Figure 3.17). Significant differences in final plant height were also observed for *tabri1-a.1d* (during GH2022) and *tabri1-b* (during GH2021), but these differences were not consistent amongst the years so could be due to some non-genetic reasons. Apart from this, no significant differences existed between the other singles or double mutants and *TaBRI1-NS* demonstrating functional redundancy amongst the *TaBRI1* homoeologues for controlling stem elongation.

Figure 3. 17 Final plant height of *tabri1* mutants. Phenotype of the triple mutants (*tabri1-a.2bd* and *tabri1-a.3bd*), a representative double mutant (*tabri1-bd*) and control *TaBRI1-NS*. The photograph was taken at GS93 (maturity) during GH2021. The bar length in left is 40cm.

A

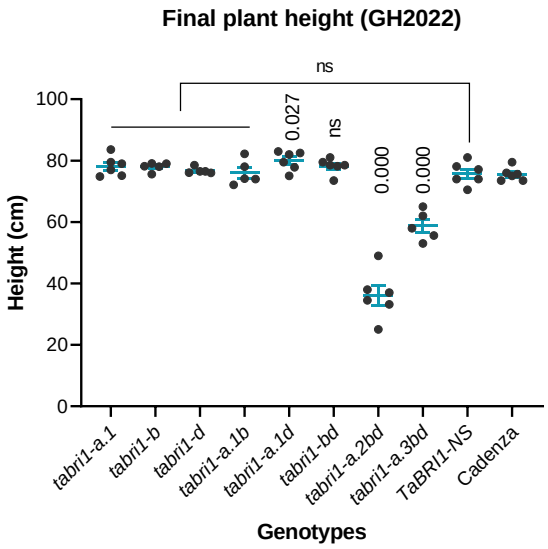

B

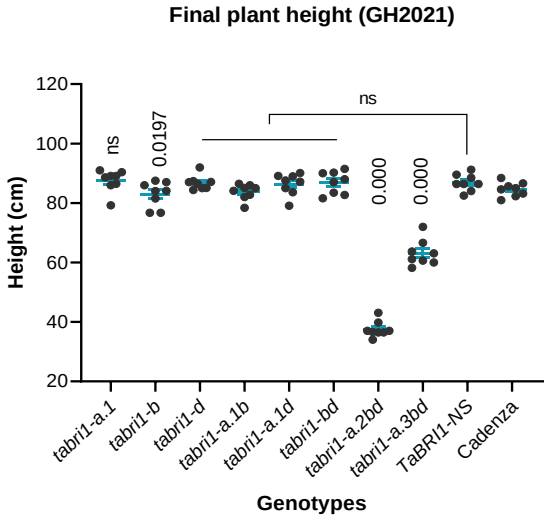

Figure 3. 18 Graphs of final plant height in *tabri1* mutants. Plant heights were recorded at maturity in GH2022 (A, n=6) and GH2021 (B, n=8). The *p*-values for the comparison between the mutants and *TaBRI1-NS* obtained using Fisher's unprotected LSD test are shown.

To determine the contribution of individual internodes to final plant height, the internode lengths from 2-3 of the longest tillers from each plant were measured. It was observed that the length of the peduncle, 2nd and 3rd internodes mainly contributed towards the differences in final plant height with little or no differences

for the 4th and 5th internode (if present). The data are presented in Table 3.6 and a stacked bar graph for the GH2021 experiment is presented in Figure 3.19.

ANOVA confirmed significant differences in the lengths of the peduncle, internode 2 (I2) and internode 3 (I3) in the triple mutants compared with *TaBRI1-NS* (*p*-values <0.001). The length of peduncle, I2 and I3 were significantly shorter in the triple mutants i.e., *tabri1-a.2bd* (8.6, 9.3 and 7.6 cm, respectively) and *tabri1-a.3bd* (23.4, 15.1 and 9.9 cm, respectively) compared with *TaBRI1-NS* (36.7, 18.5 and 12.2 cm, respectively) which caused a significant reduction in the final plant height in these mutants compared to the *TaBRI1-NS*. Internode lengths in the other mutants were not significantly different from those in *TaBRI1-NS*, except for peduncle length of *tabri1-b*, which was significantly different to *TaBRI1-NS* during GH2021.

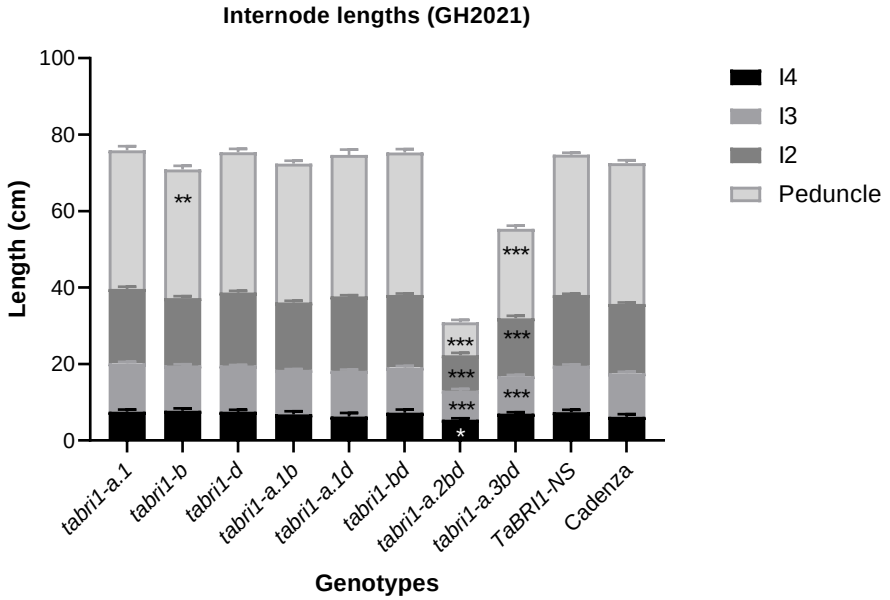

Figure 3. 19 Internode lengths in *tabri1* mutants. Internode lengths were recorded at maturity in *tabri1* mutants along with Cadenza during GH2021. ***, ** and * indicate significant difference from *TaBRI1-NS*, $p < 0.001$, <0.01 and <0.05 respectively, obtained using Fisher's unprotected LSD test.

Table 3. 6 Internode lengths in *tabri1* mutants. Internode lengths (mean ± SD) of various mutants were recorded at maturity during GH2021. The % difference compared with *TaBRI1-NS* is also shown. General ANOVA output i.e., *p*-values, SED, and LSD at 5% level of significance are also shown. Statistical significant difference between mutant and *TaBRI1-NS* were denoted **P* < 0.05, ***P* < 0.01, ****P* < 0.001 (obtained from Fisher's LSD unprotected test).

Genotype	Peduncle (cm)	% Change compared to *TaBRI1-NS*	Internode 2 (cm)	% Change compared to *TaBRI1-NS*	Internode 3 (cm)	% Change compared to *TaBRI1-NS*	Internode 4 (cm)	% Change compared to *TaBRI1-NS*
tabri1-a.1	36.2 ± 3.2	-1.36	19.4 ± 1.5	4.86	12.7 ± 1.1	4.1	7.5 ± 1.6	1.35
tabri1-b	33.6 ± 2.9**	-8.45	17.7 ± 1.3	-4.32	11.9 ± 0.9	-2.46	7.7 ± 1.9	4.05
tabri1-d	36.7 ± 2.6	0	19.1 ± 1.3	3.24	12.1 ± 0.4	-0.82	7.4 ± 1.4	0
tabri1-a.1b	36.3 ± 2.2	-1.1	17.6 ± 1.3	-4.86	11.6 ± 0.4	-4.91	6.8 ± 2.3	-8.11
tabri1-a.1d	37 ± 3.9	0.82	19.4 ± 0.9	4.8	12 ± 0.8	-1.64	6.2 ± 2.7	-16.21
tabri1-bd	37.2 ± 2.7	1.36	18.9 ± 1.1	2.16	11.8 ± 1.1	-3.27	7.3 ± 2.2	-1.35
tabri1-a.2bd	8.6 ± 1.8***	-76.56	9.3 ± 1.7***	-49.72	7.6 ± 1.3***	-37.7	5.4 ± 1.1*	-27.02
tabri1-a.3bd	23.4 ± 2.3***	-36.23	15.1 ± 1.8***	-18.37	9.9 ± 0.8***	-18.85	7 ± 1.0	-5.4
TaBRI1-NS	36.7 ± 1.5	_	18.5 ± 0.8	_	12.2 ± 0.8	_	7.4 ± 1.9	_
Cadenza	36.8 ± 2.2	0.27	18.1 ± 1.1	-2.16	11.4 ± 1.0	-6.55	6.2 ± 1.9	-16.21
***p*-value**	**<0.001**		**<0.001**		**<0.001**		**0.22**	
SED	1.167		0.631		0.465		0.899	
LSD	2.332		1.261		0.929		1.797	

3.2.8.3 Seed characteristics

Seed size, number and weight are important yield components. The Marvin Seed Analyser (INDOSAW, Haryana, India) was used to measure grain length (mm), width (mm), area (mm^2) and 1000-grain weight (TGW). The data, analysed by ANOVA, are presented n Table 3.7 and Figures 3.21 and 3.22.

ANOVA confirmed statistical significant differences in the TGW between the mutants in the 2022 and 2021 experiments [F (9,55) = 4.54 p<.001], [F (9,77) = 6.17 p<.001], respectively. Interestingly, we observed a significant increase in the TGW in some of *tabri1* mutants (i.e., *tabri1-a.1*, *tabri1-b*, *tabri1-a1.b* and *tabri1-a1.d*) with slight to no effects in *tabri1-d* and *tabri1-bd* and a decrease in grain weight in the triple mutants (*tabri1-a.2bd* and *tabri1-a.3bd*) compared with *TaBRI1-NS* in both of the independent experiments. For instance, we observed 6% and 9% reduction in the triple mutants and nearly 10% increase in some single and double mutants (i.e., *tabri1-a.1*, *tabri1-b*, *tabri1-a1.b* and *tabri1-a1.d*) compared to *TaBRI1-NS* in the GH2021 trial.

Additionally, ANOVA confirmed statistically significant differences in seed area amongst the mutants in the GH2022 and GH2021 experiments [F (9,55) = 7.38, p<.001], [F (9,77) = 15.71, p<.001], respectively. We observed a decrease in the seed area in the triple mutants *tabri1-a.2bd* and *tabri1-a.3bd* by approximately 7-15% compared to *TaBRI1-NS* (as shown in Figure 3.20) and an increase in seed area in some single and double mutants (i.e., *tabri1-a.1*, *tabri1-b*, *tabri1-a.1b* and *tabri1-a1.d*) which is consistent with their heavier grain in these mutants.

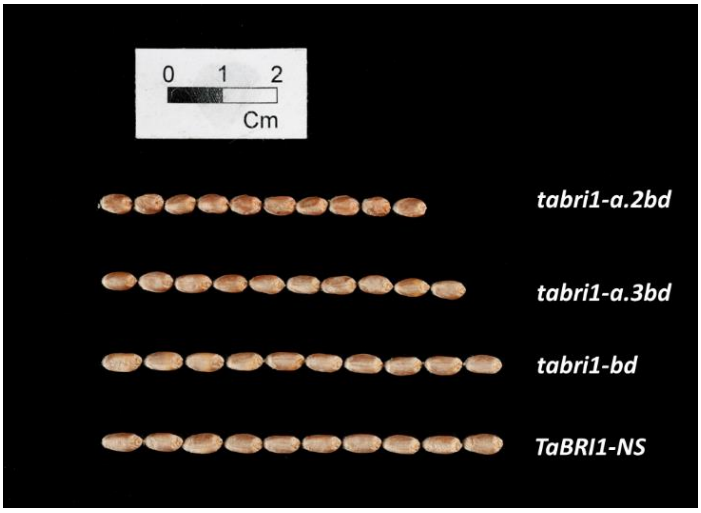

A

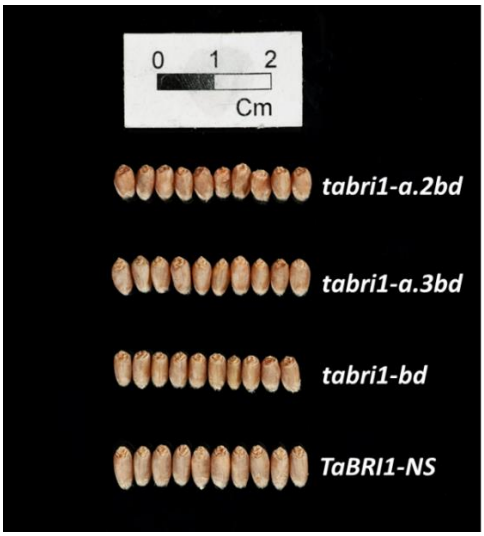

B

Figure 3. 20 Grain morphology of *tabri1* mutants. (A) Grain length of ten seeds of *tabri1-a.2bd, tabri1-a.3bd, tabri1-bd* and *TaBRI1-NS*. (B) Grain width of ten seeds of *tabri1-a.2bd, tabri1-a.3bd, tabri1-bd* and *TaBRI1-NS*. The photograph was taken on mature grains after harvesting. The bar length is 1cm.

A

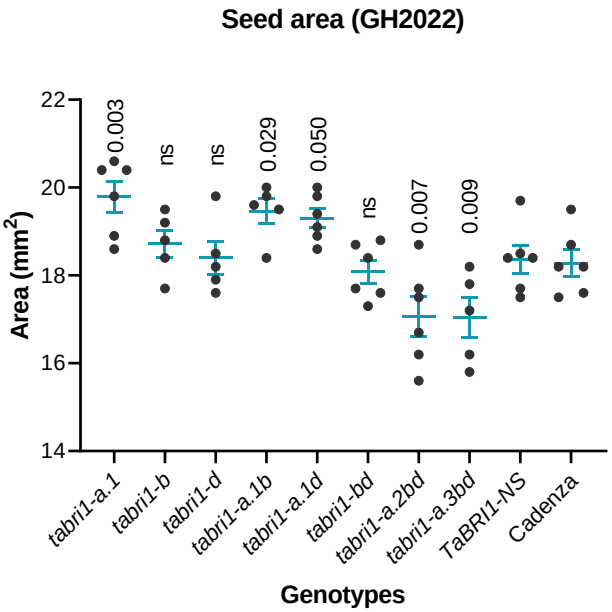

B

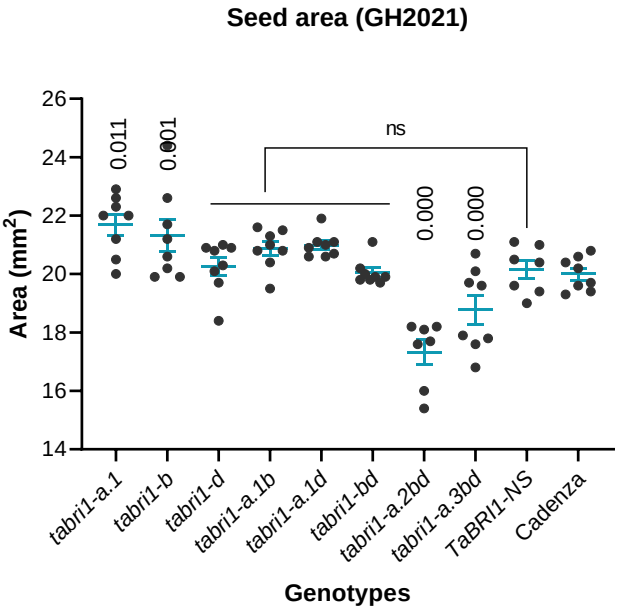

Figure 3. 21 Graphs of seed area for the *tabri1* mutants. The data for mature grains (obtained using the Marvin seed analyser) for *tabri1* mutants are presented along with Cadenza during GH2022 (A, n=6) and GH2021 (B, n=8). The *p*-values for differences between mutants and *TaBRI1-NS* obtained using Fisher's unprotected LSD test are shown.

A

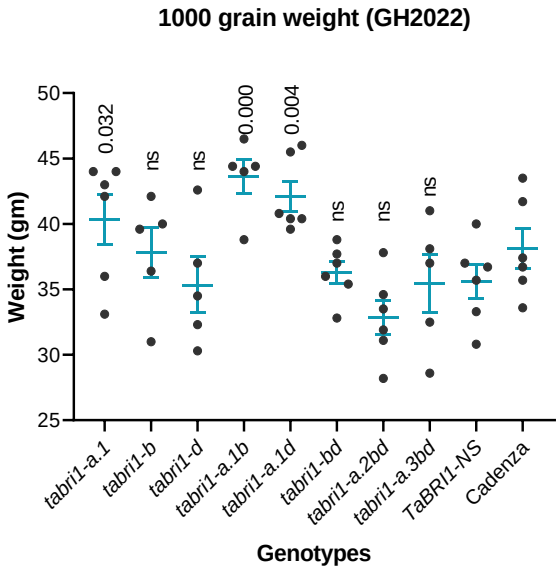

B

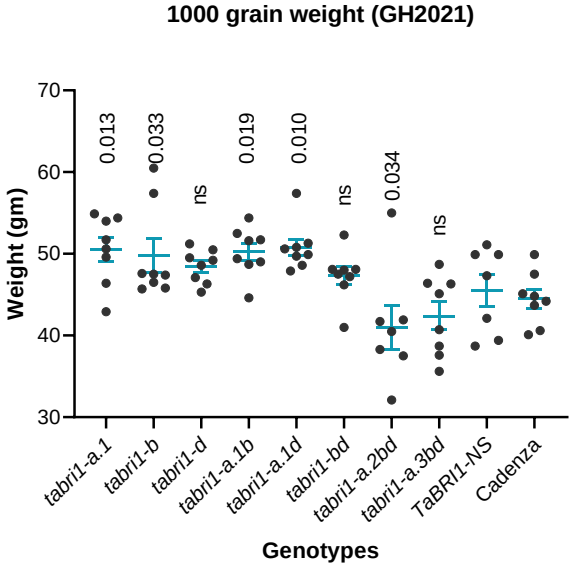

Figure 3. 22 Graphs of 1000 grain weight for the *tabri1* mutants. The data collected on mature grains (using weighing balance) on *tabri1* mutants are presented along with Cadenza during GH2022 (A, n=6) and GH2021 (B, n=8). The *p*-values for differences between mutants and *TaBRI1-NS* obtained using Fisher's unprotected LSD test are shown.

Table 3. 7 Seed area and thousand grain weights of *tabri1* mutants. The data (mean ± SD) for the *tabri1* mutants recorded from mature grains harvested during GH2022 and GH2021. The % change in these parameters compared with *TaBRI1-NS* is shown. ANOVA output *p*-values, SED, and LSD at 5% level of significance is also presented. Statistical significant difference between mutant and *TaBRI1-NS* were denoted *$p < 0.05$, **$p < 0.01$, ***$p < 0.001$ (obtained from Fisher's LSD unprotected test).

Genotype	Seed area (mm^2) [GH2022]	% Change	Seed area (mm^2) [GH2021]	% Change	TGW (gm) [GH2022]	% Change	TGW (gm) [GH2021]	% Change
tabri1-a.1	19.8 ± 0.8**	7.6	21.7 ± 1.0*	8	40.3 ± 4.6*	13.2	50.6 ± 4.2*	11.4
tabri1-b	18.7 ± 0.7	1.6	21.3 ± 1.6**	6	37.8 ± 4.3	6.2	49.8 ± 5.7*	9.7
tabri1-d	18.4 ± 0.8	0	20.3 ± 0.9	1	35.3 ± 4.7	-0.8	48.5 ± 2.1	6.8
tabri1-a.1b	19.5 ± 0.6*	6	20.9 ± 0.7	4	43.6 ± 2.9***	22.5	50.3 ± 3.0*	10.8
tabri1-a.1d	19.3 ± 0.5*	4.9	21 ± 0.4	4.5	42.1 ± 2.8**	18.2	50.8 ± 3.0*	11.9
tabri1-bd	18.1 ± 0.6	-1.6	20 ± 0.4	-0.5	36.3 ± 2.1	2	47.3 ± 3.1	4.2
tabri1-a.2bd	17.1 ± 1.1**	-7.1	17.3 ± 1.1***	-14	32.8 ± 3.3	-7.9	41.1 ± 7.0*	-9.5
tabri1-a.3bd	17 ± 1.0**	-7.6	18.8 ± 1.4***	-6.5	35.4 ± 4.9	-0.6	42.4 ± 4.8	-6.6
TaBRI1-NS	18.4 ± 0.8	_	20.1 ± 0.8	_	35.6 ± 3.2	_	45.4 ± 5.3	_
Cadenza	18.3 ± 0.7	-0.5	20 ± 0.6	-0.5	38.1 ± 3.7	7	44.5 ± 3.2	-2
***p*-value**	<0.001		<0.001		<0.001		<0.001	
SED	0.482		0.459		2.238		2.02	
LSD	0.97		0.918		4.504		4.03	

3.2.8.4 Spike characteristics

To investigate the effect of these mutations on the wheat spikes, we measured spike length (mm) and counted the number of spikelets in 6-8 spikes at maturity. General ANOVA was then performed, and the data are shown below in Table 3.8 and Figures 3.24 and 3.25. Morphologically, we observed reduced grain set in the triple mutants i.e., *tabri1-a.2bd*, *tabri1-a.3bd* compared to *TaBRI1-NS* as shown in Figure 3.23. The compromised fertility is a common feature of some *BRI1* mutants in rice (Yamamuro et al., 2000; Morinaka et al., 2006).

ANOVA confirmed significant differences in spike length in experiments GH2022 and GH2021 [F (9,55) = 73.46, p<.001], [F (9,79) = 88.15, p<.001], respectively. Reductions in spike lengths of 35% and 22% in the triple mutants *tabri1-a.2bd* and *tabri1-a.3bd*, respectively, compared with *TaBRI1-NS* were observed, resulting in compact spikes in these mutants as shown in Figure 3.23. There was no significant effect on spike lengths in the single or double *tabri1* mutants.

ANOVA confirmed significant differences existed for the number of spikelets per spike in experiments GH2022 and GH2021 [F (9,55) = 3.64, p =0.002], [F (9,79) = 8.52, p<0.001], respectively. However, there was not a consistent trend for the two independent experiments, other than a reduction in the number of spikelets in one of the severe triple *bri*1 mutants i.e., *tabri1-a.2bd* compared to other mutants and null-segregant control.

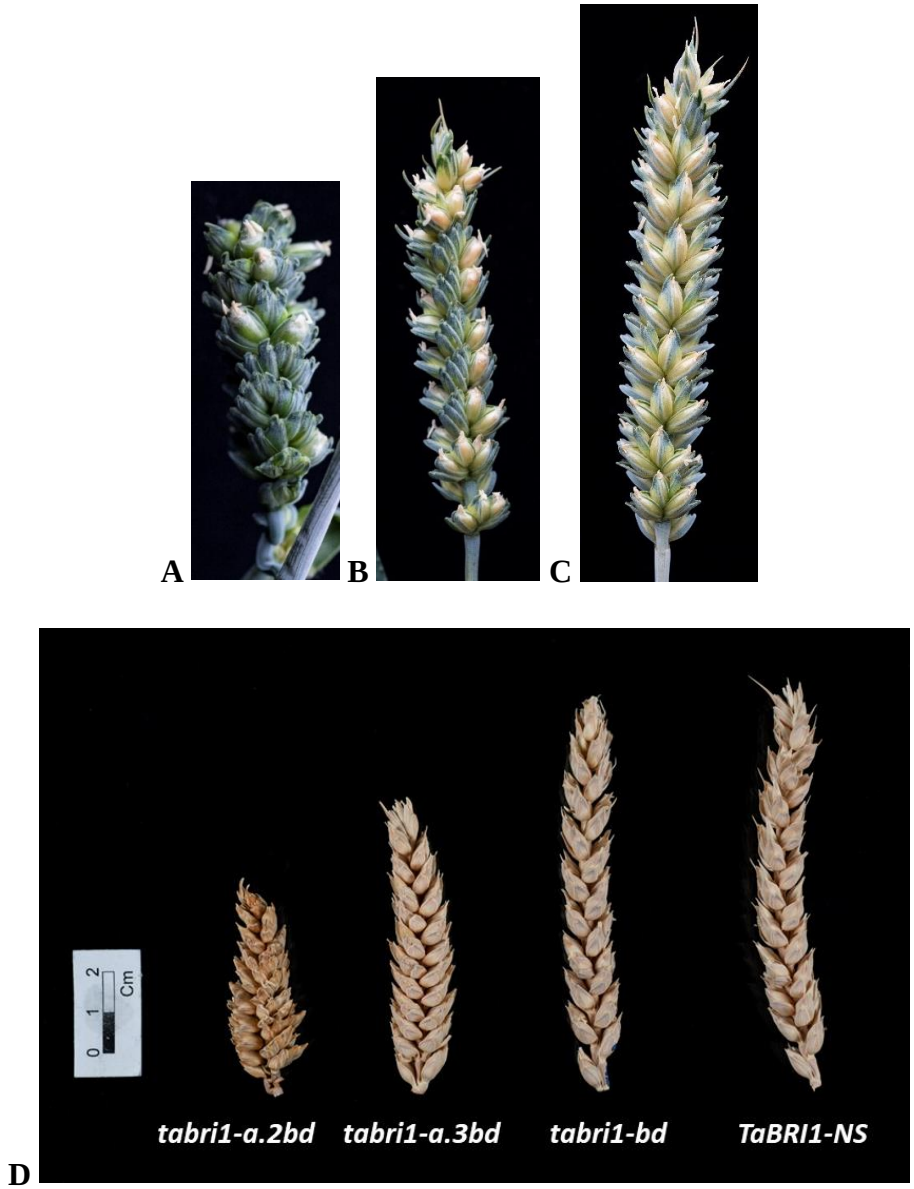

Figure 3. 23 Spike morphology of *tabri1* mutants. Triple mutants *tabri1-a.2bd* (A) and *tabri1-a.3bd* (B) have reduced seed set compared to *TaBRI1-NS* (C) at GS83 (soft dough stage). (D) Spike length of the triple mutants (*tabri1-a.2bd* and *tabri1-a.3bd*), a representative double mutant (*tabri1-bd*) and control *TaBRI1-NS*. This photograph was taken at maturity. The scale bar length (on the left) is 1cm.

A

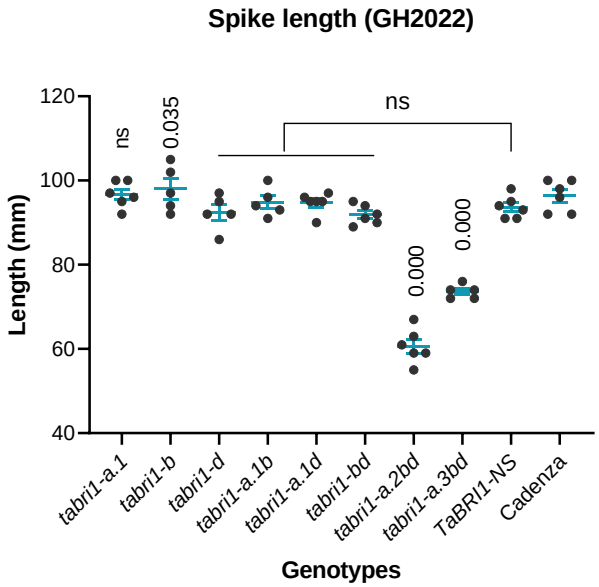

B

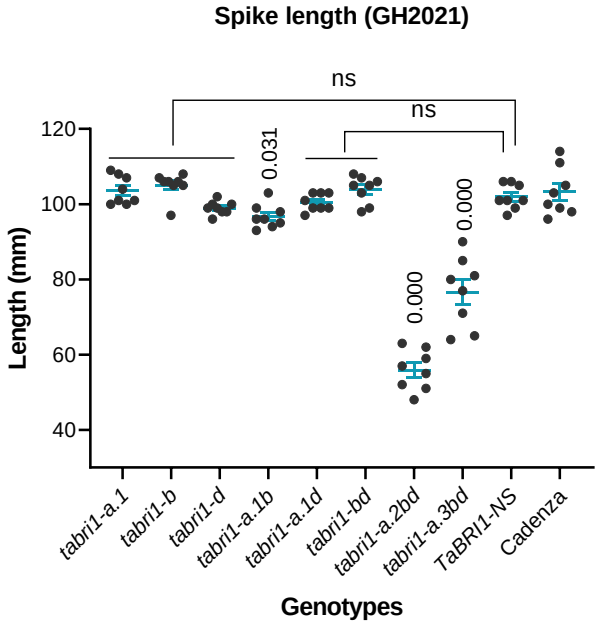

Figure 3. 24 Graphs of spike length in *tabri1* mutants. The data were recorded at maturity in the *tabri1* mutants along with Cadenza during GH2022 (A, n=6) and GH2021 (B, n=8). The *p*-values for the differences between mutants and *TaBRI1-NS* obtained using Fisher's unprotected LSD test are shown.

A

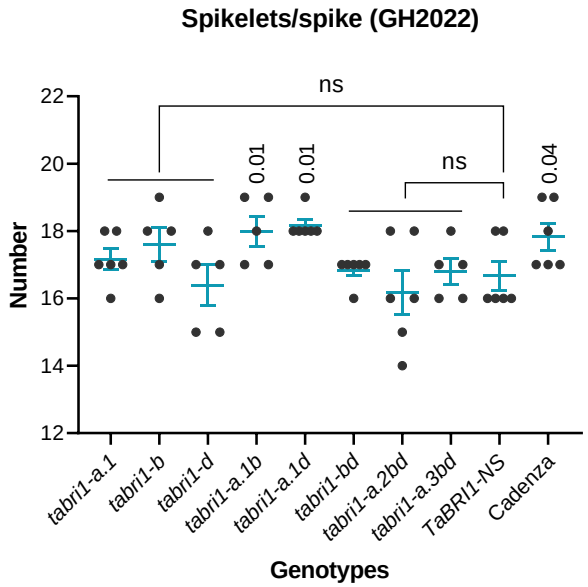

B

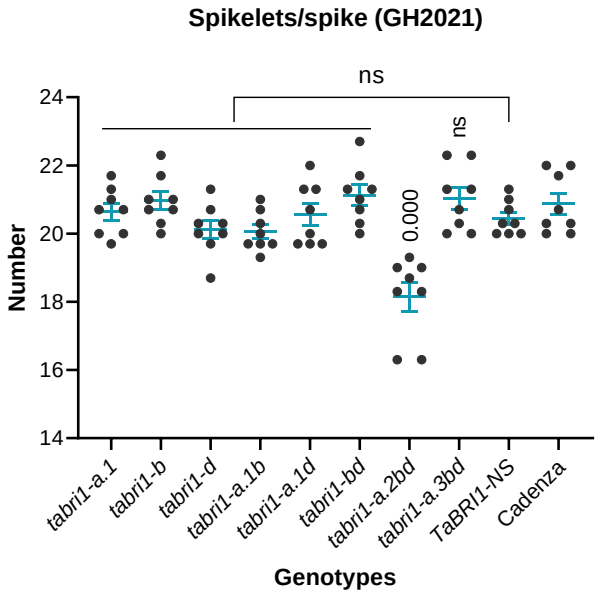

Figure 3. 25 Graphs of spikelets per spike in *tabri1* mutants. The data were recorded at maturity in the *tabri1* mutants along with Cadenza in GH2022 (A, n=6) and GH2021 (B, n=8). We also included *p*-values for the differences between the mutants and *TaBRI1-NS* obtained using Fisher's unprotected LSD test.

Table 3. 8 Spike length and number of spikelets per spike in *tabri1* mutants. The data (mean ± SD) for the *tabri1* mutants was recorded during GH2022 and GH2021. The % difference in these parameters compared to *TaBRI1-NS* was also measured. ANOVA output such as *p*-values, SED, and LSD at 5% level of significance is shown below. Statistical significant difference between mutant and *TaBRI1-NS* were denoted **P* < 0.05, ***P* < 0.01, ****P* < 0.001 (obtained from Fisher's LSD unprotected test).

Genotype	Spike length (mm) (GH2022)	% Change compared to *TaBRI1-NS*	Spike length (mm) (GH2021)	% Change compared to *TaBRI1-NS*	Spikelets/spike (GH2022)	% Change compared to *TaBRI1-NS*	Spikelets/spike (GH2021)	% Change compared to *TaBRI1-NS*
tabri1-a.1	9.7 ± 0.3	3.2	10.4 ± 0.3	1.9	17 ± 0.6	0	20.6 ± 0.7	0.5
tabri1-b	9.8 ± 0.5*	4.2	10.5 ± 0.3	2.9	17 ± 0.9	0	21 ± 0.7	2.4
tabri1-d	9.2 ± 0.4	-2.1	9.9 ± 0.2	-2.9	16 ± 1.4	-5.9	20.1 ± 0.8	-2
tabri1-a.1b	9.5 ± 0.3	1.1	9.7 ± 0.3*	-4.9	18 ± 0.8*	5.9	20 ± 0.6	-2.4
tabri1-a.1d	9.5 ± 0.2	1.1	10.1 ± 0.2	-1	18 ± 0.3*	5.9	20.5 ± 0.9	0
tabri1-bd	9.2 ± 0.2	-2.1	10.4 ± 0.4	-2	17 ± 0.6	0	21.1 ± 0.8	2.9
tabri1-a.2bd	6.1 ± 0.4***	-35.1	5.6 ± 0.5***	-45.1	16 ± 1.4	-5.9	18.2 ± 1.2***	-11.2
tabri1-a.3bd	7.3 ± 0.2***	-22.3	7.7 ± 0.9***	-24.5	17 ± 0.8	0	21 ± 0.9	2.4
TaBRI1-NS	9.4 ± 0.2	_	10.2 ± 0.3	_	17 ± 0.8	_	20.5 ± 0.5	_
Cadenza	9.6 ± 0.4	2.1	10.3 ± 0.6	1	18 ± 0.8*	5.9	20.9 ± 0.9	2
P-value	<.001		<0.001		0.002		<0.001	
SED	0.2		0.24		0.5		0.42	
LSD	0.41		0.48		1		0.84	

3.3 Discussion

The objective of this study was to characterize the *TaBRI1* genes and establish their roles in controlling growth and development in wheat. This was achieved by generating combinatorial *bri1* mutants in hexaploid wheat background using a TILLING-based screening approach. We observed a severe phenotypic abnormality in the *tabri1-a.1bd* triple mutant, including extreme dwarfism, small and wrinkled dark green leaves and an inability to transition into the reproductive phase. This demonstrated that the three *TaBRI1* homoeologues have an essential role in controlling BR-responsive growth in wheat. In contrast the single and double mutants displayed only subtle phenotypic differences compared to the controls (for instance erect leaf angles and larger seeds in some singles and double knockout mutants), indicating that the *TaBRI1* homoeologues are largely functionally redundant in controlling growth and development in hexaploid wheat.

The overarching objective of this work is to generate new architecture alleles that can be deployed by breeders to improve agronomic traits in wheat. We hypothesized that weaker *tabri1* alleles would be required to achieve this objective. For which we performed a forward genetics-based screen (using an EMS-mutagenized *tabri1-bd* double mutant). This led to the identification of two BR-insensitive dwarf mutants, displaying erect flag leaves, reduced height, and defects in reproductive development.

We wanted to uncover the effect of *tabri1* mutations on the flux through the BR pathway. To this end, BR hormone levels and transcript profiling on these mutants were performed. Elevated hormone levels and transcript abundance of the BR biosynthesis pathway and down-regulation of few signalling components in severe triple mutants demonstrated the role of *BRI1* in regulating BR homeostasis in wheat. Additionally, the triple mutants displayed reduced sensitivity to external BR application thereby strengthening our hypothesis that mutations in *TaBRI1* genes leads to BR-insensitivity and altered growth and development.

3.3.1 *BRI* genes controls growth and development in wheat

The *BRI1* genes encode a BR receptor which, in the presence of bioactive BRs, is responsible for initiating a signalling cascade that leads to the activation of downstream transcription factors which regulate multiple aspects of BR-dependent

growth and development. The role of the *BRI1* gene in controlling whole plant architecture has been established in various plant species such as Arabidopsis (Clouse et al., 1996), pea (Namura et al., 2003), barley (Chono et al., 2003), rice (Yamamuro et al., 2000; Morinaka et al., 2006), tomato (Montoya et al., 2002), Medicago (Cheng et al., 2017), cotton (Wang et al., 2014); Brachipodium (Feng et al., 2015), soyabean (Peng et al., 2016) and maize (Kir et al., 2015). There are also two recent reports describing the partial characterising the *BRI1* genes in wheat (Navarro et al., 2015; Fang et al., 2020). In model plants, these studies have demonstrated a role for *BRI1* in various developmental processes including stem elongation, leaf expansion, leaf angle determination, root growth, fertility, and seed germination.

To establish the role of this gene in wheat, we identified premature stop codon mutations in the three homoeologues of *TaBRI1* from Cadenza TILLING population developed by Krasileva et al., 2017. This enabled generation of a complete set of combinatorial mutants. The position of the nonsense mutations at codons 509, 273 and 447 within the respective *TaBRI1-A*, *TaBRI1-B* and *TaBRI1-D* coding sequences are expected to result in truncated receptor proteins lacking critical domains. (Clouse, 2011; Wang et al., 2012; Hothorn et al., 2011; Li and Chory, 1997; She et al., 2011; Wang et al., 2001) causing severe abnormality in the triple knockout mutant *tabri1-a.bd*.

Mutational analysis enables better understanding of gene function and key domains. This approach was widely followed to understand the function of the *BRI1* gene in rice, barley, and Arabidopsis in which a range of mutants were identified (Yamamuro et al., 2000; Morinaka et al., 2006; Dockter et al., 2014; Gruszka et al., 2011; Neff et al., 1999; Sun et al., 2017). For instance, large scale screening of mutants generated via Tos17 retrotransposon and gamma radiation enabled identification of seven novel *OsBRI1* mutants (Morinaka et al., 2006). *d61-7* had the weakest mutant allele, producing erect leaves and semi-dwarf stature (Morinaka et al., 2006). To produce weaker alleles in *TaBRI1A*, one of the double knockout mutants i.e., *tabri1-bd* was mutagenized with 0.4% EMS (Steve Thomas personal communications). A large number of M2 individuals were visually screened under the field conditions, enabling identification of two novel missense mutations in TaBRI1-A, one creating a P671S substitution in M3-31 (later called *tabri1-a.2bd*) and the second a G1008E substitution in M3-49 (later called *tabri1-a.3bd*). These mutants were backcrossed

once with the parent *tabri1-bd* mutant to produce BC1F2 seed which could be characterised further. A 3:1 segregation ratio was observed at this stage (mutant allele being recessive) by bulked segregation analysis thus confirming single gene segregation for the observed phenotypic differences.

Phenotypically, some subtle differences were observed in the *tabri1* single and double mutants that suggested that the homoeologues do not display complete functional redundancy. Leaf angle is regulated by BR signalling, with reduced BR signalling causing a reduction in leaf angle and a more erect architecture (Morinaka et al., 2006; Dockter et al., 2014; Feng et al., 2020; Kir et al., 2015). For instance, in rice *bri1* mutants such as *d61-1, d61-2* and *d61-7* demonstrate an erect-leaf phenotype compared to the wild-types whose leaves bend away from the stem (Morinaka et al., 2006). Significant reductions in the flag-leaf angle (at anthesis stage) were observed in single *tabri1-d* (only in experiment GH2021) and all double knockout mutants i.e., *tabri1-a.1b*, *tabri1-a.1d* and *tabri1-bd* indicating a gene-dosage effect for the trait of interest. Reduced BR-signalling in the lamina joint region (potentially affecting cell division/ differentiation) might be controlling leaf angle in the *tabri1* mutants. Additionally, nearly 65% reduction in the flag-leaf angle at anthesis was observed in the *tabri1-a.3bd* mutant compared to *TaBRI1-NS*. However, due to malformed and wrinkled leaves in *tabri1-a.2bd*, it was not possible to record leaf angles in this very severe mutant.

In contrast to leaf angle, no differences in the final plant height of the single or double mutants were observed. This indicates that the *BRI1* homoeologues have functionally redundant roles in controlling stem elongation. This contrasts with the findings of Fang and colleagues (2020), who reported a reduction in final plant height in the single *tabri1-a1* and *tabri1-d1* mutants. Final plant height was reduced in *tabri1-a.2bd* and *tabri1-a.3bd* mutant due to restricted internode elongation of the peduncle and internodes 2 and 3 compared to *TaBRI1-NS*. BRs play a role in controlling plant height and internode elongation as usually BR-deficient mutants are dwarfed in various cereals. For instance, *d61* mutant (having mutation in *OsBRI1*) causes semi-dwarfism in rice and *093AR* mutant (changing threonine to lysine at 573rd position) leads to semi-dwarfism in barley (Gruszka et al., 2011; Morinaka et al., 2006). It is established that the reduced final plant height in the *BRI1* mutants is due to restricted internode elongation. For instance, *ZmBRI1*-RNAi lines had significantly shorter

internodes compared to non-transgenic siblings leading to reduced final plant height in the mutant (Kir et al., 2015). Another study in rice suggests that restricted internode elongation is specific to effects on the second and third internodes (Yamamuro et al., 2000). The reduction in the final plant height observed could be due to reduced cell elongation in the internodes as observed in other *bri1* mutants in *Brachypodium distachyon*, maize and rice (Feng et al., 2015; Kir et al., 2015; Yamamuro et al., 2000). The reduction in plant height in the *tabri1* triple mutants is due to all internodes being shorter as observed in maize (Kir et al., 2015), but contrasts the observation in rice, where the lengths only of uppermost and 4th internodes were affected by *osbri1* mutations (Yamamuro et al., 2000).

Differences in grain weight were observed in some of the *tabri1* mutants including *tabri1-a.1*, *tabri1-b* (GH2021), *tabri1-a.1b*, *tabri1-a.1d* mutants during GH2021 and GH2022. However, as this was not completely consistent across different experiments, it is not clear whether this is due to altered BR sensitivity or indirect effects such as altered fertility and will need to be further investigated. In the study by Fang et al 2020, they noted a reduction in grain size in their *tabri1-a1* and *tabri1-d1* mutants. However, this was not observed in the current study conducted under glasshouse conditions. It is conceivable that the phenotypic differences observed by Fang and colleagues are due to the ion-beam mutagenesis used to generate the mutants which is likely to have caused large deletions in the genome that influence multiple growth characteristics. In the current study, grain size was reduced in the *tabri1* triple mutants causing reductions in thousand grain weight, although this was not observed consistently in GH experiments. Reduced grain size was also reported in various *osbri1* mutants such as *d61-1*, *d61-2* and *d61-7* isolated through chemical screens (Sinclair and Sheehy, 1999; Morinaka et al., 2006). Spike length was significantly reduced in the triple mutants *tabri1-a.2bd* and *tabri1-a.3bd* compared to *TaBRI1-NS*. Spike and panicle length are altered in *BRI1* mutants of barley and rice, respectively. For example, spike length is significantly shorter in the *uzu1.a* mutant of barley compared to the wild type due to reduced rachis internode length at the bottom and top of the spike (Dockter et al., 2014). In rice, the panicle length is either similar (*d61-1* mutant) or longer (*d61-2* and *d61-7* mutants) in the mutants compared to the wild type (Yamamuro et al., 2000; Morinaka et al., 2006).

The severe phenotype observed in *tabri1-a.2bd* mutant (P671S) is a characteristic of BR-deficient mutants in Arabidopsis. Loss-of-function or severe mutations have been reported in either island domain or island-LRR interface such as *bri1-9* (P662F), *bri1-113* (G611E) and *bri1-6* (G644D) in Arabidopsis (Noguchi et al., 1999; Li and Chory, 1997). Structure analysis revealed that these mutations probably interfere with hydrogen bonding with BR diol moiety consequently having a negative effect on the recognition of BRs by BRI1 (Hothorn et al., 2011; She et al., 2011). A range of mutants from severe to subtle have been identified in kinase domain of *AtBRI1* gene (Sun et al., 2017; Vert et al., 2005). Nonsynonymous mutation identified in *tabri1-a.3bd* mutant (G1008E) corresponds to IX subdomain of AtBRI1 protein and mutations identified in this region are reported to have strong phenotype due to their proximity to activation loop of the protein (Sun et al., 2017; Vert et al., 2005). Interestingly in rice, *d61-1* mutant (T989I) having spontaneous mutation near the region displayed dwarf height, erect leaves, reduced grain number per panicle due to defects in reproductive development as observed in *tabri1-a.3bd* mutant (Morinaka et al., 2006).

To estimate sensitivity of these mutants to external BR application, lamina joint inclination assays were performed at the seedling stage (Li et al., 2017) Leaf angles were measured in *tabri1-a.2bd*, *tabri1-a.3bd*, *tabri1-bd* mutants against *TaBRI1-NS* after treatment with epiBL (10^{-5}M) and without epiBL (water). We observed significant increase in the leaf angle in *tabri1-bd* and *TaBRI1-NS* when treated with 10^{-5}M epiBL. Interestingly, the leaf angle of *tabri1-a.2bd* and *tabri1-a.3bd* mutant was at par when treated with 10^{-5}M epiBL compared to water. Demonstrating that the triple mutants have altered sensitivity to external BR application. This is consistent with work with *bri1* mutants of rice and barley (having missense mutations), which were shown to have reduced sensitivity to external BR application (Yamamuro et al., 2000; Chono et al., 2003; Dockter et al., 2014). Thus, it can be concluded that the altered BR-signalling in the *tabri1* triple mutants is responsible for the differential growth and development at seedling stage.

3.3.2 Altered BR homeostasis in *tabri1* mutants

While limited amounts of applied BR can enhance growth excessive levels are known to be destructive for growth and development (Clouse et al., 1996). Therefore, maintenance of BR homeostasis by regulating biosynthesis and catabolism is an

important mechanism that forms part of BR signalling (Zhao and Li, 2012; Ye et al., 2011; Symons and Reid, 2004). The reduced responsiveness of the *tabri* mutants is predicted to result in loss of homeostasis and an accumulation of active BRs.

There is limited knowledge available on the endogenous BRs in wheat and the effect of *BRI1* mutations on the flux through the BR-pathway in this species. This was addressed by comparing BR concentrations and transcript levels in selected *tabri1* triple and double mutants with those in *TaBRI1-NS* and Cadenza control lines harvested at seedling stage (2nd leaf) growing under continuous light in controlled environment.

Nine BRs, including brassinolide (BL) were detected, some for the first time in wheat. BL was also detected in wheat seedlings by Janeczko and Swaczynova, 2010), but its presence in other cereals has not been reported (Chono et al., 2003, Yamamuro et al., 2000; Kim et al., 2008). Intermediates in the late C6 oxidation pathway were more abundant than those in the early C6 oxidation pathway, but both pathways are present as observed in Arabidopsis, rice, pea, and zinnia (Hong et al., 2002; Yamamuro et al., 2000; Nomura et al., 1999; Nomura et al., 1997; Yamamoto et al., 2001).

The most striking differences in the levels of bioactive BRs were found in the *tabri1-a.1bd* and *tabri1-a.2bd* triple mutants that displayed the most severe developmental defects, whereas no significant differences were observed in other mutants including *tabri1-a.3bd* and *tabri1-bd*. Accumulation of BRs in BR-insensitive mutants is common in other *BRI1* mutants isolated in Arabidopsis, rice, and barley (Noguchi et al., 1999; Nomura et al., 1999; Yamamuro et al., 2000; Chono et al., 2003, Choe et al., 2002; Montoya et al., 2002).

Consistent with the results from the BR analysis, RNA-seq revealed up-regulation of many BR-biosynthesis pathway genes, such as *DWF4*, *D2*, *CPD1*, *ROT3*, *BR6oxs* in *tabri1-a.1bd* compared to *TaBRI1-NS*. There was significant upregulation of *DWF4*, *CPD* and *BR6oxs* in the less severe triple mutant *tabri1-a.2bd* compared to *TaBRI1-NS*. Interestingly, there was also significant upregulation of *TaBRI1-A*, *-B* and *-D* genes in triple mutants (*tabri-a.1bd*, *tabri1-a.2bd* and *tabri1-a.3bd*). Upregulation of the rice BR receptor gene was also observed in the *osbri1* mutant *d61-1* compared to wild-type rice seedlings. Expression of *OsBRI1* and BR-biosynthetic genes was

shown to be regulated by RAV-Like1 controlling BR-homeostasis in rice (Je et al., 2010). Additionally, in the current study there was significant downregulation of the BR-catabolism genes *BAS1* and *BEN1* and the negative signalling genes *BKI1* and *BES1/ BZR1*, in the *tabri1-a.1bd* mutant compared to *TaBRI1-NS*, consistent with their involvement in BR homeostasis (He et al., 2005; Turk et al., 2005; Yuan et al., 2007; Neff et al., 1999; Sandhu et al., 2013; Wang et al., 2017). These results demonstrate the role of BR signal transduction mediated by BRI1 in BR homeostasis acting on both metabolism and signalling as part of the network by which BRs regulate plant development and responses to the environment.

3.3.3 Conclusion

The aim of this study was to understand the role of the *BRI1* gene in regulating plant architecture in wheat. This was approached by induced mutations in the gene using forward and reverse genetics, resulting in the isolation of a range of mutants affecting many aspects of BR-regulated development processes such as leaf angle, plant height and internode elongation, seed, and spike characteristics. Some of the mutants (knockouts in two *BRI1* homoeologues) had more erect leaf architecture without any pleotropic effects on height and grain development thus being potential targets for yield improvement under field conditions. The more severe mutants with mutations in all three *BRI1* homoeologues (*tabri1-a.2bd* and *tabri1-a.3bd*), showed abnormalities in reproductive and grain morphology and the search for new *tabri1* alleles is still underway. BR analysis provided new information on BR status in wheat and, in combination with mRNA sequencing, led to better understanding of BR homeostasis in this crop species.

Chapter 4: Characterisation of the roles of *TaDWF1* and *TaDWF4* in regulating wheat architecture

4.1 Introduction

4.1.1 Role of *DWF1* gene in plant growth and development

In Arabidopsis, the *DWF1*/*DIM* gene encodes an enzyme that catalyses the conversion of 24-methylenecholesterol to campesterol, in the sterol pathway (Klahre et al., 1998; Choe et al., 1999). The protein contains a flavin adenine dinucleotide-binding domain, which is common in oxidoreductase enzymes (Choe et al., 1999). The Arabidopsis *dim* mutant displayed extremely short hypocotyls, stems, petioles, and roots due to reduced cell elongation on the longitudinal axis of these organs (Takahashi et al., 1994). The phenotype of the *dim* mutant can be restored by application of external BL and its precursors, demonstrating that the mutants are deficient in BRs (Klahre et al., 1998).

Loss-of-function mutations in the *DWF1*/*DIM* gene also modifies whole plant architecture in cereals such as rice, maize and barley (Hong et al., 2005; Best et al., 2016; Dockter et al., 2014). For example, in rice the *brd2* mutant (defective in *DIM*/*DWF1* gene) displays erect leaves, semi-dwarf height, reduced root elongation, shortened grains and abnormal panicle development (Hong et al., 2005). Similarly, in barley, near-isogenic lines containing mutations in *HvDIM* have erect leaves, reduced stem elongation and a condensed spike phenotype (Dockter et al., 2014).

4.1.2 Role of *DWF4* gene in plant growth and development

DWF4 catalyses a rate limiting step within the BR biosynthetic pathway, that involves a 22α-hydroxylation reaction (Choe et al., 1998). DWF4 is a member of cytochrome P450 monoxygenase family, having signature domains including the heme binding domain, domain A (dioxygen binding), domain B (steroid binding) and domain C (Nebert and Gonzalez, 1987; Kalb and Loper, 1988). In Arabidopsis, *DWF4* expression was observed in growing tissues such as root and shoot apices and

joints (Kim et al., 2006). Overexpressing the *DWF4* gene has been demonstrated to produce increases in biomass and yield in Arabidopsis, maize, rice, and wheat (Choe et al., 2001; Li et al., 2018; Liu et al., 2020; Milner et al., 2022).

Altering expression of *DWF4* gene results in architectural and agronomic advantage in cereals. For instance, the rice *osdwf4-1* mutant has an upright canopy architecture with a slight reduction in final plant height and no negative effects on reproductive development ultimately leading to increased grain yield under a dense planting regime (Sakamoto et al., 2006). In wheat, overexpression of *TaDWF4-B* (which is the dominant shoot expressed homolog of *OsDWF4*) resulted in increased productivity and yield in wheat, primarily due to modified carbon partitioning and maintenance of photosystem II under low and sufficient nitrogen conditions (Milner et al., 2022).

4.1.3 Objectives of current study

The aim of the current study was to alter the canopy architecture in wheat by manipulating BR biosynthesis. Based on studies in other cereals, the BR biosynthetic genes *DWF1* and *DWF4* will be targeted in wheat, using a reverse genetics approach known as TILLING. To determine the effects of these mutations on BR signalling, BR hormone estimation and BR response assays will be conducted on the mutants.

An extensive phenotypic characterisation of the *tadwf1* and *tadwf4* mutants will be conducted under glasshouse conditions to establish the effects of these mutations on a range of traits. Traits such as flag-leaf angle, final plant height, internode lengths, spike and grain characteristics will be recorded to establish the role of these genes in controlling growth and development in wheat.

To establish how underlying changes in leaf architecture are caused, the anatomical differences existing in the lamina joint of these mutants will be investigated using scanning electron microscopy (SEM) and laser ablation tomography (LAT).

4.2 Results

4.2.1 Identification of the *DWF1* orthologues in wheat

To identify orthologs of the *DWF1/ DIM1* gene in wheat, the Arabidopsis *AtDWF1* gene sequence was used to blast (BlastP) against the wheat genome. This enabled the identification of three genes in wheat (present on chromosomes 7A, 7B and 7D) namely TraesCS7A02G559400, TraesCS7B02G484200 and TraesCS7D02G550700. This was followed by identification of orthologues of *DWF1* gene (by using protein sequence of *AtDWF1*) in various cereal species. The results of the blast analysis are given in Table 4.1. A phylogenetic tree was constructed using Neighbor end joining methods in Geneious 10.2.3 software (Figure 4.1). This enabled better understanding of the relatedness of *TaDWF1* genes with other related species.

Table 4. 1 Similarity of *DWF1* genes amongst species. BlastP was performed on Ensembl to identify orthologues of the gene using the predicted amino acid sequence of *AtDWF1*. The table provides the gene identifiers and their % identity with respect to *AtDWF1*.

S. No.	Species	Gene ID	Target %id
1	*Oryza sativa Japonica group*	Os10g0397400	79.32
2	*Triticum aestivum*	TraesCS7B02G484200	79.32
3	*Triticum aestivum*	TraesCS7A02G559400	78.61
4	*Triticum aestivum*	TraesCS7D02G550700	74.2
5	*Zea mays*	Zm00001eb228910	78.83
6	*Sorghum bicolor*	SORBI_3010G277300	76.78
7	*Hordeum vulgare*	HORVU.MOREX.r3.7HG0749940	73.31

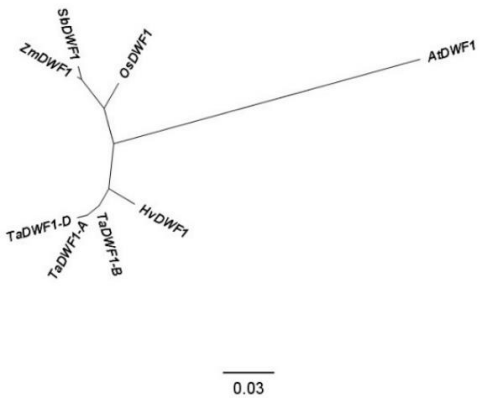

Figure 4. 1 Phylogenetic tree for *DWF1*. The tree was constructed using DWF1 protein sequence isolated from wheat, barley, maize, sorghum, rice, and Arabidopsis. This tree was constructed in Geneious10.2.3 software using Neighbor-joining method. The scale bar shows length of the branch.

4.2.2 Key domains in *DWF1* gene

Amino acid alignment predicted the presence of flavin adenine dinucleotide (FAD) domain in the encoded *DWF1* protein, implying gene belongs to oxidoreductase family and has enzymatic roles (Choe et al 1999). It was predicted to have a N-terminal hydrophobic stretch whose tentative function is to bind the protein to the cytosolic face of the membrane and transmembrane α helices enabling proper orientation of the protein (Tao et al 2004).

Based on a literature review, we attempted to annotate the various domains present in the wheat DWF1 proteins. The amino acid sequences of the DWF1 proteins in Arabidopsis, barley (*Hordeum vulagare*), rice (*Oryza sativa*), maize (*Zea mays*), sorghum (*Sorghum bicolor*) was aligned against the TaDWF1 sequences encoded by TraesCS7A02G559400, TraesCS7B02G484200 and TraesCS7D02G550700 (using ClustalW program on Geneious 10.2.3 software; Figure 4.2). Two domains have been identified in the ZmDWF1 protein (Tao et al., 2004). The first is a transmembrane domain required for membrane localisation and the second is a flavin adenine dinucleotide (FAD) domain required for oxidoreductase enzymatic activity of the protein. A high level of amino acid sequence identity was observed between the DWF1 proteins, included the conserved transmembrane and FAD domains.

Figure 4. 2 Alignment of DWF1 proteins showing conserved domains. The amino acid alignment of DWF1 proteins from Arabidopsis, maize, rice (*O. sativa*), barley (*H. vulgare*), and wheat (TraesCS7A02G559400, TraesCS7B02G484200 and TraesCS7D02G550700). The positions of various domains and motifs are annotatedon the ZmDWF1 protein sequence (Tao et al 2004). They include the transmembrane domain (maroon), FAD domain (green). The amino acid alignment was generated using ClustalW programme in Geneious 10.2.3 software.

4.2.3 Identification of mutations in *TaDWF1* genes using TILLING

Many mutations have been reported and characterised in the *DWF1/DIM* genes in Arabidopsis, rice, and barley (Choe et al 1999; Hong et al 2005 and Dockter et al 2014). Interestingly, these mutations do not confer the extreme phenotypic abnormalities that are observed in *BRI1* mutants. Therefore, to establish the function of the wheat *DWF1* genes the hexaploid wheat TILLING population (Krasileva et al., 2017) was screened for deleterious mutations within the three homoeologous *TaDWF1* genes. The Cadenza TILLING lines CAD-381, 1444 and 1339 were identified as containing nonsense mutations resulting in premature termination at codons 92, 23 and 252 in the coding sequence of the *TaDWF1-A*, *TaDWF1-B* and *TaDWF1-D*, respectively. To confirm the presence of these mutations, the respective regions of the *TaDWF1* genes were amplified by PCR from gDNA isolated from the TILLING lines and then confirmed by sequencing (supplementary table 1). As premature stop codons occur before the region encoding the transmembrane (*TADWF1-B*) or FAD domain (*TADWF1-A* and *TADWF1-D*) of the protein it is expected that they result in non-functional proteins. The positions of these mutations at DNA and protein levels are illustrated schematically below in Figure 4.3. A detailed description of the mutations is given in Table 4.2 below.

Table 4. 2 *DWF1* homoeologues in wheat and the position of TILLING mutations. The position of nonsense mutations identified in the *TaDWF1* homoeologues of Cadenza TILLING lines are indicated.

S. No.	Gene	Chromosome	Gene Id	Variant	Amino Acid substitution	Line No.
1	*TaDWF1A*	7A	TraesCS7A02G559400	stop_gained	W92*	381
2	*TaDWF1B*	7B	TraesCS7B02G484200	stop_gained	Q23*	1444
3	*TaDWF1D*	7D	TraesCS7D02G550700	stop_gained	Q252*	1339

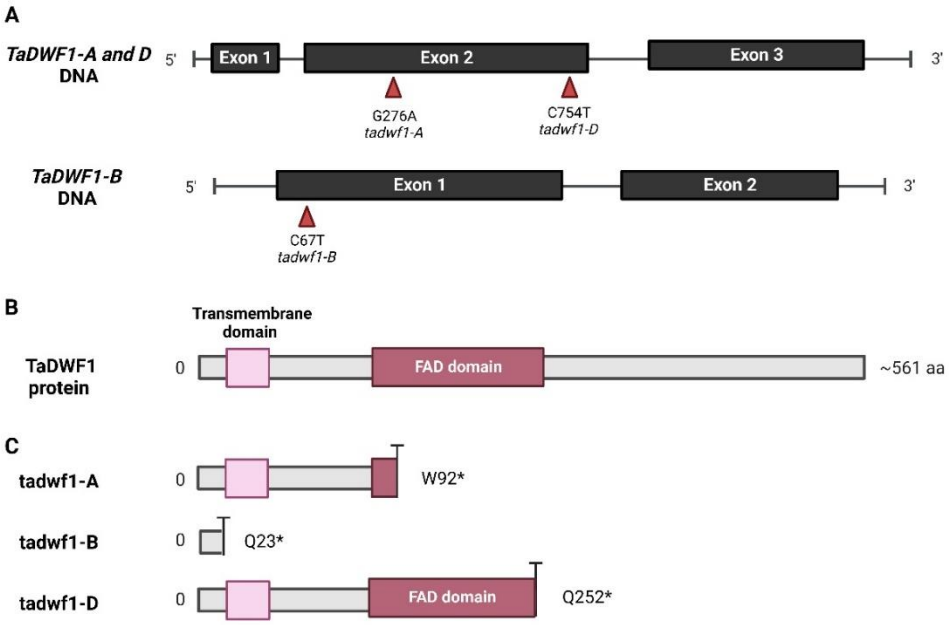

Figure 4. 3 Schematic diagram of *TaDWF1* gene, protein and position of mutations. (A) Shows the *DWF1* gene with the position of introns, exons and deleterious TILLING mutations in *tadwf1-A*, *tadwf1-B* and *tadwf1-D* gene. *TaDWF1-A* and *TaDWF1-D* genes contain 3 exons, whereas *TaDWF1-B* contains 2 exons. (B) The position of conserved domains present in the *TaDWF1* protein including the transmembrane (pink) and FAD (maroon) domains which are critical for protein function. (C) Shows the positions of the premature stop codons that results in predicted truncations at W92*, Q23* and Q252* on the tadwf1-A, -B and -D, respectively.

4.2.4 Identification of *DWF4* orthologues in wheat

To identify the *DWF4* orthologues in wheat, a Blast analysis (BlastP) was conducted using the sequences of *AtDWF4*. The analysis resulted in the identification of two putative orthologues in wheat (*TaDWF4* and *TaDWF4L*) as reported in Milner et al., 2022. Three putative *TaDWF4* homoeologues were identified on chromosome 4 (TraesCS4A02G078000, TraesCS4B02G234100 and TraesCS4D02G235200). In contrast, four *TaDWF4L* homoeologues were identified in chromosome 3 (TraesCS3A02G519000, TraesCS3B02G586500, TraesCS3D02G526400 and TraesCS3D02G526300), which include a duplication on chromosome 3D. This was followed by identification of orthologues of *DWF4* gene (by using protein sequence of *AtDWF4*) in various cereal species. The results of the blast analysis are given in Table 4.3. A phylogenetic tree was constructed to see relatedness of *TaDWF4* and *TaDWF4L* genes with other species as shown in Figure 4.4.

Table 4. 3 Blast search results for identification of orthologues of *DWF4* gene in various species. BlastP was performed on Ensembl to identify orthologues of the gene using amino acid sequence of *AtDWF4*. The table gives information of the gene Id, identity % w.r.t. sequence of *AtDWF4*.

S.No.	Species	Gene ID	Target %id
1	*Oryza sativa Japonica Group*	Os03g0227700	67.79
2	*Triticum aestivum*	TraesCS4A02G078000	61.03
3	*Triticum aestivum*	TraesCS4B02G234100	67.59
4	*Triticum aestivum*	TraesCS4D02G235200	67.72
5	*Sorghum bicolor*	SORBI_3001G445900	66.53
6	*Triticum aestivum*	TraesCS3A02G519000	66
7	*Triticum aestivum*	TraesCS3B02G586500	66.13
8	*Triticum aestivum*	TraesCS3D02G526300	66.67
9	*Triticum aestivum*	TraesCS3D02G526400	64.4
10	*Zea mays*	Zm00001eb009730	65.55

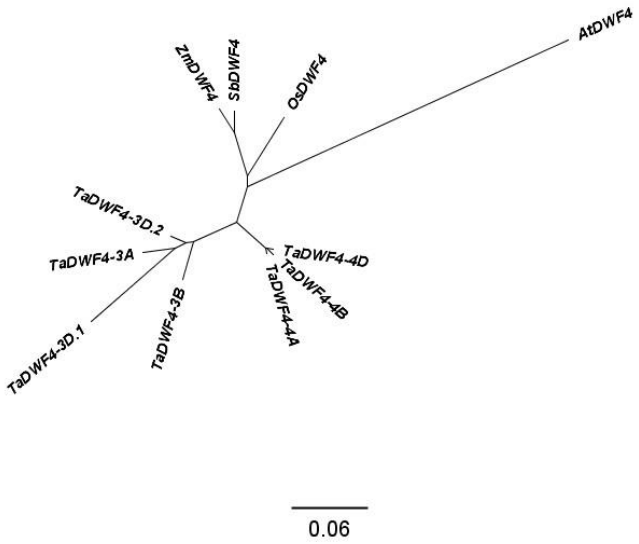

Figure 4. 4 Phylogenetic tree for *DWF4*. The tree was constructed using DWF4 protein sequences isolated from wheat, maize, sorghum, rice, and Arabidopsis were used for building the tree. The tree was constructed using a Neighbor-joining method in Geneious10.2.3 software. The scale bar shows length of the branch.

4.2.5 Key domains in *DWF4* gene

The amino acid sequences of the DWF4 proteins from Arabidopsis, rice (*Oryza sativa*), maize (*Zea mays*), sorghum (Sorghum bicolor) was aligned against the *TaDWF4* sequences, including TraesCS4A02G078000 (TaDWF4-4A), TraesCS4B02G234100 (TaDWF4-4B) and TraesCS4D02G235200 (TaDWF4-4D) and TaDWF4L sequences i.e., TraesCS3A02G519000 (TaDWF4-3A), TraesCS3B02G586500 (TaDWF4-3B), TraesCS3D02G526400 (TaDWF4-3D.1) and TraesCS3D02G526300 (TaDWF4-3D.2). A high level of amino acid sequence identity was observed between the proteins from different plant species as indicated in Figure 4.5.

Figure 4. 5 Domains and motifs present in DWF4 proteins. The amino acid alignment of putative DWF4 proteins from Arabidopsis, maize (*Zea mays*), rice (*O. sativa*), sorghum (*Sorghum bicolor*), and wheat.The positions of conserved domains and motifs are annotated on the ZmDWF4 protein and include domain A, B, and C and a Heme binding site (Liu et al 2007). The amino acid alignment was generated using ClustalW programme in Geneious 10.2.3 software.

4.2.6 Identification of mutations in the *TaDWF4* genes using TILLING

To establish whether the *TaDWF4* and *TaDWF4L* paralogues have a major role in controlling BR-responsive growth in wheat, their expression profiles were investigated. Interrogating the publicly available wheat expression database (Gonzalez et al 2018 on www.wheat-expression.com) and the mRNA-seq results described in the previous chapter (section 3.2.5) demonstrated that the *TaDWF4* homoeologues had significantly higher expression levels than the *TaDWF4L* genes at seedling stage (Figure 4.6 and 4.7). In fact, the levels of expression of *TaDWF4L* genes were undetectable or extremely low in most tissues. This suggests that *TaDWF4* is the predominant paralogue involved in BR biosynthesis in wheat and was therefore selected for further characterisation.

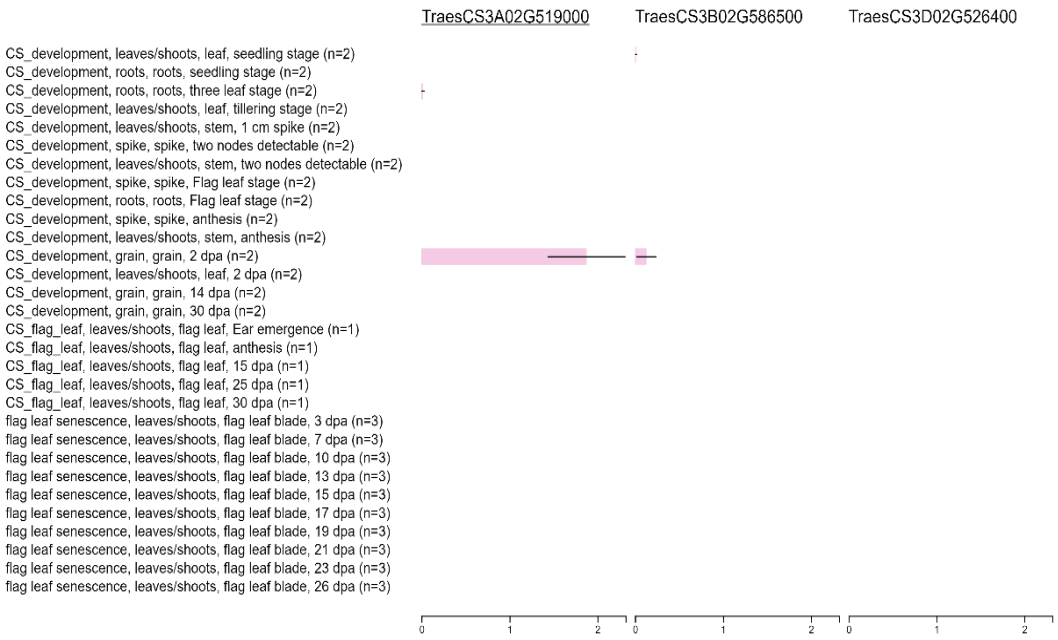

Figure 4. 6 *TaDWF4L* gene expression levels in different tissues. The expression of three homoeologues of *TaDWF4L* i.e. TraesCS3A02G519000, TraesCS3B02G586500, TraesCS3D02G526400 (transcripts per million i.e. tpm) was established using the wheat expression browser (www.wheat-expression.com) at various growth stages in the wheat variety Chinese spring. The expression scale is 0-2 tpm.

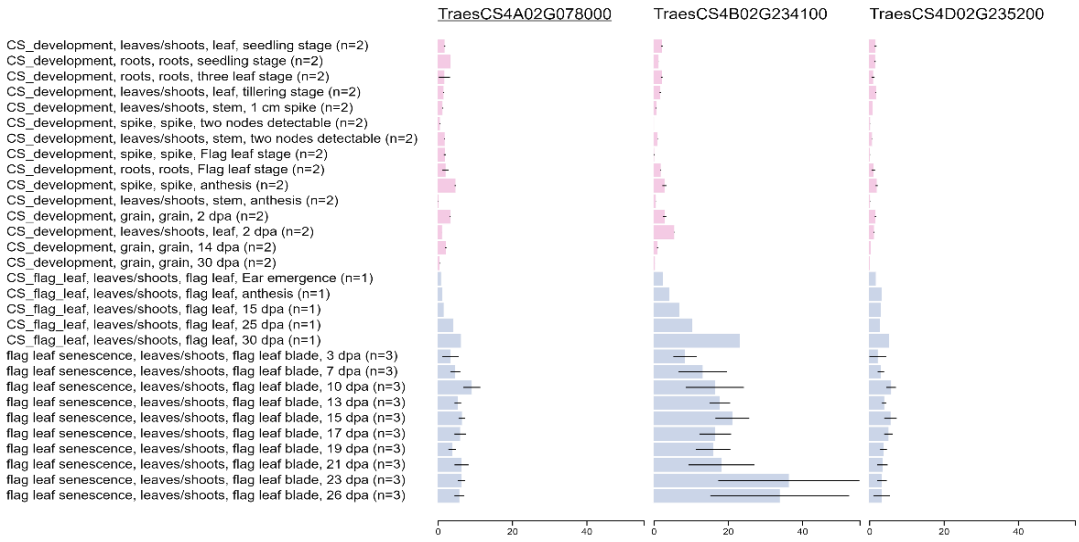

Figure 4. 7 *TaDWF4* gene expression levels in different tissues. The expression of three *TaDWF4* homoeologues of i.e. TraesCS4A02G078000, TraesCS4B02G234100 and TraesCS4D02G235200 (transcripts per million i.e. tpm) was established using the wheat expression browser (www.wheat-expression.com) at various growth stages in the wheat variety Chinese spring. The expression scale is 0-40 tpm.

To characterise the roles of the *TaDWF4* genes, deleterious mutations were identified in the Cadenza TILLING population. The TILLING lines CAD4-1353, 0012 and 0934 were identified as containing nonsense mutations in *TaDWF4A*, *TaDWF4B* and *TaDWF4D*, respectively (Table 4.4). These mutations are expected to introduce premature stop codons at the coding positions W168*, W39* and W353* *TaDWF4A*, *TaDWF4B* and *TaDWF4D*, respectively. To confirm the presence of the mutations the regions of *TaDWF4* genes were amplified using gene-specific markers and sequenced (supplementary table 1). A summary of the *TaDWF4* TILLING mutations and their positions in the gene are shown in Table 4.4. The mutations are expected to result in production of truncated proteins lacking essential domains required for functionality and are therefore expected to be null alleles. The schematic diagram of the tadwf4 proteins is shown in Figure 4.8.

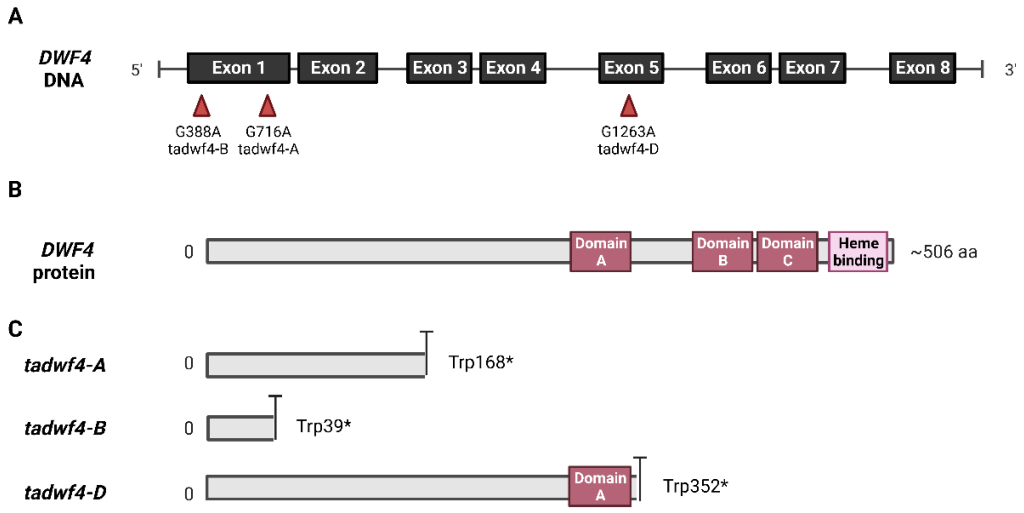

Figure 4. 8 Schematic diagram of *TaDWF4* gene, encoded protein and sites of mutations. (A) Schematic diagram of *DWF4* gene with the position of exons and introns and location of the deleterious mutations in homoeologous genes. (B) Illustrates the key domains i.e. A, B, C and heme binding, present in TaDWF4. (C) The predicted TaDWF4 truncations caused by the TILLING mutations.

Table 4. 4 *TaDWF4* homoeologues and the position of TILLING mutations. The gene identifiers and position of nonsense mutations identified in the *TaDWF4* homoeologues of Cadenza TILLING lines are indicated.

S. No.	Gene	Chromosome	Gene Id	Variant	Position	Line No.
1	*TaDWF4A*	4A	TraesCS4A02G078000	stop_gained	W168*	1353
2	*TaDWF4B*	4B	TraesCS4B02G234100	stop_gained	W39*	12
3	*TaDWF4D*	4D	TraesCS4D02G235200	stop_gained	W352*	934

4.2.7 Generation of *tadwf1* and *tadwf4* combinatorial mutants for gene characterization

At the start of this project, mutations in *TaDWF1* had previously been identified, stacked, and backcrossed to generate BC_2F_2 seed (Steve Thomas, personal communications). KASP markers were generated (supplementary table 2) for targeting these mutations and used to identify combinatorial groups i.e., single (*tadwf1-a*, *tadwf1-b*, and *tadwf1-d*), double (*tadwf1-ab*, *tadwf1-ad*, and *tadwf1-bd*) and triple mutants (*TaDWF1-NS* and *tadwf1-abd*). In contrast, *TaDWF4* was selected as a new target, therefore it was necessary to identify and stack TILLING mutations and perform backcrossing with the aim of conducting a phenotypic characterization.

The scheme followed for generation of the *tadwf4* combinatorial mutants is discussed in detail in section 2.3.2 of material and methods chapter.

4.2.8 Phenotypic characterization of *tadwf1* and *tadwf4* mutants under glasshouse conditions

Mutations in the *DWF1* gene result in erect-leaf architecture, reduced final plant height (due to restricted internode elongation), production of malformed panicles with reduced spikelet number and fertility in rice (Hong et al., 2005). Similarly, reduced stem height due to restricted internode elongation was also reported in the *dwf1* mutants of barley and maize (Dockter et al., 2014; Best et al., 2016). In contrast knocking out the *DWF4* gene caused upright canopy architecture, slight dwarfism, and normal grain development in rice (Sakamoto et al., 2006). Whereas, overexpressing *DWF4* resulted in increased leaf angles, tiller number, thousand grain weight, and grain yield/plant in rice mutants (Li et al., 2018).

To establish the phenotype associated with knocking-out *DWF1* and *DWF4* genes in wheat, we performed preliminary evaluation of all the singles, doubles, and triple knockout mutants at the BC2F2 generation under glasshouse conditions. Subsequently, a more detailed phenotypic characterisation of only the triple mutants (*tadwf1-abd*, *TaDWF1-NS*, *tadwf4-abd* and *TaDWF4-NS*) along with Cadenza was conducted in the glasshouse. Traits such as flag-leaf angle, plant height, internode elongation, spike and grain characteristics were recorded. The aim of this experiment was to determine the effect of these mutations on above ground phenotype under glasshouse conditions.

4.2.8.1 Preliminary phenotypic evaluation of all the combinatorial mutants of *TaDWF1* gene

We performed a preliminary phenotypic characterisation experiment with various mutants at the BC2F2 generation) under glasshouse conditions. Four biological replicates of each combinatorial mutant i.e., singles (*tadwf1-a*, *tadwf1-b*, and *tadwf1-d*), doubles (*tadwf1-ab*, *tadwf1-ad*, and *tadwf1-bd*) and triples (*TaDWF1-NS* and *tadwf1-abd*) were grown with Cadenza and planted in a randomised complete block design. The flag-leaf angles (at 22 days after anthesis) and final plant height of these mutants was recorded as described below.

4.2.8.1.1 Flag-leaf angles

To establish the effects of *tadwf1* mutations on canopy architecture in wheat, we recorded the flag-leaf angles (LA) at 22 days post-anthesis (22DPA) stage on the primary tillers. The data collected was analysed using ANOVA (details under the statistical analysis section 2.9 of material and methods chapter) and is presented below in Table 4.5 and Figure 4.9.

ANOVA confirmed statistical significant differences in flag leaf angle (LA) amongst these mutants in the experiment [F (8,31) = 17.61, p <.001]. No significant differences existed between the LA of Cadenza and *TaDWF1-NS*. Therefore, both genotypes could be considered as the control. We observed significant reductions in the flag-leaf angle in all the mutants with the exception of *tadwf1-ad* when compared against *TaDWF1-NS*. The *tadwf1-abd* mutant displayed a striking reduction in LA of approximately 80% when compared against *TaDWF1-N*S. This demonstrates an important role for the *DWF1* gene in regulating flag leaf angle in wheat.

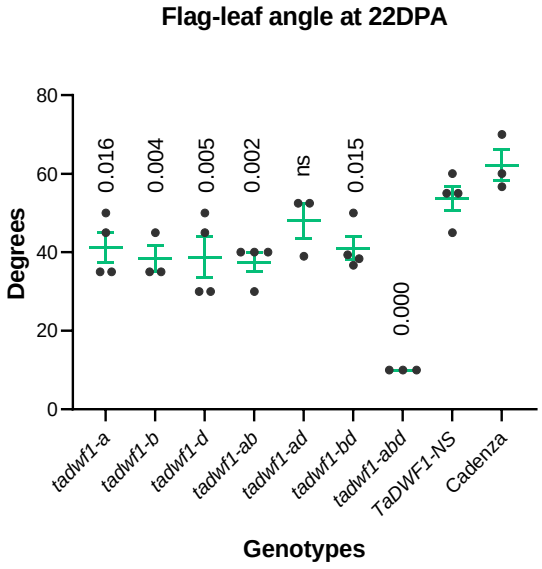

Figure 4. 9 Flag-leaf angles of *tadwf1* mutants. LA was recorded at 22 days post-anthesis (DPA) in combinatorial *tadwf1* mutants compared against Cadenza and *TaDWF1-NS* (n=4). *P*-values for differences between mutants and *TaDWF1-NS* obtained using Fisher's unprotected LSD test are shown above.

Table 4. 5 Flag-leaf angles of *tadwf1* mutants. LA (mean ± SD) of the various *tadwf1* mutants and control lines were recorded at 22 DPA during GH2019. The % change in the leaf angles was compared against *TaDWF1-NS* control. General ANOVA output i.e., *p*-values, SED, and LSD at 5% level of significance are also shown. Statistical significant difference between mutant and *TaDWF1-NS* were denoted $*P < 0.05$, $**P < 0.01$, $***P < 0.001$, $****P < 0.0001$ (obtained from Fisher's LSD unprotected test).

Genotypes	FLA (degrees) at 22DPA	% Change
tadwf1-a	41.2 ± 7.5*	-23.3
tadwf1-b	38.3 ± 5.8**	-28.7
tadwf1-d	38.7 ± 10.3**	-27.9
tadwf1-ab	37.5 ± 5**	-30.2
tadwf1-ad	48 ± 7.8	-10.6
tadwf1-bd	41.1 ± 6*	-23.5
tadwf1-abd	10 ± 0****	-81.4
TaDWF1-NS	53.7 ± 6.3	_
Cadenza	62.2 ± 6.9	15.8
***p*-value**	<.001	
SED	4.83	
LSD	10	

4.2.8.1.2 Final plant height

To understand the effects of *tadwf1* mutation on final plant height, the length of the tallest tiller/plant (including the ear) was recorded on four biological replicates. The data collected, was analysed using ANOVA and the data are described below in Table 4.6 and Figure 4.10. ANOVA confirmed significant differences amongst the mutants for final plant height [$F(8,34) = 14.91$, $p < .001$]. We observed an approximate 37% reduction in the final plant height in the *tadwf1-abd* triple mutant, compared to *TaBRI1-NS*, but no significant differences existed between the singles or double mutants and *TaBRI1-NS.* These results demonstrate a role for the *TaDWF1* gene in regulating stem elongation in wheat. It also demonstrates that the *TaDWF1* homoeologues have functionally redundant roles in controlling stem elongation in wheat.

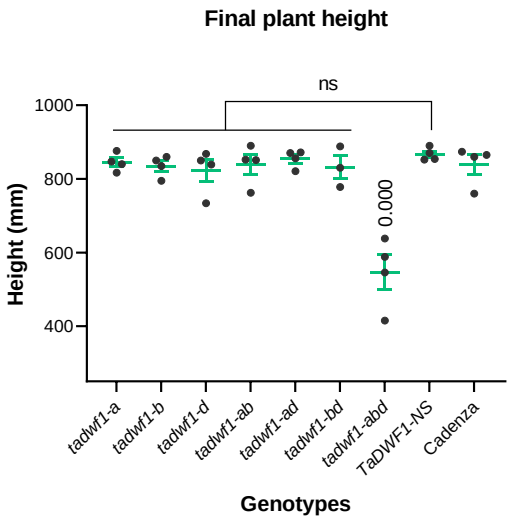

Figure 4. 10 Final plant height of *tadwf1* mutants. The data was recorded in *tadwf1* combinatorial mutants and the controls *TaDWF1-NS* and Cadenza (n=4) at maturity. *P*-values for differences between mutants and *TaDWF1-NS* obtained using Fisher's unprotected LSD test are also shown.

Table 4. 6 Final plant height of *tadwf1* mutants. Final plant height (mean ± SD) was recorded in combinatorial *tadwf1* mutants and control lines at maturity. The % difference in the plant height compared to *TaDWF1-NS* control is also shown. General ANOVA output i.e., *p*-values, SED, and LSD at 5% level of significance are described below. Statistical significant difference between mutant and *TaDWF1-NS* were denoted **P* < 0.05, ***P* < 0.01, ****P* < 0.001, *****P* < 0.0001 (obtained from Fisher's LSD unprotected test).

Genotypes	Final plant height (mm)	% Change
tadwf1-a	845 ± 24.3	-2.5
tadwf1-b	835 ± 28.6	-3.6
tadwf1-d	822.7 ± 60.6	-5
tadwf1-ab	838.8 ± 54.3	-3.2
tadwf1-ad	854.8 ± 23.6	-1.3
tadwf1-bd	832 ± 55	-3.9
tadwf1-abd	546.8 ± 95.5****	-36.9
TaDWF1-NS	866.5 ± 17.6	_
Cadenza	839.7 ± 53.5	-3.1
***p*-value**	<.001	
SED	36.33	
LSD	74.67	

4.2.8.2 Phenotypic evaluation of *tadwf4* combinatorial mutants.

To establish the phenotype associated with loss-of-function mutations in the wheat *DWF4* genes, a preliminary phenotypic characterisation experiment was conducted including *tadwf4* combinatorial mutants (BC2F2 generation) under glasshouse conditions (GH2022). Four biological replicates of each combinatorial mutant i.e., singles (*tadwf4-a*, *tadwf4-b*, and *tadwf4-d*), doubles (*tadwf4-ab*, *tadwf4-ad*, and *tadwf4-bd*) and triples (*TaDWF4-NS* and *tadwf4-abd*) along with Cadenza were planted in a randomised complete block design. The flag-leaf angles (at anthesis stage) and final plant height was recorded on these mutants as described below.

4.2.8.2.1 Flag leaf angle

To establish the effects of *tadwf4* mutations on canopy architecture in wheat, we recorded the flag-leaf angles (LA) on the primary tillers of all combinatorial mutants at anthesis stage. The data collected was analysed using ANOVA and is presented below in Table 4.7 and Figure 4.11.

ANOVA confirmed statistical significant differences in flag-leaf angle amongst these mutants in the experiment [F (8,35) = 7.08, p <.001]. We observed an approximate 65% reduction in LA in the *tadwf4-abd* triple mutant compared to *TaDWF4-NS* which was statistically significant as the *P*-value obtained by Fisher's unprotected LSD test was <0.05. In contrast, except for *tadwf4-abd*, we observed no significant differences amongst the singles and double mutants compared to *TaDWF4-NS*. Only a small difference was observed in the *tadwf4-bd* mutant (P = 0.034) and the significance is not clearly apparent. These results demonstrate a role for the *TaDWF4* homoeologues in regulating flag leaf angle in wheat and highlights that they have functionally redundant roles.

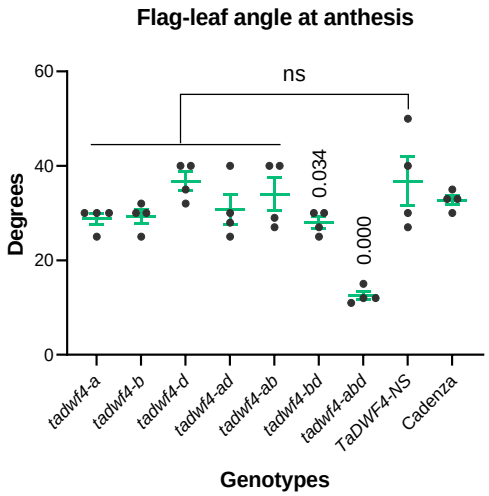

Figure 4. 11 Flag-leaf angles of *tadwf4* mutants. The data was recorded at anthesis in combinatorial*tadwf4* mutants along with Cadenza and *TaDWF4-NS* (n=4). *P*-values for differences between mutants and *TaDWF4-NS* obtained using Fisher's unprotected LSD test are also shown. 'ns' refers to no-significant differences existing amongst the pair of genotypes being compared.

Table 4. 7 Flag-leaf angles of *tadwf4* mutants. Flag leaf angle (mean ± SD) of the various *tadwf4* mutants and control lines recorded at anthesis during GH2022. The % change in the leaf angles in mutants was compared against *TaDWF4-NS* control. General ANOVA output i.e., *p*-values, SED, and LSD at 5% level of significance is also described below. Statistical significant difference between mutant and *TaDWF4-NS* were denoted $*P < 0.05$, $**P < 0.01$, $***P < 0.001$, $****P < 0.0001$ (obtained from Fisher's LSD unprotected test).

Genotypes	FLA at anthesis (degrees)	% Change
tadwf4-a	28.7 ± 2.5	-21.8
tadwf4-b	29.2 ± 3	-20.4
tadwf4-d	36.7 ± 3.9	0
tadwf4-bd	28 ± 2.4*	-23.7
tadwf4-ad	30.7 ± 6.5	-16.3
tadwf4-ab	34 ± 7	-7.3
tadwf4-abd	12.5 ± 1.7****	-65.9
TaDWF4-NS	36.7 ± 10.4	_
Cadenza	32.7 ± 2.1	-10.9
p-value	<.001	
SED	3.8	
LSD	8.02	

4.2.8.2.2 Final plant height

To establish the effects of *tadwf4* mutation on final plant height, we recorded the length of the tallest tiller/plant (including the ear) on four biological replicates of each line. The data was analysed using ANOVA and presented below in Table 4.8 and Figure 4.12. ANOVA confirmed no significant differences amongst the mutants for final plant height [F (8,32) = 1.11, p = 0.39]. This demonstrates that *TaDWF4* gene has no obvious role in regulating final plant height in wheat under glasshouse conditions.

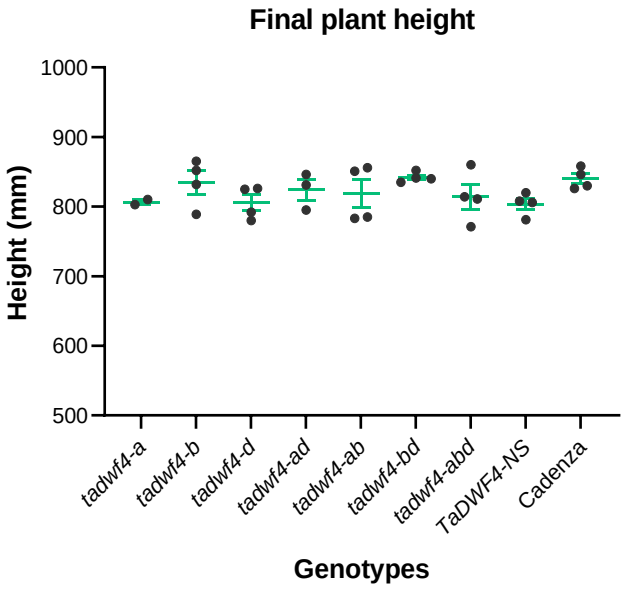

Figure 4. 12 Final plant height in *tadwf4* mutants. The data was recorded in combinatorial *tadwf4* mutants along with Cadenza and *TaDWF4-NS* controls (n=4). No significant differences were observed for the trait as the *p*-value obtained by ANOVA was 0.39 which was significantly greater than 0.05.

Table 4. 8 Final plant height in *tadwf4* mutants. Plant height (mean ± SD) of the various *tadwf4* mutants and control lines was recorded at maturity. The % change in the height was compared against *TaDWF4-NS*. General ANOVA output i.e., *p*-values, SED, and LSD at 5% level of significance are also described below.

Genotypes	Final plant height (mm)	% Change
tadwf4-a	806.5 ± 4.0	0.36
tadwf4-b	834.5 ± 33.2	3.8
tadwf4-d	805.7 ± 23.3	0.2
tadwf4-bd	824 ± 26.2	2.5
tadwf4-ad	818.7 ± 40.2	1.8
tadwf4-ab	842 ± 7.2	4.7
tadwf4-abd	814 ± 36.4	1.3
TaDWF4-NS	803.7 ± 16.4	_
Cadenza	840 ± 14.8	4.5
p-value	0.396	
SED	19.3	
LSD	40.2	

4.2.8.3 Detailed phenotypic characterization of *tadwf1* and *tadwf4* triple mutants

Based on the phenotypic characterization of *tadwf1* and *tadwf4* combinatorial mutants, it was found that major architectural changes were most apparent in the triple mutants. This indicates the existence of a high level of functional redundancy in the roles of the respective homoeologous genes. Therefore, a more detailed phenotypic characterization of the triple *tadwf1-abd* and *tadwf4-abd* mutants was conducted along with *TaDWF1-NS, TaDWF4-NS* and Cadenza controls. The experiment included 6 biological replicates of each genotype which were planted in randomised complete block design in the glasshouse. We recorded the flag-leaf angle, final plant height, internode lengths, spike, and grain characteristics in the genotypes.

4.2.8.3.1 Flag-leaf angle

To establish the effect of *tadwf1* and *tadwf4* mutations on leaf architecture, flag-leaf angles were recorded on these genotypes at 14 DPA. ANOVA was then performed to analyse the data which is presented in Figure 4.14 and Table 4.9. ANOVA confirmed statistically significant differences for flag-leaf angle [$F(4,29) = 12.81$, $p<.001$]. The flag leaf angle of the controls *TaDWF1-NS, TaDWF4-NS* and Cadenza

were 73, 87 and 74 degrees, respectively, but statistically they were not significant. In contrast, a striking reduction in the LA of the *tadwf1-abd* and *tadwf4-abd* triple mutants was observed compared to the respective *TaDWF1-NS* and *TaDWF4-NS* controls. The results obtained in this experiment were similar to the differences observed in the preliminary glasshouse experiment (Figures 4.9 and 4.11). The erect stature of the *tadwf1-abd* and *tadwf4-abd* triple mutants at GS87 is shown in Figure 4.13. This demonstrates the roles of *TaDWF1* and *TaDWF4* in regulating flag-leaf angle in wheat.

Figure 4. 13 Gross morphology of *tadwf1-abd, tadwf4-abd* mutants. Phenotype of the *tadwf1-abd* and *tadwf4-abd* triple mutants compared with Cadenza. Plants were grown in a glasshouse and photographed at GS87 stage. Scale-bar length is equivalent to 20cm.

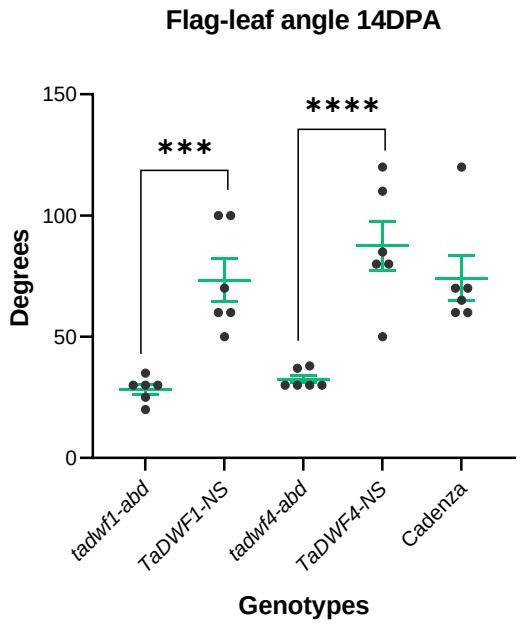

Figure 4. 14 Flag-leaf angles of *tadwf1* and *tadwf4* triple mutants. The data was recorded at 14 DPA in the triple mutants along with Cadenza (n=6). Statistical significant difference between triple knockout mutants and respective null-segregants (NS) were denoted as ***$P < 0.001$, ****$P < 0.0001$ (obtained from Fisher's LSD unprotected test).

Table 4. 9 Flag-leaf angles in *tadwf1* and *tadwf4* triple mutants. Flag leaf angle (mean ± SD) of the various mutants and control lines were recorded at 14 days post-anthesis (DPA) during GH2022. The % change in the leaf angles was compared against respective NS control. General ANOVA output i.e., *p*-values, SED, and LSD at 5% level of significance are also described below. Statistical significant difference between mutant and NS were denoted as ***$P < 0.001$, ****$P < 0.0001$ (obtained from Fisher's LSD unprotected test).

Genotypes	FLA 14DPA (degrees)	% Change
tadwf1-abd	28.3 ± 5.1***	-61.4
TaDWF1-NS	73.3 ± 21.6	_
tadwf4-abd	32.5 ± 3.8****	-62.8
TaDWF4-NS	87.6 ± 24.8	_
Cadenza	74.2 ± 22.8	
p- value	<.001	
SED	10.6	
LSD	22.15	

4.2.8.3.2 Final plant height and internode elongation

To establish the effect of *tadwf1* and *tadwf4* mutations on final plant height, we measured the length of the tallest tiller/plant (including ear/ spike) for all of the genotypes. Data was analysed using ANOVA and the results are presented in Figure 4.15 and Table 4.10. ANOVA confirmed statistically significant differences amongst the genotypes for final plant height [F (4, 29) = 52.93, p<.001]. The final plant height of the *tadwf1-abd* mutant was reduced by approximately 27% compared to the *TaDWF1-NS*. No significant reduction was observed in the final plant height of the *tadwf4-abd* mutant compared to *TaDWF4-NS*. This demonstrated a specific role of *TaDWF1* genes in regulating final plant height in wheat. In contrast, *TaDWF4* does not appear to have a role in controlling stem elongation.

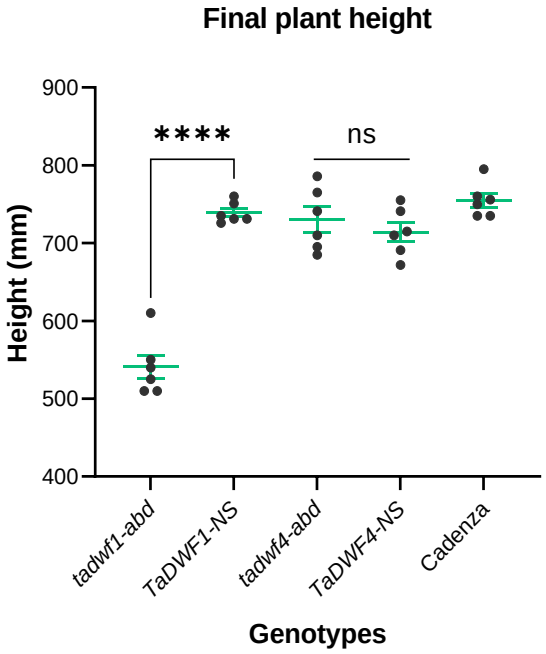

Figure 4. 15 Final plant height of *tadwf1* and *tadwf4* triple mutants. The data was collected (n=6) when the genotypes had reached maturity during GH2022. Statistically significant differences between triple mutants and respective null-segregants (NS) were denoted as ****$P < 0.0001$ (obtained from Fisher's LSD unprotected test).

Table 4. 10 Final plant height in *tadwf1* and *tadwf4* triple mutants. Final plant height (mean ± SD) was recorded at maturity during GH2022. The % change in the height was compared with the respective NS control is indicated. General ANOVA output i.e., *p*-values, SED, and LSD at 5% level of significance are also described below. Statistically significant differences between mutant and NS were denoted as ****$P < 0.0001$ (obtained from Fisher's LSD unprotected test).

Genotypes	Final plant height (mm)	% Change
tadwf1-abd	540.8 ± 37.4****	-26.7
TaDWF1-NS	739 ± 13.4	_
tadwf4-abd	730.3 ± 40.3	2.2
TaDWF4-NS	714 ± 30.7	_
Cadenza	755.2 ± 22.1	
p- value	<.001	
SED	17.09	
LSD	35.65	

To determine the contribution of individual internodes (peduncle, I2, I3 and I4 as they were present in the genotypes that were assessed) to final plant height, the internode lengths from 2-3 of the longest tillers from each plant were measured. The data are presented in Table 4.11 and a stacked bar graph in Figure 4.16. ANOVA confirmed significant differences in the lengths of the peduncle, I2 and I3 and I4 in the *tadwf1-abd* triple mutant compared with *TaDWF1-NS* (*p*-values <0.05). We observed approximately 35%, 18%, 18% and 23% reduction in the lengths of peduncle, I2, I3 and I4 in *tadwf1-abd* mutant, respectively, when compared to *TaDWF1-NS*. This demonstrates the trends of reduced internode elongation in the *tadwf1* triple mutant is similar to that observed in maize rather than in rice and barley. No significant differences in internode elongation were observed in the *tadwf4-abd* mutant compared to the controls, which is consistent with the lack of height reduction seen in this mutant.

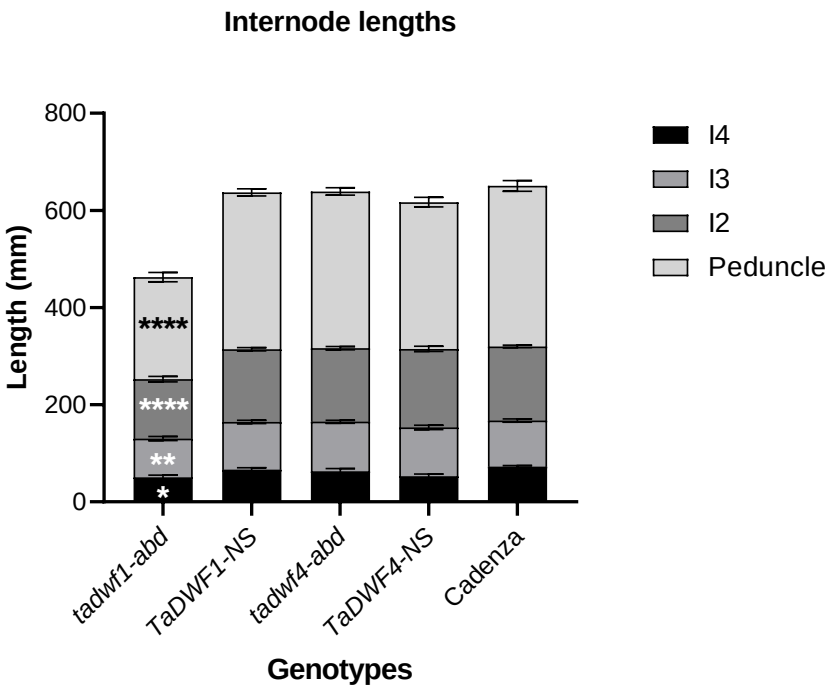

Figure 4. 16 Internode lengths of *tadwf1* and *tadwf4* triple mutants. The lengths of the peduncle, I2, I3 and I4 were recorded at maturity in *tadwf1-abd*, *TaDWF1-NS*, *tadwf4-abd* and *TaDWF4-NS* mutants along with Cadenza. The data are presented in the form of stacked bar graph. Statistical significant difference between the triple mutant and respective NS were denoted *$P < 0.05$, **$P < 0.01$, ***$P < 0.001$, ****$P < 0.0001$ (obtained from Fisher's LSD unprotected test).

Table 4. 11 Internode lengths in *tadwf1* and *tadwf4* triple mutants. The internode lengths (mm) of the peduncle, I2, I3 and I4 (mean ± SD) for *tadwf1-abd*, *TaDWF1-NS*, *tadwf4-abd* and *TaDWF4-NS* mutants were recorded along with Cadenza at maturity. The % change in the internode elongation of triple mutants was compared with respective NS. General ANOVA output i.e., *p*-values, SED, and LSD at 5% level of significance are also shown. Statistical significant difference between mutant and NS were denoted **P* < 0.05, ***P* < 0.01, ****P* < 0.001 (obtained from Fisher's LSD unprotected test).

Genotypes	**L of Peduncle (mm)**	**% Change**	**L of I2 (mm)**	**% Change**	**L of I3 (mm)**	**% Change**	**L of I4 (mm)**	**% Change**
tadwf1-abd	209.8 ± 34.7****	-35	122.3 ± 19.2****	-18.3	79.9 ± 14.6**	-18.7	50.4 ± 15.4*	-23.7
TaDWF1-NS	323 ± 25.2	_	149.7 ± 11.2	_	98.45 ± 10.4	_	66.1 ± 13.2	_
tadwf4-abd	322.6 ± 25.0	6.8	151.3 ± 11.4	-6.4	101.7 ± 10.3	1.3	63.2 ± 17.2	19.7
TaDWF4-NS	302 ± 30	_	161.7 ± 19.3	_	100.4 ± 16.3	_	52.8 ± 15.1	_
Cadenza	330.5 ± 39.4		152.6 ± 8.5		94.8 ± 11.3		72.4 ± 7.5	
p- value	<.001		<.001		0.001		0.002	
SED	13.35		5.96		5.47		5.96	
LSD	26.84		11.99		11		11.99	

4.2.8.3.3 Spike characteristics

To understand the effect of *tadwf1* and *tadwf4* mutations on spike development, we measured the number of spikelets/spike and spike length on six mature spikes/mutant in experiment GH2022. ANOVA was performed to analyse the data which is presented in Figures 4.17 and Table 4.12. below. For spike length, ANOVA confirmed statistically significant differences amongst the mutants [$F(4,29) = 76.41$, $p<.001$]. We observed higher reduction in spike length in *tadwf1-abd* mutant (approx. 20% smaller) compared to *TaDWF1-NS* and slight reduction in spike length of *tadwf4-abd* mutant (approximately 4% smaller) compared to *TaDWF4-NS*. ANOVA confirmed significant differences for number of spikelets/spike, amongst the mutants [$F(4,29) = 11.03$, $p<.001$]. We observed significant reduction in *tadwf1-abd* mutant, which produced 15 spikelets/spike compared to 17 in *TaDWF1-NS* and no significant differences were observed amongst *tadwf4* mutants. This demonstrates a role for *TaDWF1* mutations in regulating spike length and number of spikelets/ spikes. In contrast, *TaDWF4* appears to have only a minor role in controlling spike length without an influence in determining spikelet number.

A

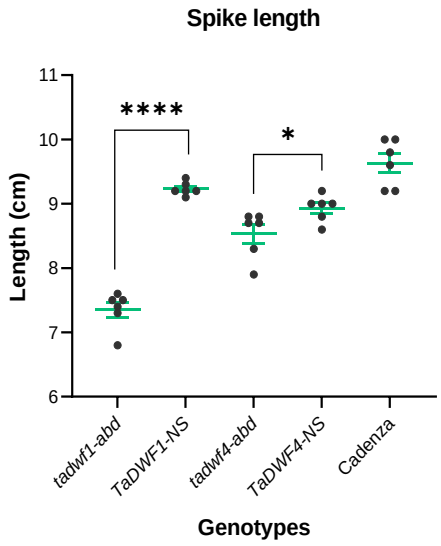

B

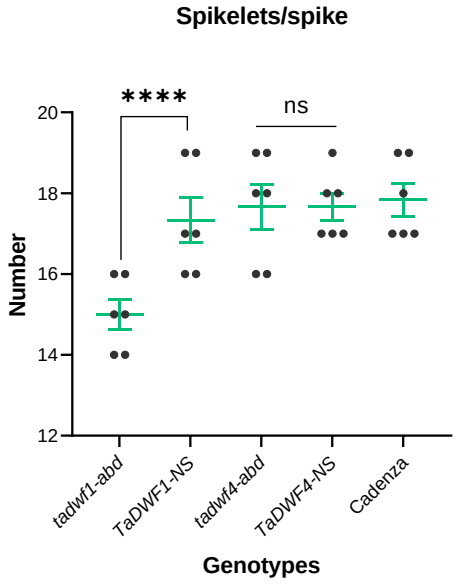

Figure 4. 17 Spike length and spikelet number in *tadwf1* and *tadwf4* triple mutants. Graph (A) shows spike length and (B) shows number of spikelets/spike recorded at maturity in *tadwf1-abd*, *TaDWF1-NS*, *tadwf4-abd* and *TaDWF4-NS* mutants along with Cadenza (n=6). Statistical significant difference between mutant and NS were denoted *$P < 0.05$, ****$P < 0.0001$ (obtained from Fisher's LSD unprotected test).

Table 4. 12 Spike length and spikelet number in *tadwf1* and*tadwf4* triple mutants. Spike length and spikelet number (mean ± SD) in *tadwf1-abd* and*tadwf4-abd* and the respective controls were recorded on mature spikes. The % change was calculated by comparing the means of triple mutants with respective NS's. General ANOVA output i.e., *p*-values, SED, and LSD at 5% level of significance are also described below. Statistically significant difference between mutant and NS were denoted *$P < 0.05$, ****$P < 0.0001$ (obtained from Fisher's LSD unprotected test).

Genotypes	Spike length (cm)	% Change	Number of spikelets/spike	% Change
tadwf1-abd	7.3 ± 0.3****	-20.6	15 ± 0.8****	-11.7
TaDWF1-NS	9.2 ± 0.1	_	17 ± 1	_
tadwf4-abd	8.5 ± 0.3*	-4.5	17 ± 1.2	-5.5
TaDWF4-NS	8.9 ± 0.2	_	18 ± 0.8	_
Cadenza	9.6 ± 0.4		18 ± 0.8	
p- value	<.001		<.001	
SED	0.14		0.5	
LSD	0.29		1.1	

4.2.8.3.4 Grain characteristics

To establish the impact of the *tadwf1* and *tadwf4* mutations on grain size (using Marvin seed analyzer, INDOSAW, India) and grain weight (weighing balance), clean grain obtained after thrashing from spike and removing chaff was analysed. The data obtained was analysed using ANOVA and is presented in Figure 4.18 and Table 4.13. ANOVA confirmed statistically significant differences for grain area amongst the various mutants [F (4,29) = 10.97, p<.001]. We observed an approximate 8.5% reduction in the grain area in the *tadwf1-abd* mutant compared to *TaDWF1-NS* and no significant differences amongst the *tadwf4* mutants. This demonstrates that *TaDWF1* promotes grain expansion in wheat. To determine grain weight the thousand grain weight (TGW) was measured, ANOVA confirmed no significant differences amongst the mutants [F (4,29) = 2.24, $p = 0.093$]. This indicates that the *tadwf1* and *tadwf4* mutations do not alter grain weight regardless of changes in seed area that were observed in the *tadwf1-abd* mutant.

A

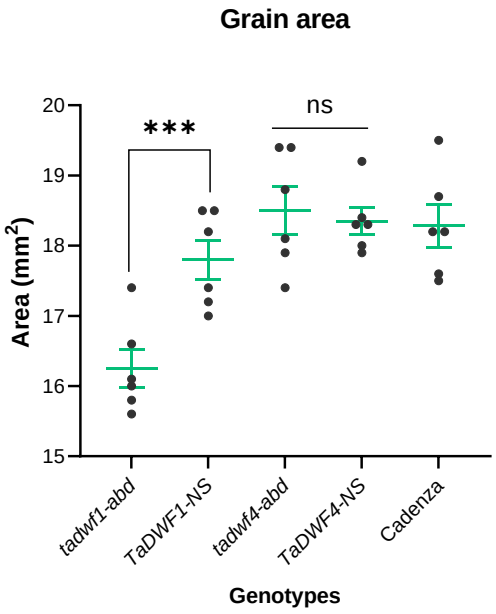

B

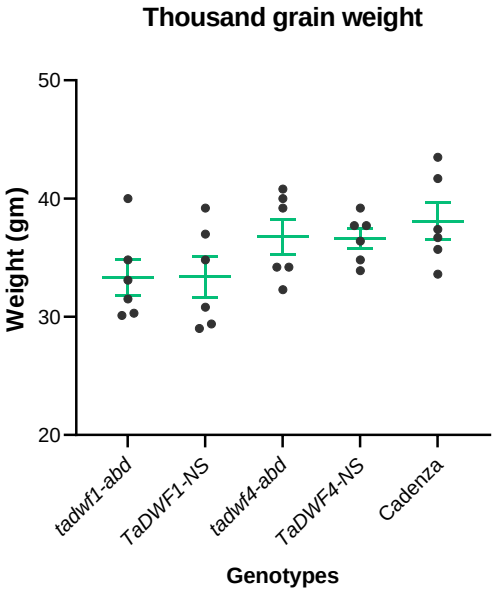

Figure 4. 18 Grain characteristics of *tadwf1* and *tadwf4* triple mutants. Graphs (A) shows grain area and (B) shows thousand grain weight (TGW) recorded in *tadwf1-abd*, *TaDWF1-NS*, *tadwf4-abd* and *TaDWF4-NS* mutants and Cadenza (n=6) on mature grains after harvesting and threshing. Statistically significant difference between the triple mutant and respective NS were denoted ***$P < 0.001$ (obtained from Fisher's LSD unprotected test).

Table 4. 13 Grain characteristics of *tadwf1* and *tadwf4* triple mutants. Thousand grain weight (TGW) and grain area (mean ± SD) of *tadwf1-abd*and *tadwf4-abd* mutants compared against the respective NS and Cadenza control. The % change was calculated by comparing the values of triple mutant with the respective NS controls. General ANOVA output i.e., *p*-values, SED, and LSD at 5% level of significance are also described below. Statistical significant difference between mutant and NS were denoted ***$P < 0.001$ (obtained from Fisher's LSD unprotected test).

Genotypes	TGW (gm)	% Change	Grain Area (mm^2)	% Change
tadwf1-abd	33.3 ± 3.7	-0.29	16.3 ± 0.6***	-8.4
TaDWF1-NS	33.4 ± 4.2	_	17.8 ± 0.6	_
tadwf4-abd	36.8 ± 3.6	0.54	18.5 ± 0.8	0.5
TaDWF4-NS	36.6 ± 2	_	18.4 ± 0.4	_
Cadenza	38.1 ± 3.7		18.3 ± 0.7	
p-value	0.093		<.001	
SED	2.05		0.39	
LSD	4.24		0.81	

4.2.8.4 Seedling phenotype of *tadwf1* and *tadwf4* triple mutants

To assess the phenotype of the *tadwf1-abd* and *tadwf4-abd* triple mutants at the seedling growth stage they were grown in a randomised block design and compared against Cadenza and the respective null segregants. Once these seedlings reached the 2nd leaf stage, after approximately 10-14 days, the traits such as leaf angle, seedling height, leaf blade length and width were recorded as described below.

4.2.8.4.1 Leaf angle

The role of *TaDWF1* and *TaDWF4* in regulating flag leaf angle at reproductive stages was established previously (section 4.2.8.3.1). Interestingly, a similar trend in leaf angle reduction was observed in the *tadwf1* and *tadwf4* triple mutants at the seedling stage. For instance, we observed around a 50% reduction in the LA in *tadwf1-abd* mutant compared to *TaDWF1-NS* and 40% reduction in LA in *tadwf4-abd* mutant compared to *TaDWF4-NS*. The data are shown in Figure 4.19 and Table 4.14 below. No significant differences existed in the leaf angles of *TaDWF1-NS, TaDWF4-NS* and Cadenza. Thus, there is strong possibility that altered leaf angle in these mutants is governed by similar regulatory processes operating at seedling and reproductive stage.

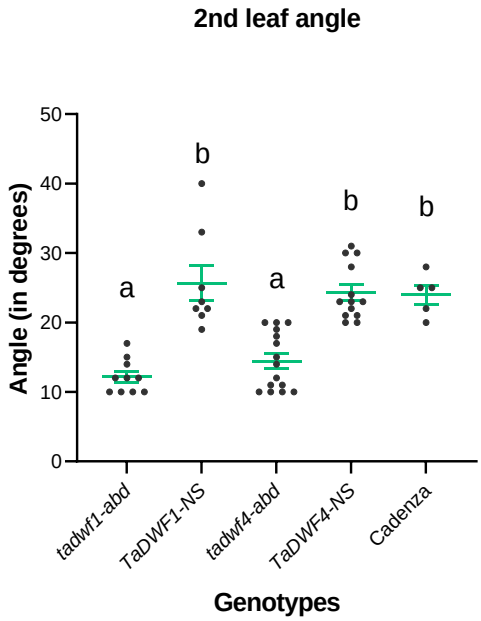

Figure 4. 19 Seedling leaf angle of *tadwf1* and *tadwf4* triple mutants. The leaf angle (in degrees) of the second leaf was recorded in *tadwf1-abd*, *TaDWF1-NS*, *tadwf4-abd* and *TaDWF4-NS* mutants along with Cadenza. ANOVA confirmed presence of statistical differences (in LA) amongst the genotypes. Different letters were used to designate significant differences amongst the genotypes.

Table 4. 14 Seedling leaf angle in *tadwf1* and *tadwf4* triple mutants. Leaf angle of the 2nd leaf (mean ± SD) was recorded on *tadwf1-abd*, *TaDWF1-NS*, *tadwf4-abd* and *TaDWF4-NS* mutants and Cadenza at the seedling stage. The percentage change was calculated by comparing these values against Cadenza. General ANOVA output including *p*-values, SED, and LSD at 5% level of significance are indicated. Statistically significant difference between mutant and Cadenza were denoted ***$P < 0.001$, ****$P < 0.0001$ (obtained from Fisher's LSD unprotected test).

Genotypes	Leaf angle in degrees (2nd leaf)	% Change
tadwf1-abd	12.2 ± 2.4****	-49.2
TaDWF1-NS	25.6 ± 7.2	6.6
tadwf4-abd	14.4 ± 4.1***	-40
TaDWF4-NS	24.3 ± 4.0	1.25
Cadenza	24 ± 3.1	_
p- value	<.001	
SED	2.076	
LSD	4.178	

4.2.8.4.2 Seedling height

It was previously established that mutations in *TaDWF1* caused a reduction in final plant height due to restricted internode elongation. In contrast, mutations in *TaDWF4* did not have any effect on final plant height or internode elongation. To establish the role of these mutations on seedling height (2nd leaf stage), *tadwf1-abd*, *TaDWF1-NS*, *tadwf4-abd*, *TaDWF4-NS* and Cadenza were grown in the glasshouse. ANOVA confirmed the presence of statistically significant differences for seedling height as shown in Figure 4.20 and Table 4.15. We observed around a 27% reduction in height of *tadwf1-abd* mutant compared to Cadenza. There was no reduction in height of *tadwf4-abd* mutant compared to Cadenza. However, a slight reduction in the height of *tadwf4-abd* was observed when compared against *TaDWF4-NS*. The seedling height of *TaDWF1-NS* and Cadenza were similar, but they were significantly shorter than *TaDWF4-NS*. The significance of the observed increased seedling elongation in *TaDWF4-NS* is currently not clear although it is conceivable that the presence of other EMS mutations in the background could have an influence.

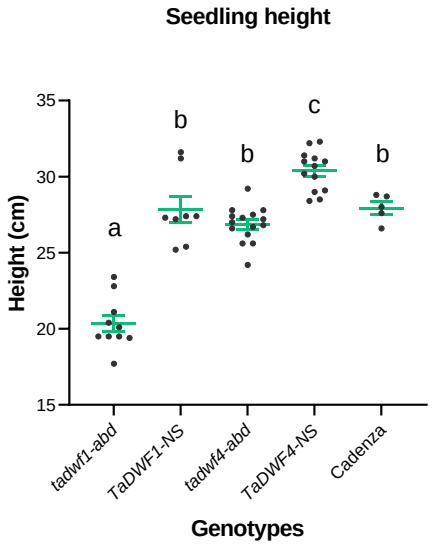

Figure 4. 20 Seedling height of *tadwf1* and *tadwf4* triple mutants. The height of seedlings (till end of first leaf) was recorded in *tadwf1-abd*, *TaDWF1-NS*, *tadwf4-abd* and *TaDWF4-NS* mutants along with Cadenza at the 2nd leaf stage. ANOVA confirmed presence of statistically significant differences amongst the genotypes. Different letters were used to designate significant differences amongst genotypes.

Table 4. 15 Seedling height of *tadwf1* and *tadwf4* triple mutants. Seedling height (mean ± SD) was recorded on *tadwf1-abd*, *TaDWF1-NS*, *tadwf4-abd* and *TaDWF4-NS* mutants and Cadenza when they reached the 2nd leaf stage. The percentage change was calculated by comparing these values against Cadenza. General ANOVA output including *p*-values, SED, and LSD at 5% level of significance are indicated. Statistically significant difference between mutant and Cadenza were denoted $^{**}P < 0.01$, $^{****}P < 0.0001$ (obtained from Fisher's LSD unprotected test).

Genotypes	Seedling height (cm)	% Change
tadwf1-abd	20.3 ± 1.7****	-27.2
TaDWF1-NS	27.8 ± 2.4	-0.4
tadwf4-abd	26.9 ± 1.2	-3.6
TaDWF4-NS	30.4 ± 1.3**	8.9
Cadenza	27.9 ± 0.9	_
p-value	<.001	
SED	0.7264	
LSD	1.462	

4.2.8.4.3 Leaf area

Leaf area is an important agronomic trait which accounts for net photosynthesis by governing radiation use efficiency. To establish the role of *TaDWF1* and *TaDWF4* in controlling leaf expansion, the *tadwf1-abd* and *tadwf4-abd* mutants were compared against Cadenza and the respective null segregants. Seedlings were grown in the glasshouse until the 2nd leaf (when it stopped elongating) seedling stage and then the leaf length, leaf blade width and leaf area (on second leaf) were measured. ANOVA confirmed the existence of significant differences in leaf length, width, and area in the *tadwf1* and *tadwf4* mutants compared to Cadenza as shown in Figure 4.21 and Table 4.16. For leaf blade length, we observed a 19% reduction in the *tadwf1-abd* mutant but didn't observe any significant reduction in the *tadwf4-abd* mutant compared to Cadenza. For leaf blade width, we observed almost a 14% increase in *tadwf1-abd* mutant but the *tadwf4-abd* mutant was non significantly different compared to Cadenza. The leaf area of the *tadwf1-abd* and *tadwf4-abd* mutants were not significantly different compared to Cadenza or the respective null segregants. Interestingly, the leaf area of *tadwf1-abd* was statistically smaller than the *tadwf4-abd* mutant.

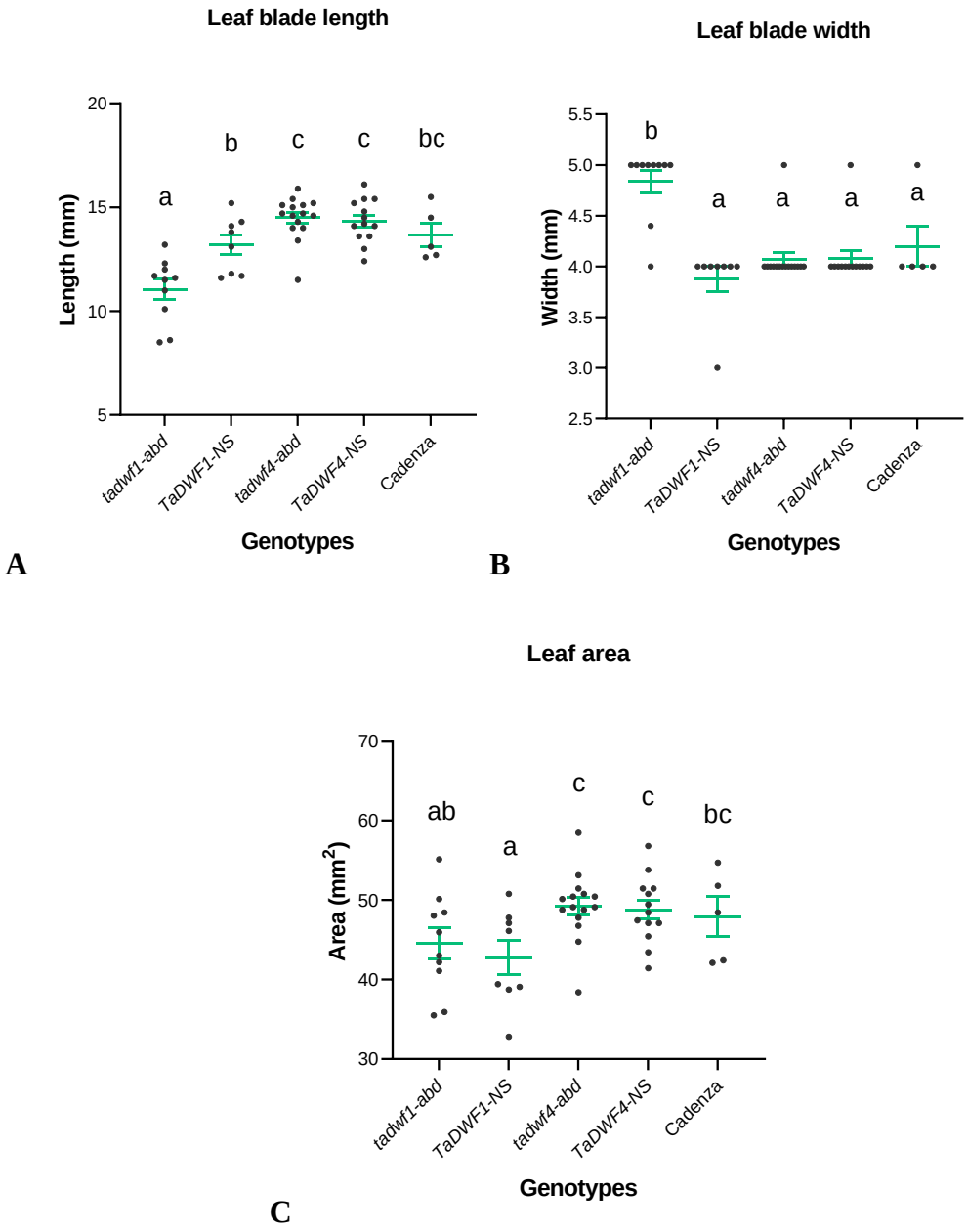

Figure 4. 21 Seedling leaf dimensions of *tadwf1* and *tadwf4* triple mutants. The data of leaf length (A), leaf width (B) and leaf area (C) was recorded on *tadwf1-abd*, *TaDWF1-NS*, *tadwf4-abd* and *TaDWF4-NS* mutants and Cadenza on 2nd leaf at seedling stage. ANOVA confirmed the presence of statistically significant differences amongst the genotypes. Different letters were used to designate significant differences amongst the genotypes.

Table 4. 16 Seedling leaf dimensions of *tadwf1* and *tadwf4* triple mutants. The data (Mean ± SD) was recorded on *tadwf1-abd*, *TaDWF1-NS, tadwf4-abd* and *TaDWF4-NS* mutants and Cadenza on the 2nd leaf (when it stopped elongating) at seedling stage. The percentage change was calculated by comparing the values against Cadenza. General ANOVA output is also described below. Statistically significant difference between mutant and Cadenza were denoted $^{**}P < 0.01$, $^{***}P < 0.001$ (obtained from Fisher's LSD unprotected test).

Genotypes	Leaf blade length (mm)	% Change	Leaf blade width (mm)	% Change	Leaf area (mm^2)	% Change
tadwf1-abd	11.1 ± 1.5***	-18.9	4.8 ± 0.3***	14.3	44.5 ± 6.2	-6.9
TaDWF1-NS	13.2 ± 1.4	-3.6	3.9 ± 0.4	-7.1	42.7 ± 6.1**	-10.7
tadwf4-abd	14.5 ± 1.0	5.8	4.1 ± 0.3	-2.4	49.2 ± 4.3	2.9
TaDWF4-NS	14.2 ± 1.0	3.6	4.1 ± 0.3	-2.4	48.7 ± 4.2	1.9
Cadenza	13.7 ± 1.3	_	4.2 ± 0.4	_	47.8 ± 5.6	_
p-value	<.001		<.001		0.006	

4.2.9 Analysis of endogenous BR levels in *tadwf1* and *tadwf4* triple mutants

It is reported that BR biosynthetic mutants having lesions in specific steps within the contain lower levels of downstream BR products substrates. For example, the OsDWF1 enzyme has been demonstrated to catalyse the conversion of 24-methylene-cholesterol (24-MC) to campesterol (CR) and in the *osdwf1* mutant (*brd2*) there is a subsequent 10-fold increase in the level of 24-MC and a 100-fold reduction in the level of CR compared to wild-type. The intermediates from CR to CS either in early or late C-6 oxidation pathway were also substantially reduced (such as CN, 6-oxoCN, 6-deoxoCT, CT, 6-deoxoTE, TE, 6-deoxoTY, TY, CS and BL etc) in the *brd2* mutant. It was noted that the os*dwf1* mutant had a moderate (semidwarf) BR-deficient phenotype as opposed to severe phenotype observed in other BR deficient mutants. Hong and colleagues provided evidence that this was due to the production of DS, via an alternative BR biosynthetic pathway, which was acting as an alternative bioactive BR that partially promoted growth (Hong et al., 2005). The *osdwf4-1/d11-*

4 double mutant (but not either single mutants i.e., *osdwf4-1* and *d11-4*) also demonstrated to result in perturbations in the levels of BR that were consistent with a block in 22α-hydroxylation (Sakamoto et al., 2006).

Currently there is no information available about the effect of *tadwf1* and *tadwf4* mutations on the levels of BR and this data are likely to provide important knowledge about the BR biosynthesis pathway in wheat. An experiment was designed to determine the BR content of the *tadwf1-abd* and *tadwf4-abd* triple mutants. This involved harvesting the above ground portion of whole seedlings when they reached at 2nd leaf stage. This material was chosen due to the phenotypic differences (section 4.2.8.4) that were observed in the *tadwf1* and *tadwf4* mutants at this developmental stage. The harvested material was analysed at The Laboratory of Growth Regulators, Palacky University, Olomouc, Czech Republic, where they determined endogenous BRs using a published protocol for measuring 22 BRs and related sterols (Tarkowska et al., 2016).

The data generated was analysed using One-way ANOVA which yielded *p*-values, SED, and LSD at 5% level of significance which are presented below in Table 4.17 and Figure 4.22. Nine BRs were detected in *tadwf1* and *tadwf4* wheat mutants namely CR, CN, 6-oxoCN, 6-deoxoCT, 6-deoxoTY, TY, CS, BL, and DS. ANOVA confirmed statistically significant differences for BR content, amongst the mutants as the *p*-values obtained were <0.05. Levels of BRs such as CR, CN, 6-oxoCN and 6-deoxoCT in *tadwf1-abd* mutant were approximately 126-, 12.8-, 3.7- and 1.1-fold lower compared to *TaDWF1-NS*. Interestingly, we observed a significant increase in the levels of the bioactive BRs CS and BL in the *tadwf1-abd* mutant. Although this is unexpected, it is conceivable that this could reflect tissue-specific differences in accumulation of BRs which will require further analyses. We didn't observe any striking differences amongst the BR levels in *tadwf4-abd* mutant compared to *TaDWF4-NS*. Although the levels of 6-deoxoCT and 6-deoxoTY were significantly different amongst these genotypes, but it was noted that the levels of these compounds were also significantly lower in *TaDWF4-NS*.

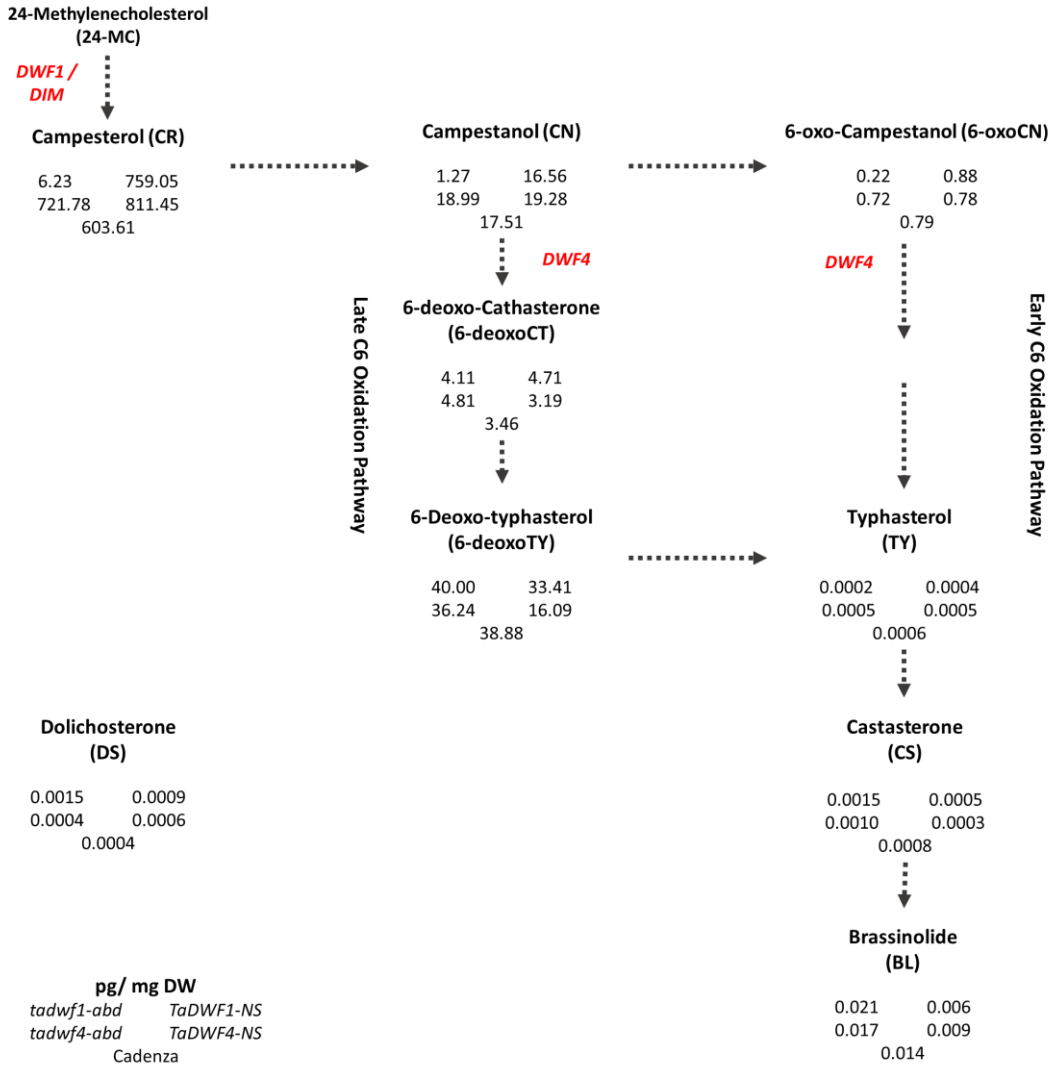

Figure 4. 22 BR levels in *tadwf1* and *tadwf4* triple mutants. The mean values of BR contents (in pg/mg DW) were determined in *tadwf1-abd, TaDWF1-NS, tadwf4-abd* and *TaDWF4-NS* mutants and Cadenza seedlings harvested at the 2nd leaf stage. CR is the first substrate of the BR-biosynthesis pathway leading to production of CN. 6-deoxoCT and 6-deoxoTY are substrates of the late C6 oxidation pathway whereas, 6-oxoCN, TY, CS and BL are BRs specific to the early C6 oxidation pathway. DS is a product of an alternative BR-biosynthesis pathway.

Table 4. 17 BR levels in *tadwf1* and *tadwf4* triple mutants. The data (mean ± SD) showing BR content (pg/mg DW) in *tadwf1* and *tadwf4* mutants along with Cadenza determined in seedling tissue (2nd leaf stage). The General ANOVA output i.e., *p*-values, SED, and LSD at 5% level of significance is described below. Fisher's unprotected LSD test was performed for multiple pair-wise comparisons. Statistical significant difference between mutant and NS were denoted **P* < 0.05, ***P* < 0.01, ****P* < 0.001, *****P* < 0.0001 (obtained from Fisher's LSD unprotected test).

		tadwf1-abd	***TaDWF1-NS***	***tadwf4-abd***	***TaDWF4-NS***	**Cadenza**	***p*-value**	**SED**	**LSD at 5%**
BR content (pg/mg DW)	**CR**	6.23 ± 0.43****	759.05 ± 67.02	721.78 ± 61.77*	811.45 ± 21.46	603.61 ± 55.63	<.001	42.165	89.872
	CN	1.27 ± 0.34****	16.56 ± 0.78	18.99 ± 0.81	19.28 ± 0.94	17.51 ± 1.84	<.001	0.868	1.85
	6-oxoCN	0.22 ± 0.03***	0.82 ± 0.12	0.72 ± 0.12	0.78 ± 0.19	0.79 ± 0.17	<.001	0.112	0.239
	6-deoxoCT	4.11 ± 0.43*	4.71 ± 0.33	4.81 ± 0.12****	3.19 ± 0.47	3.46 ± 0.10	<.001	0.27	0.575
	6-deoxoTY	40.00 ± 5.20	33.41 ± 1.98	36.24 ± 3.80****	16.09 ± 1.45	38.88 ± 5.57	<.001	3.238	6.903
	TY	0.0002 ± 0.0001**	0.0004 ± 0.0001	0.0005 ± 0.0000	0.0005 ± 0.0002	0.0006 ± 0.0001	0.002	0.000078	0.00016
	CS	0.0015 ± 0.0008**	0.0005 ± 0.0001	0.0010 ± 0.0002	0.0003 ± 0.0001	0.0008 ± 0.0003	0.015	0.00031	0.00067
	BL	0.021 ± 0.003****	0.006 ± 0.003	0.017 ± 0.003**	0.009 ± 0.002	0.014 ± 0.002	<.001	0.0025	0.0054
	DS	0.0015 ± 0.0006	0.0009 ± 0.001	0.0004 ± 0.0003	0.0006 ± 0.0004	0.0004 ± 0.0002	0.018	0.0003	0.0006

4.2.10 Sensitivity of *tadwf1* and *tadwf4* mutants to external BR application

Plants exhibiting a BR-deficient phenotype caused by mutations in the BR-biosynthesis pathway genes can be restored by the application of external BRs (Klahre et al., 1998, Choe et al., 1998).

To test the sensitivity of *tadwf1-abd* and *tadwf4-abd* mutants to external BR application a lamina joint inclination assay was performed (Li et al., 2017). Leaf angles were measured after treating the genotypes with 10^{-5}M epiBL or a control solution. A paired *t*-test was performed to establish statistically significant differences amongst the genotypes following treatments. The results are shown in Figure 4.23.

We observed hypersensitivity of *tadwf1-abd* mutant to external BR, as leaf angle increased by approx. 184% when leaf segments were dipped in BR solution compared to water. Which was statistically significant as the adjusted *P*-value was <0.000001. The sensitivity of *TaDWF1-NS* and Cadenza was lower as LA increased following BL treatment by approximately 33% and 56%, respectively.

Similarly, we observed hypersensitivity of *tadwf4-abd* mutant to external BR, as leaf angle increased by approx. 83% when leaf segments were dipped in BR solution compared to water. The sensitivity of *TaDWF4-NS* to BL was lower as LA increased by only 29% (water to 10^{-5}M epi-BL).

These assays suggest that leaf inclination in the *tadwf1-abd* and *tadwf4-abd* mutants is hypersensitive to external BR application compared to the controls.

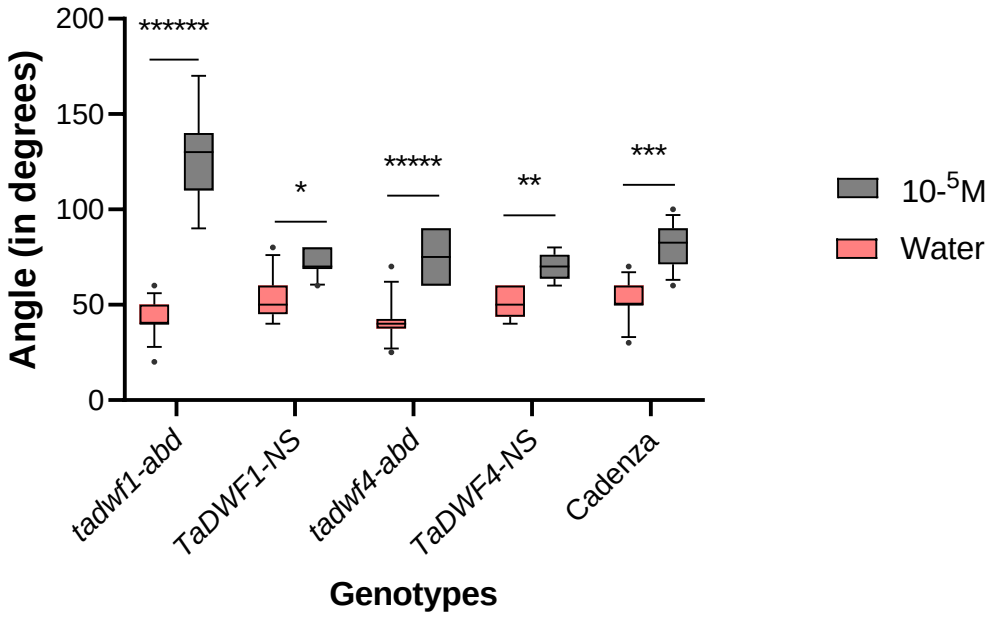

Figure 4. 23 Response of *tadwf1* and *tadwf4* triple mutants to external BR application. A lamina joint inclination assay was performed on *tadwf1-abd*, *TaDWF1-NS*, *tadwf4-abd* and *TaDWF4-NS* mutants along with Cadenza. Leaf angles were noted in these genotypes with and without 10^{-5}M epiBL treatment. The data are plotted as a box and whisker plot. The line in the middle (of the box) is median, edges of the box representing 25 and 75 percentiles, whiskers are 10 and 90 percentiles and dots above/ below these indicate outliers. Statistical significances were denoted by adjusted *P* values * < 0.05, ** < 0.01, *** < 0.001 and so on (obtained by Pairwise *t*-test).

4.2.11 Identification of anatomical differences in the lamina joint of *tadwf1* and *tadwf4* mutants

To understand the anatomical differences that underlie changes in leaf architecture *tadwf1* and *tadwf4* further analysis of the lamina joint was conducted. As we observed a reduction in leaf angle in the second leaf of mutant seedlings, this stage of development was chosen to establish anatomical differences. To investigate the anatomical differences within the lamina joint of the mutants, scanning electron microscopy (SEM) and laser ablation tomography (LAT) were conducted.

4.2.11.1 SEM on adaxial end of lamina joint

The wheat *cpa* mutant contains a lesion in *TaSPL8*, has altered response to auxin and BR biosynthesis, displays an erect leaf phenotype. SEM imaging demonstrated that the LJ was smaller in the mutant due to a reduced number of cells (Liu et al., 2019).

This observation demonstrates that cell proliferation is important for controlling leaf angle in wheat and highlights the importance of phytohormone signalling.

SEM imaging on the adaxial end of the LJ of *tadwf1-abd* and *tadwf4-abd* mutants to understand the anatomical differences associated with the observed changes in leaf angle. Initially, it was that the leaf blade was more tightly packed around the ligule in *tadwf1-abd* and *tadwf4-abd* and compared to the Cadenza control (Figure 4.24), as previously observed by Liu and colleagues (2018).

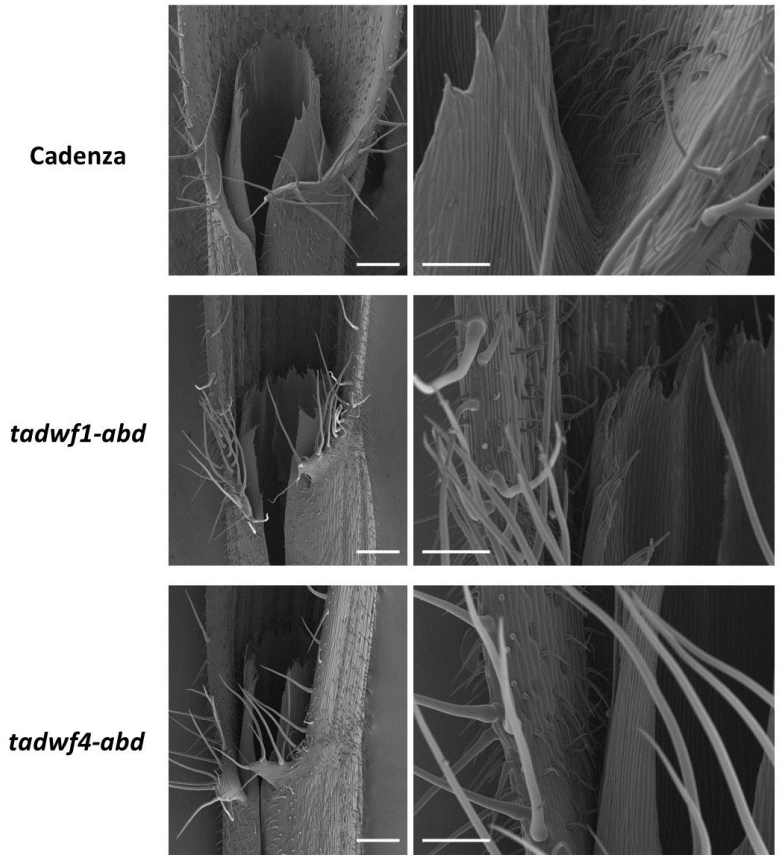

Figure 4. 24 Gross morphology of the adaxial side of the lamina joint in *tadwf1-abd* and *tadwf4-abd* mutants. The images were from the 2nd leaf using low-vac SEM. Images on left were captured at 30X and the scale bar represents 500µm. Images on right are close-ups near the auricle region of the LJ captured at 120X and scale bar represents 200µm.

4.2.11.2 SEM imaging of the auricle region of the lamina joint

It has been reported that a reduction in the cell length of the adaxial end of the auricle region of LJ results in erect-leaf architecture of some maize and rice mutants (Feng et al., 2016; Tian et al., 2019).

We performed SEM imaging on the auricle region of LJ of the *tadwf1-abd* and *tadwf4-abd* mutants along with the Cadenza control. The cell lengths were then measured from the images using ImageJ software. ANOVA was performed on the cell lengths and the data are presented below in Figure 4.26 and Table 4.18. It was observed that significant differences existed for cell lengths in the auricle region amongst the genotypes [$F(2, 527) = 159.28$, $p<.001$]. Average cell length was approximately 88 and 104µm in *tadwf1-abd* and *tadwf4-abd* respectively, compared to 154.5µm in Cadenza. This represents reductions in cell length of approximately 43% and 32% in the *tadwf1-abd* and *tadwf4-abd* mutants compared to Cadenza, respectively.

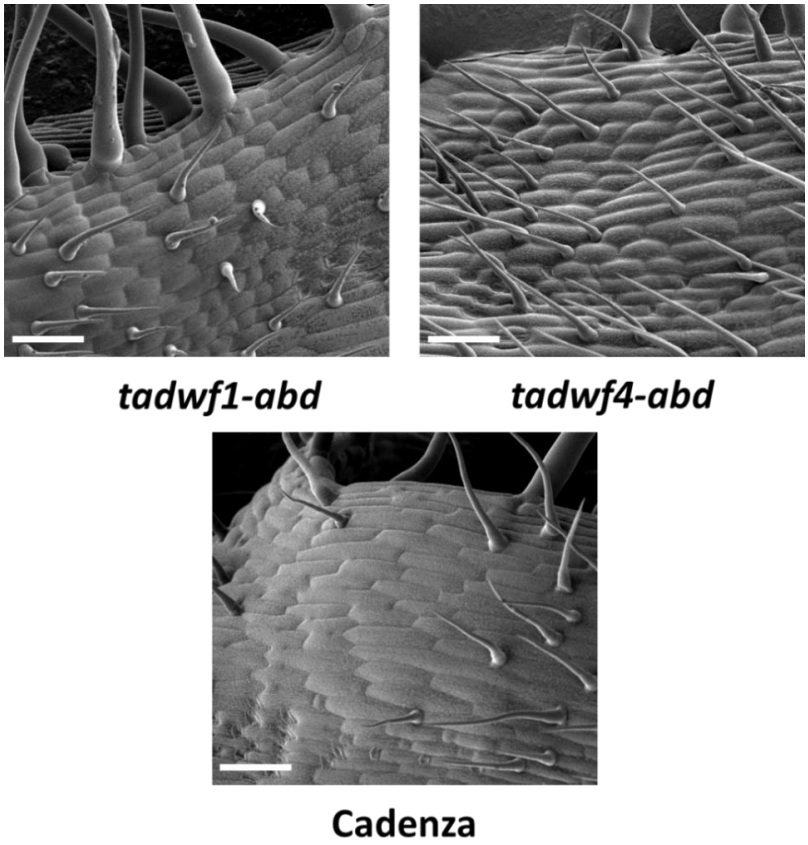

Figure 4. 25 SEM imaging of the auricle region of the LJ in *tadwf1-abd* and *tadwf4-abd* mutants. To measure cell lengths on the auricle region of lamina joint of *tadwf1-abd* (n=197), *tadwf4-abd* (n=200) and Cadenza (n=131), images were captured at 130X on 2nd leaf at seedling stage using low-vac SEM. The scale bar represents 100µm.

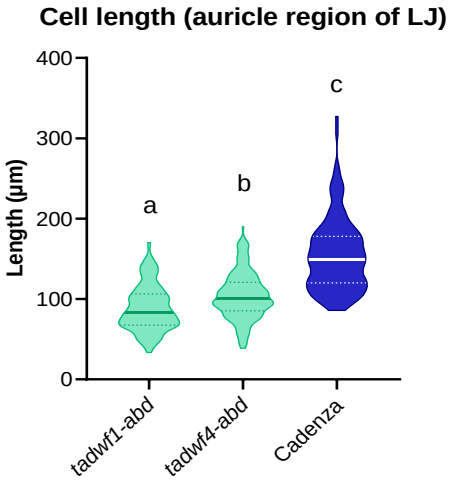

Figure 4. 26 Cell lengths at the auricle region of the LJ in *tadwf1-abd* and *tadwf4-abd* mutants. SEM imaging was performed at seedling stage i.e., 2nd leaf stage on these mutants. The data are presented in the form of violin plot. Different letters are used to designate significant differences amongst the genotypes (obtained from Fisher's LSD unprotected test).

Table 4. 18 Cell lengths at the auricle region of the LJ in *tadwf1-abd* and *tadwf4-abd* mutants. The data on cell lengths (mean ± SD) was collected using ImageJ software. The percentage change was calculated by comparing the values with Cadenza. General ANOVA output i.e., *p*-values, SED, and LSD at 5% level of significance are also described below. Statistical significant difference between mutant and Cadenza were denoted $*P < 0.05$, $**P < 0.01$, $***P < 0.001$, $****P < 0.0001$ (obtained from Fisher's LSD unprotected test).

Genotypes	Cell length (µm)	% Change	*p*-value	SED	LSD
tadwf1-abd	88.6 ± 28.3****	-43	<.001	3.635	7.14
tadwf4-abd	103.9 ± 28.7****	-32			
Cadenza	154.5 ± 45.3	_			

4.2.11.3 Laser ablation tomography (LAT)

Changes in cellular organisation due to altered cell proliferation patterns at either the abaxial or adaxial sclerenchyma region has been linked to changes in final leaf angle in maize and rice (Tian et al., 2019; Sun et al., 2015). In the maize *UPA2*-NIL^{8759} mutant, having altered BR content has a greater number of sclerenchyma cell layers in the adaxial side of ligule, leading to upright canopy architecture in maize (Tian et al., 2019). In contrast, a greater number of cell layers on the abaxial side of the LJ in rice *d61-1* and *d2-2* mutants also leads to erect leaves (Sun et al., 2015). Therefore, to establish role of BRs in regulating cell proliferation we performed LAT (laser ablation tomography) imaging of cross-sections of *tadwf1-abd* and *tadwf4-abd* mutants along with Cadenza. LAT is an innovative high-throughput imaging technology capable of sectioning the sample rapidly and allowing three-dimensional visualization of the biological samples in full-colour with special scales from 0.1 mm to 1 cm and a resolution at micron level (Strock et al., 2019). The images were then used to calculate the number of sclerenchyma cell layers on the abaxial (D2) and adaxial (D3) sides. In addition, the length of D1, D2, D3, C in LJ was also determined (Figure 4.27).

ANOVA confirmed the presence of statistical differences for measurements of regions D1, D2, D3 and C amongst these genotypes as shown in Figure 4.29 and Table 4.19. Significant differences existed amongst the genotypes for the length of region D1 [$F(2, 164) = 25.68$, $p<.001$]. There were approximately 11% and 14% increases in the length of D1 region in the *tadwf1-abd* and *tadwf4-abd* mutants,

respectively, when compared to Cadenza. Significant differences existed in the length of the D2 region amongst the genotypes [F (2, 164) = 32.88, p<.001]. There was a 7.8% decrease and 9.5% increase in the length of D2 in *tadwf1-abd* and *tadwf4-abd* mutant, respectively, compared to Cadenza. Similarly, significant differences existed for length of D3 amongst the genotypes, [F (2, 100) = 9.03, p<.001]. There was approximately a 19% increase in the length of D3 in *tadwf4-abd*, but no significant difference was observed in *tadwf1-abd* compared to Cadenza. Significant differences in the length of widest region of the LJ (C) existed amongst the genotypes [F (2, 164) = 22.95, p<.001]. This region was 5.6% and 9.5% wider in *tadwf1-abd* and *tadwf4-abd* mutants, respectively, compared to Cadenza. The LAT images are shown in Figure 4.28.

Statistically significant differences existed for the number of sclerenchyma cell layers in the abaxial (D2) and adaxial (D3) region of LJ amongst the genotypes (Figure 4.29 and Table 4.20). Within the D2 region, significant differences in the number of cell layers existed amongst the genotypes [F (2, 110) = 11.68, p<.001]. Increases of 6% and 9% in the number of sclerenchyma cell layers in abaxial region of LJ were observed in *tadwf1-abd* and *tadwf4-abd* mutants, respectively, compared to Cadenza. Similarly, for the number of cell layers in region D3, significant differences existed amongst the genotypes [F (2, 110) = 23.21, p<.001]. There were approximately 40% and 21% more sclerenchyma cell layers in the adaxial (D3) region of the LJ of the *tadwf1-abd* and *tadwf4-abd* mutants, respectively compared to Cadenza.

These results demonstrate a role for BRs in regulating the number of sclerenchyma cell layers in abaxial (D2) and adaxial (D3) end of LJ. Interestingly, the lengths of the D2 and D3 regions were either similar or decreased in the *tadwf1-abd* mutant compared to Cadenza regardless of the greater number of cell layers, which could potentially indicate restricted cell expansion. in contrast, a greater number of D2 and D3 sclerenchyma cell layers in the *tadwf4-abd* mutant, led to significantly larger D2 and D3 regions compared to Cadenza.

Figure 4. 27 LAT image showing a cross section of a LJ (*tadwf4-abd*) and the different regions. Widths of cell layers forming the abaxial sclerenchyma (D2) and adaxial sclerenchyma (D3). D1 region indicates the length between the mid vein and adaxial end of LJ. The widest region of entire LJ region is indicated by C. were recorded on LAT images using ImageJ software. The number of sclerenchyma cell layers in the abaxial end of LJ (D2) and adaxial side of the LJ (D3) were manually counted from LAT images produced on LJ region.

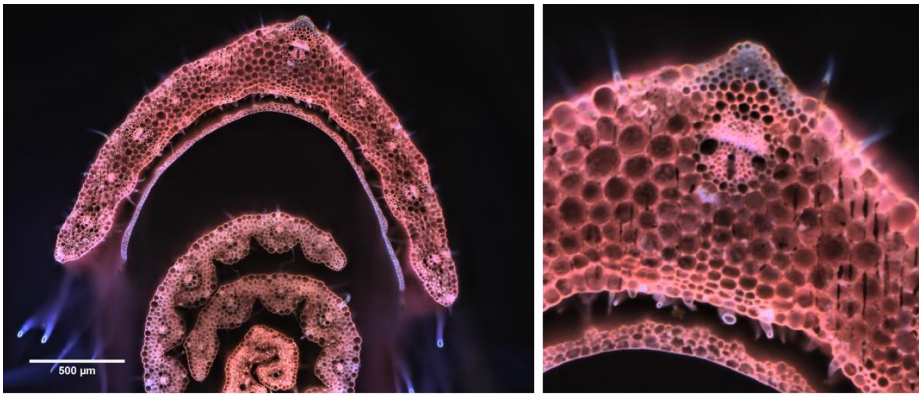

Cadenza

A

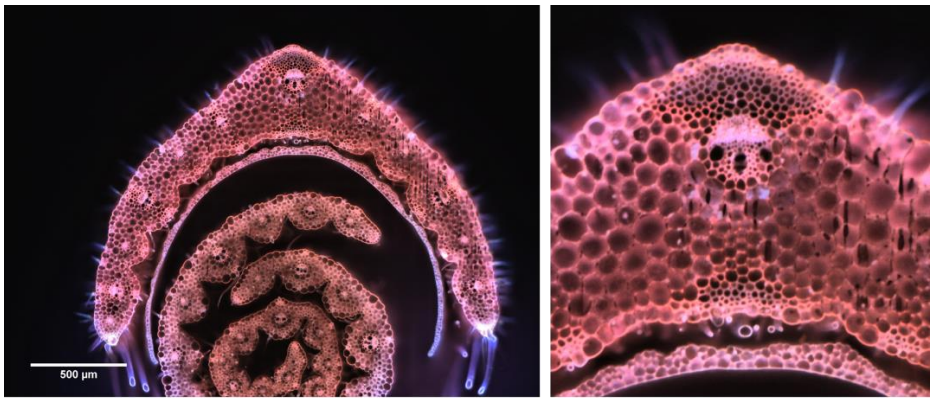

tadwf1-abd

B

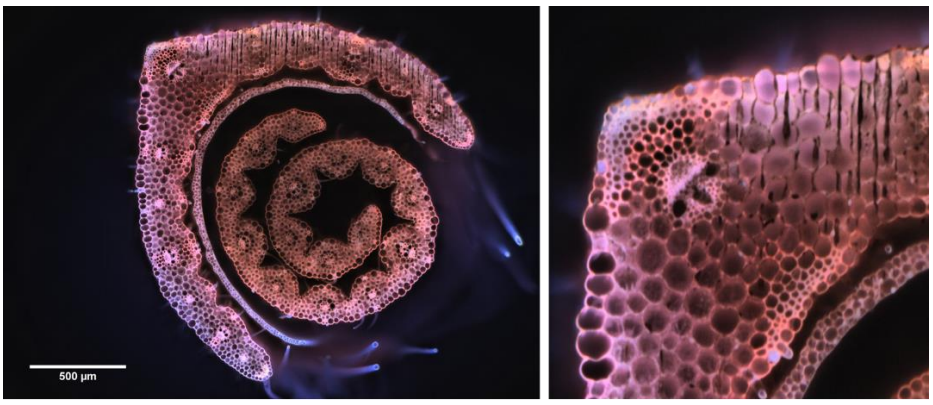

tadwf4-abd

C

Figure 4. 28 LAT images of *tadwf1-abd* and *tadwf4-abd* mutants. The LAT images of the LJ were captured from Cadenza (A), *tadwf1-abd* (B) and *tadwf4-abd* mutant (C) at 2nd leaf seedling stage. Images on the left show the entire LJ section (scale bar length is 500um) and on right shows a close-up of the abaxial end LJ in the mutants. The images were captured at 5X magnification.

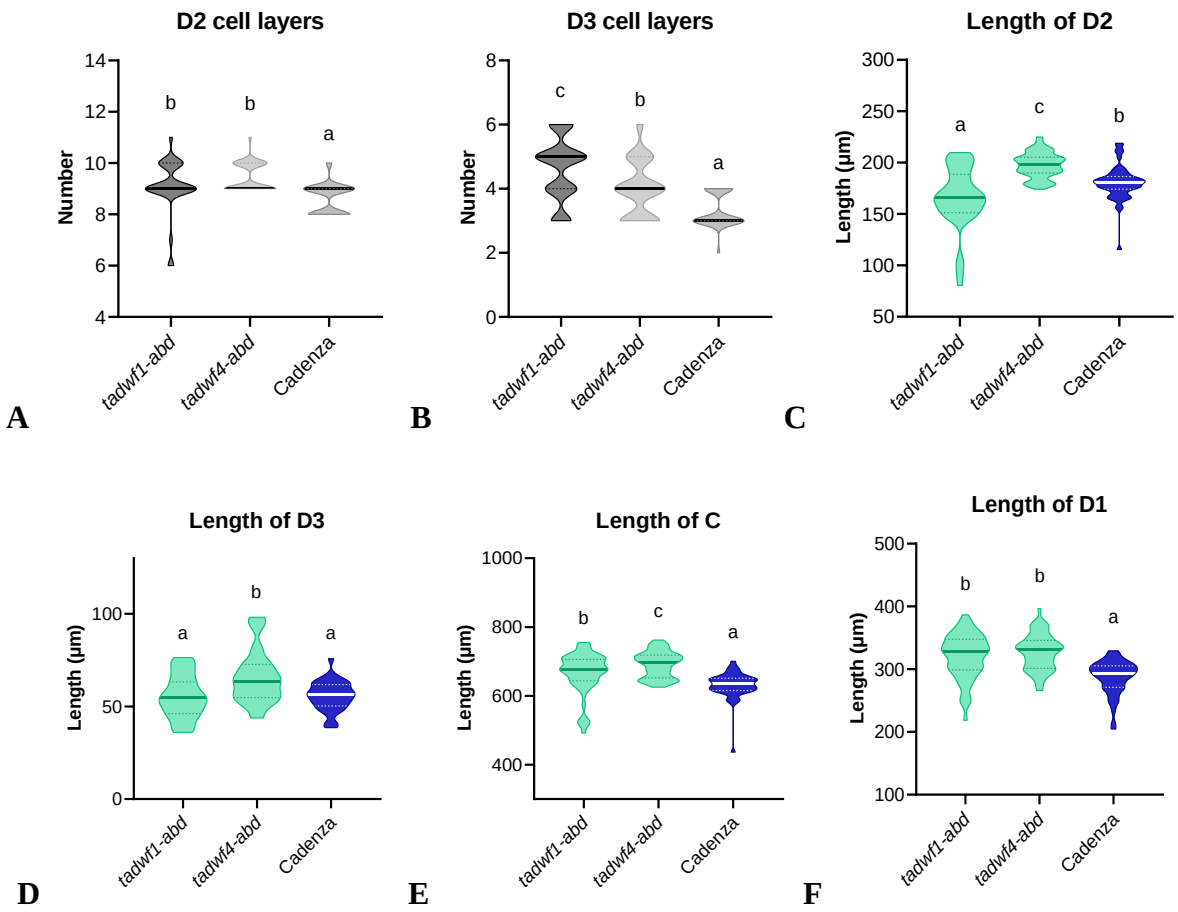

Figure 4. 29 Number of sclerenchyma cell layers and dimensions of *tadwf1-abd* and *tadwf4-abd* mutants. Number of sclerenchyma cell layers in D2 (A) and D3 (B) region were manually counted on LAT images of the LJ region. Widths of cell layers D1 (F), D2 (C), D3 (D) and C (E) were measured from LAT images using ImageJ software. The data are presented in the form of violin plot. ANOVA confirmed statistical significance for these traits. Different letters on the graphs designate significant differences amongst the genotypes (obtained from Fisher's LSD unprotected test).

Table 4. 19 Dimensions of cell layers in the *tadwf1-abd* and *tadwf4-abd* mutants. The width (Mean ± SD) of cell layers D1, D2, D3 and C were measured from LAT images using ImageJ software. The percentage change was calculated by comparing the values with Cadenza. General ANOVA output including, *p*-values, SED, and LSD at 5% level of significance are indicated. Statistically significant difference between mutant and Cadenza were denoted **P* < 0.05, ***P* < 0.01, ****P* < 0.001, *****P* < 0.0001 (obtained from Fisher's LSD unprotected test).

Genotypes	**Length of D1 (µm)**	**% Change**	**Length of D2 (µm)**	**% Change**	**Length of D3 (µm)**	**% Change**	**Length of C (µm)**	**% Change**
tadwf1-abd	320.6 ± 35.5****	11.4	166.1 ± 29.7***	-7.8	55.4 ± 11.5	-0.2	666.4 ± 59.8****	5.6
tadwf4-abd	327.2 ± 28.1****	13.7	197.5 ± 12.1***	9.5	65.8 ± 14.2***	18.5	691.1 ± 37.4****	9.5
Cadenza	287.7 ± 26.9	_	180.3 ± 16.5	_	55.5 ± 7.9	_	631.3 ± 38.0	_
***p*-value**	<.001		<.001		<.001		<.001	
SED	5.814		3.961		2.82		8.838	
LSD	11.48		7.823		5.596		17.45	

Table 4. 20 Number of sclerenchyma cell layers in *tadwf1-abd* and *tadwf4-abd* mutants. The measurements (Mean ± SD) of D2 and D3 cell layers were recorded from LAT images. The percentage change was calculated by comparing the values against Cadenza. General ANOVA output including *p*-values, SED, and LSD at 5% level of significance are indicated. Statistically significant differences between mutant and Cadenza were denoted $*P < 0.05$, $**P < 0.01$, $***P < 0.001$, $****P < 0.0001$ (obtained from Fisher's LSD unprotected test).

Genotypes	Cell layers in D2	% Change	Cell layers in D3	% Change
tadwf1-abd	9.1 ± 1.1**	5.8	4.6 ± 0.9****	39.4
tadwf4-abd	9.4 ± 0.5****	9.3	4 ± 0.9***	21.2
Cadenza	8.6 ± 0.6	_	3.3 ± 0.5	_
***p*- value**	<.001		<.001	
SED	0.17		0.187	
LSD	0.34		0.372	

4.3 Discussion

The objective of this study was to establish the role of *DWF1* and *DWF4* genes in controlling above ground architecture in wheat. This was achieved by identifying orthologous genes in wheat, which were then characterised by generating loss-of-function mutants using the Cadenza TILLING population. This enabled the identification of combinatorial mutants which were backcrossed and then assessed for alterations in plant architecture.

The phenotypic characterisation of *tadwf1* and *tadwf4* combinatorial mutants demonstrated that differences in plant architecture were only observed in the triple mutants. This demonstrated that the *TaDWF1* and *TaDWF4* homoeologues have functionally redundant roles in controlling BR-responsive growth in wheat. The *tadwf1-abd* triple mutant displayed striking architectural changes including a semi-dwarf stature with erect leaves, compact spikes with fewer spikelets and smaller grains. Similarly, we observed erect leaf architecture in the *tadwf4-abd* triple mutant, but with no negative effects on final plant height, spikelet number and grain size and weight. Interestingly, we observed similar leaf angle reductions in *tadwf1-abd* and

tadwf4-abd mutant at multiple stages of development, implying that a similar mechanisms is regulating this trait at seedling and reproductive stages.

As *DWF1* and *DWF4* are BR biosynthetic genes, their inactivation is expected to lower the levels of bioative BRs and subsequently reduce BR signalling. To test this hypothesis, we conducted BR analysis on the *tadwf1-abd* and *tadwf4-abd*, *mutants* at using UHPLC-ESI-MS/MS. Interestingly, there was 126-fold reduction in accumulation of campesterol (CR) in *tadwf1-abd* mutant compared to the control and a significant reduction in levels of CR, CN, 6-oxoCN and 6-deoxoCT BR's which are downstream in the BR-biosynthesis pathway beyond this step. In contrast, we didn't observe any notable differences in the *tadwf4-abd* mutant. A possible explanation is that harvesting whole seedlings masks the temporal and/or tissue-specific activity of this gene. This hypothesis needs to be tested by conducting detailed hormonal and transcriptomic studies specifically within the LJ region at different timepoints during development.

To establish the anatomical basis of erect leaf architecture in the *tadwf1* and *tadwf4* triple mutants, laser ablation tomography (LAT) and scanning electron microscopy (SEM) was conducted. A reduction in the cell lengths of auricle region in the LJ was observed in the *tadwf1-abd* and *tadw4-abd* triple mutants compared to Cadenza. Lateral sections of the leaf sheath using LAT also demonstrated an increase in the number of sclerenchyma cell layers in the *tadwf1-abd* and *tadw4-abd* mutants compared to Cadenza. Additionally, the length of abaxial and adaxial sclerenchyma cell layers in *tadwf4-abd* mutant was significantly increased compared to Cadenza. However, this effect was not observed in *tadwf1-abd* potentially due to a restriction in the widths of the cells.

4.3.1 *TaDWF1* gene alters above-plant architecture

To establish the role of the *DWF1* gene on growth and development in wheat, we identified potential deleterious mutations in the three homoeologous genes, by screening the Cadenza TILLING population (Krasileva et al., 2017). The mutations that were identified in *TaDWF1-A*, *TaDWF1-B* and *TaDWF1-D* resulted in premature stop codons within the coding sequences at codons 92, 23 and 252, respectively. These are predicted to lead to partial or complete loss of the FAD domain in the encoded proteins which is essential for oxidoreductase activity of the

enzyme (Choe et al., 1999). It is therefore expected that they result in complete loss of enzymatic activity in the encoded DWF1 proteins. The *tadwf1* triple mutant displayed striking developmental defects at maturity, including restricted internode elongation, erect leaf angles, reduced leaf elongation, a condensed spike, as well as smaller and lighter grains. Which was also observed in other cereals such as rice, barley, and maize (Hong et al., 2005; Dockter et al., 2014; Best et al., 2016). For instance, in rice, the *brassinosteroid-deficient dwarf2* (*brd2*) mutant orthologous to Arabidopsis *DIMINUTO/DWARF1* gene, displayed dark-green, erect statured and shortened leaves in rice (Hong et al., 2005). In cereals the *DWF1* genes have been demonstrated to have an important role controlling stem elongation. However, the extent to which they control this process varies in different species. In maize, the *ZmDWF1* mutant has a striking reduction in stem elongation exhibiting a height that is 90% reduced compared to wild type at maturity (Best et al., 2016). In contrast, the rice *brd2* mutant of rice has a 60% reduction in height compared to the wild type (Hong et al., 2005). Additionally, it has been reported that the reduced final plant height in cereal *DWF1* mutants is due to restricted internode elongation. For example, in the maize *na2-1* mutant there is an evenly distributed reduction in elongation of all the internodes (Best et al., 2016). In contrast, the rice *brd2* mutant was observed to have restricted elongation of the second and lower internodes, but the peduncle elongation is comparable to wild type (Hong et al., 2005). Furthermore, in barley, *hvdim* mutants displayed restricted elongation of specifically the second internode, leading to semi-dwarf stature (Dockter et al., 2014). These findings indicate that in different cereals the *DWF1* genes have diverging roles in controlling elongation of specific internodes. In general, cereal BR-deficient mutants often display spike or panicle abnormalities. For instance, in rice, the *brd2* mutant (containing lesions in *DWF1*) produces malformed panicles with a reduced number of spikelets/panicle and decreased fertility (Hong et al., 2005). Lastly, knocking out the *OsDWF1* gene (*brd2* mutant) significantly reduces grain size in the mutants compared to wild-type (Hong et al., 2005). Thus, demonstrating multiple roles of *DWF1* gene in controlling diverse developmental processes in wheat as has been observed in other cereals such as rice, maize, and barley.

We also observed phenotypic defects during seedling development of the *tadwf1-abd* triple mutant. These abnormalities included reduced leaf elongation and an erect leaf

angle. To establish whether these phenotypic changes were due to reduced accumulation of BRs, we conducted lamina joint inclination assays (Li et al., 2017) and analysed the endogenous BR levels (Tarkowská et al., 2016). In leaf inclination assays we observed hypersensitivity of *tadwf1-abd* mutant to external BR, as leaf angle increased by approx. 184% when leaf segments were treated with BR. The sensitivity of the controls was much lower as LA increased by about 33% and 56%, respectively. This restoration of leaf angle in *tadwf1-abd* mutant supports our hypothesis that BR-deficiency leads to defects in growth and development which can be restored by BR (Youn et al., 2018; Klahre et al., 1998).

Analysis of endogenous BR levels in the *tadwf1-abd* triple mutant demonstrated that it contained a dramatic reduction (126-fold) in CR levels compared to control plants. This is consistent with the *DWF1* genes encoding an enzyme catalysing the conversion of 24-MC to CR (Klahre et al., 1998; Hong et al., 2005). Furthermore, there was a reduction in the levels of some later BR intermediates, such as CN, 6-oxoCN, 6-deoxoCT in the *tadwf1-abd* mutant which was also reported in the equivalent rice and Arabidopsis *dwf1* mutants (Hong et al., 2005; Choe et al., 1999; Klahre et al., 1998). It is interesting to note that the levels of bioactive BRs, CS and BL were significantly increased in the *tadwf1-abd* triple mutant compared to the controls. This result was unexpected given that the in *tadwf1-abd* mutant displays a BR-deficient phenotype. It is likely that BL and CS are being produced by an alternative route. In the rice *brd2* mutant, the production of DS which is acting as a BR with bioactivity has been suggested as an explanation for the weak BR-deficient phenotype in the mutant (Hong et al., 2005). However, in wheat we demonstrate that the *tadwf1* mutant does not contain elevated levels of DS compared against *TaDWF1-NS*. Thus, it's not clear which pathway leads to production of BL and CS and the reason for less severe phenotype in *tadwf1-abd* mutant. It is conceivable that tissue-specific effects in the regulation of BR biosynthesis are occurring during the development of wheat seedlings. This hypothesis can potentially be addressed by conducting a more detailed spatial and temporal analysis of BR levels in the *tadwf1* mutant.

4.3.2 *TaDWF4* specifically alters canopy architecture without having negative pleiotropic effects

The *DWF4* gene encodes a cytochrome P450 monooxygenase that catalyses the C-22 hydroxylation of BR intermediates cytochrome P450 (Choe et al., 1998; Sakamoto et al., 2006). In rice, a second paralogue, *DWF11* is present and encodes an enzyme that catalyses the same reaction within the BR biosynthesis pathway. Based on the phenotype of the respective rice *dwf4* and *dwf11* mutants the genes have tissue-specific roles in controlling plant development. The os*dwf4-1* has erect canopy architecture, but only a slight reduction in plant height without any defects in reproductive development (Sakamoto et al., 2006). This phenotype has been demonstrated to improve grain yields in rice under dense planting conditions. In contrast, the *osdwf11* mutants show a more substantial reduction in stem elongation, erect leaves, and smaller grains, thus demonstrating that *OsD11* has an essential role in maintaining levels of BRs needed for shoot elongation and reproductive development (Sakamoto et al., 2006). Interestingly, overexpression of *DWF4* is reported to improve vegetative and grain yield in Arabidopsis, *Brassica napus*, rice and maize (Milner et al., 2022; Choe et al., 2001; Sahni et al., 2016; Liu et al., 2020; Li et al., 2018; Wu et al., 2008). These findings highlight *DWF4* as a potential target for manipulating canopy architecture in wheat for increasing grain yields without negative pleotropic effects on other agronomically important traits.

In wheat, there were two orthologues of the rice *DWF4* gene, designated *TaDWF4* and *TaDWF4L* and which are located on chromosomes 3 and 4, respectively. It was observed that expression of *TaDWF4* genes were significantly higher as compared to *TaDWF4L*, which was largely undetectable in wheat (Milner et al., 2022; Section 3.2.7 describing mRNA-seq results at seedling seedling). It therefore seems likely that *TaDWF4* gene has a similar role to *OsDWF4* in controlling architectural traits. To establish its role, TILLING was used to generate *tadwf4* combinatorial mutants (Krasileva et al., 2017). Mutations that result in premature stop codons were identified for the three *TaDWF4* homoeologues at codon positions 168, 39 and 353 in *TaDWF4-A*, *TaDWF4-B* and *TaDWF4-D*, respectively. The predicted truncated forms of the proteins that are encoded are lacking the A, B, C and Heme-binding domains which are critical for DWF4 activity, and it is therefore expected that they are null alleles (Choe et al., 1998). Phenotypic characterization of the combinatorial

tadwf4 mutants was conducted under glasshouse conditions along with Cadenza. We observed a significant reduction in flag-leaf angle at anthesis, smaller spikes, no reduction in final plant height, seed area or thousand grain weight in *tadwf4-abd* compared to the control. The organ-specific effect of *TaDWF4*, specifically controlling leaf angle without any impact on height, internode elongation, spike and grain characteristics were also reported in rice (Sakamoto et al., 2006). Thus, making it a potential target for yield improvement in wheat.

As significant reductions in leaf angle were observed in *tadwf4-abd*, we hypothesised this is caused by reduced BR-signalling in the mutant. To establish whether this was the case, lamina joint inclination assays (Li et al., 2017) and analysis of BR levels was performed in this mutant. We observed hypersensitivity of *tadwf4-abd* mutant to BR treatment compared to the controls. This restoration of leaf angle by BR treatment demonstrates that *tadwf4-abd* mutant is deficient in endogenous BRs controlling leaf inclination (Choe et al., 1998). Interestingly, no obvious differences in BR levels were observed in *tadwf4-abd* seedlings compared to the controls. This was similar to reports in rice, where the levels of BR intermediates in *osdwf4-1/d11-4* double mutant were significantly changed compared to either *osdwf4-1* or *d11-4* single mutants (Sakamoto et al., 2006). This could potentially be due to tissue-specific expression of *TaDWF4* that only influences LJ development. Our analysis of the entire above ground seedling (as was also reported in Sakamoto et al., 2006), might have obscured these tissue-specific effects. A more detailed spatial and temporal analysis of BR levels during lamina joint development will be required to test this hypothesis.

4.3.3 Erect leaf architecture in *tadwf1* and *tadwf4* mutants is due to altered lamina joint development

Lesions in BR biosynthetic genes are reported to affect lamina joint development leading to altered leaf angles in cereals such as rice, maize, barley, sorghum, and wheat (Morinaka et al., 2006; Sakamoto et al., 2006; Dockter et al 2014; Sun et al., 2015; Feng et al., 2016; Tian et al., 2019; Liu et al., 2017).BRs alter leaf angle by regulating cell elongation and/or proliferation patterns in the auricle region of lamina joint (Sun et al., 2015). There are also reports to suggest that BRs control leaf angle by regulating proliferation of sclerenchyma cell layers in either the abaxial or adaxial side of the lamina joint in rice and maize (Sun et al., 2015; Tian et al., 2019).

We were interested to understand the anatomical basis of the erect leaf phenotype in the *tadwf1-abd* and *tadwf4-abd* mutants. A comparable and significant reduction in leaf angles were observed in both triple mutants at the seedling and reproductive stage. It is conceivable that similar underlying molecular mechanisms involving the alteration of BR signalling is occurring in the lamina joint region of these mutants.

Leaf angle in cereals is determined by the size of ligule (or lamina joint), which links the blade and sheath. The lamina joint has two regions of outgrowth, the ligule and the auricles. The auricles consist of wedge sharped structures which controls the extent of leaf bending away from the axis. To uncover differences in cell elongation on adaxial and auricle/collar region of LJ, scanning electron microscopy (SEM) was conducted. Morphologically, the leaf blade in Cadenza was loosely packed, whereas it was tightly packed around ligule in *tadwf1-abd* and *tadwf4-abd*. This phenotype was also observed in the wheat *cpa* mutant, which has altered auxin and BR biosynthesis due to mutation in the *TaSPL8* gene (Liu et al., 2019). Additionally, SEM imaging was performed on the auricle region of LJ in these genotypes. We observed a significant reduction in cell lengths of auricle region, in *tadwf1-abd* and *tadwf4-abd* mutants compared to the control. It is likely that reduced longitudinal cell elongation in the auricle region is inhibiting the bending of the leaves away from the axis and potentially also causing them to be tightly packed around the ligule. This feature is commonly reported in erect statured rice and maize BR-related mutants (Feng et al., 2016; Zhang et al., 2015; Tian et al., 2019; Zhang et al., 2009; Zhao et al., 2013).

The lamina joint is composed of vascular bundles surrounded by parenchyma and sclerenchyma cells. The sclerenchyma cell layers provide mechanical strength to the midrib, thereby determining the leaf angle in rice and maize (Méchin et al., 2005; Strable et al., 2017). To quantify the number of sclerenchyma cell layers surrounding the vascular bundles of the lamina joint (adaxial and abaxial end) and the width of D1, D2, D3 and C regions, laser ablation tomography (LAT) was conducted. We observed a significant increase in abaxial and adaxial cell layers in the *tadwf1-abd* and *tadwf4-abd* mutants compared to Cadenza. These results demonstrate that although there is significant increase in number of sclerenchyma cell layers in abaxial and adaxial end of LJ in the triple knockout mutants, there is potentially a reduction in cell width in the *tadwf1-abd* mutant compared to Cadenza.

4.3.4 Conclusions

The objective of this study was to understand the roles of the wheat *DWF1* and *DWF4* genes in regulating growth and development, with a focus on establishing effects on lamina joint development that governs leaf angle. To achieve this aim, loss-of-function mutants were generated using TILLING and subsequent phenotypic assessments performed. The *tadwf1-abd* triple mutant displayed pleiotropic developmental defects in BR-regulated growth processes including leaf angle, plant height and internode elongation, seed, and spike characteristics. In contrast, the *tadwf4-abd* triple mutant only displayed significant phenotypic changes in leaf angle without other pleiotropic effects on other traits such as stem elongation. BR-hormone estimation and BR-responsive lamina joint inclination assays led to a better understanding of the physiological roles of these *tadwf1 and tadwf4* genes in modulating endogenous BR-levels in wheat. As we were interested in uncovering the anatomical basis of erect architecture in *tadwf1-abd* and *tadwf4-abd* mutant compared to Cadenza, we performed anatomical studies using advanced microscopic technologies such as low-vac SEM and LAT. These studies provided some evidence of a role for BR in regulating lamina joint development and subsequent leaf angle. Taken together, the *tadwf4-abd* mutant has the ideotype that could potentially improve grain yields in field conditions.

Chapter 5: Assessment of wheat *bri1*, *dwf4* and *dwf1* mutants under field conditions

5.1 Introduction

5.1.1 Importance of field phenotyping in plant breeding

Field phenotyping is a critical component of breeding for superior cultivars, as it enables testing of phenotypic and physiological performance of varieties under field conditions. This data enables scientists and breeders to take informed decisions based on genotypic and environmental interactions. With advances in high-throughput genotyping and genomics, many lines can be screened for the presence of superior alleles in a cost-effective manner. Phenotyping large breeding material using conventional approaches can be laborious and inaccurate when thousands of lines are being screened simultaneously at a particular GS or time. Therefore, advances in high throughput phenotyping platforms (HTPPs) can bridge this gap ensuring genetic improvement of crops for maintaining food security.

5.1.2 Erect statured and semi-dwarf cereals improved grain yields

Erect statured maize hybrids showed consistent increase in grain yield due to increased planting density from 30,000 plants per ha in the 1930s to 82,500 plants per ha in the 2000s (Ma et al., 2014). In addition to higher planting density, these lines allowed greater light penetration and improved photosynthetic efficiency that improved maize yields in farmers' fields (Tian et al., 2011; Fischer and Edmeades, 2010; Duvick, 2005; Pendleton et al., 1968). Similarly, in rice, erect statured lines had better light interception, photosynthesis rate and lower photoinhibition under higher light saturation leading to increased grain yield compared to plants having less erect canopies (Tanaka et al., 1968; Yoshida, 1981; Murchie et al., 1999; Sakamoto et al., 2006; Kumagai et al., 2014). The rice hybrid 'Liangyoupeijiu' having erect leaves and higher photosynthetic rate had 8-15% higher grain yield compared to less erect variety 'Shanyou63' in the field (Yao et al., 2000; Chen et al., 2002; Zong et al., 2000). Similarly, in spring wheat, genotypes with erectophile canopies had 13% higher grain yields (due to 11% higher above-ground biomass) compared to

planophile genotypes under field conditions (Richards et al., 2019). This demonstrates the huge potential of erect statured genotypes for improving grain yields in cereals.

5.1.3 Objectives of the study

We established the above-ground phenotypes of *tabri1*, *tadwf1* and *tadwf4* mutants in the glasshouse (as discussed in depth in results chapters 3 and 4). As the glasshouse trials were conducted under controlled environment, field-based characterisation is essential to access performance of the mutants under real conditions to select genotypes which could be crossed with elite breeding lines for trait improvement. To fulfil this objective two independent preliminary field trials were planted having separate aims:

In a trial with the *tabri1*, *tadwf1* and *tadwf4* mutants in 2022 the agronomic performance of the mutants was assessed under field conditions. Traits such as flag-leaf angles, final plant height, internode elongation, spike and seed characteristics were recorded on mutants generated through forward- and reverse- genetic approaches.

Secondly, a detailed phenotypic comparison of the *tadwf1-abd* mutant with Cadenza was undertaken under the Field Scanalyzer during 2020-21. The aim of this trial was to assess the impact of changed canopy architecture of a representative BR mutant, *tadwf1-abd*, on green canopy cover, spike density and plant height throughout the life cycle. The mutant and Cadenza were sown in Autumn 2020-21 under the Field Scanalyzer, which is a fully automated high-throughput phenotyping platform (HTPP) at Rothamsted Research, Harpenden (Virlet et al., 2017). The images collected over these genotypes at various GS stages (through different sensors) enabled quantification of these above-mentioned traits.

5.2 Results

5.2.1 Phenotypic evaluation of *tabri1*, *tadwf1* and *tadwf4* mutants in 2022

Field evaluation allows to test the performance of genotypes in real-world conditions, which can provide valuable information on how the mutant will perform in the environment for which they were primarily designed, as opposed to controlled greenhouse conditions, which may not accurately reflect the conditions (such as soil type, temperature, precipitation, and pest and disease pressures) in the field.

The phenotype of *tabri1*, *tadwf1* and *tadwf4* mutants was assessed under field conditions in 2022. The following *tabri1* mutants were sown: *tabri1-a.1*, *tabri1-b*, *tabri1-d*, *tabri1-a.1b*, *tabri1-a.1d*, *tabri1-bd*, *tabri1-a.3bd* and the *TaBRI1-NS*. The severe mutants *tabri1a.1bd* and *tabri1-a.2bd* were not included due to shortage of seed. In addition, *tadwf1-abd* and *TaDWF1-NS*, and *tadwf4-abd* were sown, but *TaDWF4-NS* was not included due to seed shortage. All the above stated lines were sown in Spring along with Cadenza in four biological replicates (1 m^2 plots) in a randomised complete block design. Flag-leaf angle at anthesis, final plant height and internode lengths, spike length and grain characteristics (grain area and weight) were recorded, and the data are described below.

5.2.1.1 Flag leaf angle

The FLAs were recorded at anthesis on approximately ten consistent tillers/plot/genotype. The data were analysed using ANOVA and are presented in Figure 5.1 and Table 5.1. ANOVA confirmed statistically significant differences between genotypes [F (11, 411), p <.001]. The FLA for *TaBRI1-NS* and *TaDWF1-NS* were comparable to Cadenza. Therefore, for simplicity the FLA of the *tabri1*, *tadwf1* and *tadwf4* mutants were compared against Cadenza as a common control. For *tabri1* mutants, FLA of various single knockouts (*tabri1-a.1*, *tabri1-b* and *tabri1-d*) was non-significantly different from that of Cadenza. In contrast, we observed approximately 30%, 28% and 34% reductions in FLA in *tabri1-a.1b*, *tabri1-a.1d* and *tabri1-bd* double knockout mutants, respectively, compared to Cadenza. An approximately 55% reduction in FLA was noted in the triple mutant, *tabri1-a.3bd* compared to Cadenza. The FLA of the *tadwf1-abd* triple knockout mutant was

reduced by 55% compared to Cadenza, while that of the *tadwf4-abd* triple knockout mutant was reduced by 46%.

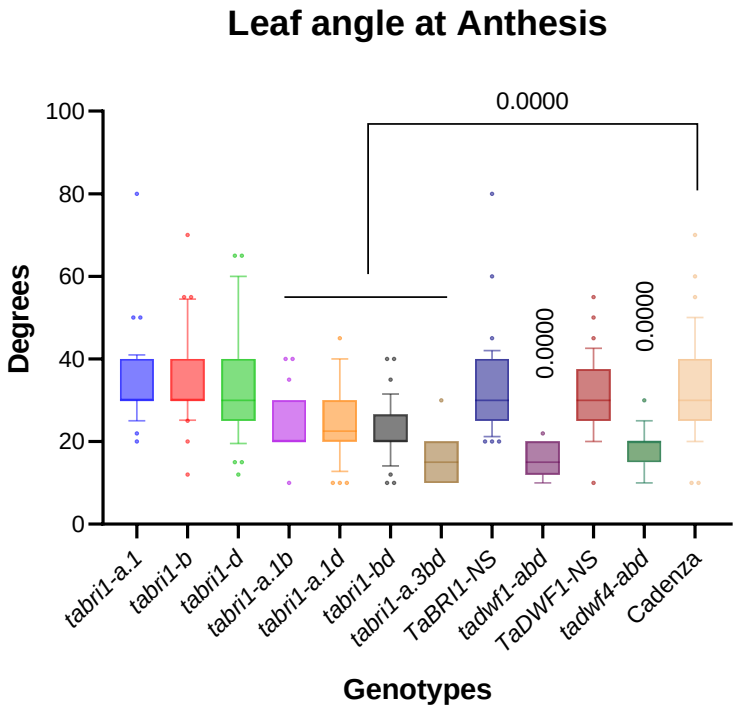

Figure 5. 1 Flag-leaf angles recorded on *tabri1*, *tadwf1* and *tadwf4* mutants. FLA was recorded on *tabri1* (singles, doubles, *tabri1-a.3bd* triple and *TaBRI1-NS*), *tadwf1* (*tadwf1-abd* and *TaDWF1-NS*) and *tadwf4-abd* lines along with Cadenza at anthesis (n~40) from a spring-sown field trail WS2232. The data are plotted as a box and whisker plot. *p*-values for significant differences between mutants and Cadenza (obtained using Fisher's unprotected LSD test) are also shown.

Table 5. 1 Flag-leaf angles recorded on *tabri1, tadwf1* and *tadwf4* mutants. The data (mean ± SD) of FLA at anthesis in *tabri1, tadwf1* and *tadwf4* lines along with Cadenza were recorded during a spring-sown field trail WS2232. The % changes in the leaf angles compared with Cadenza are also shown. General ANOVA output i.e., *p*-values, SED, and LSD at 5% level of significance are also included. Statistically significant differences between mutant and Cadenza were denoted ****$p < 0.0001$ (obtained from Fisher's LSD unprotected test).

Genotypes	Mean FLA (degrees) ± SD	% Change
tabri1-a.1	34.4 ± 9.9	-0.28
tabri1-b	35.9 ± 11.9	4.05
tabri1-d	33.8 ± 13.3	-2.02
tabri1-a.1b	24.2 ± 6.3****	-29.85
tabri1-a.1d	24.8 ± 8.6****	-28.11
tabri1-bd	22.6 ± 6.9****	-34.49
TaBRI1-NS	32.6 ± 11.7	-5.5
tabri1-a.3bd	15.5 ± 4.9****	-55.07
tadwf1-abd	15.8 ± 4.0****	-54.2
tadwf4-abd	18.6 ± 4.7****	-46.08
TaDWF1-NS	30.5 ± 9.3	-11.59
Cadenza	34.5 ± 13.1	_
***p*-value (Genotype)**	<0.001	
***p*-value (Block)**	<0.001	
LSD	4.422	
SED	2.249	

5.2.1.2 Final plant height and internode elongation

Final plant height (including the ear) was recorded on 15 tillers harvested from each 4 plot/genotype at maturity. The data were analysed using ANOVA and is presented in Figure 5.2 and Table 5.2. ANOVA confirmed statistically significant differences between genotypes [F (11, 648) = 254.69, p <.001]. As there was no significant difference between *TaBRI1-NS* and Cadenza the height of *tabri1* mutants were compared with Cadenza as a common control. There were no significant differences for final plant height between the single and double mutants and Cadenza, except for *tabri1-a.1b* which could be due to an unrelated genetic reason. The final plant height of the triple mutant *tabri1-a.3bd* was 343.4 mm compared to 534.2 mm for Cadenza, which is approximately 36% shorter.

The final plant height of the *tadwf1-abd* mutant was reduced by approximately 50% compared to Cadenza, but there was only a 14% decrease in the height of *tadwf4-abd*. This slight height reduction in the height of *tadwf4-abd* was observed only under field conditions, and was not observed in the glasshouse, as described in detail under section 4.2.8.2 and 4.2.8.3.

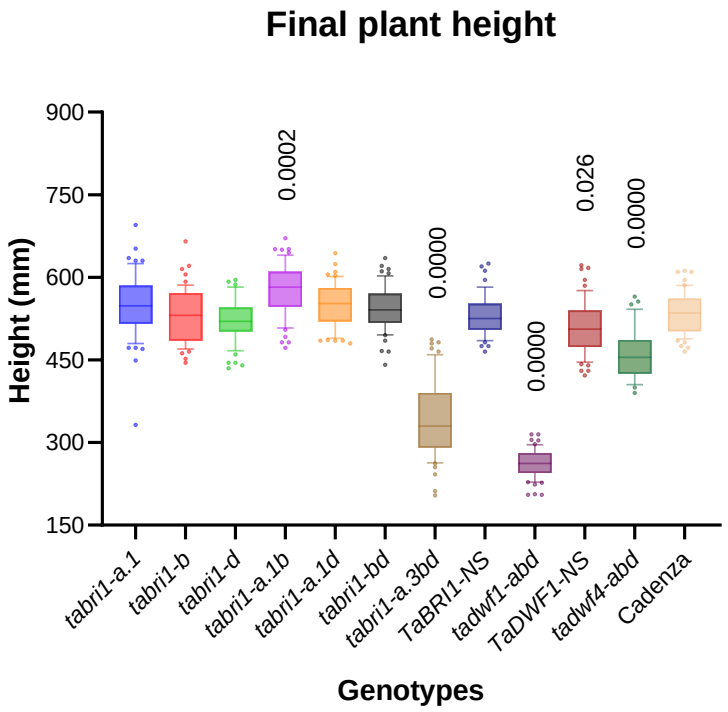

Figure 5. 2 Final plant height in *tabri1*, *tadwf1* and *tadwf4* mutants. Height was recorded on *tabri1* (singles, doubles, *tabri1-a.3bd* and *TaBRI1-NS*), *tadwf1* (*tadwf1-abd* and *TaDWF1-NS*) and *tadwf4-abd* lines along with Cadenza at harvest (n~60) from a spring-sown field trail WS2232. The data are plotted as box and whisker plots. *p*-values for significant differences between mutants and Cadenza (obtained using Fisher's unprotected LSD test) are also shown.

Table 5. 2 Final plant height of *tabri1*, *tadwf1* and *tadwf4* mutants. Final plant height of *tabri1, tadwf1* and *tadwf4* mutants along with Cadenza were recorded at maturity from a spring-sown field trail WS2232. The % change in the height compared with Cadenza is also shown. General ANOVA output i.e., *p*-values, SED, and LSD at 5% level of significance are also described below. Statistically significant differences between mutant and Cadenza were denoted *$p < 0.05$, **$p < 0.01$, ***$p < 0.001$, ****$p < 0.0001$ (obtained from Fisher's LSD unprotected test).

Genotype	Mean height (mm) ± SD	% Change
tabri1-a.1	548.3 ± 57.6	2.63
tabri1-b	532.5 ± 48.5	-0.31
tabri1-d	520.6 ± 39.0	-2.54
tabri1-a.1b	577.5 ± 47.3***	8.1
tabri1-a.1d	551.0 ± 39.7	3.14
tabri1-bd	541.5 ± 40.5	1.36
TaBRI1-NS	529.3 ± 37.2	-0.91
tabri1-a.3bd	343.4 ± 72.2****	-35.71
tadwf1-abd	262.4 ± 26.4****	-50.87
tadwf4-abd	460.6 ± 46.3****	-13.77
TaDWF1-NS	508.8 ± 47.9*	-4.75
Cadenza	534.2 ± 37.6	_
***p*-value (Genotype)**	<0.001	
***p*-value (Block)**	<0.001	
LSD	16.99	
SED	8.65	

To determine the contribution of individual internodes to final plant height, we measured internode lengths on 10 representative tillers per plot at maturity. The data were analysed using ANOVA and the results are presented in Figure 5.3 and Table 5.3. ANOVA confirmed statistical significant differences for the lengths of peduncle, internode 2 and internode 3 between genotypes [F (11, 463) = 56.31, p <.001], [F (11, 463) = 51.30, p <.001] and [F (11, 446) = 35.09, p <.001], respectively.

Peduncle lengths of *TaBRI1-NS* and *TaDWF1-NS* were like that of Cadenza. Therefore, for simplicity we compared the lengths of the peduncle in the mutants to Cadenza. We observed significant reductions in peduncle length in all the triple mutants i.e., *tabri1-a.3bd*, *tadwf1-abd* and *tadwf4-abd* i.e., 47%, 55% and 26%,

respectively, compared to Cadenza. Peduncle lengths of other single or double *tabri1* mutants were not significantly different from Cadenza.

Similarly, the length of the second internode of *TaBRI1-NS* and *TaDWF1-NS* did not differ significantly from that in Cadenza, which was used as control for the mutants. We observed significant reductions in the length of the 2nd internode in *tabri1-a.3bd* and *tadwf1-abd*, i.e., 31% and 45%, respectively, compared to Cadenza. No significant differences were observed for this trait between *tadwf4-abd* and Cadenza. In contrast, there was an increase in the length of the 2nd internode of *tabri1-a.1* and *tabri1-a.1b* compared to Cadenza. Otherwise, no significant differences from Cadenza existed for 2nd internode length in other single or double *tabri1* mutants.

The length of the 3rd internode of *TaBRI1-NS* and *TaDWF1-NS* were not significantly different from Cadenza, which was used as control. There were 30% and 75% reductions in 3rd internode lengths in the *tabri1-a.3bd* and *tadwf1-abd* mutants, respectively, compared to Cadenza. The lengths of the 3rd internode of *tadwf4-abd* and of *tabri1* single and double mutants did not differ significantly from Cadenza, although there was an increased length in *tabri1-a.1b*.

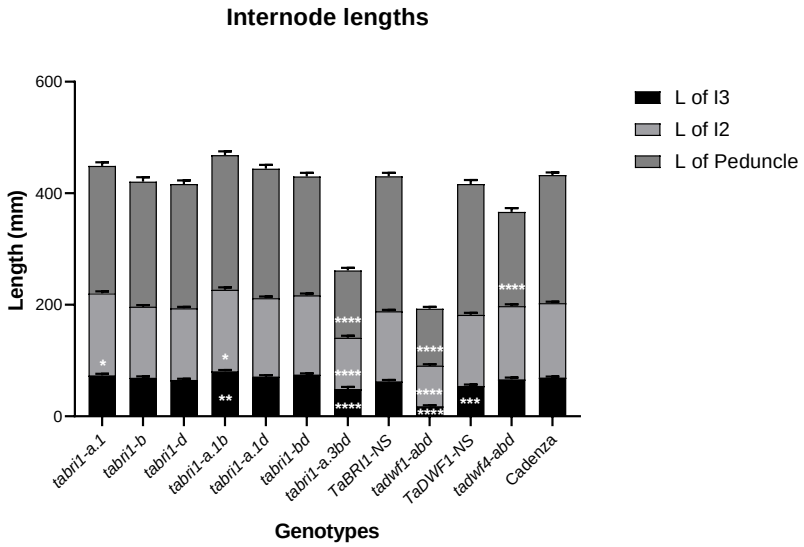

Figure 5. 3 Internode lengths in *tabri1, tadwf1* and *tadwf4* mutants. Internode lengths (peduncle, internode 2 and 3) were recorded at maturity in *tabri1* (*singles, doubles, tabri1-a.3bd, TaBRI1NS*), *tadwf1* (*tadwf1-abd* and *TaDWF1-NS*) and *tadwf4-abd* lines along with Cadenza (n~40) from the spring-sown field trail WS2232. The data are presented in the form of a stacked bar graph. Statistically significant differences between mutants and Cadenza are denoted *$p < 0.05$, **$p < 0.01$, ***$p < 0.001$, ****$p < 0.0001$ (obtained from Fisher's LSD unprotected test).

Table 5. 3 Internode lengths in *tabri1*, *tadwf1* and *tadwf4* mutants. Peduncle, I2 and I3 lengths for *tabri1* (*singles*, *doubles*, *tabri1-a.3bd* and *TaBRI1-NS*), *tadwf1* (*tadwf1-abd* and *TaDWF1-NS*) and *tadwf4-abd* lines along with Cadenza were recorded at maturity during a spring-sown field trial WS2232. The % difference compared with Cadenza are also shown. General ANOVA output i.e., *p*-values, SED, and LSD at 5% level of significance are provided. Statistically significant differences between mutant and Cadenza are denoted *$p < 0.05$, **$p < 0.01$, ***$p < 0.001$, ****$P < 0.0001$ (obtained from Fisher's LSD unprotected test).

	Peduncle		**Internode 2**		**Internode 3**	
Genotype	**Mean length ± SD (mm)**	**% Change**	**Mean length ± SD (mm)**	**% Change**	**Mean length ± SD (mm)**	**% Change**
tabri1-a.1	228.4 ± 40.7	-0.52	147.2 ± 21.3*	10.01	73.5 ± 18.3	5.9
tabri1-b	224.4 ± 49.4	-2.26	127.4 ± 18.7	-4.78	69.1 ± 14.5	-0.43
tabri1-d	222.9 ± 41.1	-2.91	128.4 ± 17.1	-4.03	65.3 ± 13.6	-5.9
tabri1-a.1b	241.4 ± 43.5	5.13	146.2 ± 26.4*	9.26	80.7 ± 15.1**	16.28
tabri1-a.1d	232.2 ± 43.1	1.13	140.8 ± 19.1	5.23	71.1 ± 16.3	2.44
tabri1-bd	213.2 ± 41.1	-7.14	142.3 ± 21.0	6.35	74.7 ± 15.3	7.63
TaBRI1-NS	242.1 ± 38.3	5.44	125.7 ± 16.7	6.05	62.8 ± 15.9	-9.51
tabri1-a.3bd	120.6 ± 31.3****	-47.47	92.2 ± 22.3****	31.09	48.7 ± 23.2****	-29.82
tadwf1-abd	102.2 ± 21.3****	-55.48	72.9 ± 16.5****	-45.5	18.0 ± 9.8****	-74.06
tadwf4-abd	168.6 ± 37.6****	-26.56	131.4 ± 15.6	-1.79	66.4 ± 17.0	-4.32
TaDWF1-NS	234.4 ± 44.9	2.09	127.8 ± 22.5	-4.48	54.3 ± 16.9***	-21.75
Cadenza	229.6 ± 29.7	_	133.8 ± 14.5	_	69.4 ± 11.5	_
***p*-value (Genotype)**	<0.001		<0.001		<0.001	
***p*-value (Block)**	<0.001		0.274		0.141	
LSD	16.83		8.43		6.964	
SED	8.564		4.289		3.543	

5.2.1.3 Spike length

To estimate the compactness of the spikes we measured the length of 15 mature spikes in each plot. The data were analysed using ANOVA and are presented in Figure 5.4 and Table 5.4. ANOVA confirmed statistically significant differences for spike length between genotypes [F (11, 669) = 55.76, p <.001]. Spike length in *TaBRI1-NS* was not significantly different from that in Cadenza, whereas there was a slight significant reduction in spike length in *TaDWF1-NS* compared to Cadenza. Spike lengths for single (except for *tabri1-b*) and double *tabri1* mutants were not significantly different from that in Cadenza. However, we observed a nearly 18% reduction in spike length in the triple *tabri1-a.3bd* mutant compared to Cadenza. Additionally, we observed nearly 21% and 8% reduction in the spike length in *tadwf1-abd* and *tadwf4-abd* compared to Cadenza. The data demonstrate a role for BRs in controlling spike length in wheat.

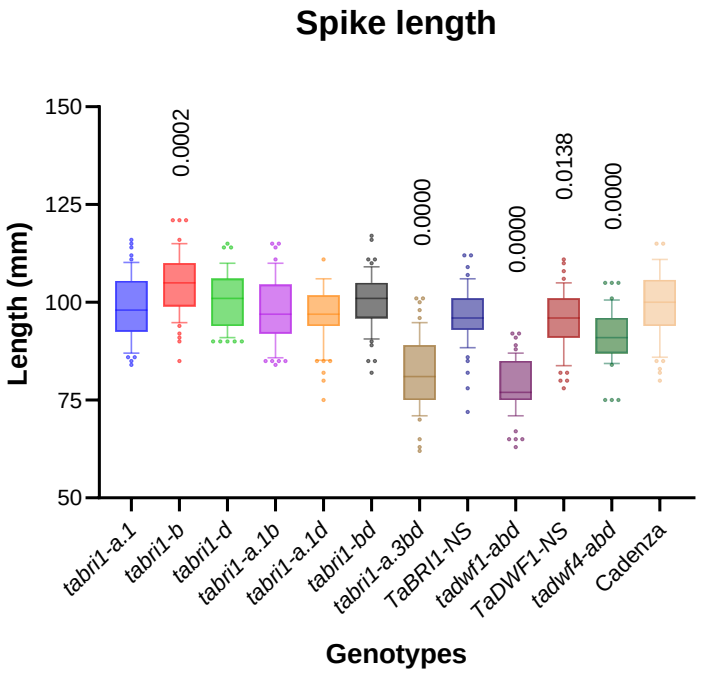

Figure 5. 4 Spike length in *tabri1*, *tadwf1* and *tadwf4* mutants. Mature spike lengths were measured on *tabri1* (*singles, doubles* and triple (*tabri1-a.3bd*) mutants and *TaBRI1-NS*), *tadwf1* (*tadwf1-abd* and *TaDWF1-NS*) and *tadwf4-abd* mutants along with Cadenza (n~60) in the spring-sown field trail WS2232. The data are plotted as a box and whisker plot. *p*-values for significant differences between mutants and Cadenza (obtained using Fisher's unprotected LSD test) are shown.

Table 5. 4 Spike length in *tabri1*, *tadwf1* and *tadwf4* mutants. The spike lengths of the *tabri1*, *tadwf1* and *tadwf4* mutants along with Cadenza were recorded at maturity in the spring-sown field trail WS2232. The % change in the spike length compared with Cadenza is also shown. General ANOVA output i.e., *p*-values, SED, and LSD at 5% level of significance are also described below. Statistically significant differences between mutant and Cadenza were denoted *$p < 0.05$, ***$p < 0.001$, ****$p < 0.0001$ (obtained from Fisher's LSD unprotected test).

Genotype	Mean length ± SD (mm)	% Change
tabri1-a.1	98.8 ± 8.1	-0.6
tabri1-b	104.8 ± 8.0***	5.43
tabri1-d	100.2 ± 7.1	0.8
tabri1-a.1b	97.9 ± 8.0	-1.5
tabri1-a.1d	97.0 ± 7.1	-2.41
tabri1-bd	100.4 ± 7.3	1
TaBRI1-NS	97.1 ± 7.7	-2.31
tabri1-a.3bd	81.8 ± 9.3****	-17.7
tadwf1-abd	78.6 ± 7.0****	-20.92
tadwf4-abd	91.5 ± 7.0****	-7.94
TaDWF1-NS	95.7 ± 7.8*	-3.72
Cadenza	99.4 ± 8.7	_
***p*-value (Genotype)**	<0.001	
***p*-value (Block)**	<0.001	
LSD	2.911	
SED	1.482	

5.2.1.4 Seed characteristics

Seed area, number and thousand grain weight (TGW) determine final grain yield in cereals. Seed areas were measured using Marvin Seed Analyser (INDOSAW, Haryana, India) and for estimating seed weight (weighing scale) was used. Values for these parameters from the mutants and control lines were analysed using ANOVA and are presented in Figure 5.5 and Table 5.5.

ANOVA confirmed statistically significant differences for seed area between the genotypes [F (11, 46) = 3.17, p= 0.005]. In *tabri1* mutants (singles, doubles, and *tabri1-a.3bd*), we found no significant differences in seed area compared to Cadenza. In contrast, seed area was significantly reduced in the *tadwf1-abd* mutant, by

approximately 7% compared to Cadenza. Additionally, there was no significant difference in seed area between the *tadwf4-abd* mutant and Cadenza.

There were statistically significant differences in TGW between the mutants [F (11,46) = 2.85, *p*= 0.010]. We observed nearly 15% reduction in the TGW in *tabri1-a.3bd* and *tadwf1-abd* compared to Cadenza. Interestingly, no significant reduction was noted in erect-statured *tadwf4-abd* and *tabri1* double mutants (*tabri1-a.1b*, *tabri1-a.1d* and *tabri1-bd*), which are potential targets for yield enhancement under dense planting conditions.

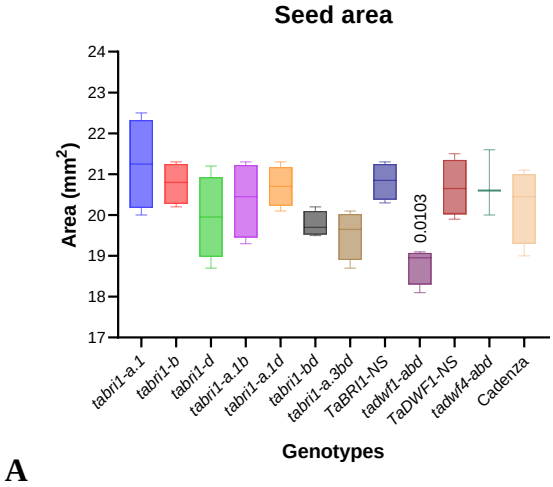

A

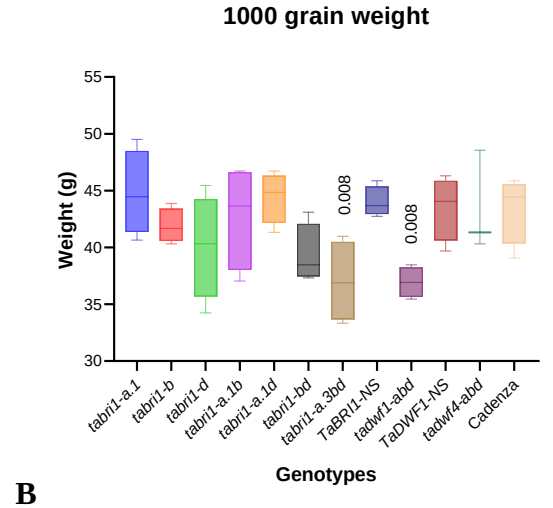

B

Figure 5. 5 Seed area and TGW in *tabri1*, *tadwf1* and *tadwf4* mutants. (A) seed area and (B) TGW of *tabri1 (singles, doubles, tabri1-a.3bd, TaBRI1-NS), tadwf1 (tadwf1-abd, TaDWF1-NS)* and *tadwf4-abd* mutants along with Cadenza (n=4) recorded on grains obtained after harvesting from the spring-sown field trial WS2232. The data are plotted as a box and whisker plot. *p*-values for significant differences between mutants and Cadenza (obtained using Fisher's unprotected LSD test) are also shown.

Table 5. 5 Seed area and TGW of *tabri1*, *tadwf1* and *tadwf4* mutants. The seed areas and TGW were recorded on mature grains harvested from the spring-sown field trial WS2232. The % change in these traits compared with Cadenza is also shown. General ANOVA output i.e., *p*-values, SED, and LSD at 5% level of significance are also given. Statistically significant differences between mutant and Cadenza were denoted *$p < 0.05$, **$p < 0.01$, obtained from Fisher's LSD unprotected test).

	Seed Area (mm^2)		TGW (gm)	
Genotype	**Mean ± SD**	**% Change**	**Mean ± SD**	**% Change**
tabri1-a.1	21.3 ± 1.1	4.92	44.8 ± 3.7	2.98
tabri1-b	20.8 ± 0.5	2.46	41.9 ± 1.5	-3.67
tabri1-d	20.0 ± 1.0	-1.47	40.1 ± 4.6	-7.81
tabri1-a.1b	20.4 ± 0.9	0.49	42.8 ± 4.6	-1.6
tabri1-a.1d	20.7 ± 0.5	1.97	44.4 ± 2.3	-2.06
tabri1-bd	19.8 ± 0.3	-2.46	39.3 ± 2.6	-9.65
TaBRI1-NS	20.8 ± 0.5	2.46	44.0 ± 1.3	1.14
tabri1-a.3bd	19.5 ± 0.6	-3.94	37.0 ± 3.6**	-14.94
tadwf1-abd	18.8 ± 0.5*	-7.38	36.9 ± 1.3**	-15.17
tadwf4-abd	20.7 ± 0.8	1.97	43.4 ± 4.5	-0.23
TaDWF1-NS	20.7 ± 0.7	1.97	43.5 ± 2.8	0
Cadenza	20.3 ± 0.9	_	43.5 ± 3.0	_
***p*-value (Genotype)**	0.006		0.013	
***p*-value (Block)**	0.884		0.667	
LSD	1.218		5.200	
SED	0.5979		2.553	

5.2.2 High-throughput phenotyping of *tadwf1-abd* mutant using a Field Scanalyzer

The Field Scanalyzer at Rothamsted Research is a fully automated high-throughput phenotyping platform (HTTP) manufactured by LemnaTec GmbH, Germany, containing an array of high-resolution sensors such as thermal infrared, 3D laser scanner, visible camera, hyperspectral imager and NDVI sensor which can monitor crop growth, physiology, morphology, and health at regular intervals throughout the lifecycle of a field-grown crop (Virlet et al., 2016).

We were interested in determining the green canopy cover, spike density and stem elongation patterns throughout the life cycle of the BR mutants. Therefore, three biological replicates of a representative erect-statured, semidwarf mutant, *tadwf1-abd* were planted under the Field Scanalyzer along with the Cadenza control in a

randomised block design. Only this mutant was stable and sufficiently backcrossed for sowing during winter 2020.

5.2.2.1 Canopy cover

Canopy cover (CC) can give an estimate of canopy architecture, leaf angles, leaf area index (LAI) and degree of light interception. The RGB camera provides a low cost, high-resolution, non-destructive, high throughput method for estimating canopy cover (Behrens and Diepenbrock, 2006; Shrestha and Steward, 2003; Thorp and Dierig, 2011; Thorp et al., 2008; Ewing and Horton, 1999; Purcell, 2000; Rasmussen et al., 2007). CC was estimated over the life cycle from the RGB images. Figure 5.6 shows original and segmented RGB image of *tadwf1-abd* mutant and Cadenza at GS-69 captured on 22nd June 2021.

Figure 5.7 (A) shows that *tadwf1-abd* has lower CC compared to Cadenza throughout its life cycle from early November 2020 to late July 2021. Over the reproductive phase, there were 23%, 26% and 28% reductions in CC for *tadwf1-abd* at ear emergence (GS-59), 50% flowering completion (GS-65) and flowering completion (GS-69) (Figure 5.7 and Table 5.6). One tail *t*-test confirmed statistical significance between *tadwf1-abd* and Cadenza with *p*-values <0.05 (using Genstat software 22nd Edition).

A

B

Figure 5. 6 Green canopy cover of the *tadwf1* mutant and Cadenza at GS-69. The RGB images were captured on *tadwf1-abd* (A) and Cadenza (B) at GS-69 under the Field Scanalyzer during 2020-21. Left panel shows the original image and the right panel shows the segmented RGB images. The CC was estimated from the RGB images using a published pipeline (Sadeghi-Tehran et al., 2017).

A

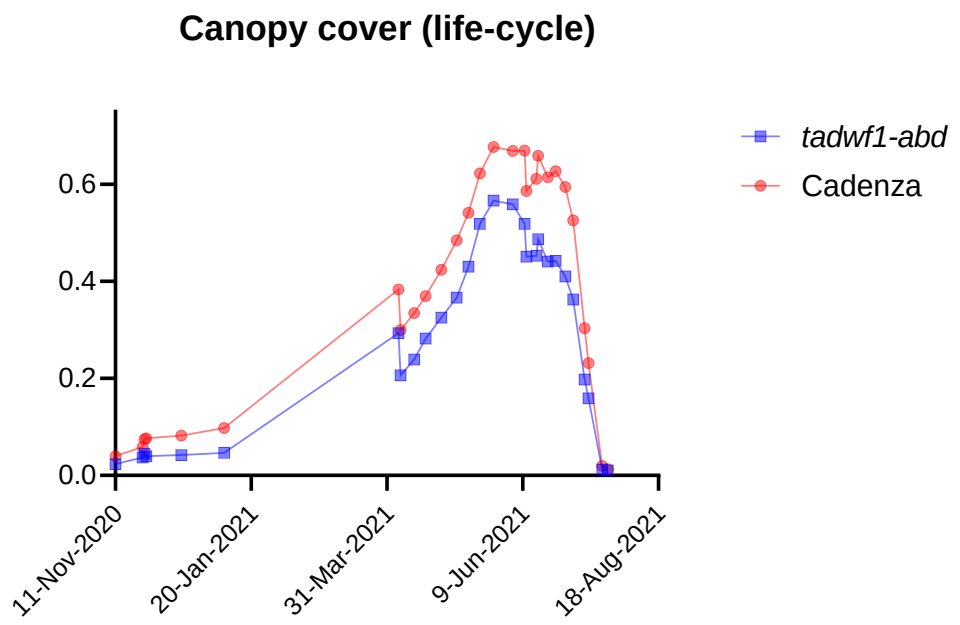

B

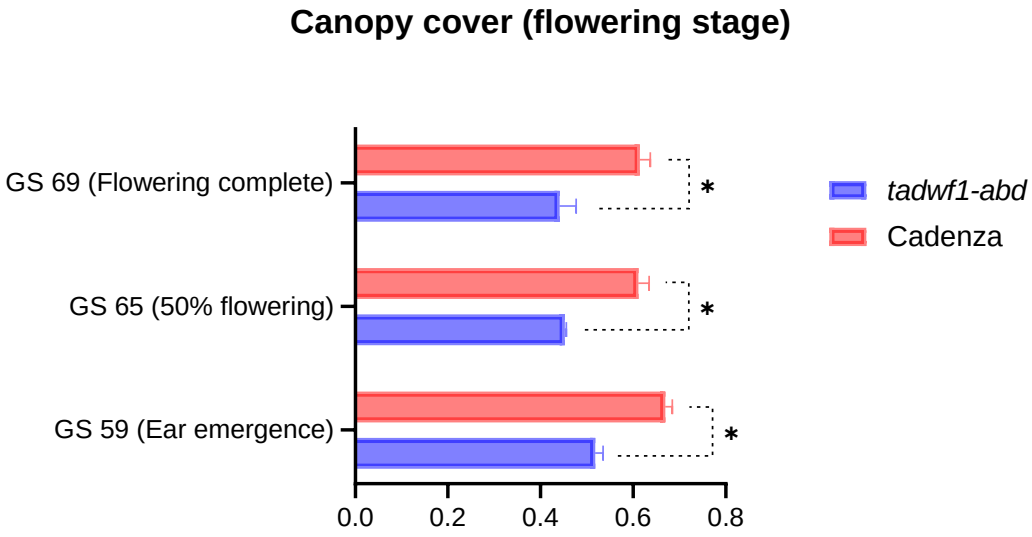

Figure 5. 7 Green canopy cover of *tadwf1-abd* and Cadenza during flowering stage. (A) Canopy cover of *tadwf1-abd* and Cadenza recorded under the Field Scanalyzer from early November 2020 until late June 2021 (n=3) (B) Canopy cover of these genotypes during flowering stages (GS-59, GS-65, and GS-69). Significant differences were denoted as *$p < 0.05$ as confirmed from one-tail *t*-test using Genstat software.

Table 5. 6 Green canopy cover of *tadwf1-abd* and Cadenza during flowering stages. CC (mean ± SED) of the *tadwf1-abd* mutant along with Cadenza recorded at GS-59, GS-65, and GS-69 under the Field Scanalyzer during 2021-22. The % change in thi trait compared with Cadenza is also shown. One-way *t*-test output i.e., t-statistic, d.f. and *p*-values at 5% level of significance are also presented in the Table. Statistically significant differences between mutant and Cadenza were denoted *$p < 0.05$ (obtained from one-way *t*-test).

	Canopy cover		
Genotypes	**GS-59**	**GS-65**	**GS-69**
tadwf1-abd	0.451 ± 0.009*	0.452 ± 0.003*	0.441 ± 0.036*
Cadenza	0.586 ± 0.030	0.611 ± 0.023	0.614 ± 0.022
% Change	23.03	25.8	28
t-statistic	4.2	6.72	4.07
d.f.	4	2.07	4
***p*-value**	0.014	0.02	0.015

5.2.2.2 Spike density

Improving yield in crop plants is one of the main objectives of plant breeders and crop scientists. Yield is determined by spike density (correlating to tillering), number of grains per spike and grain weight. We quantified the number of grains per spike and grain weight for this mutant under glasshouse and field conditions but estimating spike density is a labour intensive and time-consuming task. Due to advances in HTTP technology and image analysis spike density can be estimated using a fully automated simple linear iterative clustering and deep convolutional neural network pipeline (Sadeghi-Tehran et al., 2019). The spike density per plot for *tadwf1-abd* and Cadenza at GS-69 (end of flowering stage) was estimated from the RGB images using a published protocol (Sadeghi-Tehran et al., 2019).

We observed a significant 26% reduction in the number of spikes per m^2 for *tadwf1-abd* compared to Cadenza with the *p*-value obtained by one-tail *t*-test significantly lower than 0.05 (Figure 5.8 and Table 5.7).

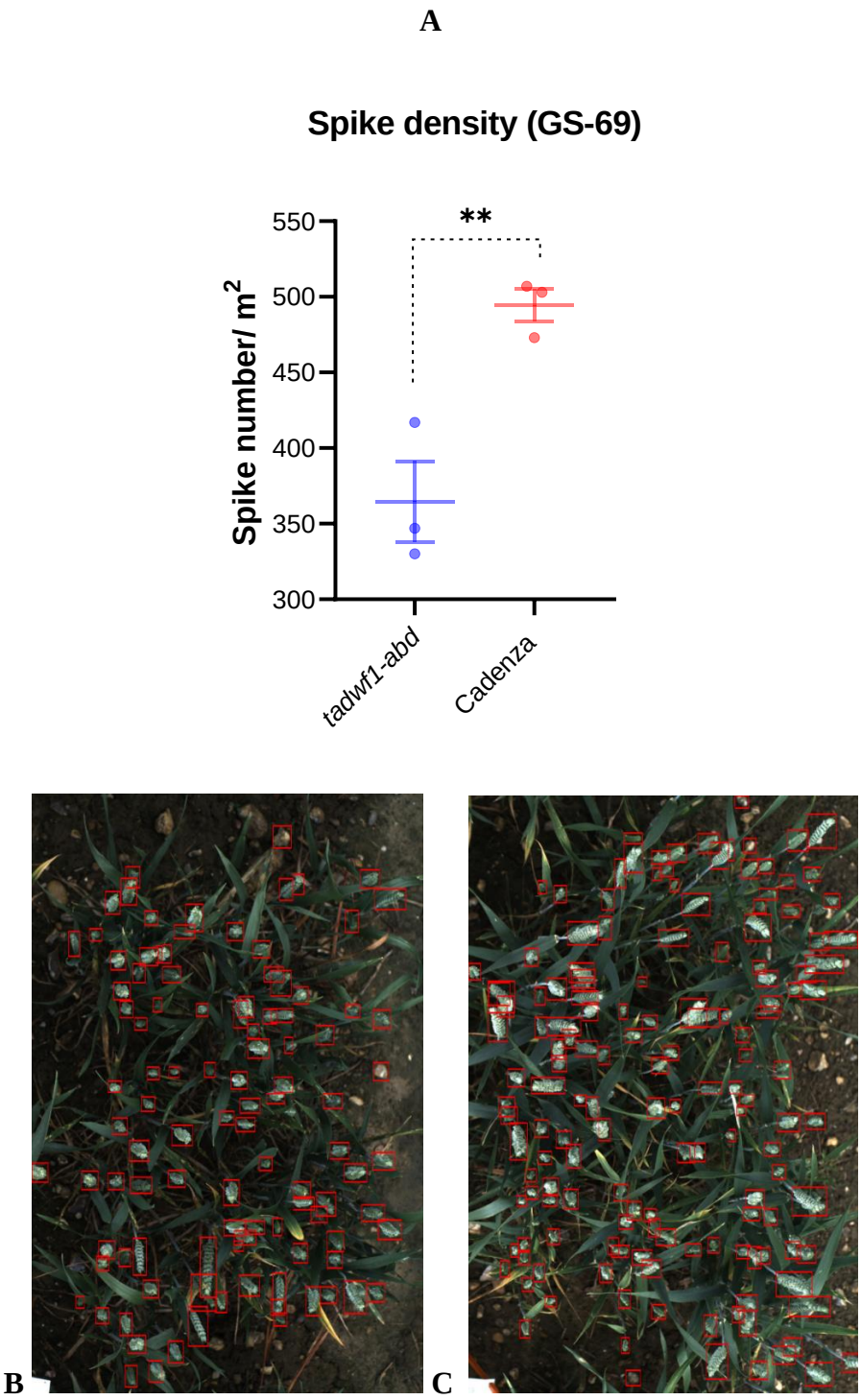

Figure 5. 8 Spike density for *tadwf1-abd* and Cadenza. (A) Spike density (number of spikes per m^2) for *tadwf1-abd* and Cadenza (n=3) were recorded at GS-69 stage under Field Scanalyzer during 2020-21 showing a statistically significant difference between the mutant and Cadenza $^{**}p < 0.01$ (obtained from one-way *t*-test). (B) and (C) RGB images showing highlighted spikes in *tadwf1-abd* and Cadenza, respectively, for estimating spike density using a published protocol (Sadeghi-Tehran et. al., 2019).

Table 5. 7 Spike density of the *tadwf1-abd* mutant and Cadenza. Spike density (mean spike number per m^2 ± SED) was recorded for the *tadwf1-abd* mutant and Cadenza at GS-69 under the Field Scanalyzer during 2021-22. The % change in these traits compared with Cadenza is also shown. One-way *t*-test output i.e., t-statistic, d.f. and *p*-values at 5% level of significance are also described below. Statistically significant differences between mutant and Cadenza were denoted $^{**}p < 0.01$ (obtained from one-way *t*-test).

Genotype	**Number of spikes /m^2 (GS-69)**
tadwf1-abd	364.4 ± 26.55**
Cadenza	494.4 ± 10.60
% Change	26.3
t-statistic	4.55
d.f.	4
***p*-value**	0.01

5.2.2.3 Plant height and internode elongation

We observed reduced plant height and restricted internode elongation in the *tadwf1-abd* mutant at maturity compared to Cadenza under glasshouse and field conditions. The height of the mutant and Cadenza were recorded under the Field Scanalyzer from GS-37 (initiation of internode elongation) until GS-91 (maturity).. As shown in Figure 5.9 there was a gradual increase in plant height reaching a maximum at flowering stage from 16th June-30th June (GS-59, GS-65, and GS-69) followed by a slight decrease near maturity (due to drying).

The statistical significance of the height difference between *tadwf1-abd* and Cadenza was assessed at two growth stages: GS-65 (midway through flowering) and GS-91 (maturity). We observed approximately 30% and 25% reduction in plant height in *tadwf1-abd* compared to Cadenza at GS-65 and GS-91, respectively, as shown in figure 5.9. The one-way *t*-test confirmed these differences to be statistically significant with *p*-values <0.05 as shown in Table 5.8.

Interestingly, we observed less reduction in final plant height (25%) in *tadwf1-abd* compared to Cadenza when sown in winter, compared to an approximately 50% reduction in the mutant when spring-grown (as discussed in 5.2.1.2).

A

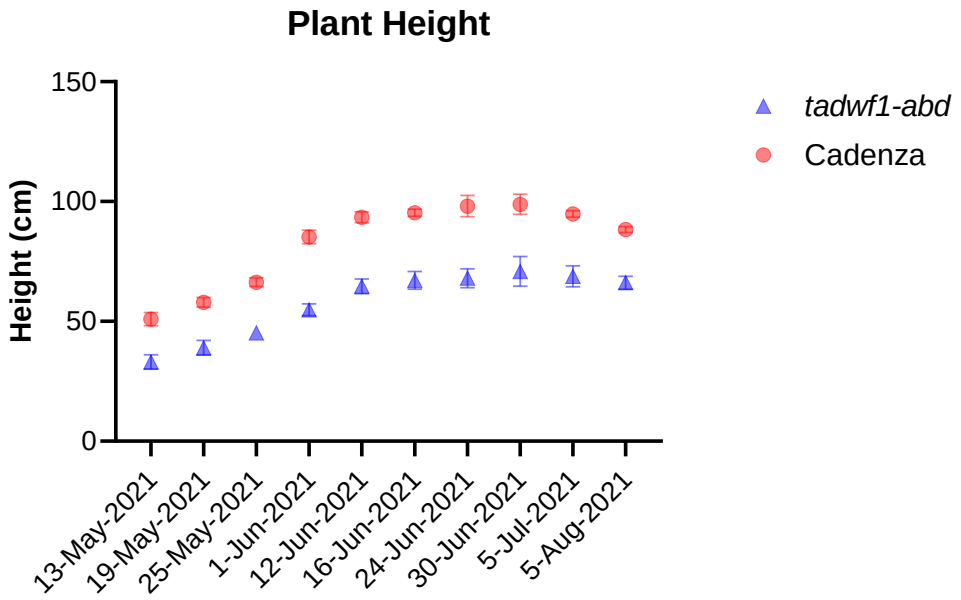

B

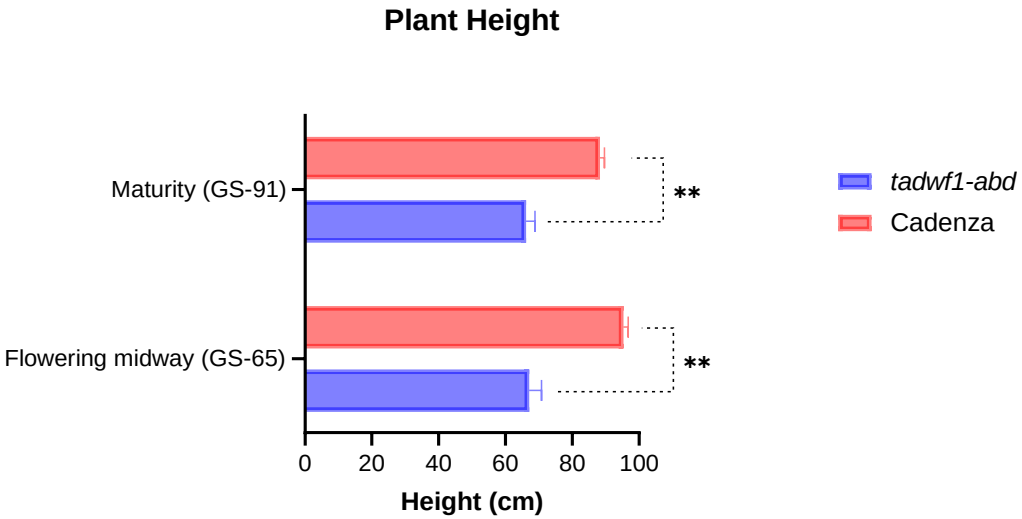

Figure 5. 9 Heights of *tadwf1-abd* and Cadenza. (A) The height of the *tadwf1-abd* mutant and Cadenza (n=3) were recorded under the Field Scanalyzer from mid May 2021 (initiation of internode elongation) until early August 2021 (maturity). (B) Heights of these genotypes were recorded at the mid flowering stage (GS-65) and at maturity (GS-91). Statistically significant differences between *tadwf1-abd* and Cadenza were found with $p < 0.01$ (obtained using one-tail *t*-test).

Table 5. 8 Plant heights of *tadwf1-abd* mutant and Cadenza at two growth stages. Heights (mean ± SED) of the *tadwf1-abd* mutant and Cadenza were recorded at GS-65 and GS-91 under the Field Scanalyzer during 2021-22. The % change in height *in tadwf1-abd* mutant compared with Cadenza is also shown. One-way *t*-test output i.e., *t*-statistic, d.f. and *p*-values at 5% level of significance are also described below. Statistically significant differences between mutant and Cadenza were denoted * **$P < 0.01$, (obtained from one-way *t*-test).

	Plant height (cm)	
Genotypes	**GS-65**	**GS-91**
tadwf1-abd	67.11 ± 3.67**	66.18 ± 2.68**
Cadenza	95.31 ± 1.47	88.34 ± 1.28
% Change	29.5	25
t-statistic	7.13	7.46
d.f.	4	4
***p*-value**	0.002	0.002

To determine the contribution of individual internodes to plant height in *tadwf1-abd* and Cadenza we measured internode lengths in the 10 tallest tillers per plot. One-way *t*-test confirmed significant differences amongst the genotypes as the *p*-value was <0.05 for all the internodes. We observed approximately 30%, 32%, 42%, 43% and 68% reduction lengths of peduncle, I2, I3, I4 and I5, respectively, in *tadwf1-abd* compared to Cadenza. (Figure 5.10 and Table 5.9).

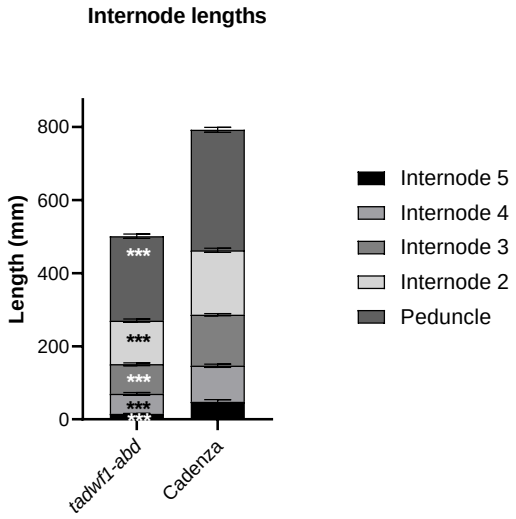

Figure 5. 10 Internode lengths in *tadwf1-abd* and Cadenza at maturity. The internode lengths (peduncle, internodes 2, 3, 4 and 5) were recorded at maturity for *tadwf1-abd* and Cadenza (n~30). The data are presented as a stacked bar graph. Statistically significant differences between mutant and Cadenza were denoted ***$P < 0.001$ (obtained from one-way *t*-test).

Table 5. 9 Internode lengths in *tadwf1-abd* and Cadenza. Internode lengths in mm (mean ± SD) for *tadwf1-abd* and Cadenza were recorded at maturity. The % difference in lengths in *tadwf1-abd* compared with Cadenza are also shown. One-way *t*-test output i.e., *t*-statistic, d.f. and *p*-values at 5% level of significance are also presented. Differences between the genotypes are statistically significant, $p < 0.001$ (obtained from one-way *t*-test).

	Internode lengths				
Genotype	**Peduncle (mm)**	**I2 (mm)**	**I3 (mm)**	**I4 (mm)**	**I5 (mm)**
tadwf1-abd	231.1 ± 5.8	119.1 ± 4.5	81.4 ± 3.8	54.3 ± 3.8	15.2 ± 0.9
Cadenza	329.7 ± 6.8	176 ± 5.5	139.6 ± 2.8	98.9 ± 4.4	47.8 ± 6.1
% Change	29.7	32.3	41.7	44.8	68.1
t-statistic	10.99	7.89	12.18	7.48	5.26
d.f.	58	58	58	54	23
***p*-value**	<0.001	<0.001	<0.001	<0.001	<0.001

5.3 Discussion

In chapters 3 and 4 the phenotypic characterisation of *tabri1*, *tadwf1* and *tadwf4* mutants growing under glasshouse conditions is described. However, the overarching objective was to assess these architectural mutants under field conditions which is required to inform their potential for future exploitation in wheat breeding. Therefore, a field trial assessment of *tabri1*, *tadwf1* and *tadwf4* mutants was conducted in 2022 to assess traits including flag leaf angle, plant height, internode elongation, spike length and grain characteristics. The *tabri1*, *tadwf1* and *tadwf4* mutants displayed similar phenotypic characteristics, including altered flag leaf angles, when grown in the field as observed under glasshouse conditions. Based on the field assessment, the *tabri1-a.1b*, *tabri1-bd*, *tabri1-a.1d* and *tadwf4-abd* mutants were identified as genotypes having reduced flag-leaf angle without displaying obvious negative pleotropic effects that could impact key agronomic traits. This raises the prospect that these new BR-related architecture alleles could provide opportunities for improving grain yields in wheat, when grown under dense planting density.

In a separate field experiment, the *tadwf1-abd* mutant was assessed using the high-throughput Field Scanalyzer phenotyping facility at Rothamsted. This allowed a

more detailed assessment of phenotype throughout the growing season. Interestingly, we observed a significant reduction in green canopy cover, spike density and plant height in the *tadwf1-abd* triple mutant compared to Cadenza. This demonstrated that alterations in wheat canopy architecture can be achieved by altering BR signalling.

5.3.1 Mutations in *tabri1, tadwf1* and *tadwf4* genes alter plant architecture in the field

Some BR-deficient or insensitive mutants have erect stature and reduced stem elongation, allowing dense planting and providing lodging resistance that can improve grain yields in cereals such as rice and maize (Sakamoto et al., 2006; Tian et al., 2019; Song et al., 2023). Our main objective was to establish whether a similar strategy can be used to improve grain yields in wheat. The generation of *tabri1*, *tadwf1* and *tadwf4* mutants (described in chapters 3 and 4) provided an opportunity to establish whether reduced BR-signalling can improve wheat traits under field conditions. Therefore, to uncover the phenotype associated with these mutations under field conditions, a spring-sown trial was conducted. For *tabri1* mutant characterisation, we sowed singles (*tabri1-a.1*, *tabri1-b* and *tabri1-d*), doubles (*tabri1-a.1b*, *tabri1-a.1d* and *tabri1-bd*) and a triple mutant (*tabri1-a.3bd*) and compared them with the controls *TaBRI1-NS* and Cadenza. The more severe triple mutants *tabri1-a.1bd* and *tabri1-a.2bd* were excluded due to insufficient seed availability as a result of severe and moderate sterility, respectively. To determine whether these mutants' exhibited changes in leaf erectness, the flag leaf angle was measured at anthesis. No differences were observed in the *tabri1* single mutants when compared to the controls. In contrast, significant reductions in the flag leaf angle were observed in all the double and triple mutants (*tabri1-ab*, *tabri1-ad*, *tabri1-bd* and *tabri1-a.3bd*) compared to either *TaBRI1-NS* or Cadenza (as observed when growing these mutants under GH conditions discussed in section 3.2.8.1). These results demonstrate that *TaBRI1* genes regulate canopy architecture in wheat in a gene dosage manner with singles having no effect, while the doubles and triple mutants show leaf erectness. This could be explained by reduced expression of *TaBRI1* genes in the double and triple mutants specifically in the lamina joint region, reducing BR-signalling in this tissue. It would need to be confirmed by hormone and transcriptomic analysis around the lamina joint, in which quite high levels of *BRI1* gene expression have been observed in wheat (Fang et al., 2020). The current results

confirm a role of *BRI1* in regulating canopy architecture in wheat as has been reported in studies with other cereals (Morinaka et al., 2006; Dockter et al., 2014; Fang et al., 2020). No significant differences existed for plant height, internode elongation, spike, and grain characteristics between the single and double *tabri1* mutants and controls demonstrating a high level of functional redundancy for these traits (except for flag-leaf angle) amongst *TaBRI1* genes. This phenotype is consistent as observed under GH trials, discussed in detail in section 3.2.8.2 and 3.2.8.3. In contrast, Fang et al. (2020) reported that single mutations in the *TaBRI1-A* or *-D* homoeologues caused reductions in final plant height, thousand grain weight and harvest index. However, these mutants were isolated from an ion-beam based mutagenesis approach which induces large deletions in the genome. As the mutants had not been backcrossed, the observed phenotypic differences could be due to background mutations. Interestingly, we observed reduction in final plant height due to restricted internode elongation, smaller spikes and lighter grains in the *tabri1-a.3bd* triple mutant compared to controls (also observed in this mutant when grown under GH, discussed in section 3.2.8.3 and 3.2.8.4) demonstrating a role of BRs in regulating these developmental processes as reported in rice and maize (Morinaka et al., 2006; Gruszka et al., 2011; Kir et al., 2015).

The field-grown *tadwf1-abd* mutant displayed erect flag leaf angle at anthesis, reduced final plant height, smaller spikes and lighter grains compared to *TaDWF1-NS* or Cadenza, as observed also in glasshouse experiments (discussed in section 4.2.8 in chapter 4). This phenotype was like that in barley and rice *dwf1* mutants, demonstrating a conserved role for this gene in controlling growth and development in cereals (Hong et al., 2005; Dockter et al., 2014). Due to negative pleiotropic effects of the *tadwf1* mutations on reproductive and grain development, loss-of-function mutations are not expected to provide improvements in wheat grain yields.

The *tadwf4-abd* mutant displayed erect flag leaves and a slight height reduction due to restricted elongation of the peduncle. The altered height phenotype was not observed when growing the mutant in the glasshouse (mentioned in section 4.2.8). The *tadwf4-abd* mutant also displayed smaller spikes but there was no reduction in seed area and TGW compared to controls consistent with GH experiment described in section 4.2.8. Phenotypically, the *tadwf4-abd* mutant resembled the rice *osdwf4-1* mutant, which also has erect leaves, a slight reduction in height but no negative

impact on reproductive tissues (Sakamoto et al., 2006). *DWF4* encodes the BR-biosynthetic enzyme C-22-hydroxylase redundantly with *DWF11*. Unlike the *osdwf4-1* mutant, the *osd11-4* mutant has substantially reduced height, and small round seeds, indicating a more restricted role for *DWF4* (Sakamoto et al., 2006). The erect leaf and semi-dwarf stature lacking negative pleiotropic effects exhibited by *tadwf4-abd* mutant provides a suitable ideotype to investigate whether these architectural changes are suitable for increasing grain yields. Future experiments will aim to establish whether altered planting density of the *tadwf4-abd* mutant can achieve this aim.

5.3.2 Mutations in *TaDWF1* reduces green canopy cover, plant height and spike density

High throughput phenotyping platforms (HTTP) allow testing of genotypes in a non-invasive manner with high precision and resolution throughout the crop life cycle under controlled or field environments (Deery et al., 2014). The Field Scanalyzer at Rothamsted Research is a fully automated, fixed site HTTP which can monitor crop physiology, growth, and development throughout the life cycle of the crop (Virlet et al., 2017). The Rothamsted HTTP was used to assess a representative BR-deficient mutant, *tadwf1-abd*, to establish how changes in canopy architecture affect traits such as green canopy cover, stem elongation and spike density. The *tadwf1-abd* mutant was assessed alongside Cadenza under the Scanalyzer in 2020. RGB images confirmed a significant reduction in green canopy cover in the *tadwf1-abd* plots compared to Cadenza throughout its life cycle. This effect could be due to multiple factors, but one possibility is that it is caused by the erect leaf angles observed in the *tadwf1-abd* mutant (Hong et al., 2005; Dockter et al., 2014). Interestingly, there was a significant 26% reduction in spike density, which is an estimate of tiller number, at GS-69 in the *tadwf1-abd* mutant compared to Cadenza. This observation is consistent with the report that BR signalling positively regulates tillering in rice by promoting bud outgrowth (Fang et al., 2020). We also observed that the *tadwf1-abd* mutant was significantly shorter than Cadenza between GS-37 and GS-91, a trait that agrees with the semi-dwarf character reported for mutants of orthologues of this gene in other cereals The reduction in plant height was due to restricted elongation of all internodes in *tadwf1-abd*, as was reported for the equivalent rice mutant, *brd2/dwf1* (Hong et

al., 2005). In contrast, the barley *dwf1/dim* mutants displayed restricted elongation of only second internode (Dockter et al., 2014).

This experiment adds more power to our previously recorded phenotypic data (glasshouse and field) as it recorded data in real-time throughout the life cycle. Future experiments with the Scanalyzer will be conducted with the most promising BR mutants, *tabri1-a.1b*, *tabri1-a.1d*, *tabri1-bd* and *tadwf4-abd*, to uncover their effects on green canopy cover and spike density under normal and dense planting density. This will provide useful information on the potential of these mutant alleles to improve grain yields.

5.3.3 Conclusions

The objective of this study was to perform a phenotypic assessment of the newly developed BR mutants under field conditions and identify candidate genotypes that would be suitable for assessing in altered density planting trials. Based on the field data, the phenotype of wheat BR mutants under GH conditions is largely replicating in the field, although there were some minor differences. In the case of the *tabri1* mutants, the *tabri1-a.1b*, *tabri1-a.1d* and *tabri1-bd* double mutants were demonstrated to display increased erectness without alterations in plant height, spike, and grain characteristics. Furthermore, the *tadwf4-abd* triple mutant displayed even more pronounced erectness with only a minor effect on plant height. Although further field testing is required, these mutants represent important candidates for improving grain yields under dense planting density.

Chapter 6: General Discussion

6.1 Project Summary

BRs are a group of steroidal phytohormones that control multiple aspects of plant growth and development including stem elongation, leaf angle determination, flowering time, pollen development, seed size and root development (Morinaka et al., 2006; Sakamoto et al., 2006; Jiang et al., 2013; Ye et al., 2010; Domagalska et al., 2010; Bao et al., 2004; Kondo et al., 2014; Nolan et al., 2020). Biosynthesis of BRs occurs through a complex pathway, with the enzymes located in the endoplasmic reticulum (Northey et al., 2016). Bioactive BRs are perceived by the BR receptor, BRI1 in the apoplast (He et al., 2000; Cano-Delgado et al., 2004; Kinoshita et al., 2005). Binding of BRs to the ectodomain of the BRI1 receptor causes BRI1 activation, initiating a cascade of downstream signalling events that activates the BZR1 and BES1 family of transcription factors responsible for controlling BR-dependent growth and development (Nolan et al., 2020). At the cellular and molecular levels, BRs control growth by regulating cell division, elongation, microtubule orientation, tracheary element differentiation and ATPase activity (Clouse et al., 1996, Li et al., 1996; Catterou et al., 2001). In addition to controlling plant development, BRs also control responses to various biotic and abiotic stresses (Krishna, 2003; Nolan et al., 2020).

The primary aim of this project was to establish the role of the BR pathway genes (such as *BRI1*, *DWF1* and *DWF4*) in regulating wheat architecture, with a view to developing new crop improvement strategies. These genes were selected based on studies in other cereals which have highlighted their potential for improving agronomic traits (Chono et al., 2003; Morinaka et al., 2006; Sakamoto et al., 2006; Hong et al., 2005; Dockter et al., 2014). To achieve these objectives, mutations in the *TaBRI1* genes were identified using forward and reverse genetics-based approaches (Chapter 3). Using the same strategy, mutations in the *TaDWF1* and *TaDWF4* genes (Chapter 4) were identified by screening a hexaploid wheat TILLING population (Krasileva et al., 2017). This allowed the generation of *tabri1*, *tadwf1* and *tadwf4*

mutants that were then assessed to establish their potential to improve architectural traits in wheat.

In chapter 3, the role of *BRI1* genes in regulating plant growth and development in wheat was established. It was observed that knocking out all three copies of *TaBRI1* gene, leads to severe dwarfism, complete infertility (due to the inability to transition into the reproductive phase) and malformed leaves. These observations demonstrated essential roles of *BRI1* in regulating BR-responsive growth and development in wheat as established in other crops (Clouse et al., 1996; Yamamuro et al., 2000). Interestingly, some of the single and double *tabri1* mutants displayed subtle phenotypic differences in some traits, including upright flag leaf angle that could provide avenues for exploitation in wheat breeding. Nevertheless, it was established that a high level of functional redundancy exists amongst the *TaBRI1* homoelogues. As a strategy to overcome the functional redundancy and generate weak *tabri1* alleles that have useful architectural traits, EMS mutagenesis of the *tabri1-bd* double mutant was conducted. This screen led to the identification, of two novel *tabri1-a* missense mutants. Phenotypically, these mutants were less severe compared to *tabri1-a.1bd* mutant and transitioned into the reproductive phase, ultimately producing seeds. Alterations in canopy architecture and stem elongation were also observed in the *tabri1* mutants.

In chapter 4, the role of the *DWF1* and *DWF4* genes in regulating above-ground architecture in wheat was established. The *tadwf1-abd* mutant displayed upright leaf angles, reduced height, a compacted spike, reduced spikelet number and smaller seeds compared to controls. The phenotype of the *tadwf1* mutant was like rice and barley *dwf1* mutants, although some differences did exist (Hong et al., 2005; Dockter et al., 2014). In contrast, the *tadwf4-abd* mutant displayed upright leaf angles and reduced spike length, but no alterations in stem elongation, seed size and weight were observed under glasshouse conditions. Interestingly, the phenotype of *tadwf4-abd* is like the rice *osdwf4-1* mutant and this highlights the potential of DWF4 genes for conferring beneficial architectural traits in cereals;(Sakamoto et al., 2006).

To establish the performance of the *tabri1*, *tadwf1* and *tadwf4* mutants under field conditions (Chapter 5) two independent field trails were conducted. In the first experiment, the agronomic performance of *tabri1*, *tadwf1* and *tadwf4* mutants was

assessed. This established that the architectural phenotypes of the mutants under field conditions was consistent with those observed in the glasshouse. It also identified the *tabri1-a.1b*, *tabri1-a.1d*, *tabri1-bd* and *tadwf4-abd* mutants as displaying upright leaf angles without any negative pleotropic effects on stem elongation, spike, and grain characteristics. In contrast, the *tabri1-a.3bd* and *tadwf1-abd* mutants displayed upright leaf angles, but also exhibited negative effects on other traits such as restricted stem elongation and reduced grain size. We wanted to establish the effect of upright canopy architecture on wheat grain yields under dense planting density but due to disruption caused by COVID-19, we couldn't perform this experiment. In the second trial, phenotypic traits of a representative BR-deficient mutant, *tadwf1-abd* were measured in real time throughout the life cycle using the Rothamsted Field Scanalyzer phenotyping platform. This HTPP analysis established reduced green canopy cover, stem elongation and spike density in *tadwf1-abd* mutant compared to Cadenza.

These studies have generated novel wheat BR mutants that have demonstrated their potential; for improving crop canopy architecture in wheat. The characterisation of these mutants has provided new knowledge about their roles controlling BR-responsive growth in wheat The following sections provide a description of how these resources can be exploited in both wheat breeding and utilised to investigate the molecular mechanisms underlying how BRs control architectural traits.

6.2 Exploitation in breeding pipelines

Grain yield improvements achieved through upright canopy architecture allowing increased planting density to have been reported in maize and rice (Duvik, 2005; Sakamoto et al., 2006). The genetic resources that we have generated which confer an erect architecture can now be exploited to establish whether improvements in grain yields can be achieved in wheat using this strategy. However, to assess this, it will be necessary to introduce these alleles into modern elite varieties. This can be achieved by simple introgression of the alleles, but it would take a considerable number of years before material was available for multi-year/location testing under different planting densities to establish their effect on wheat yields. Using recent advances in genome editing technologies (CRISPR-Cas9), these mutations could be directly introduced in elite wheat cultivars without the requirement for backcrossing, thereby substantially reducing the time taken to generate material for testing (Li et al., 2018).

With recent legislation on 'Genetic Technology (Precision Breeding)' being approved into law on Thursday, 23rd March 2023 (https://www.gov.uk/government/news/genetic-technology-act-key-tool-for-uk food-security), approving commercial application of gene editing technology for crop improvement in the UK is a more feasible and straightforward process.

6.3 Accessing radiation use efficiency (RUE)

Erect leaf architecture near the top of crop canopy enables even light distribution across the different layers and improves grain yields in rice and maize (Pendleton et al., 1968; Lee and Tollenaar, 2007; Yao et al., 2000; Chen et al., 2002; Yuan, 2001). For instance, maize lines containing the *lg2* allele exhibit upright canopy architecture and yielded 40% more grain compared to lines having horizontal canopy architecture (Pendleton et al., 1968). Erect leaf architecture improves leaf area index (LAI), net photosynthesis rate, reduces photoinhibition under light saturation even under lower nitrogen levels (Lee and Tollenaar, 2007; Sinclair and Sheehy, 1999; Tanaka et al., 1968; Murchie et al., 1999; 2009). This phenotype can lead to improvements in grain yields in rice hybrids due to higher net photosynthesis (Zong et al., 2000). Based on these observations, genotypes having an erect leaf angle were proposed as 'ideal ideotype' for breeding high yielding wheat cultivars in CIMMYT (Shearman et al., 2005). Based on this information, we can now establish the effect of upright canopy architecture on radiation use efficiency (RUE) using the wheat BR mutants generated in this study.

6.4 Role of BRs in lamina joint development

The lamina joint is the tissue connecting the leaf blade and sheath which determines the leaf angle formation in cereals such as rice, maize, and wheat. Brassinosteroids are known to have an important role in controlling lamina joint development in cereals, because altering BR levels or sensitivity results in altered leaf angle (Hong et al., 2005; Sakamoto et al., 2006; Zhang et al., 2014). At the cellular level, BRs control cell elongation at the adaxial side of the collar region and sclerenchyma cell proliferation at the abaxial or adaxial side of the LJ (Sun et al., 2015; Zhang et al., 2009; Tian et al., 2019). The upright leaf angles observed in the *tadwf1-abd* and *tadwf4-abd* mutants appears to be caused by restricted cell elongation in the collar

region of the LJ and an increased number of sclerenchyma cell layers in abaxial and adaxial regions of the LJ.

To gain a better understanding of the anatomical changes and underlying transcriptional regulatory networks controlling lamina joint development, the wheat BR mutants that have been generated within this project provide important tools. It will be necessary to conduct an in-depth dissection of anatomical changes occurring during LJ organogenesis and leaf angle formation, combined coupled with spatial mRNA sequencing and hormone analyses. These studies are likely to identify specific regulators enriched in the lamina joint region that directly control leaf erectness. Ultimately, these components could be targeted specifically to alter wheat leaf angle in an organ-specific manner without affecting other agronomic traits such as plant height, tillering and reproductive development which are usually affected in BR-deficient mutants (Morinaka et al., 2006; Hong et al., 2005).

6.5 Potential in abiotic stress tolerance

In plants, BRs are known to regulate growth in response to abiotic stresses including drought, heat and cold (Nolan et al., 2017; Manghwar et al., 2022). For example, overexpression of *BRL3* (*BRI1-like3*) increased drought tolerance in Arabidopsis without pleotropic effects on growth (Fabregas et al., 2018). Similarly, in wheat altering TaBZR2 activity led to changes in drought tolerance sensitivity (Cui et al., 2019). Mechanistically, this effect was mediated through the interaction of TaBZR2 with TaGST1 to induce scavenging of superoxide anions and antioxidant gene expression. This study indicated that increased BR signalling improved drought tolerance in wheat. However, there are conflicting reports demonstrating that reduced BR signalling can confer drought tolerance (Feng et al., 2015; Northey et al., 2016; Nolan et al., 2017). For instance, blockage in CYP85A2 (catalysing last step in BR biosynthesis pathway) led to elevated accumulation of BL (and reduced BR signalling) leading to increased response to ABA causing drought tolerance in Arabidopsis (Northey et al., 2016). Similarly, downregulation of *BdBri1* gene resulted in drought tolerance in *Brachypodium distachyon* (Feng et al., 2015).

In response to heat stress, external BR application leads to increased photosynthetic efficiency in both heat susceptible and resistant cultivars of melon (Zhang et al., 2013). Similarly, higher temperatures led to accumulation of BES1 and BZR1 (TF of

BR signalling) which interact with PIF4 leading to thermogenic growth (Martinez et al., 2018). However, high temperatures led to *BRI1* degradation leading to reduced BR signalling (Martins et al., 2017). In barley, reduced BR signalling has been shown to confer heat tolerance (Sadura et al., 2019). These studies demonstrate that BRs play diverse roles in regulating heat stress tolerance in different plant species (Kagale et al., 2007; J Ahammed et al., 2014).

Like heat stress, cold stress leads to ROS accumulation causing degradation of membranes (Chen et al., 2013). ROS scavenging enzymes are required to avoid photoinhibition. In tomato, BR deficiency leads to cold susceptibility whereas, overexpression of the BR biosynthetic gene (*DWRF*) leads to cold tolerance in tomato (Xia et al., 2018). Similarly, it is also demonstrated that cold stress results in the accumulation of BZR1, leading to elevated *RBOH1* and apoplastic H_2O_2 production which enables photoprotection (Fang et al., 2019).

References

Al-Babili, S. and Bouwmeester, H.J., 2015. Strigolactones, a novel carotenoid-derived plant hormone. *Annual review of plant biology*, *66*, pp.161-186.

Asahina, M., Tamaki, Y., Sakamoto, T., Shibata, K., Nomura, T. and Yokota, T., 2014. Blue light-promoted rice leaf bending and unrolling are due to up-regulated brassinosteroid biosynthesis genes accompanied by accumulation of castasterone. *Phytochemistry*, *104*, pp.21-29.

Asseng, S., Ewert, F., Martre, P., Rötter, R.P., Lobell, D.B., Cammarano, D., Kimball, B.A., Ottman, M.J., Wall, G.W., White, J.W. and Reynolds, M.P., 2015. Rising temperatures reduce global wheat production. *Nature climate change*, *5*(2), pp.143-147.

Attia, K.A., Abdelkhalik, A.F., Ammar, M.H., Wei, C., Yang, J., Lightfoot, D.A., El-Sayed, W.M. and El-Shemy, H.A., 2009. Antisense phenotypes reveal a functional expression of OsARF1, an auxin response factor, in transgenic rice. *Current issues in molecular biology*, *11*(s1), pp.29-34.

Bai, M.Y., Shang, J.X., Oh, E., Fan, M., Bai, Y., Zentella, R., Sun, T.P. and Wang, Z.Y., 2012. Brassinosteroid, gibberellin and phytochrome impinge on a common transcription module in Arabidopsis. *Nature cell biology*, *14*(8), pp.810-817.

Bai, X., Luo, L., Yan, W., Kovi, M.R., Zhan, W. and Xing, Y., 2010. Genetic dissection of rice grain shape using a recombinant inbred line population derived from two contrasting parents and fine mapping a pleiotropic quantitative trait locus qGL7. *BMC genetics*, *11*, pp.1-11.

Bajguz, A. and Hayat, S., 2009. Effects of brassinosteroids on the plant responses to environmental stresses. *Plant physiology and biochemistry*, *47*(1), pp.1-8.

Bajguz, A., Chmur, M. and Gruszka, D., 2020. Comprehensive overview of the brassinosteroid biosynthesis pathways: substrates, products, inhibitors, and connections. *Frontiers in plant science*, *11*, p.1034.

Bao, F., Shen, J., Brady, S.R., Muday, G.K., Asami, T. and Yang, Z., 2004. Brassinosteroids interact with auxin to promote lateral root development in Arabidopsis. *Plant physiology*, *134*(4), pp.1624-1631.

Barkley, N.A. and Wang, M.L., 2008. Application of TILLING and EcoTILLING as reverse genetic approaches to elucidate the function of genes in plants and animals. *Current genomics*, *9*(4), pp.212-226.

Becraft, P.W., Bongard-Pierce, D.K., Sylvester, A.W., Poethig, R.S. and Freeling, M., 1990. The liguleless-1 gene acts tissue specifically in maize leaf development. *Developmental biology*, *141*(1), pp.220-232.

Behrens, T. and Diepenbrock, W., 2006. Using digital image analysis to describe canopies of winter oilseed rape (Brassica napus L.) during vegetative developmental stages. *Journal of Agronomy and Crop Science*, *192*(4), pp.295-302.

Best, N. B., Hartwig, T., Budka, J., Fujioka, S., Johal, G., Schulz, B., and Dilkes, B. P., 2016. nana plant2 encodes a maize ortholog of the Arabidopsis brassinosteroid biosynthesis gene DWARF1, identifying developmental interactions between brassinosteroids and gibberellins. *Plant Physiology*, *171*(4), pp.2633-2647.

Bian, H., Xie, Y., Guo, F., Han, N., Ma, S., Zeng, Z., Wang, J., Yang, Y. and Zhu, M., 2012. Distinctive expression patterns and roles of the miRNA393/TIR1 homolog module in regulating flag leaf inclination and primary and crown root growth in rice (Oryza sativa). *New Phytologist*, *196*(1), pp.149-161.

Bingsong, C., Yunhua, Z., Xia, L. and Demao, J., 2002. Photosynthetic characteristic and assimilate distribution in super hybrid rice Liangyoupeijiu at late growth stage. *Zuo wu xue bao*, *28*(6), pp.777-782.

Bishop, G.J., Nomura, T., Yokota, T., Harrison, K., Noguchi, T., Fujioka, S., Takatsuto, S., Jones, J.D. and Kamiya, Y., 1999. The tomato DWARF enzyme catalyses C-6 oxidation in brassinosteroid biosynthesis. *Proceedings of the National Academy of Sciences*, *96*(4), pp.1761-1766.

Bolger, A.M., Lohse, M. and Usadel, B., 2014. Trimmomatic: a flexible trimmer for Illumina sequence data. *Bioinformatics*, *30*(15), pp.2114-2120.

Borlaug, N. E., 1983. Contributions of conventional plant breeding to food production. *Science*, *219*(4585), pp.689-693.

Bouquin, T., Meier, C., Foster, R., Nielsen, M.E. and Mundy, J., 2001. Control of specific gene expression by gibberellin and brassinosteroid. *Plant Physiology*, *127*(2), pp.450-458.

Caño-Delgado, A., Yin, Y., Yu, C., Vafeados, D., Mora-García, S., Cheng, J.C., Nam, K.H., Li, J. and Chory, J., 2004. BRL1 and BRL3 are novel brassinosteroid receptors that function in vascular differentiation in Arabidopsis. *Development*, *131* (21), pp.5341-5351.

Carland, F., Fujioka, S. and Nelson, T., 2010. The sterol methyltransferases SMT1, SMT2, and SMT3 influence Arabidopsis development through nonbrassinosteroid products. *Plant physiology*, *153*(2), pp.741-756.

Castorina, G., Persico, M., Zilio, M., Sangiorgio, S., Carabelli, L. and Consonni, G., 2018. The maize lilliputian1 (lil1) gene, encoding a brassinosteroid cytochrome P450 C-6 oxidase, is involved in plant growth and drought response. *Annals of botany*, *122*(2), pp.227-238.

Catterou, M., Dubois, F., Schaller, H., Aubanelle, L., Vilcot, B., Sangwan-Norreel, B.S. and Sangwan, R.S., 2001. Brassinosteroids, microtubules and cell elongation in Arabidopsis thaliana. II. Effects of brassinosteroids on microtubules and cell elongation in the bul1 mutant. *Planta*, *212*, pp.673-683.

Cecchetti, V., Altamura, M.M., Falasca, G., Costantino, P. and Cardarelli, M., 2008. Auxin regulates Arabidopsis anther dehiscence, pollen maturation, and filament elongation. *The Plant Cell*, *20*(7), pp.1760-1774.

Chen, S., Jin, W., Liu, A., Zhang, S., Liu, D., Wang, F., Lin, X. and He, C., 2013. Arbuscular mycorrhizal fungi (AMF) increase growth and secondary metabolism in cucumber subjected to low temperature stress. *Scientia Horticulturae*, *160*, pp.222-229.

Cheng, X., Gou, X., Yin, H., Mysore, K.S., Li, J. and Wen, J., 2017. Functional characterisation of brassinosteroid receptor MtBRI1 in Medicago truncatula. *Scientific Reports*, *7*(1), p.9327.

Choe, S., Dilkes, B.P., Fujioka, S., Takatsuto, S., Sakurai, A. and Feldmann, K.A., 1998. The DWF4 gene of Arabidopsis encodes a cytochrome P450 that mediates multiple 22α-hydroxylation steps in brassinosteroid biosynthesis. *The Plant Cell*, *10*(2), pp.231-243.

Choe, S., Dilkes, B.P., Gregory, B.D., Ross, A.S., Yuan, H., Noguchi, T., Fujioka, S., Takatsuto, S., Tanaka, A., Yoshida, S. and Tax, F.E., 1999. The Arabidopsis dwarf1 mutant is defective in the conversion of 24-methylenecholesterol to campesterol in brassinosteroid biosynthesis. *Plant physiology*, *119*(3), pp.897-908.

Choe, S., Fujioka, S., Noguchi, T., Takatsuto, S., Yoshida, S. and Feldmann, K.A., 2001. Overexpression of DWARF4 in the brassinosteroid biosynthetic pathway results in increased vegetative growth and seed yield in Arabidopsis. *The Plant Journal*, *26*(6), pp.573-582.

Choe, S., Schmitz, R.J., Fujioka, S., Takatsuto, S., Lee, M.O., Yoshida, S., Feldmann, K.A. and Tax, F.E., 2002. Arabidopsis brassinosteroid-insensitive dwarf12 mutants are semidominant and defective in a glycogen synthase kinase 3β-like kinase. *Plant physiology*, *130*(3), pp.1506-1515.

Choe, S., Tanaka, A., Noguchi, T., Fujioka, S., Takatsuto, S., Ross, A.S., Tax, F.E., Yoshida, S. and Feldmann, K.A., 2000. Lesions in the sterol Δ7 reductase gene of Arabidopsis cause dwarfism due to a block in brassinosteroid biosynthesis. *The Plant Journal*, *21*(5), pp.431-443.

Choi, S., Cho, Y.H., Kim, K., Matsui, M., Son, S.H., Kim, S.K., Fujioka, S. and Hwang, I., 2013. BAT 1, a putative acyltransferase, modulates brassinosteroid levels in A rabidopsis. *The Plant Journal*, *73*(3), pp.380-391.

Choi, Y.H., Fujioka, S., Harada, A., Yokota, T., Takatsuto, S. and Sakurai, A., 1996. A brassinolide biosynthetic pathway via 6-deoxocastasterone. *Phytochemistry*, *43*(3), pp.593-596.

Chono, M., Honda, I., Zeniya, H., Yoneyama, K., Saisho, D., Takeda, K., Takatsuto, S., Hoshino, T. and Watanabe, Y., 2003. A semidwarf phenotype of barley uzu results from a nucleotide substitution in the gene encoding a putative brassinosteroid receptor. *Plant physiology*, *133*(3), pp.1209-1219.

Chory, J., Nagpal, P. and Peto, C.A., 1991. Phenotypic and genetic analysis of det2, a new mutant that affects light-regulated seedling development in Arabidopsis. *The Plant Cell*, *3*(5), pp.445-459.

Choudhury, B.J., 2000. A sensitivity analysis of the radiation use efficiency for gross photosynthesis and net carbon accumulation by wheat. *Agricultural and Forest Meteorology*, *101*(2-3), pp.217-234.

Chung, Y. and Choe, S., 2013. The regulation of brassinosteroid biosynthesis in Arabidopsis. *Critical reviews in plant sciences*, *32*(6), pp.396-410.

Clavijo, B.J., Venturini, L., Schudoma, C., Accinelli, G.G., Kaithakottil, G., Wright, J., Borrill, P., Kettleborough, G., Heavens, D., Chapman, H. and Lipscombe, J., 2017. An improved assembly and annotation of the allohexaploid wheat genome identifies complete families of agronomic genes and provides genomic evidence for chromosomal translocations. *Genome research*, *27*(5), pp.885-896.

Clouse, S.D. and Sasse, J.M., 1998. Brassinosteroids: essential regulators of plant growth and development. *Annual review of plant biology*, *49*(1), pp.427-451.

Clouse, S.D., 2008. The molecular intersection of brassinosteroid-regulated growth and flowering in Arabidopsis. *Proceedings of the National Academy of Sciences*, *105*(21), pp.7345-7346.

Clouse, S.D., 2011. Brassinosteroid signal transduction: from receptor kinase activation to transcriptional networks regulating plant development. *The Plant Cell*, *23*(4), pp.1219-1230.

Clouse, S.D., Langford, M. and McMorris, T.C., 1996. A brassinosteroid-insensitive mutant in Arabidopsis thaliana exhibits multiple defects in growth and development. *Plant physiology*, *111*(3), pp.671-678.

Cui, X.Y., Gao, Y., Guo, J., Yu, T.F., Zheng, W.J., Liu, Y.W., Chen, J., Xu, Z.S. and Ma, Y.Z., 2019. BES/BZR transcription factor TaBZR2 positively regulates drought responses by activation of TaGST1. *Plant physiology*, *180*(1), pp.605-620.

Cutler, H.G., Yokota, T. and Adam, G. eds., 1991. *Brassinosteroids: chemistry, bioactivity, and applications*. American Chemical Society.

Diener, A.C., Li, H., Zhou, W.X., Whoriskey, W.J., Nes, W.D. and Fink, G.R., 2000. Sterol methyltransferase 1 controls the level of cholesterol in plants. *The Plant Cell*, *12*(6), pp.853-870.

Divi, U.K. and Krishna, P., 2009. Brassinosteroid: a biotechnological target for enhancing crop yield and stress tolerance. *New biotechnology*, *26*(3-4), pp.131-136.

Dobin, A., Davis, C.A., Schlesinger, F., Drenkow, J., Zaleski, C., Jha, S., Batut, P., Chaisson, M. and Gingeras, T.R., 2013. STAR: ultrafast universal RNA-seq aligner. *Bioinformatics*, *29*(1), pp.15-21.

Dockter, C., Gruszka, D., Braumann, I., Druka, A., Druka, I., Franckowiak, J., Gough, S.P., Janeczko, A., Kurowska, M., Lundqvist, J. and Lundqvist, U., 2014. Induced variations in brassinosteroid genes define barley height and sturdiness, and expand the green revolution genetic toolkit. *Plant Physiology*, *166*(4), pp.1912-1927.

Domagalska, M.A., Sarnowska, E., Nagy, F. and Davis, S.J., 2010. Genetic analyses of interactions among gibberellin, abscisic acid, and brassinosteroids in the control of flowering time in Arabidopsis thaliana. *PloS one*, *5*(11), p.e14012.

Dong, J., Kim, S.T. and Lord, E.M., 2005. Plantacyanin plays a role in reproduction in Arabidopsis. *Plant physiology*, *138*(2), pp.778-789.

Du, H., Wu, N., Fu, J., Wang, S., Li, X., Xiao, J. and Xiong, L., 2012. A GH3 family member, OsGH3-2, modulates auxin and abscisic acid levels and differentially affects drought and cold tolerance in rice. *Journal of experimental botany*, *63*(18), pp.6467-6480.

Dubcovsky, J., and Dvorak, J., 2007. Genome plasticity a key factor in the success of polyploid wheat under domestication. *Science*, *316*(5833), pp.1862-1866.

Duvick, D.N., 2005. The contribution of breeding to yield advances in maize (Zea mays L.). *Advances in agronomy*, *86*, pp.83-145.

Duvick, D.N., Smith, J.S.C., Cooper, M. and Janick, J., 2004. Plant Breeding Reviews Part 2 Long Term Selection: Crops, Animals and Bacteria.

Evenson, R. E., and Rosegrant, M., 2003. The economic consequences 23 of crop genetic improvement programmes. *Crop variety improvement and its effect on productivity: The impact of international agricultural research*, pp.473-497.

Ewing, R.P. and Horton, R., 1999. Quantitative color image analysis of agronomic images. *Agronomy Journal*, *91*(1), pp.148-153.

Fàbregas, N., Lozano-Elena, F., Blasco-Escámez, D., Tohge, T., Martínez-Andújar, C., Albacete, A., Osorio, S., Bustamante, M., Riechmann, J.L., Nomura, T. and Yokota, T., 2018. Overexpression of the vascular brassinosteroid receptor BRL3 confers drought resistance without penalizing plant growth. *Nature communications*, *9*(1), p.4680.

Fang, N., Xu, R., Huang, L., Zhang, B., Duan, P., Li, N., Luo, Y. and Li, Y., 2016. SMALL GRAIN 11 controls grain size, grain number and grain yield in rice. *Rice*, *9*, pp.1-11.

Fang, P., Yan, M., Chi, C., Wang, M., Zhou, Y., Zhou, J., Shi, K., Xia, X., Foyer, C.H. and Yu, J., 2019. Brassinosteroids act as a positive regulator of photoprotection in response to chilling stress. *Plant physiology*, *180*(4), pp.2061-2076.

Fang, Z., Ji, Y., Hu, J., Guo, R., Sun, S. and Wang, X., 2020. Strigolactones and brassinosteroids antagonistically regulate the stability of the D53–OsBZR1 complex to determine FC1 expression in rice tillering. *Molecular plant*, *13*(4), pp.586-597.

Feldman, M., 2001. Origin of cultivated wheat. *The world wheat book: a history of wheat breeding*, pp.3-53.

Feldman, M., Lupton, F. G. H., and Miller, T. E. 1995. Wheats, pp. 184–192 in *Evolution of Crop Plants*, Ed. 2nd, edited by J. Smartt, NW Simmonds.

Feng, Y., Yin, Y. and Fei, S., 2015. Down-regulation of BdBRI1, a putative brassinosteroid receptor gene produces a dwarf phenotype with enhanced drought tolerance in Brachypodium distachyon. *Plant Science*, *234*, pp.163-173.

Feng, Z., Wu, C., Wang, C., Roh, J., Zhang, L., Chen, J., Zhang, S., Zhang, H., Yang, C., Hu, J. and You, X., 2016. SLG controls grain size and leaf angle by modulating brassinosteroid homeostasis in rice. *Journal of Experimental Botany*, *67*(14), pp.4241-4253.

Fischer, R.A. and Edmeades, G.O., 2010. Breeding and cereal yield progress. Crop Sei 50: S85–S98.

Friedrichsen, D. and Chory, J., 2001. Steroid signaling in plants: from the cell surface to the nucleus. *Bioessays*, *23*(11), pp.1028-1036.

Fujioka, S., and Yokota, T., 2003. Biosynthesis and metabolism of brassinosteroids. *Annual review of plant biology*, *54*(1), pp.137-164.

Fujioka, S., Li, J., Choi, Y.H., Seto, H., Takatsuto, S., Noguchi, T., Watanabe, T., Kuriyama, H., Yokota, T., Chory, J. and Sakurai, A., 1997. The Arabidopsis deetiolated2 mutant is blocked early in brassinosteroid biosynthesis. *The Plant Cell*, *9*(11), pp.1951-1962.

Fujioka, S., Noguchi, T., Watanabe, T., Takatsuto, S. and Yoshida, S., 2000. Biosynthesis of brassinosteroids in cultured cells of Catharanthus roseus. *Phytochemistry*, *53*(5), pp.549-553.

Fujioka, S., Takatsuto, S. and Yoshida, S., 2002. An early C-22 oxidation branch in the brassinosteroid biosynthetic pathway. *Plant Physiology*, *130*(2), pp.930-939.

Fujita, S., Ohnishi, T., Watanabe, B., Yokota, T., Takatsuto, S., Fujioka, S., Yoshida, S., Sakata, K. and Mizutani, M., 2006. Arabidopsis CYP90B1 catalyses the early C-22 hydroxylation of C27, C28 and C29 sterols. *The Plant Journal*, *45*(5), pp.765-774.

Gallego-Bartolomé, J., Minguet, E.G., Grau-Enguix, F., Abbas, M., Locascio, A., Thomas, S.G., Alabadí, D. and Blázquez, M.A., 2012. Molecular mechanism for the interaction between gibberellin and brassinosteroid signaling pathways in Arabidopsis. *Proceedings of the National Academy of Sciences*, *109*(33), pp.13446-13451.

Gan, L., Wu, H., Wu, D., Zhang, Z., Guo, Z., Yang, N., Xia, K., Zhou, X., Oh, K., Matsuoka, M. and Ng, D., 2015. Methyl jasmonate inhibits lamina joint inclination by repressing brassinosteroid biosynthesis and signaling in rice. *Plant Science*, *241*, pp.238-245.

Gan, S., Rozhon, W., Varga, E., Unterholzner, S.J., Berthiller, F. and Poppenberger, B., 2020. The BAHD acyltransferase BIA1 uses acetyl-CoA for catabolic inactivation of brassinosteroids. *Plant physiology*, *184*(1), p.23.

Gasperini, D., Greenland, A., Hedden, P., Dreos, R., Harwood, W. and Griffiths, S., 2012. Genetic and physiological analysis of Rht8 in bread wheat: an alternative source of semi-dwarfism with a reduced sensitivity to brassinosteroids. *Journal of experimental botany*, *63*(12), p.4419.

Gilchrist, E.J. and Haughn, G.W., 2005. TILLING without a plough: a new method with applications for reverse genetics. *Current opinion in plant biology*, *8*(2), pp.211-215.

Gou, X., Yin, H., He, K., Du, J., Yi, J., Xu, S., Lin, H., Clouse, S.D. and Li, J., 2012. Genetic evidence for an indispensable role of somatic embryogenesis receptor kinases in brassinosteroid signaling. *PLoS genetics*, *8*(1), p.e1002452.

Grove, M. D., Spencer, G. F., Rohwedder, W. K., Mandava, N., Worley, J. F., Warthen, J. D., ... and Cook, J. C., 1979. Brassinolide, a plant growth-promoting steroid isolated from Brassica napus pollen. *Nature*, *281*(5728), pp.216-217.

Gruszka, D., Szarejko, I. and Maluszynski, M., 2011. New allele of HvBRI1 gene encoding brassinosteroid receptor in barley. *Journal of applied genetics*, *52*, pp.257-268.

Guo, J., Li, W., Shang, L., Wang, Y., Yan, P., Bai, Y., Da, X., Wang, K., Guo, Q., Jiang, R. and Mao, C., 2021. OsbHLH98 regulates leaf angle in rice through transcriptional repression of OsBUL1. *New Phytologist*, *230*(5), pp.1953-1966.

Hayat, S., Hasan, S.A., Yusuf, M., Hayat, Q. and Ahmad, A., 2010. Effect of 28-homobrassinolide on photosynthesis, fluorescence and antioxidant system in the presence or absence of salinity and temperature in Vigna radiata. *Environmental and Experimental Botany*, *69*(2), pp.105-112.

He, J.X., Gendron, J.M., Sun, Y., Gampala, S.S., Gendron, N., Sun, C.Q. and Wang, Z.Y., 2005. BZR1 is a transcriptional repressor with dual roles in brassinosteroid homeostasis and growth responses. *Science*, *307*(5715), pp.1634-1638.

He, J.X., Gendron, J.M., Yang, Y., Li, J. and Wang, Z.Y., 2002. The GSK3-like kinase BIN2 phosphorylates and destabilizes BZR1, a positive regulator of the brassinosteroid signaling pathway in Arabidopsis. *Proceedings of the National Academy of Sciences*, *99*(15), pp.10185-10190.

He, Z., Wang, Z.Y., Li, J., Zhu, Q., Lamb, C., Ronald, P. and Chory, J., 2000. Perception of brassinosteroids by the extracellular domain of the receptor kinase BRI1. *Science*, *288*(5475), pp.2360-2363.

Hedden, P., 2003. The genes of the Green Revolution. *TRENDS in Genetics*, *19*(1), pp.5-9.

Honda, I., Zeniya, H., Yoneyama, K., Chono, M., Kaneko, S. and Watanabe, Y., 2003. Uzu mutation in barley (Hordeum vulgare L.) reduces the leaf unrolling response to brassinolide. *Bioscience, biotechnology, and biochemistry*, *67*(5), pp.1194-1197.

Hong, Z., Ueguchi-Tanaka, M., Fujioka, S., Takatsuto, S., Yoshida, S., Hasegawa, Y., Ashikari, M., Kitano, H. and Matsuoka, M., 2005. The rice brassinosteroid-deficient dwarf2 mutant, defective in the rice homolog of Arabidopsis DIMINUTO/DWARF1, is rescued by the endogenously accumulated alternative bioactive brassinosteroid, dolichosterone. *The Plant Cell*, *17*(8), pp.2243-2254.

Hong, Z., Ueguchi-Tanaka, M., Shimizu-Sato, S., Inukai, Y., Fujioka, S., Shimada, Y., Takatsuto, S., Agetsuma, M., Yoshida, S., Watanabe, Y. and Uozu, S., 2002. Loss-of-function of a rice brassinosteroid biosynthetic enzyme, C-6 oxidase, prevents the organized arrangement and polar elongation of cells in the leaves and stem. *The Plant Journal*, *32*(4), pp.495-508.

Hong, Z., Ueguchi-Tanaka, M., Umemura, K., Uozu, S., Fujioka, S., Takatsuto, S., Yoshida, S., Ashikari, M., Kitano, H. and Matsuoka, M., 2003. A rice brassinosteroid-deficient mutant, ebisu dwarf (d2), is caused by a loss of function

Hothorn, M., Belkhadir, Y., Dreux, M., Dabi, T., Noel, J.P., Wilson, I.A. and Chory, J., 2011. Structural basis of steroid hormone perception by the receptor kinase BRI1. *Nature*, *474*(7352), pp.467-471.

Hu, X., Qian, Q., Xu, T., Zhang, Y.E., Dong, G., Gao, T., Xie, Q. and Xue, Y., 2013. The U-box E3 ubiquitin ligase TUD1 functions with a heterotrimeric G α subunit to regulate brassinosteroid-mediated growth in rice. *PLoS Genetics*, *9*(3), p.e1003391.

Huang, S., Cerny, R.E., Qi, Y., Bhat, D., Aydt, C.M., Hanson, D.D., Malloy, K.P. and Ness, L.A., 2003. Transgenic studies on the involvement of cytokinin and gibberellin in male development. *Plant Physiology*, *131*(3), pp.1270-1282.

J Ahammed, G., Xia, X.J., Li, X., Shi, K., Yu, J.Q. and Zhou, Y.H., 2015. Role of brassinosteroid in plant adaptation to abiotic stresses and its interplay with other hormones. *Current protein and peptide science*, *16*(5), pp.462-473.

Jaillais, Y., Hothorn, M., Belkhadir, Y., Dabi, T., Nimchuk, Z. L., Meyerowitz, E. M., and Chory, J., 2011. Tyrosine phosphorylation controls brassinosteroid receptor activation by triggering membrane release of its kinase inhibitor. *Genes and development*, *25*(3), pp.232-237.

Janeczko, A. and Swaczynová, J., 2010. Endogenous brassinosteroids in wheat treated with 24-epibrassinolide. *Biologia plantarum*, *54*, pp.477-482.

Jang, J.C., Fujioka, S., Tasaka, M., Seto, H., Takatsuto, S., Ishii, A., Aida, M., Yoshida, S. and Sheen, J., 2000. A critical role of sterols in embryonic patterning and meristem programming revealed by the fackel mutants of Arabidopsis thaliana. *Genes & development*, *14*(12), pp.1485-1497.

Jang, S., Cho, J.Y., Do, G.R., Kang, Y., Li, H.Y., Song, J., Kim, H.Y., Kim, B.G. and Hsing, Y.I., 2021. Modulation of Rice Leaf Angle and Grain Size by Expressing OsBCL1 and OsBCL2 under the Control of OsBUL1 Promoter. *International Journal of Molecular Sciences*, *22*(15), p.7792

Jiang, W.B. and Lin, W.H., 2013. Brassinosteroid functions in Arabidopsis seed development. *Plant signaling and behavior*, *8*(10), p.e25928.

Jing, Z. and Wanxia, Z., 2003. Tracing sources of dwarfing genes in barley breeding in China. *Euphytica*, *131*(3), pp.285-293.

Kagale, S., Divi, U.K., Krochko, J.E., Keller, W.A. and Krishna, P., 2007. Brassinosteroid confers tolerance in Arabidopsis thaliana and Brassica napus to a range of abiotic stresses. *Planta*, *225*, pp.353-364.

Kalb VF, Loper JC. Proteins from eight eukaryotic cytochrome P-450 families share a segmented region of sequence similarity. Proceedings of the National Academy of Sciences. 1988 Oct;85(19):7221-5.

Kauschmann, A., Jessop, A., Koncz, C., Szekeres, M., Willmitzer, L. and Altmann, T., 1996. Genetic evidence for an essential role of brassinosteroids in plant development. *The Plant Journal*, *9*(5), pp.701-713.

Khripach, V., Zhabinskii, V. and de Groot, A., 2000. Twenty years of brassinosteroids: steroidal plant hormones warrant better crops for the XXI century. *Annals of botany*, *86*(3), pp.441-447.

Khush, G. S., 2001. Green revolution: the way forward. *Nature reviews genetics*, *2*(10), pp.815.

Khush, G.S., 1993. Breeding rice for sustainable agricultural systems. *International Crop Science I*, pp.189-199.

Kieber, J.J., Rothenberg, M., Roman, G., Feldmann, K.A. and Ecker, J.R., 1993. CTR1, a negative regulator of the ethylene response pathway in Arabidopsis, encodes a member of the raf family of protein kinases. *Cell*, *72*(3), pp.427-441.

Kim, B.K., Fujioka, S., Takatsuto, S., Tsujimoto, M. and Choe, S., 2008. Castasterone is a likely end product of brassinosteroid biosynthetic pathway in rice. *Biochemical and biophysical research communications*, *374*(4), pp.614-619.

Kim, G.T., Fujioka, S., Kozuka, T., Tax, F.E., Takatsuto, S., Yoshida, S. and Tsukaya, H., 2005. CYP90C1 and CYP90D1 are involved in different steps in the brassinosteroid biosynthesis pathway in Arabidopsis thaliana. *The Plant Journal*, *41*(5), pp.710-721.

Kim, H.B., Kwon, M., Ryu, H., Fujioka, S., Takatsuto, S., Yoshida, S., An, C.S., Lee, I., Hwang, I. and Choe, S., 2006. The regulation of DWARF4 expression is likely a critical mechanism in maintaining the homeostasis of bioactive brassinosteroids in Arabidopsis. *Plant physiology*, *140*(2), pp.548-557.

Kim, S., Moon, J., Roh, J. and Kim, S.K., 2018. Castasterone can be biosynthesized from 28-homodolichosterone in Arabidopsis thaliana. *Journal of plant biology*, *61*, pp.330-335.

Kim, T.W. and Wang, Z.Y., 2010. Brassinosteroid signal transduction from receptor kinases to transcription factors. *Annual review of plant biology*, *61*, pp.681-704.

Kim, T.W., Guan, S., Burlingame, A.L. and Wang, Z.Y., 2011. The CDG1 kinase mediates brassinosteroid signal transduction from BRI1 receptor kinase to BSU1 phosphatase and GSK3-like kinase BIN2. *Molecular cell*, *43*(4), pp.561-571.

King, R., Bird, N., Ramirez-Gonzalez, R., Coghill, J.A., Patil, A., Hassani-Pak, K., Uauy, C. and Phillips, A.L., 2015. Mutation scanning in wheat by exon capture and next-generation sequencing. *PLoS One*, *10*(9), p.e0137549.

Kinoshita, T., Caño-Delgado, A., Seto, H., Hiranuma, S., Fujioka, S., Yoshida, S. and Chory, J., 2005. Binding of brassinosteroids to the extracellular domain of plant receptor kinase BRI1. *Nature*, *433*(7022), pp.167-171.

Kir, G., Ye, H., Nelissen, H., Neelakandan, A.K., Kusnandar, A.S., Luo, A., Inzé, D., Sylvester, A.W., Yin, Y. and Becraft, P.W., 2015. RNA interference knockdown of BRASSINOSTEROID INSENSITIVE1 in maize reveals novel functions for brassinosteroid signaling in controlling plant architecture. *Plant Physiology*, *169*(1), pp.826-839.

Klahre, U., Noguchi, T., Fujioka, S., Takatsuto, S., Yokota, T., Nomura, T., Yoshida, S. and Chua, N.H., 1998. The Arabidopsis DIMINUTO/DWARF1 gene encodes a protein involved in steroid synthesis. *The Plant Cell*, *10*(10), pp.1677-1690.

Koka, C.V., Cerny, R.E., Gardner, R.G., Noguchi, T., Fujioka, S., Takatsuto, S., Yoshida, S. and Clouse, S.D., 2000. A putative role for the tomato genes DUMPY and CURL-3 in brassinosteroid biosynthesis and response. *Plant physiology*, *122*(1), pp.85-98.

Kondo, Y., Ito, T., Nakagami, H., Hirakawa, Y., Saito, M., Tamaki, T., Shirasu, K. and Fukuda, H., 2014. Plant GSK3 proteins regulate xylem cell differentiation downstream of TDIF–TDR signalling. *Nature communications*, *5*(1), p.3504.

Kowalski, A.M., Gooding, M., Ferrante, A., Slafer, G.A., Orford, S., Gasperini, D. and Griffiths, S., 2016. Agronomic assessment of the wheat semi-dwarfing gene Rht8 in contrasting nitrogen treatments and water regimes. *Field crops research*, *191*, pp.150-160.

Krasileva, K.V., Vasquez-Gross, H.A., Howell, T., Bailey, P., Paraiso, F., Clissold, L., Simmonds, J., Ramirez-Gonzalez, R.H., Wang, X., Borrill, P. and Fosker, C.,

2017. Uncovering hidden variation in polyploid wheat. *Proceedings of the National Academy of Sciences*, *114*(6), pp.E913-E921.

Krishna, P., 2003. Brassinosteroid-mediated stress responses. *Journal of Plant Growth Regulation*, *22*, pp.289-297.

Kumagai, E., Hamaoka, N., Araki, T. and Ueno, O., 2014. Dorsoventral asymmetry of photosynthesis and photoinhibition in flag leaves of two rice cultivars that differ in nitrogen response and leaf angle. *Physiologia plantarum*, *151*(4), pp.533-543.

Kurowska, M., Daszkowska-Golec, A., Gruszka, D., Marzec, M., Szurman, M., Szarejko, I. and Maluszynski, M., 2011. TILLING-a shortcut in functional genomics. *Journal of applied genetics*, *52*, pp.371-390.

Kwon, M., Fujioka, S., Jeon, J.H., Kim, H.B., Takatsuto, S., Yoshida, S., An, C.S. and Choe, S., 2005. A double mutant for the CYP85A1 and CYP85A2 genes of Arabidopsis exhibits a brassinosteroid dwarf phenotype. *Journal of Plant Biology*, *48*, pp.237-244.

Lambert, R.J. and Johnson, R.R., 1978. Leaf angle, tassel morphology, and the performance of maize hybrids 1. *Crop Science*, *18*(3), pp.499-502.

Lauer, S., Hall, B.D., Mulaosmanovic, E., Anderson, S.R., Nelson, B. and Smith, S., 2012. Morphological changes in parental lines of pioneer brand maize hybrids in the US central corn belt. *Crop Science*, *52*(3), pp.1033-1043.

Law, C. N., Snape, J. W., and Worland, A. J., 1978. The genetical relationship between height and yield in wheat. *Heredity*, *40*(1), pp.133.

Lee, E.A. and Tollenaar, M., 2007. Physiological basis of successful breeding strategies for maize grain yield. *Crop Science*, *47*, pp.S-202.

Li, H.Y., Wang, H.M. and Jang, S., 2017. Rice lamina joint inclination assay. *Bio-protocol*, *7*(14), pp.e2409-e2409.

Li, J. and Chory, J., 1997. A putative leucine-rich repeat receptor kinase involved in brassinosteroid signal transduction. *Cell*, *90*(5), pp.929-938.

Li, J. and Jin, H., 2007. Regulation of brassinosteroid signaling. *Trends in plant science*, *12*(1), pp.37-41.

Li, J., Nagpal, P., Vitart, V., McMorris, T.C. and Chory, J., 1996. A role for brassinosteroids in light-dependent development of Arabidopsis. *Science*, *272*(5260), pp.398-401.

Li, J., Nam, K.H., Vafeados, D. and Chory, J., 2001. BIN2, a new brassinosteroid-insensitive locus in Arabidopsis. *Plant physiology*, *127*(1), pp.14-22.

Li, Q.F., Yu, J.W., Lu, J., Fei, H.Y., Luo, M., Cao, B.W., Huang, L.C., Zhang, C.Q. and Liu, Q.Q., 2018. Seed-specific expression of OsDWF4, a rate-limiting gene involved in brassinosteroids biosynthesis, improves both grain yield and quality in rice. *Journal of agricultural and food chemistry*, *66*(15), pp.3759-3772.

Li, X., Sun, S., Li, C., Qiao, S., Wang, T., Leng, L., Shen, H. and Wang, X., 2014. The Strigolactone-related mutants have enhanced lamina joint inclination phenotype at the seedling stage. *Journal of genetics and genomics= Yi chuan xue bao*, *41*(11), pp.605-608.

Li, X., Zhang, X., Liu, G., Tang, Y., Zhou, C., Zhang, L. and Lv, J., 2020. The spike plays important roles in the drought tolerance as compared to the flag leaf through the phenylpropanoid pathway in wheat. *Plant physiology and biochemistry*, *152*, pp.100-111.

Lichtenthaler, H.K., 2000. Non-mevalonate isoprenoid biosynthesis: enzymes, genes and inhibitors. *Biochemical Society Transactions*, *28*(6), pp.785-789.

Liu, K., Cao, J., Yu, K., Liu, X., Gao, Y., Chen, Q., Zhang, W., Peng, H., Du, J., Xin, M. and Hu, Z., 2019. Wheat TaSPL8 modulates leaf angle through auxin and brassinosteroid signaling. *Plant Physiology*, *181*(1), pp.179-194.

Liu, N., Zhao, Y.J., Wu, J.W., Wei, Y.M., Ren, R.C., Zang, J., Zhang, W.T., Zhang, L., Shen, Q., Zhang, X.S. and Zhao, X.Y., 2020. Overexpression of ZmDWF4 improves major agronomic traits and enhances yield in maize. *Molecular Breeding*, *40*, pp.1-12.

Liu, T., Zhang, J., Wang, M., Wang, Z., Li, G., Qu, L. and Wang, G., 2007. Expression and functional analysis of ZmDWF4, an ortholog of Arabidopsis DWF4 from maize (Zea mays L.). *Plant cell reports*, *26*, pp.2091-2099.

Liu, X., Yang, C.Y., Miao, R., Zhou, C.L., Cao, P.H., Lan, J., Zhu, X.J., Mou, C.L., Huang, Y.S., Liu, S.J. and Tian, Y.L., 2018. DS1/OsEMF1 interacts with OsARF11 to control rice architecture by regulation of brassinosteroid signaling. *Rice*, *11*, pp.1-12.

Love, M.I., Huber, W. and Anders, S., 2014. Moderated estimation of fold change and dispersion for RNA-seq data with DESeq2. *Genome biology*, *15*(12), pp.1-21.

Lyra, D.H., Griffiths, C.A., Watson, A., Joynson, R., Molero, G., Igna, A.A., Hassani-Pak, K., Reynolds, M.P., Hall, A. and Paul, M.J., 2021. Gene-based mapping of trehalose biosynthetic pathway genes reveals association with source-and sink-related yield traits in a spring wheat panel. *Food and Energy Security*, *10*(3), p.e292.

Ma, D.L., Xie, R.Z., Niu, X.K., Li, S.K., Long, H.L. and Liu, Y.E., 2014. Changes in the morphological traits of maize genotypes in China between the 1950s and 2000s. *European Journal of Agronomy*, *58*, pp.1-10.

Manghwar, H., Hussain, A., Ali, Q. and Liu, F., 2022. Brassinosteroids (BRs) role in plant development and coping with different stresses. *International Journal of Molecular Sciences*, *23*(3), p.1012.

Marsolais, F., Boyd, J., Paredes, Y., Schinas, A.M., Garcia, M., Elzein, S. and Varin, L., 2007. Molecular and biochemical characterization of two brassinosteroid sulfotransferases from Arabidopsis, AtST4a (At2g14920) and AtST1 (At2g03760). *Planta*, *225*, pp.1233-1244.

Martínez, C., Espinosa-Ruíz, A., de Lucas, M., Bernardo-García, S., Franco-Zorrilla, J.M. and Prat, S., 2018. PIF 4-induced BR synthesis is critical to diurnal and thermomorphogenic growth. *The EMBO Journal*, *37*(23), p.e99552.

Martínez, C., Espinosa-Ruíz, A., de Lucas, M., Bernardo-García, S., Franco-Zorrilla, J.M. and Prat, S., 2018. PIF 4-induced BR synthesis is critical to diurnal and thermomorphogenic growth. *The EMBO Journal*, *37*(23), p.e99552.

Martins, S., Montiel-Jorda, A., Cayrel, A., Huguet, S., Roux, C.P.L., Ljung, K. and Vert, G., 2017. Brassinosteroid signaling-dependent root responses to prolonged elevated ambient temperature. *Nature communications*, *8*(1), p.309.

Mathur, J., Molnár, G., Fujioka, S., Takatsuto, S., Sakurai, A., Yokota, T., Adam, G., Voigt, B., Nagy, F., Maas, C. and Schell, J., 1998. Transcription of the Arabidopsis CPD gene, encoding a steroidogenic cytochrome P450, is negatively controlled by brassinosteroids. *The Plant Journal*, *14*(5), pp.593-602.

Méchin, V., Argillier, O., Rocher, F., Hébert, Y., Mila, I., Pollet, B., Barriére, Y. and Lapierre, C., 2005. In search of a maize ideotype for cell wall enzymatic degradability using histological and biochemical lignin characterization. *Journal of Agricultural and Food Chemistry*, *53*(15), pp.5872-5881.

Milner, M.J., Swarbreck, S.M., Craze, M., Bowden, S., Griffiths, H., Bentley, A.R. and Wallington, E.J., 2022. Over-expression of TaDWF4 increases wheat productivity under low and sufficient nitrogen through enhanced carbon assimilation. *Communications Biology*, *5*(1), p.193.

Miralles, D.J., Calderini, D.F., Pomar, K.P. and D'ambrogio, A., 1998. Dwarfing genes and cell dimensions in different organs of wheat. *Journal of Experimental Botany*, *49*(324), pp.1119-1127.

Mitchell, J. W., Mandava, N., Worley, J. F., Plimmer, J. R., and Smith, M. V., 1970. Brassins—a new family of plant hormones from rape pollen. *Nature*, *225*(5237), pp.1065-1066.

Miyake, K., and Imai, Y., 1922. Genetic studies in barley. I. *Bot. Mag. Tokyo*, *36*, pp.25-38.

Mo, Y., Howell, T., Vasquez-Gross, H., De Haro, L.A., Dubcovsky, J. and Pearce, S., 2018. Mapping causal mutations by exome sequencing in a wheat TILLING population: a tall mutant case study. *Molecular Genetics and Genomics*, *293*, pp.463-477.

Montoya, T., Nomura, T., Farrar, K., Kaneta, T., Yokota, T. and Bishop, G.J., 2002. Cloning the tomato curl3 gene highlights the putative dual role of the leucine-rich repeat receptor kinase tBRI1/SR160 in plant steroid hormone and peptide hormone signaling. *The Plant Cell*, *14*(12), pp.3163-3176.

Morinaka, Y., Sakamoto, T., Inukai, Y., Agetsuma, M., Kitano, H., Ashikari, M. and Matsuoka, M., 2006. Morphological alteration caused by brassinosteroid

insensitivity increases the biomass and grain production of rice. *Plant physiology*, *141*(3), pp.924-931.

Murchie, E.H., Chen, Y.Z., Hubbart, S., Peng, S. and Horton, P., 1999. Interactions between senescence and leaf orientation determine in situ patterns of photosynthesis and photoinhibition in field-grown rice. *Plant physiology*, *119*(2), pp.553-564.

Murchie, E.H., Pinto, M. and Horton, P., 2009. Agriculture and the new challenges for photosynthesis research. *New Phytologist*, *181*(3), pp.532-552.

Nakamura, A., Nakajima, N., Goda, H., Shimada, Y., Hayashi, K.I., Nozaki, H., Asami, T., Yoshida, S. and Fujioka, S., 2006. Arabidopsis Aux/IAA genes are involved in brassinosteroid-mediated growth responses in a manner dependent on organ type. *The Plant Journal*, *45*(2), pp.193-205.

Nalam, V. J., Vales, M. I., Watson, C. J., Kianian, S. F., and Riera-Lizarazu, O., 2006. Map-based analysis of genes affecting the brittle rachis character in tetraploid wheat (Triticum turgidum L.). *Theoretical and Applied Genetics*, *112*(2), pp.373-381.

Nam, K.H. and Li, J., 2002. BRI1/BAK1, a receptor kinase pair mediating brassinosteroid signaling. *Cell*, *110*(2), pp.203-212.

Navarro, C., Moore, J., Ott, A., Baumert, E., Mohan, A., Gill, K.S. and Sandhu, D., 2015. Evolutionary, comparative and functional analyses of the brassinosteroid receptor gene, BRI1, in wheat and its relation to other plant genomes. *PLoS One*, *10*(5), p.e0127544.

Nebert, D.W. and Gonzalez, F.J., 1987. P450 genes: structure, evolution, and regulation. *Annual review of biochemistry*, *56*(1), pp.945-993.

Neff, M.M., Nguyen, S.M., Malancharuvil, E.J., Fujioka, S., Noguchi, T., Seto, H., Tsubuki, M., Honda, T., Takatsuto, S., Yoshida, S. and Chory, J., 1999. BAS1: A gene regulating brassinosteroid levels and light responsiveness in Arabidopsis. *Proceedings of the National Academy of Sciences*, *96*(26), pp.15316-15323.

Noguchi, T., Fujioka, S., Choe, S., Takatsuto, S., Tax, F.E., Yoshida, S. and Feldmann, K.A., 2000. Biosynthetic pathways of brassinolide in Arabidopsis. *Plant Physiology*, *124*(1), pp.201-210.

Noguchi, T., Fujioka, S., Choe, S., Takatsuto, S., Yoshida, S., Yuan, H., Feldmann, K.A. and Tax, F.E., 1999. Brassinosteroid-insensitive dwarf mutants of Arabidopsis accumulate brassinosteroids. *Plant physiology*, *121*(3), pp.743-752.

Nolan, T., Chen, J. and Yin, Y., 2017. Cross-talk of Brassinosteroid signaling in controlling growth and stress responses. *Biochemical Journal*, *474*(16), pp.2641-2661.

Nolan, T.M., Vukašinović, N., Liu, D., Russinova, E. and Yin, Y., 2020. Brassinosteroids: multidimensional regulators of plant growth, development, and stress responses. *The Plant Cell*, *32*(2), pp.295-318.

Nomura, T., Bishop, G.J., Kaneta, T., Reid, J.B., Chory, J. and Yokota, T., 2003. The LKA gene is a BRASSINOSTEROID INSENSITIVE 1 homolog of pea. *The Plant Journal*, *36*(3), pp.291-300.

Nomura, T., Kitasaka, Y., Takatsuto, S., Reid, J.B., Fukami, M. and Yokota, T., 1999. Brassinosteroid/sterol synthesis and plant growth as affected by lka and lkb mutations of pea. *Plant Physiology*, *119*(4), pp.1517-1526.

Nomura, T., Nakayama, M., Reid, J.B., Takeuchi, Y. and Yokota, T., 1997. Blockage of brassinosteroid biosynthesis and sensitivity causes dwarfism in garden pea. *Plant Physiology*, *113*(1), pp.31-37.

Northey, J.G., Liang, S., Jamshed, M., Deb, S., Foo, E., Reid, J.B., McCourt, P. and Samuel, M.A., 2016. Farnesylation mediates brassinosteroid biosynthesis to regulate abscisic acid responses. *Nature plants*, *2*(8), pp.1-7.

Oh, M.H., Ray, W.K., Huber, S.C., Asara, J.M., Gage, D.A. and Clouse, S.D., 2000. Recombinant brassinosteroid insensitive 1 receptor-like kinase autophosphorylates on serine and threonine residues and phosphorylates a conserved peptide motif in vitro. *Plant physiology*, *124*(2), pp.751-766.

Oh, M.H., Wang, X., Clouse, S.D. and Huber, S.C., 2012. Deactivation of the Arabidopsis BRASSINOSTEROID INSENSITIVE 1 (BRI1) receptor kinase by

autophosphorylation within the glycine-rich loop. *Proceedings of the National Academy of Sciences*, *109*(1), pp.327-332.

Ohnishi, T., Godza, B., Watanabe, B., Fujioka, S., Hategan, L., Ide, K., Shibata, K., Yokota, T., Szekeres, M. and Mizutani, M., 2012. CYP90A1/CPD, a brassinosteroid biosynthetic cytochrome P450 of Arabidopsis, catalyzes C-3 oxidation. *Journal of Biological Chemistry*, *287*(37), pp.31551-31560.

Ohnishi, T., Szatmari, A.M., Watanabe, B., Fujita, S., Bancos, S., Koncz, C., Lafos, M., Shibata, K., Yokota, T., Sakata, K. and Szekeres, M., 2006. C-23 hydroxylation by Arabidopsis CYP90C1 and CYP90D1 reveals a novel shortcut in brassinosteroid biosynthesis. *The Plant Cell*, *18*(11), pp.3275-3288.

Park, J.H., Halitschke, R., Kim, H.B., Baldwin, I.T., Feldmann, K.A. and Feyereisen, R., 2003. A knock-out mutation in allene oxide synthase results in male sterility and defective wound signal transduction in Arabidopsis due to a block in jasmonic acid biosynthesis. *The Plant Journal*, *31*(1), pp.1-12.

Parry, M.L., 2019. *Climate change and world agriculture*. Routledge.

Pendleton, J.W., Smith, G.E., Winter, S.R. and Johnston, T.J., 1968. Field investigations of the relationships of leaf angle in corn (zea mays l.) to grain yield and apparent photosynthesis 1. *Agronomy Journal*, *60*(4), pp.422-424.

Pendleton, J.W., Smith, G.E., Winter, S.R. and Johnston, T.J., 1968. Field investigations of the relationships of leaf angle in corn (zea mays l.) to grain yield and apparent photosynthesis 1. *Agronomy Journal*, *60*(4), pp.422-424.

Peng, S., Khush, G.S., Virk, P., Tang, Q. and Zou, Y., 2008. Progress in ideotype breeding to increase rice yield potential. *Field Crops Research*, *108*(1), pp.32-38.

Peng, S., Tao, P., Xu, F., Wu, A., Huo, W. and Wang, J., 2016. Functional characterization of soybean Glyma04g39610 as a brassinosteroid receptor gene and evolutionary analysis of soybean brassinosteroid receptors. *International Journal of Molecular Sciences*, *17*(6), p.897.

Pilu, R., Cassani, E., Villa, D., Curiale, S., Panzeri, D., Badone, F.C. and Landoni, M., 2007. Isolation and characterization of a new mutant allele of brachytic 2 maize gene. *Molecular Breeding*, *20*, pp.83-91.

Poppenberger, B., Rozhon, W., Khan, M., Husar, S., Adam, G., Luschnig, C., Fujioka, S. and Sieberer, T., 2011. CESTA, a positive regulator of brassinosteroid biosynthesis. *The EMBO Journal*, *30*(6), pp.1149-1161.

Ptošková, K., Szecówka, M., Jaworek, P., Tarkowská, D., Petřík, I., Pavlović, I., Novák, O., Thomas, S.G., Phillips, A.L. and Hedden, P., 2022. Changes in the concentrations and transcripts for gibberellins and other hormones in a growing leaf and roots of wheat seedlings in response to water restriction. *BMC Plant Biology*, *22*(1), p.284.

Pullen, M., Clark, N., Zarinkamar, F., Topping, J. and Lindsey, K., 2010. Analysis of vascular development in the hydra sterol biosynthetic mutants of Arabidopsis. *PLoS One*, *5*(8), p.e12227.

Purcell, L.C., 2000. Soybean canopy coverage and light interception measurements using digital imagery. *Crop science*, *40*(3), pp.834-837.

Putri, G.H., Anders, S., Pyl, P.T., Pimanda, J.E. and Zanini, F., 2022. Analysing high-throughput sequencing data in Python with HTSeq 2.0. *Bioinformatics*, *38*(10), pp.2943-2945.

Rajaram, S. and Van Ginkel, M., 1996. Yield potential debate: Germplasm vs. methodology, or both. *Increasing yield potential in wheat: breaking the barriers. Mexico, DF: CIMMYT*, pp.11-18.

Rasmussen, J., Nørremark, M. and Bibby, B.M., 2007. Assessment of leaf cover and crop soil cover in weed harrowing research using digital images. *Weed Research*, *47*(4), pp.299-310.

Ray, D. K., Mueller, N. D., West, P. C., and Foley, J. A., 2013. Yield trends are insufficient to double global crop production by 2050. *PloS one*, *8*(6), e66428.

Richards, R.A., Cavanagh, C.R. and Riffkin, P., 2019. Selection for erect canopy architecture can increase yield and biomass of spring wheat. *Field Crops Research*, *244*, p.107649.

Rouleau, M., Marsolais, F., Richard, M., Nicolle, L., Voigt, B., Adam, G. and Varin, L., 1999. Inactivation of brassinosteroid biological activity by a salicylate-inducible

steroid sulfotransferase from Brassica napus. *Journal of Biological Chemistry*, *274*(30), pp.20925-20930.

Rozhon, W., Akter, S., Fernandez, A. and Poppenberger, B., 2019. Inhibitors of brassinosteroid biosynthesis and signal transduction. *Molecules*, *24*(23), p.4372.

Sadeghi-Tehran, P., Sabermanesh, K., Virlet, N. and Hawkesford, M.J., 2017. Automated method to determine two critical growth stages of wheat: heading and flowering. *Frontiers in Plant Science*, *8*, p.252.

Sadeghi-Tehran, P., Virlet, N., Ampe, E.M., Reyns, P. and Hawkesford, M.J., 2019. DeepCount: in-field automatic quantification of wheat spikes using simple linear iterative clustering and deep convolutional neural networks. *Frontiers in plant science*, *10*, p.1176.

Sadura, I., Libik-Konieczny, M., Jurczyk, B., Gruszka, D. and Janeczko, A., 2020. Plasma membrane ATPase and the aquaporin HvPIP1 in barley brassinosteroid mutants acclimated to high and low temperature. *Journal of plant physiology*, *244*, p.153090.

Sadura, Iwona, Ewa Pociecha, Michał Dziurka, Jana Oklestkova, Ondrej Novak, Damian Gruszka, and Anna Janeczko. "Mutations in the HvDWARF, HvCPD and HvBRI1 genes-involved in brassinosteroid biosynthesis/signalling: Altered photosynthetic efficiency, hormonal homeostasis and tolerance to high/low temperatures in barley." *Journal of Plant Growth Regulation* 38 (2019): 1062-1081.

Sahni, S., Prasad, B.D., Liu, Q., Grbic, V., Sharpe, A., Singh, S.P. and Krishna, P., 2016. Overexpression of the brassinosteroid biosynthetic gene DWF4 in Brassica napus simultaneously increases seed yield and stress tolerance. *Scientific Reports*, *6*(1), pp.1-14.

Saisho, D., Tanno, K.I., Chono, M., Honda, I., Kitano, H. and Takeda, K., 2004. Spontaneous brassinolide-insensitive barley mutants ‘uzu’adapted to east Asia. *Breeding science*, *54*(4), pp.409-416.

Saisho, D., Tanno, K.I., Chono, M., Honda, I., Kitano, H. and Takeda, K., 2004. Spontaneous brassinolide-insensitive barley mutants ‘uzu’adapted to east Asia. *Breeding science*, *54*(4), pp.409-416.

Sakamoto, T., Kawabe, A., Tokida-Segawa, A., Shimizu, B.I., Takatsuto, S., Shimada, Y., Fujioka, S. and Mizutani, M., 2011. Rice CYP734As function as multisubstrate and multifunctional enzymes in brassinosteroid catabolism. *The Plant Journal*, *67*(1), pp.1-12.

Sakamoto, T., Morinaka, Y., Ohnishi, T., Sunohara, H., Fujioka, S., Ueguchi-Tanaka, M., Mizutani, M., Sakata, K., Takatsuto, S., Yoshida, S. and Tanaka, H., 2006. Erect leaves caused by brassinosteroid deficiency increase biomass production and grain yield in rice. *Nature biotechnology*, *24*(1), pp.105-109.

Sandhu, K.S., Koirala, P.S. and Neff, M.M., 2013. The ben1-1 brassinosteroid-catabolism mutation is unstable due to epigenetic modifications of the intronic T-DNA insertion. *G3: Genes, Genomes, Genetics*, *3*(9), pp.1587-1595.

Schneider, H.M., Lor, V.S., Zhang, X., Saengwilai, P., Hanlon, M.T., Klein, S.P., Davis, J.L., Borkar, A.N., Depew, C.L., Bennett, M.J. and Kaeppler, S.M., 2023. Transcription factor bHLH121 regulates root cortical aerenchyma formation in maize. *Proceedings of the National Academy of Sciences*, *120*(12), p.e2219668120.

Schneider, K., Breuer, C., Kawamura, A., Jikumaru, Y., Hanada, A., Fujioka, S., Ichikawa, T., Kondou, Y., Matsui, M., Kamiya, Y. and Yamaguchi, S., 2012. Arabidopsis PIZZA has the capacity to acylate brassinosteroids. e46805.

Schrick, K., Mayer, U., Horrichs, A., Kuhnt, C., Bellini, C., Dangl, J., Schmidt, J. and Jürgens, G., 2000. FACKEL is a sterol C-14 reductase required for organized cell division and expansion in Arabidopsis embryogenesis. *Genes & development*, *14*(12), pp.1471-1484.

Shao, G., Tang, S., Luo, J., Jiao, G., Wei, X., Tang, A., Wu, J., Zhuang, J. and Hu, P., 2010. Mapping of qGL7-2, a grain length QTL on chromosome 7 of rice. *Journal of Genetics and Genomics*, *37*(8), pp.523-531.

Sharma, N. and Khurana, P., 2022. Genome-wide identification, characterization and expression analysis of the BRI1 gene family in Triticum aestivum L. *Plant Biotechnology Reports*, *16*(6), pp.777-791.

She, J., Han, Z., Kim, T.W., Wang, J., Cheng, W., Chang, J., Shi, S., Wang, J., Yang, M., Wang, Z.Y. and Chai, J., 2011. Structural insight into brassinosteroid perception by BRI1. *Nature*, *474*(7352), pp.472-476.

Shearman, V.J., Sylvester-Bradley, R., Scott, R.K. and Foulkes, M.J., 2005. Physiological processes associated with wheat yield progress in the UK. *Crop science*, *45*(1), pp.175-185.

Shewry, P. R., 2009. Wheat. *Journal of experimental botany*, *60*(6), pp. 1537-1553.

Shimada, A., Ueguchi-Tanaka, M., Sakamoto, T., Fujioka, S., Takatsuto, S., Yoshida, S., Sazuka, T., Ashikari, M. and Matsuoka, M., 2006. The rice SPINDLY gene functions as a negative regulator of gibberellin signaling by controlling the suppressive function of the DELLA protein, SLR1, and modulating brassinosteroid synthesis. *The Plant Journal*, *48*(3), pp.390-402.

Shrestha, D.S. and Steward, B.L., 2003. Automatic corn plant population measurement using machine vision. *Transactions of the ASAE*, *46*(2), p.559.

Simons, K. J., Fellers, J. P., Trick, H. N., Zhang, Z., Tai, Y. S., Gill, B. S., and Faris, J. D., 2006. Molecular characterization of the major wheat domestication gene Q. *Genetics*, *172*(1), pp.547-555.

Sinclair, T.R. and Sheehy, J.E., 1999. Erect leaves and photosynthesis in rice. *Science*, *283*(5407), pp.1455-1455.

Sinclair, T.R. and Sheehy, J.E., 1999. Erect leaves and photosynthesis in rice. *Science*, *283*(5407), pp.1455-1455.

Singh, D.P., Jermakow, A.M. and Swain, S.M., 2002. Gibberellins are required for seed development and pollen tube growth in Arabidopsis. *The Plant Cell*, *14*(12), pp.3133-3147.

Soeno, K., Fujioka, S., Hiranuma, S., Seto, H. and Yoshida, S., 2006. Metabolic conversion of castasterone and brassinolide into their glucosides in higher plants. *Journal of Plant Growth Regulation*, *25*, pp.195-202.

Sonawane, P.D., Pollier, J., Panda, S., Szymanski, J., Massalha, H., Yona, M., Unger, T., Malitsky, S., Arendt, P., Pauwels, L. and Almekias-Siegl, E., 2016. Plant

cholesterol biosynthetic pathway overlaps with phytosterol metabolism. *Nature plants*, *3*(1), pp.1-13.

Song, J., Sun, S., Ren, H., Grison, M., Boutté, Y., Bai, W. and Men, S., 2019. The SMO1 family of sterol 4α-methyl oxidases is essential for auxin-and cytokinin-regulated embryogenesis. *Plant physiology*, *181*(2), pp.578-594.

Song, L., Liu, J., Cao, B., Liu, B., Zhang, X., Chen, Z., Dong, C., Liu, X., Zhang, Z., Wang, W. and Chai, L., 2023. Reducing brassinosteroid signalling enhances grain yield in semi-dwarf wheat. *Nature*, pp.1-7.

Song, Y., You, J. and Xiong, L., 2009. Characterization of OsIAA1 gene, a member of rice Aux/IAA family involved in auxin and brassinosteroid hormone responses and plant morphogenesis. *Plant molecular biology*, *70*, pp.297-309.

Souter, M., Topping, J., Pullen, M., Friml, J., Palme, K., Hackett, R., Grierson, D. and Lindsey, K., 2002. hydra mutants of Arabidopsis are defective in sterol profiles and auxin and ethylene signaling. *The Plant Cell*, *14*(5), pp.1017-1031.

Stirnberg, P., van De Sande, K. and Leyser, H.O., 2002. MAX1 and MAX2 control shoot lateral branching in Arabidopsis.

Strable, J., Wallace, J.G., Unger-Wallace, E., Briggs, S., Bradbury, P.J., Buckler, E.S. and Vollbrecht, E., 2017. Maize YABBY genes drooping leaf1 and drooping leaf2 regulate plant architecture. *The Plant Cell*, *29*(7), pp.1622-1641.

Strock, C.F., Schneider, H.M., Galindo-Castañeda, T., Hall, B.T., Van Gansbeke, B., Mather, D.E., Roth, M.G., Chilvers, M.I., Guo, X., Brown, K. and Lynch, J.P., 2019. Laser ablation tomography for visualization of root colonization by edaphic organisms. *Journal of experimental botany*, *70*(19), pp.5327-5342.

Sun, C., Yan, K., Han, J.T., Tao, L., Lv, M.H., Shi, T., He, Y.X., Wierzba, M., Tax, F.E. and Li, J., 2017. Scanning for new BRI1 mutations via TILLING analysis. *Plant Physiology*, *174*(3), pp.1881-1896.

Sun, S., Chen, D., Li, X., Qiao, S., Shi, C., Li, C., Shen, H. and Wang, X., 2015. Brassinosteroid signaling regulates leaf erectness in Oryza sativa via the control of a specific U-type cyclin and cell proliferation. *Developmental Cell*, *34*(2), pp.220-228.

Sun, Y., Fan, X.Y., Cao, D.M., Tang, W., He, K., Zhu, J.Y., He, J.X., Bai, M.Y., Zhu, S., Oh, E. and Patil, S., 2010. Integration of brassinosteroid signal transduction with the transcription network for plant growth regulation in Arabidopsis. *Developmental cell*, *19*(5), pp.765-777.

Suzuki, H., Inoue, T., Fujioka, S., Saito, T., Takatsuto, S., Yokota, T., Murofushi, N., Yanagisawa, T. and Sakurai, A., 1995. Conversion of 24-methylcholesterol to 6-oxo-24-methylcholestanol, a putative intermediate of the biosynthesis of brassinosteroids, in cultured cells of Catharanthus roseus. *Phytochemistry*, *40*(5), pp.1391-1397.

Sylvester, A.W., Cande, W.Z. and Freeling, M., 1990. Division and differentiation during normal and liguleless-1 maize leaf development. *Development*, *110*(3), pp.985-1000.

Symons, G.M. and Reid, J.B., 2004. Brassinosteroids do not undergo long-distance transport in pea. Implications for the regulation of endogenous brassinosteroid levels. *Plant physiology*, *135*(4), pp.2196-2206.

Symons, G.M., Ross, J.J., Jager, C.E. and Reid, J.B., 2008. Brassinosteroid transport. *Journal of experimental botany*, *59*(1), pp.17-24.

Szekeres, M., Németh, K., Koncz-Kálmán, Z., Mathur, J., Kauschmann, A., Altmann, T., Rédei, G.P., Nagy, F., Schell, J. and Koncz, C., 1996. Brassinosteroids rescue the deficiency of CYP90, a cytochrome P450, controlling cell elongation and de-etiolation in Arabidopsis. *Cell*, *85*(2), pp.171-182.

Takahashi, R. and Yamamoto, J., 1951. Studies on the Classification and the Geographical Distribution of the Japanese Barley Varieties. III On the Linkage Relation and the Origin of the ‘uzu’or Semi-Brachytic Character in Barley. *Berichte des Ohara Instituts für landwirtschaftliche Forschungen*, *9*(4), pp.399-410.

Takahashi, T., Gasch, A., Nishizawa, N. and Chua, N.H., 1995. The DIMINUTO gene of Arabidopsis is involved in regulating cell elongation. *Genes & Development*, *9*(1), pp.97-107.

Tanabe, S., Ashikari, M., Fujioka, S., Takatsuto, S., Yoshida, S., Yano, M., Yoshimura, A., Kitano, H., Matsuoka, M., Fujisawa, Y. and Kato, H., 2005. A novel cytochrome P450 is implicated in brassinosteroid biosynthesis via the

characterization of a rice dwarf mutant, dwarf11, with reduced seed length. *The Plant Cell*, *17*(3), pp.776-790.

Tanaka, A., 1968. Historical changes in the plant type of rice cultivars in Hokkaido. *J. Sci. Soil and Manure, Japan*, *39*, pp.526-534.

Tanaka, A., Nakagawa, H., Tomita, C., Shimatani, Z., Ohtake, M., Nomura, T., Jiang, C.J., Dubouzet, J.G., Kikuchi, S., Sekimoto, H. and Yokota, T., 2009. BRASSINOSTEROID UPREGULATED1, encoding a helix-loop-helix protein, is a novel gene involved in brassinosteroid signaling and controls bending of the lamina joint in rice. *Plant physiology*, *151*(2), pp.669-680.

Tanaka, K., Asami, T., Yoshida, S., Nakamura, Y., Matsuo, T. and Okamoto, S., 2005. Brassinosteroid homeostasis in Arabidopsis is ensured by feedback expressions of multiple genes involved in its metabolism. *Plant physiology*, *138*(2), pp.1117-1125.

Tang, W., Deng, Z., Oses-Prieto, J. A., Suzuki, N., Zhu, S., Zhang, X., ... and Wang, Z. Y., 2008. Proteomics studies of brassinosteroid signal transduction using prefractionation and two-dimensional DIGE. *Molecular and Cellular Proteomics*, *7*(4), pp.728-738.

Tao, Y., Zheng, J., Xu, Z., Zhang, X., Zhang, K. and Wang, G., 2004. Functional analysis of ZmDWF1, a maize homolog of the Arabidopsis brassinosteroids biosynthetic DWF1/DIM gene. *Plant Science*, *167*(4), pp.743-751.

Tarkowská, D. and Strnad, M., 2016. Plant ecdysteroids: plant sterols with intriguing distributions, biological effects and relations to plant hormones. *Planta*, *244*, pp.545-555.

Thorp, K.R. and Dierig, D.A., 2011. Color image segmentation approach to monitor flowering in lesquerella. *Industrial crops and products*, *34*(1), pp.1150-1159.

Thorp, K.R., Steward, B.L., Kaleita, A.L. and Batchelor, W.D., 2007. Using aerial hyperspectral remote sensing imagery to estimate corn plant stand density. *Transactions of the ASABE*, *51*(1), pp.311-320.

Tian, F., Bradbury, P.J., Brown, P.J., Hung, H., Sun, Q., Flint-Garcia, S., Rocheford, T.R., McMullen, M.D., Holland, J.B. and Buckler, E.S., 2011. Genome-wide

association study of leaf architecture in the maize nested association mapping population. *Nature genetics*, *43*(2), pp.159-162.

Tian, J., Wang, C., Xia, J., Wu, L., Xu, G., Wu, W., Li, D., Qin, W., Han, X., Chen, Q. and Jin, W., 2019. Teosinte ligule allele narrows plant architecture and enhances high-density maize yields. *Science*, *365*(6454), pp.658-664.

Till, B.J., Reynolds, S.H., Greene, E.A., Codomo, C.A., Enns, L.C., Johnson, J.E., Burtner, C., Odden, A.R., Young, K., Taylor, N.E. and Henikoff, J.G., 2003. Large-scale discovery of induced point mutations with high-throughput TILLING. *Genome research*, *13*(3), pp.524-530.

Tollenaar, M. and Wu, J., 1999. Yield improvement in temperate maize is attributable to greater stress tolerance. *Crop science*, *39*(6), pp.1597-1604.

Tong, H., Liu, L., Jin, Y., Du, L., Yin, Y., Qian, Q., Zhu, L. and Chu, C., 2012. DWARF AND LOW-TILLERING acts as a direct downstream target of a GSK3/SHAGGY-like kinase to mediate brassinosteroid responses in rice. *The Plant Cell*, *24*(6), pp.2562-2577.

Tong, H., Xiao, Y., Liu, D., Gao, S., Liu, L., Yin, Y., Jin, Y., Qian, Q. and Chu, C., 2014. Brassinosteroid regulates cell elongation by modulating gibberellin metabolism in rice. *The Plant Cell*, *26*(11), pp.4376-4393.

Trnka, M., Hlavinka, P. and Semenov, M.A., 2015. Adaptation options for wheat in Europe will be limited by increased adverse weather events under climate change. *Journal of the Royal Society Interface*, *12*(112), p.20150721.

Truong, S.K., McCormick, R.F., Rooney, W.L. and Mullet, J.E., 2015. Harnessing genetic variation in leaf angle to increase productivity of Sorghum bicolor. *Genetics*, *201*(3), pp.1229-1238.

Turk, E.M., Fujioka, S., Seto, H., Shimada, Y., Takatsuto, S., Yoshida, S., Wang, H., Torres, Q.I., Ward, J.M., Murthy, G. and Zhang, J., 2005. BAS1 and SOB7 act redundantly to modulate Arabidopsis photomorphogenesis via unique brassinosteroid inactivation mechanisms. *The Plant Journal*, *42*(1), pp.23-34.

Turk, E.M., Fujioka, S., Seto, H., Shimada, Y., Takatsuto, S., Yoshida, S., Denzel, M.A., Torres, Q.I. and Neff, M.M., 2003. CYP72B1 inactivates brassinosteroid

hormones: an intersection between photomorphogenesis and plant steroid signal transduction. *Plant Physiology*, *133*(4), pp.1643-1653.

Virlet, N., Sabermanesh, K., Sadeghi-Tehran, P. and Hawkesford, M.J., 2016. Field Scanalyzer: An automated robotic field phenotyping platform for detailed crop monitoring. *Functional Plant Biology*, *44*(1), pp.143-153.

Vukašinović, N. and Russinova, E., 2018. BRexit: Possible brassinosteroid export and transport routes. *Trends in plant science*, *23*(4), pp.285-292.

Wang, D., Fahad, S., Saud, S., Kamran, M., Khan, A., Khan, M.N., Hammad, H.M. and Nasim, W., 2019. Morphological acclimation to agronomic manipulation in leaf dispersion and orientation to promote "Ideotype" breeding: Evidence from 3D visual modeling of "super" rice (Oryza sativa L.). *Plant Physiology and Biochemistry*, *135*, pp.499-510.

Wang, L., Xu, Y., Zhang, C., Ma, Q., Joo, S.H., Kim, S.K., Xu, Z. and Chong, K., 2008. OsLIC, a novel CCCH-type zinc finger protein with transcription activation, mediates rice architecture via brassinosteroids signaling. *PloS one*, *3*(10), p.e3521.

Wang, M., Wang, D., Zhang, Q., Chai, J., Peng, Y. and Cai, X., 2017. Identification and cytochemical immunolocalization of acetyl-CoA acetyltransferase involved in the terpenoid mevalonate pathway in Euphorbia helioscopia laticifers. *Botanical studies*, *58*(1), pp.1-11.

Wang, T., Salazar, A., Zabotina, O.A. and Hong, M., 2014. Structure and dynamics of Brachypodium primary cell wall polysaccharides from two-dimensional 13C solid-state nuclear magnetic resonance spectroscopy. *Biochemistry*, *53*(17), pp.2840-2854.

Wang, X., and Chory, J. 2006. Brassinosteroids regulate dissociation of BKI1, a negative regulator of BRI1 signaling, from the plasma membrane. *Science*, *313*(5790), pp.1118-1122.

Wang, X., Goshe, M. B., Soderblom, E. J., Phinney, B. S., Kuchar, J. A., Li, J., ... and Clouse, S. D. 2005. Identification and functional analysis of in vivo phosphorylation sites of the Arabidopsis BRASSINOSTEROID-INSENSITIVE1 receptor kinase. *The Plant Cell*, *17*(6), pp.1685-1703.

Wang, Y., Sun, S., Zhu, W., Jia, K., Yang, H. and Wang, X., 2013. Strigolactone/MAX2-induced degradation of brassinosteroid transcriptional effector BES1 regulates shoot branching. *Developmental cell*, *27*(6), pp.681-688.

Wang, Z.Y., Bai, M.Y., Oh, E. and Zhu, J.Y., 2012. Brassinosteroid signaling network and regulation of photomorphogenesis. *Annual review of genetics*, *46*, pp.701-724.

Wang, Z.Y., Nakano, T., Gendron, J., He, J., Chen, M., Vafeados, D., Yang, Y., Fujioka, S., Yoshida, S., Asami, T. and Chory, J., 2002. Nuclear-localized BZR1 mediates brassinosteroid-induced growth and feedback suppression of brassinosteroid biosynthesis. *Developmental cell*, *2*(4), pp.505-513.

Wang, Z.Y., Seto, H., Fujioka, S., Yoshida, S. and Chory, J., 2001. BRI1 is a critical component of a plasma-membrane receptor for plant steroids. *Nature*, *410*(6826), pp.380-383.

Wei, Z. and Li, J., 2020. Regulation of brassinosteroid homeostasis in higher plants. *Frontiers in Plant Science*, *11*, p.583622.

Wei, Z., Yuan, T., Tarkowská, D.E., Kim, J., Nam, H.G., Novák, O., He, K., Gou, X. and Li, J., 2017. Brassinosteroid biosynthesis is modulated via a transcription factor cascade of COG1, PIF4, and PIF5. *Plant Physiology*, *174*(2), pp.1260-1273.

Wendeborn, S., Lachia, M., Jung, P.M., Leipner, J., Brocklehurst, D., De Mesmaeker, A., Gaus, K. and Mondière, R., 2017. Biological activity of brassinosteroids–direct comparison of known and new analogs in planta. *Helvetica Chimica Acta*, *100*(2).

Weng, J., Gu, S., Wan, X., Gao, H., Guo, T., Su, N., Lei, C., Zhang, X., Cheng, Z., Guo, X. and Wang, J., 2008. Isolation and initial characterization of GW5, a major QTL associated with rice grain width and weight. *Cell research*, *18*(12), pp.1199-1209.

Wu, C.Y., Trieu, A., Radhakrishnan, P., Kwok, S.F., Harris, S., Zhang, K., Wang, J., Wan, J., Zhai, H., Takatsuto, S. and Matsumoto, S., 2008. Brassinosteroids regulate grain filling in rice. *The Plant Cell*, *20*(8), pp.2130-2145.

Wu, X., Cheng, R., Xue, S., Kong, Z., Wan, H., Li, G., Huang, Y., Jia, H., Jia, J., Zhang, L. and Ma, Z., 2014. Precise mapping of a quantitative trait locus interval for spike length and grain weight in bread wheat (Triticum aestivum L.). *Molecular breeding*, *33*, pp.129-138.

Xia, X.J., Fang, P.P., Guo, X., Qian, X.J., Zhou, J., Shi, K., Zhou, Y.H. and Yu, J.Q., 2018. Brassinosteroid-mediated apoplastic H2O2-glutaredoxin 12/14 cascade regulates antioxidant capacity in response to chilling in tomato. *Plant, Cell and Environment*, *41*(5), pp.1052-1064.

Yamamoto, R., Fujioka, S., Demura, T., Takatsuto, S., Yoshida, S. and Fukuda, H., 2001. Brassinosteroid levels increase drastically prior to morphogenesis of tracheary elements. *Plant Physiology*, *125*(2), pp.556-563.

Yamamuro, C., Ihara, Y., Wu, X., Noguchi, T., Fujioka, S., Takatsuto, S., Ashikari, M., Kitano, H. and Matsuoka, M., 2000. Loss of function of a rice brassinosteroid insensitive1 homolog prevents internode elongation and bending of the lamina joint. *The Plant Cell*, *12*(9), pp.1591-1605.

Yao, Y., Lv, L., Zhang, L., Yao, H., Dong, Z., Zhang, J., Ji, J., Jia, X. and Wang, H., 2019. Genetic gains in grain yield and physiological traits of winter wheat in Hebei Province of China, from 1964 to 2007. *Field crops research*, *239*, pp.114-123.

Yao, Y., Yamamoto, Y., Yoshida, T., Nitta, Y., and Miyazaki, A., 2000. Response of differentiated and degenerated spikelets to top-dressing, shading and day/night temperature treatments in rice cultivars with large panicles. *Soil Science and Plant Nutrition*, *46*(3), pp.631-641.

Ye, H., Li, L. and Yin, Y., 2011. Recent Advances in the Regulation of Brassinosteroid Signaling and Biosynthesis Pathways F. *Journal of Integrative Plant Biology*, *53*(6), pp.455-468.

Ye, Q., Zhu, W., Li, L., Zhang, S., Yin, Y., Ma, H. and Wang, X., 2010. Brassinosteroids control male fertility by regulating the expression of key genes involved in Arabidopsis anther and pollen development. *Proceedings of the National Academy of Sciences*, *107*(13), pp.6100-6105.

Yin, Y., Vafeados, D., Tao, Y., Yoshida, S., Asami, T. and Chory, J., 2005. A new class of transcription factors mediates brassinosteroid-regulated gene expression in Arabidopsis. *Cell*, *120*(2), pp.249-259.

Yin, Y., Wang, Z.Y., Mora-Garcia, S., Li, J., Yoshida, S., Asami, T. and Chory, J., 2002. BES1 accumulates in the nucleus in response to brassinosteroids to regulate gene expression and promote stem elongation. *Cell*, *109*(2), pp.181-191.

Yokota, T., Arima, M. and Takahashi, N., 1982. Castasterone, a new phytosterol with plant-hormone potency, from chestnut insect gall. *Tetrahedron Letters*, *23*(12), pp.1275-1278.

Yokota, T., Sato, T., Takeuchi, Y., Nomura, T., Uno, K., Watanabe, T. and Takatsuto, S., 2001. Roots and shoots of tomato produce 6-deoxo-28-norcathasterone, 6-deoxo-28-nortyphasterol and 6-deoxo-28-norcastasterone, possible precursors of 28-norcastasterone. *Phytochemistry*, *58*(2), pp.233-238.

Yoshida, S., 1981. *Fundamentals of rice crop science*. Int. Rice Res. Inst..

Yoshikawa, T., Ito, M., Sumikura, T., Nakayama, A., Nishimura, T., Kitano, H., Yamaguchi, I., Koshiba, T., Hibara, K.I., Nagato, Y. and Itoh, J.I., 2014. The rice FISH BONE gene encodes a tryptophan aminotransferase, which affects pleiotropic auxin-related processes. *The Plant Journal*, *78*(6), pp.927-936.

Youn, J.H., Kim, T.W., Joo, S.H., Son, S.H., Roh, J., Kim, S., Kim, T.W. and Kim, S.K., 2018. Function and molecular regulation of DWARF1 as a C-24 reductase in brassinosteroid biosynthesis in Arabidopsis. *Journal of Experimental Botany*, *69*(8), pp.1873-1886.

Yu, X., Li, L., Zola, J., Aluru, M., Ye, H., Foudree, A., Guo, H., Anderson, S., Aluru, S., Liu, P. and Rodermel, S., 2011. A brassinosteroid transcriptional network revealed by genome-wide identification of BESI target genes in Arabidopsis thaliana. *The Plant Journal*, *65*(4), pp.634-646.

Yu, X., Lu, H., Lu, G., Chen, Z., Cao, J. and Hirata, Y., 2010. Analysis of genetic diversity in cytoplasmic male sterility, and association of mitochondrial genes with petaloid-type cytoplasmic male sterility in tuber mustard (Brassica juncea var. tumida Tsen et Lee). *Molecular biology reports*, *37*, pp.1059-1067.

Yuan, G.F., Jia, C.G., Li, Z., Sun, B., Zhang, L.P., Liu, N. and Wang, Q.M., 2010. Effect of brassinosteroids on drought resistance and abscisic acid concentration in tomato under water stress. *Scientia Horticulturae*, *126*(2), pp.103-108.

Yuan, L., 2001. Breeding of super hybrid rice. In *Rice research for food security and poverty alleviation. Proceedings of the International Rice Research Conference, Los Baños, Philippines, 31 March-3 April, 2000* (pp. 143-149). International Rice Research Institute (IRRI).

Yuan, L., Yuan, Y., Du, J., Sun, J. and Guo, S., 2012. Effects of 24-epibrassinolide on nitrogen metabolism in cucumber seedlings under Ca (NO3) 2 stress. *Plant Physiology and Biochemistry*, *61*, pp.29-35.

Yuan, T., Fujioka, S., Takatsuto, S., Matsumoto, S., Gou, X., He, K., Russell, S.D. and Li, J., 2007. BEN1, a gene encoding a dihydroflavonol 4-reductase (DFR)-like protein, regulates the levels of brassinosteroids in Arabidopsis thaliana. *The Plant Journal*, *51*(2), pp.220-233.

Yue, J., You, Y., Zhang, L., Fu, Z., Wang, J., Zhang, J. and Guy, R.D., 2019. Exogenous 24-epibrassinolide alleviates effects of salt stress on chloroplasts and photosynthesis in Robinia pseudoacacia L. seedlings. *Journal of Plant Growth Regulation*, *38*, pp.669-682.

Zampieri, M., Ceglar, A., Dentener, F. and Toreti, A., 2017. Wheat yield loss attributable to heat waves, drought and water excess at the global, national and subnational scales. *Environmental Research Letters*, *12*(6), p.064008.

Zhan, H., Lu, M., Luo, Q., Tan, F., Zhao, Z., Liu, M. and He, Y., 2022. OsCPD1 and OsCPD2 are functional brassinosteroid biosynthesis genes in rice. *Plant Science*, *325*, p.111482.

Zhang, C., Bai, M.Y. and Chong, K., 2014. Brassinosteroid-mediated regulation of agronomic traits in rice. *Plant cell reports*, *33*, pp.683-696.

Zhang, C., Xu, Y., Guo, S., Zhu, J., Huan, Q., Liu, H., Wang, L., Luo, G., Wang, X. and Chong, K., 2012. Dynamics of brassinosteroid response modulated by negative regulator LIC in rice. *PLoS Genetics*, *8*(4), p.e1002686.

Zhang, D., Ye, H., Guo, H., Johnson, A., Zhang, M., Lin, H. and Yin, Y., 2014. Transcription factor HAT 1 is phosphorylated by BIN 2 kinase and mediates brassinosteroid repressed gene expression in a rabidopsis. *The Plant Journal*, *77*(1), pp.59-70.

Zhang, D.W., Deng, X.G., Fu, F.Q. and Lin, H.H., 2015. Induction of plant virus defense response by brassinosteroids and brassinosteroid signaling in Arabidopsis thaliana. *Planta*, *241*, pp.875-885.

Zhang, S., Cai, Z. and Wang, X., 2009. The primary signaling outputs of brassinosteroids are regulated by abscisic acid signaling. *Proceedings of the National Academy of Sciences*, *106*(11), pp.4543-4548.

Zhang, S., Wang, S., Xu, Y., Yu, C., Shen, C., Qian, Q., Geisler, M., Jiang, D.A. and Qi, Y., 2015. The auxin response factor, OsARF 19, controls rice leaf angles through positively regulating OsGH 3-5 and OsBRI 1. *Plant, Cell and Environment*, *38*(4), pp.638-654.

Zhang, Y.P., Zhu, X.H., Ding, H.D., Yang, S.J. and Chen, Y.Y., 2013. Foliar application of 24-epibrassinolide alleviates high-temperature-induced inhibition of photosynthesis in seedlings of two melon cultivars. *Photosynthetica*, *51*, pp.341-349.

Zhang, Z. and Xu, L., 2018. Arabidopsis BRASSINOSTEROID INACTIVATOR2 is a typical BAHD acyltransferase involved in brassinosteroid homeostasis. *Journal of Experimental Botany*, *69*(8), pp.1925-1941.

Zhao, B. and Li, J., 2012. Regulation of brassinosteroid biosynthesis and inactivation F. *Journal of Integrative Plant Biology*, *54*(10), pp.746-759.

Zhao, S. Q., Hu, J., Guo, L. B., Qian, Q., and Xue, H. W., 2010. Rice leaf inclination2, a VIN3-like protein, regulates leaf angle through modulating cell division of the collar. *Cell research*, *20*(8), pp.935.

Zhao, S. Q., Xiang, J. J., and Xue, H. W., 2013. Studies on the rice LEAF INCLINATION1 (LC1), an IAA–amido synthetase, reveal the effects of auxin in leaf inclination control. *Molecular plant*, *6*(1), pp.174-187.

Zhou, A., Wang, H., Walker, J.C. and Li, J., 2004. BRL1, a leucine-rich repeat receptor-like protein kinase, is functionally redundant with BRI1 in regulating Arabidopsis brassinosteroid signaling. *The Plant Journal*, *40*(3), pp.399-409.

Zhu, W., Wang, H., Fujioka, S., Zhou, T., Tian, H., Tian, W. and Wang, X., 2013. Homeostasis of brassinosteroids regulated by DRL1, a putative acyltransferase in Arabidopsis. *Molecular Plant*, *6*(2), pp.546-558.

Zong, S., Lu, C., Zhao, L., Wang, C., Dai, Q. and Zou, J., 2000. Physiological basis of high yield of an intersubspecific hybrid rice, Liangyoupeijiu. *J. Nanjing Agric. Tech. College*, *16*, pp.8-12.

Zong, X., Wang, S., Ling, Y., Sang, X. and He, G., 2009. Characteristics of photosynthesis in two leaf color mutants of rice. *Acta Agronomica Sinica*, *35*(12), pp.2304-2308.

Zuo, J. and Li, J., 2014. Molecular genetic dissection of quantitative trait loci regulating rice grain size. *Annual review of genetics*, *48*, pp.99-118.

Appendix

Supplementary table 1 Homeologue specific primers designed to amplify fragments around the novel mutations in *TaBRI1*, *TaDWF1* and *TaDWF4* genes.

S. No.	Gene	Chromosome	Gene ID	Forward primer	Reverse primer	Fragment length	Tm (°C)
1	BRI1	3A	TraesCS3A02G245000	GAGCATCTCATCCTGGACTAC	TCGGAGTCGAGCTGATTAAAT	533	64
2		3B	TraesCS3B02G275000	TCCGGCGATGCGGTTGGTGCC	GAGAGGTTGAGCGCCCTGAGA	311	66
3		3D	TraesCS3D02G246500	GAGCATCTCATCCTGGACTAC	TGCTCCCCATGTACATCCTC	463	64
4	DWF1	7A	TraesCS7A02G559400	ATGTGGTCCGCCATGAAGTCC	TCGACCTCGAAGTGCCTGACG	188	66
5		7B	TraesCS7B02G484200	TCAGCTAACATCTCTTTGTACA	TCACGACCTTCTGCACGTTC	265	60
6		7D	TraesCS7D02G550700	TCAGCTAACATCTCTTTGTACT	TGGGGATGAGCTTGATCTCA	745	60
7	DWF4	4A	TraesCS4A02G078000	TCAGTACAGGCATGCGAGCAG	CGCGGACACCACCCCCTTCAT	660	66
8		4B	TraesCS4B02G234100	TCTCTCTCTCTCCAACCCATCATC	CGCATGCCTGTACTGATGTATA	403	62
9		4D	TraesCS4D02G235200	GATCTGTGCTAAACTAGACACT	ACGCATATATCTTGCACTGAT	293	62

TaBRI1A (TraesCS3A02G245000) sequencing				
F1.4-R1	CCACGACGATGATGATGAGG	TTGCTGGACAGGTCGAGAGT	1100	63
F2-R2	TGAATCTGTCCGGTGGTGCA	TCGGAGTCGAGCTGATTAAAT	1400	66.2
F3-R3	AGTTCTCAAGCATCCGATCT	CATGCACACGCGATTTTCAG	1560	63
I-F3	CCAATGGCTTCCACAATGAGAGC			
F4-R4.2	CCACCAAGGGCGATGTGTAT	CTTGCTTGCTGGACATGGAG	1400	63

Supplementary table 2 KASP primers designed to differentiate the mutant and wild type allele in segregating *TaBRI1, TaDWF1* and *TaDWF4* populations.

S. No.	Gene	Chromosome	Forward Primer (MT)	Forward Primer (WT)	Common primer
1	BRI1	3A (*tabri1-a.1*)	CCCGACTGCTCTGCCAGTT**A**	CCCGACTGCTCTGCCAGTT**G**	TGGTGACTGCAAGAGCTTGG
2		3B	CGAGGCCGGCACCCACCAT**T**	CGAGGCCGGCACCCACCAT**C**	CCTGTCCAGCAACAAGATCA
3		3D	GGTTGCTCGCCAAGGATAT**T**	GGTTGCTCGCCAAGGATAT**C**	GCTCACCGGCAGTATCCC
4		3A (*tabri1-a.2*)	AATCAGCTGAATGGGACAATT**T**	AATCAGCTGAATGGGACAATT**C**	GAGCCTTGCCCAGTATGCGA
5		3A (*tabri1-a.3*)	primers didn't work		
4	DWF1	7A	CACGTTGCGCATGCCGACGGCGAT**T**	CACGTTGCGCATGCCGACGGCGAT**C**	ACCCCAAGAAGGACGGCCTC
5		7B	ACGAGGATCCATCGGAACT**A**	ACGAGGATCCATCGGAACT**G**	CGACCAAAGAGGAAGAAGGTC
6		7D	GGAACCCGAGAGTGCCCT**A**	GGAACCCGAGAGTGCCCTG	CGAGTACTCCGACCTCTTCTA
7	DWF4	4A	GGCGGCATCCTTGGCAAAT**A**	GGCGGCATCCTTGGCAAAT**G**	CTGAGGAAGTTGAGGGAGATGG
8		4B	TTCGTCCGGCCGCTCCAC**T**	TTCGTCCGGCCGCTCCAC**C**	CATCCTCCTGGCCCTGCTCA
9		4D	AACCATCTCTTTGTAGTCTTC**T**	AACCATCTCTTTGTAGTCTTC**C**	ATGGAAATATTGACAGTGAATCCA
10	Tails added to 5' end of forward primers		GAAGGTGACCAAGTTCATGCT	GAAGGTCGGAGTCAACGGATT	

Supplementary table 3 Describes log2fold change in expression of the BR pathway genes in *tabri1* mutants compared to *TaBRI1-NS* (A), BR biosynthesis (B) and BR signalling (C and D) pathway in *tabri1-a.1bd*, *tabri1-a.2bd* and *tabri1-a.3bd* mutant compared to *TaBRI1-NS*. The significant differences (having adjusted *p*-values lower than 0.05) are highlighted in bold.

A

Sterol pathway genes							
		tabri1-a.1bd* vs *TaBRI1-NS		***tabri1-a.2bd* vs *TaBRI1-NS***		***tabri1-a.3bd* vs *TaBRI1-NS***	
Gene	Gene ID	log2fold change	p-value Adj	log2fold change	p-value Adj	log2fold change	p-value Adj
TaFACKEL1-A	TraesCS1A03G1015700	-0.366	0.212	-0.356	0.331	-0.113	0.874
TaFACKEL1-B	TraesCS1B03G1197500	-0.459	0.192	-0.544	0.186	-0.436	0.429
TaFACKEL1-D	TraesCS1D03G0976100	0.035	0.875	0.043	0.898	0.116	0.759
TaHYD1-A	TraesCS3A03G0174700	-0.311	0.054	0.048	0.877	0.032	0.949
TaHYD1-B	TraesCS3B03G0219900	-0.429	0.226	-0.182	0.753	0.021	0.985
TaHYD1-D	TraesCS3D03G0156100	0.169	0.207	0.074	0.729	-0.087	0.749
TaDWF7-A	TraesCS3A03G0076800	-0.036	0.891	0.341	0.172	0.023	0.972
TaDWF7-B	TraesCS3B03G0104500	-0.001	0.999	0.120	0.695	0.162	0.655
TaDWF7-D	TraesCS3D03G0075300	1.178	**0.000**	0.454	**0.022**	0.209	0.516
TaDWF5-A	TraesCS3A03G1145800	1.024	**0.000**	0.405	**0.031**	0.136	0.699
TaDWF5-B	TraesCS3B03G1336100	0.118	0.431	0.160	0.382	0.148	0.538
TaDWF5-D	TraesCS3D03G1072400	-0.138	0.457	-0.099	0.721	0.030	0.954
TaDWF1-A	TraesCS7A03G1363000	-0.025	0.931	-0.236	0.420	-0.050	0.937
TaDWF1-B	TraesCS7B03G1304200	0.311	0.334	-0.483	0.179	-0.337	0.512
TaDWF1-D	TraesCS7D03G1291100	0.258	0.270	-0.252	0.396	-0.011	0.988

BR-specific biosynthesis pathway genes							
		tabri1-a.1bd* vs *TaBRI1-NS		***tabri1-a.2bd* vs *TaBRI1-NS***		***tabri1-a.3bd* vs *TaBRI1-NS***	
Gene	Gene ID	log2fold change	p-value Adj	log2fold change	p-value Adj	log2fold change	p-value Adj
TaDET2-A	TraesCS3A03G0869900	1.202	**0.001**	0.093	0.896	0.275	0.717
TaDET2-B	TraesCS3B03G0993100	-0.549	0.463	-0.071	0.961	-0.158	0.936
TaDET2-D	TraesCS3D03G0796800	1.942	**0.000**	0.228	0.749	-0.060	0.964
TaCPD1-A/CYP90A3	TraesCS5A03G0368600	-0.702	**0.005**	-0.809	**0.002**	-0.563	0.096
TaCPD1-B/CYP90A3	TraesCS5B03G0369000	-0.446	**0.020**	-0.455	**0.034**	-0.323	0.261
TaCPD1-D/CYP90A3	TraesCS5D03G0351000	-0.908	**0.000**	-0.636	**0.002**	-0.469	0.069
TaDWARF4-4A/CYP90B2	TraesCS4A03G0157500	-1.769	**0.000**	-0.644	**0.042**	-0.542	0.170
TaDWARF4-4B/CYP90B2	TraesCS4B03G0638000	-3.997	**0.000**	-0.718	**0.059**	-0.531	0.297
TaDWARF4-4D/CYP90B2	TraesCS4D03G0567600	-2.235	**0.000**	-1.359	**0.000**	-1.127	0.002
TaDWARF4-3A/CYP90B2	TraesCS3A03G1224700	#N/A	#N/A	#N/A	#N/A	#N/A	#N/A
TaDWARF4-3B/CYP90B2	TraesCS3B03G1464900	#N/A	#N/A	#N/A	#N/A	#N/A	#N/A
TaDWARF4-3D/CYP90B2	TraesCS3D03G1164000	#N/A	#N/A	#N/A	#N/A	#N/A	#N/A
TaD11-A/CYP724B1	TraesCS2A03G0818100	-0.455	0.540	0.219	0.859	0.005	0.999
TaD11-B/CYP724B1	TraesCS2B03G0904700	-1.053	0.129	-0.487	0.650	-0.629	0.624
TaD11-D/CYP724B1	TraesCS2D03G0759600	-1.519	**0.008**	-0.234	0.832	-0.051	0.980
TaROT3-A/CYP90D1	TraesCS3A03G0227000	1.357	**0.000**	0.205	0.499	0.053	0.930
TaROT3-B/CYP90D1	TraesCS3B03G0278600	0.840	**0.019**	0.093	0.894	-0.377	0.563
TaROT3-D/CYP90D1	TraesCS3D03G0218600	-0.269	0.310	-0.232	0.515	-0.065	0.927
TaD2-A/CYP90D2	TraesCS3A03G0227000	1.357	**0.000**	0.205	0.499	0.053	0.930
TaD2-B/CYP90D2	TraesCS3B03G0278600	0.840	**0.019**	0.093	0.894	-0.377	0.563
TaD2-D/CYP90D2	TraesCS3D03G0218600	-0.269	0.310	-0.232	0.515	-0.065	0.927
TaBR6ox1-A1/CYP85A1	TraesCS2A03G0029200	-4.187	**0.000**	-2.613	**0.000**	-1.345	0.034
TaBR6ox1-B1/CYP85A1	TraesCS2B03G0038000	#N/A	#N/A	#N/A	#N/A	#N/A	#N/A
TaBR6ox1-D1/CYP85A1	TraesCS2D03G0028100	-3.802	**0.000**	-2.728	**0.000**	-0.829	0.490
TaBR6ox1-A2/CYP85A1	TraesCS2A03G0027900	-3.177	**0.000**	-2.245	**0.000**	-1.362	0.047
TaBR6ox1-B2/CYP85A1	TraesCS2B03G0038200	-4.158	**0.000**	-3.044	**0.000**	-1.347	0.118
TaBR6ox1-D2/CYP85A1	TraesCS2D03G0027500	-2.799	**0.000**	-1.939	**0.002**	-0.772	0.458
TaBR6ox1-A3/CYP85A1	TraesCS2A03G0028800	-6.963	**0.000**	-4.846	**0.000**	-2.835	**0.012**
TaBR6ox1-B3/CYP85A1	TraesCS2B03G0038400	-7.728	**0.009**	-4.868	**0.207**	-3.625	0.507
TaBR6ox1-D3/CYP85A1	TraesCS2D03G0027700	-5.278	**0.000**	-3.608	**0.000**	-0.868	0.550

B

C

BR signalling pathway genes (wall components)							
		tabri1-a.1bd* vs *TaBRI1-NS		***tabri1-a.2bd* vs *TaBRI1-NS***		***tabri1-a.3bd* vs *TaBRI1-NS***	
Gene	Gene ID	log2fold change	p-value Adj	log2fold change	p-value Adj	log2fold change	p-value Adj
TaBRI1-A	TraesCS3A03G0629800	-0.398	**0.005**	-0.375	**0.016**	-0.508	**0.001**
TaBRI1-B	TraesCS3B03G0712100	-0.621	**0.002**	-0.512	**0.026**	-0.614	**0.012**
TaBRI1-D	TraesCS3D03G0579600	-0.595	**0.000**	-0.407	**0.011**	-0.448	**0.010**
TaBAK1-A1	TraesCS7A03G0714700	-0.634	0.279	-0.909	0.170	-0.034	0.985
TaBAK1-B1	TraesCS7B03G0504900	0.142	0.809	-0.951	0.070	-0.225	0.844
TaBAK1-D1	TraesCS7D03G0688600	-0.176	0.520	-0.613	0.016	-0.225	0.622
TaBAK1-A2	TraesCS2A03G0801300	-0.136	0.660	0.315	0.368	-0.106	0.873
TaBAK1-B2	TraesCS2B03G0887400	0.224	0.196	0.363	0.049	-0.033	0.948
TaBAK1-D2	TraesCS2D03G0741000	0.013	0.960	0.360	0.117	0.028	0.965
TaBKI1-A	TraesCS5A03G0604200	2.867	**0.000**	0.780	0.079	0.358	0.623
TaBKI1-B	TraesCS5B03G0623000	1.617	**0.002**	1.075	0.079	0.558	0.560
TaBKI1-D	TraesCS5D03G0569800	2.423	**0.000**	0.312	0.787	-0.181	0.921

D

BR signalling pathway genes (signalling components)							
		tabri1-a.1bd* vs *TaBRI1-NS		***tabri1-a.2bd* vs *TaBRI1-NS***		***tabri1-a.3bd* vs *TaBRI1-NS***	
Gene	Gene ID	log2fold change	p-value Adj	log2fold change	p-value Adj	log2fold change	p-value Adj
TaBZR-A1/BES1	TraesCS2A03G0389800	0.903	**0.000**	0.008	0.987	-0.285	0.461
TaBZR-B1/BES1	TraesCS2B03G0529800	1.277	**0.000**	0.174	0.694	-0.194	0.731
TaBZR-D1/BES1	TraesCS2D03G0418200	0.839	**0.006**	-0.105	0.859	0.065	0.947
TaBZR-A2	TraesCS3B03G0374100	0.046	0.858	-0.112	0.744	-0.169	0.668
TaBZR-B2	TraesCS3A03G0309300	-0.239	0.411	-0.210	0.603	-0.205	0.703
TaBZR-D2	TraesCS3D03G0292400	-0.459	**0.031**	-0.378	0.144	-0.357	0.259
TaBZR-A3	TraesCS7A03G0867300	-0.675	**0.002**	-0.263	0.416	0.258	0.547
TaBZR-B3	TraesCS7B03G0746500	0.112	0.694	-0.197	0.582	-0.130	0.814
TaBZR-D3	TraesCS7D03G0867600	-0.528	**0.032**	-0.336	0.301	-0.131	0.828
TaBZR-A4	TraesCS6A03G0871600	#N/A	#N/A	#N/A	#N/A	#N/A	#N/A
TaBZR-B4	TraesCS6B03G1042400	-3.318	0.375	-4.340	NA	0.000	NA
TaBZR-D4	TraesCS6D03G0742700	#N/A	#N/A	#N/A	#N/A	#N/A	#N/A
TaBSK1-B	TraesCS4B03G0849600	-0.317	0.181	-0.212	0.523	-0.364	0.281
TaBSK1-D	TraesCS4D03G0756100	-0.122	0.575	-0.073	0.834	-0.368	0.147
TaCDG1-A	TraesCS2A03G0713500	0.247	**0.047**	0.199	0.196	-0.067	0.817
TaCDG1-B	TraesCS2B03G0792100	0.320	**0.043**	0.174	0.426	0.019	0.971
TaCDG1-D	TraesCS2D03G0658800	0.183	0.269	0.081	0.760	-0.130	0.669
TaBSU1-B	TraesCS1B03G0288400	-0.469	**0.001**	0.008	0.981	-0.177	0.501
TaBSU1-D	TraesCS1D03G0207300	-0.233	0.164	-0.153	0.513	-0.181	0.522
TaBIN2-A/TaSKetha	TraesCS1A03G0310500	-0.057	0.737	-0.159	0.401	-0.059	0.866
TaBIN2-B/TaSKetha	TraesCS1B03G0389300	-0.155	0.351	-0.042	0.888	-0.017	0.973
TaBIN2-D/TaSKetha	TraesCS1D03G0308200	-0.133	0.506	0.011	0.977	-0.125	0.739

Supplementary Figure 1 Relationship of Flag leaf angle between ear emergence and anthesis (A), anthesis and water endosperm (B), watery endosperm and soft dough (C) and soft dough and ripening (D) growth stages. Very strong 1:1 relationship was observed in flag leaf angle between subsequent growth stages ($p < 0.001$).

A

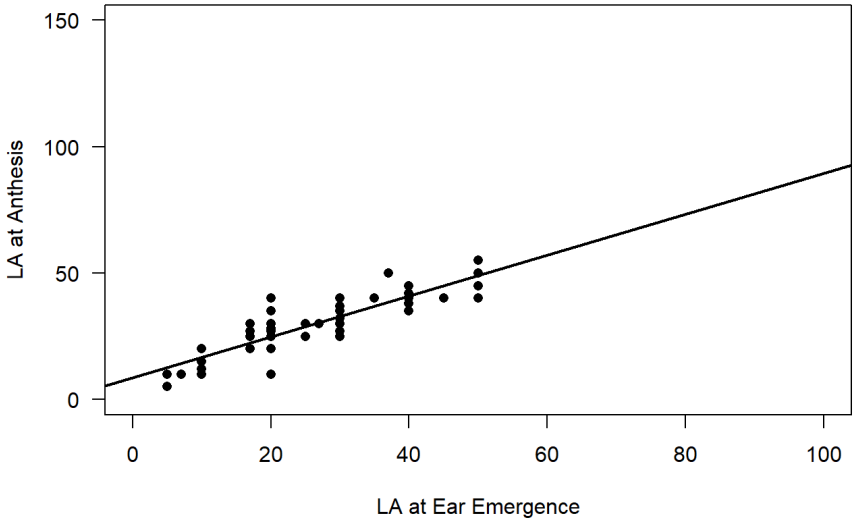

B

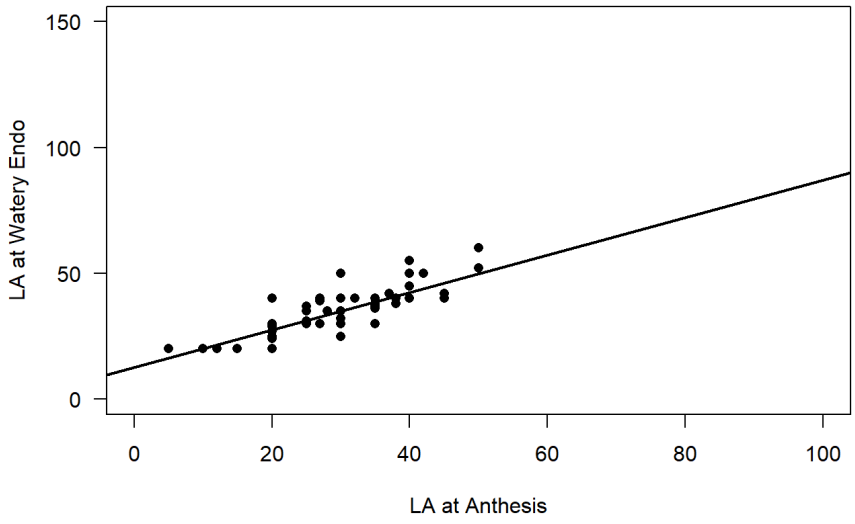

C

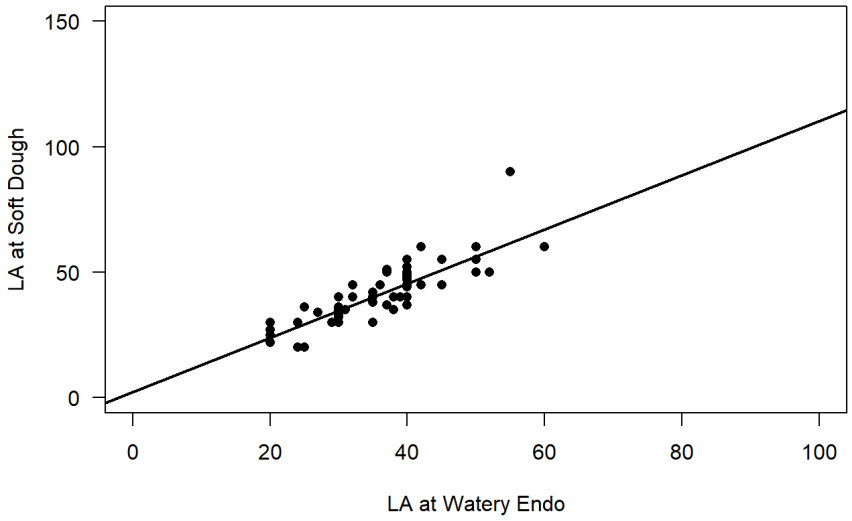
LA at Soft Dough
150
100
50
0
0
20
40
60
80
100
LA at Watery Endo

D

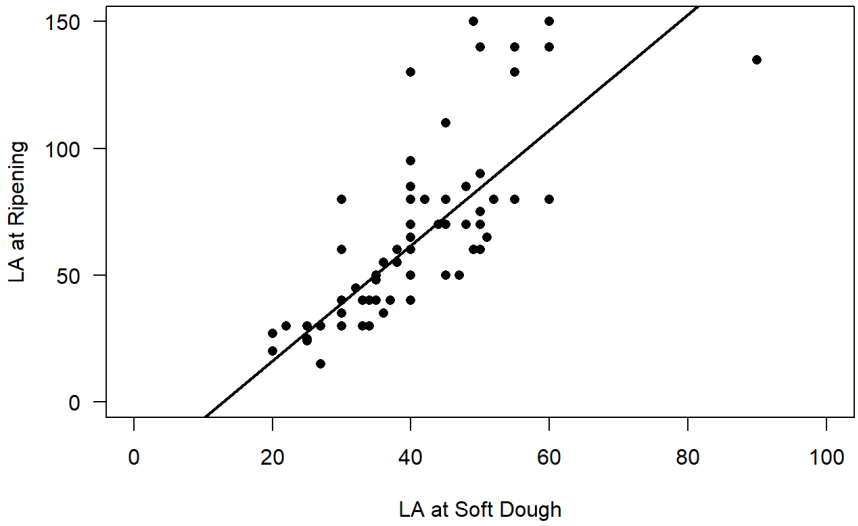
LA at Ripening
150
100
50
0
0
20
40
60
80
100
LA at Soft Dough